Theoretical Analysis of Laterally Vibrating Hammerhead Microcantilever Sensors in a Viscous Liquid

Jinjin Zhang
Marquette University

THEORETICAL ANALYSIS OF LATERALLY VIBRATING HAMMERHEAD MICROCANTILEVER SENSORS IN A VISCOUS LIQUID

By

Jinjin Zhang, B.E., M.E.

A Dissertation submitted to the Faculty of the Graduate School,
Marquette University,
in Partial Fulfillment of the Requirements for
the Degree of Doctor of Philosophy

Milwaukee, Wisconsin

December 2013

ABSTRACT
THEORETICAL ANALYSIS OF LATERALLY VIBRATING HAMMERHEAD MICROCANTILEVER SENSORS IN A VISCOUS LIQUID

Jinjin Zhang, B.E., M.E.

Marquette University, 2013

Dynamically driven prismatic microcantilevers excited in the in-plane flexural mode have been investigated and used in liquid-phase sensing applications. However, the performance is restricted due to their limited surface sensing area and higher stiffness in shorter and wider prismatic microcantilevers. To increase the surface sensing area, and further improve sensing characteristics, it has been proposed to investigate symmetric hammerhead microcantilevers vibrating laterally in viscous liquid media. In this work, a theoretical model is proposed and the characteristics of the microcantilevers with symmetric shaped hammerheads (isosceles trapezoid, semi-circle, uniform rectangle and composite rectangle) are investigated. In the analysis, the stem of the structure is modeled as an Euler-Bernoulli beam while the head is modeled as a rigid body. Since the arbitrary, symmetric head has a varying width, $2b_2(x)$, in the length direction, a new semi-analytical expression for the hydrodynamic function in terms of the Reynolds number, $Re(x)$, and aspect ratio, $h/[2b_2(x)]$ is obtained and the resonance frequency, quality factor and mass sensitivity are investigated as a function of both the hammerhead microcantilever geometry and liquid media properties.

For the investigated geometries, the results show that, for a hammerhead microcantilever with a fixed head area, as the mass center of the head moves towards the support end of the stem, the resulting resonance frequency and mass sensitivity will first increase and then decrease, because the total kinetic energy will first decrease and then increase. The quality factor will keep increasing, due to a more rapid decrease in the energy dissipation. It is also found that, hammerhead microcantilevers with wider heads tend to have higher quality factors. For instance, the highest quality factors are found for the hammerhead microcantilevers with the isosceles trapezoid-shaped, uniform rectangular and composite rectangular head as 140, 72 and 129, respectively, due to the possible shift of the mass center of the head towards the support end of the stem. Such trends can be used to optimize sensor device geometry and frequency stability. By further increasing the surface sensing area (additional mass), the resonance frequency and the mass sensitivity will significantly decrease. Such trade-offs must be considered when designing the geometry of the hammerhead microcantilever devices. For appropriately designed hammerhead microcantilevers, the improvement in the sensing area and quality factor are expected to yield much lower limits of detection in (bio) chemical sensing applications.

ACKNOWLEDGMENTS

Jinjin Zhang, B.E., M.E.

The completion of this work cannot be possibly achieved without the guidance, help, support and patience of many individuals. In this page, I will sincerely express my gratitude to all the people that have been through the happiest and toughest time with me in the past four years.

Foremost, I would like to thank my advisor, Dr. Fabien Josse, for his hard work, understanding, and patience over the entire course of this investigation. His guidance has been essential in the preparation and completion of this work. Without his enormous help, this work will not be presented in a well-organized way. Due to his strict standard, my work ethic, research spirit, and writing skill have improved greatly after these years. I would like to thank him for giving me many opportunities to grow and develop both as a researcher and as a person.

I would like to thank Dr. Nicholas Nigro for many hours of discussions and insights into the theoretical model of the problem. It is those casual and helpful discussions with him that motived me to keep investigating the theoretical model. Thanks to his encouragement and high expectations of my success, my morale has been constantly boosted.

I would also like to thank Dr. Stephen Heinrich for his continued advice regarding the theoretical model. I am amazed by his dedication, motivation, thoroughness, diligence and relentless pursuit of excellence in every discussion. His high standard motivated me in research and will keep guiding me throughout my career.

Thanks are given to Dr. Oliver Brand, Dr. Isabelle Dufour and my entire research committee (Dr. Fabien Josse, Dr. Stephen Heinrich, Dr. Nicholas Nigro, Dr. Edwin Yaz, and Dr. Chung Hoon Lee) for their corrections and suggestions on how to improve this dissertation. I must thank the current and former members of the Microsensor Research Group, especially Mr. Tao Cai, Dr. Russell Cox, and Dr. Florian Bender for helpful discussions.

Mom and dad, without your truly understanding, lifelong support and encouragement in these four years, I will not be able to complete this dissertation and earn this degree. It is you two that make this work possible.

TABLE OF CONTENTS

LIST OF TABLES

LIST OF FIGURES

1. INTRODUCTION

1.1 Microcantilevers as Chemical Sensor Platforms

Microcantilevers are devices that are being investigated and used in sensor applications due to their large surface area-mass ratio, which allows ultrahigh mass detection sensitivity. Compared to conventional analytical techniques, microcantilever-based sensors have several advantages which include high mass loading sensitivity, low cost, low analyte volume requirement, and rapid response [1-5].

Diverse microcantilever-based sensing applications have been explored. These applications range from detecting toxic gases [6-18], such as mercury vapor [6-9], volatile organic compounds [10,11], to detection of specific biological compounds applications such as the detection of bacillus anthracis spores[19], specific antigens [20], myocardial infarction [21, 22] and glucose monitoring [23]. In addition to these applications in the sensor fields, many other microcantilever-based applications span other diverse fields such as atomic force microscopy [24-27, 28], cooling devices [29-30], biomimetic robotic propulsion [31-33] and micro-scale energy harvesting through smart materials[34-36].

In chemical sensing applications, a microcantilever-based sensor consists of a microcantilever, which is usually made of a chemically inert material, and a layer of chemically sensitive coating. The microcantilevers are fabricated on silicon or silicon-on-insulator (SOI) wafers using surface micromachining and deep reactive ion etching processes [37-41]. The chemically sensitive polymers are deposited on the surface of the substrate by spin-coating [42], spray-coating [43], vapor deposition or dip-coating [44]. The chemically sensitive coating is used to absorb or adsorb the target molecules in the

surrounding medium. By coating a layer of chemically sensitive coating on the surface of the microcantilever, microcantilever-based sensor devices are able to detect mass in the range of picograms (10^{-12}g) [45], with the predicted minimum detectable mass in the range of femtograms (10^{-15}g) [6,46].

The polymer layer coated on the microcantilever is not only chemically sensitive but also partially selective. This layer selectively absorbs or adsorbs particular analyte of interest from the surrounding medium, which results in the changes in the polymer layer's characteristics such as mass, volume and viscoelastic properties [3, 19, 23, 45-48]. These changes will result in the changes in the static deflection or the resonance frequency of the coated microcantilever. By measuring the changes in the static deflection or the resonance frequency of the microcantilever, the concentration of the target analyte in the surrounding medium can be estimated. Furthermore, applying the advanced signal processing schemes to the sensor's response, the target signals can be relatively easier identified and characterized and the time required for the measurement can be significantly reduced [53-56].

Because the polymer coating layer is partially selective, it preferably responds to a particular group of analytes which have similar chemical characteristics [49]. As a result, the response of the chemical sensor, which includes the change of the resonance frequency and the amplitude of the tip deflection, is not specific to a particular analyte, but rather to a class of analytes [54]. One approach to solve this selectivity problem is to use an array of sensors, as proposed by Zaromb and Stetter in 1984 [50]. In this strategy, identical sensor platforms having different partially selective coatings are used to study multicomponent samples. The response of the entire sensor array to known chemical

analytes or to an unknown complex mixture forms a pattern, which can be analyzed using pattern recognition techniques for analyte identification, quantification and classification.

Since microcantilevers can be fabricated with very small surface areas, the implementation of micro-scale arrays of microcantilever-based sensors becomes possible [57]. Using these arrays of microcantilever-based sensors, measurements can be carried out in real-time and in-situ [51-52]. Recently, the development of nanocantilevers has further scaled down the technology, with the capability of ultrasensitive detection of analytes combined with high throughput [58].

To-date, microcantilever devices are designed and fabricated in various shapes (rectangular, T-shape, inverse T-shape, V-shape, long- and short- based U-shape) for detecting changes in mass or surface stress[59-76], as shown in Fig. 1-1. The objective is to further improve the characteristics in each field of application. For instance, T-shape microcantilevers are designed to achieve higher sensitivity in mass detection and surface force measurement [60, 73]. A piezoresistive silicon microcantilever paddle is designed for efficiently measuring gas flow [61]. It is presented in Ref 59, that for biochemical applications, inverse T-shape microcantilevers can achieve higher surface stress sensitivity but lower displacement sensitivity compared to the T-shape microcantilevers with the same surface area. Composite rectangular hammerhead microcantilevers with two additional exciting arms are also designed and fabricated to achieve better sensing characteristics [76]. Besides the microcantilevers with uniform thickness, some microfabricated resonant structures with patterned perforations have also been investigated to study the liquid effects on the resonating devices [62]. The relative size of the perforations with respect to the depth of penetration is a key factor that determines the

viscous damping and the effective liquid mass effects. These two effects play an important role in determining the performance of the microcantilever-based sensors in liquid phase detection. Several theoretical and experimental investigations on the effects of hydrodynamic loading, which includes the viscous damping and effective liquid mass, have been conducted in some early studies [27, 34, 63-65]. It is found that the hydrodynamic loading decreases the quality factor of the microcantilever-based resonant sensor device, which decreases its usefulness as an effective sensor platform. As a result, to achieve an effective microcantilever-based sensor, several studies including optimizing the geometry [71], increasing the stiffness of the microcantilever [47], improving the fabrication process and design of the circuitry [77], and using different modes of operation or vibration (in-plane, torsional and longitudinal modes) have been reported recently [28-29, 78-80].

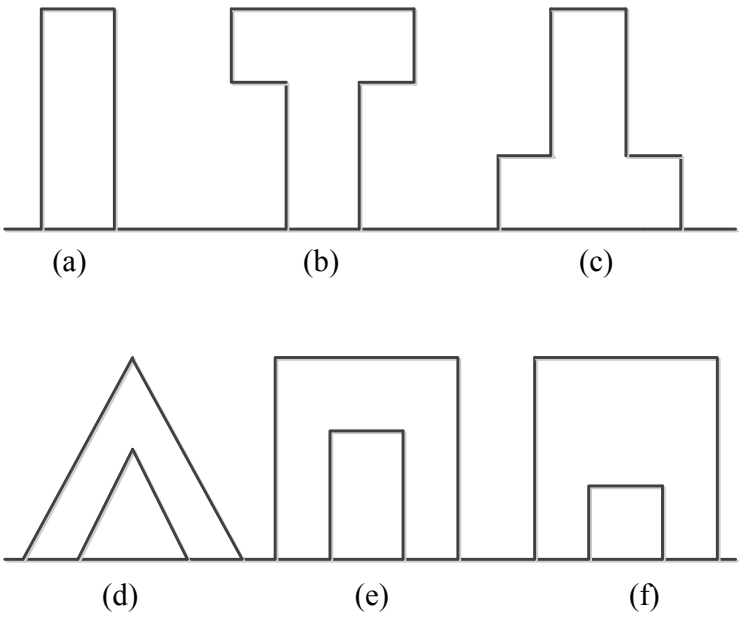

Figure 1-1: Different shapes of microcantilevers including rectangular-(a), T-shape-(b), inverse T-shape-(c), V-shape (d), long- and short- based U-shape-(e) and (f).

1.2 Modes of Operation and Vibration

Microcantilevers can be operated in two fundamental modes: the static mode and the dynamic mode [78-79]. In the static mode, as the microcantilever is operating in the target environment, the analyte molecules of interest will absorb or adsorb into the polymer layer. The interaction between the polymer layer and the target analyte causes the polymer layer to expand, which causes a stress differential between the sensing layer and the substrate of the microcantilever, which, in turn, causes a deformation in the microcantilever. By measuring the magnitude of the tip deflection, the concentration of the target analyte can be calculated [81-82]. Because the response time for a microcantilever operating in the static mode is determined by the characteristics of the microcantilever, the polymer, and the rate of absorption and diffusion of the analyte through the polymer layer [54, 82], one of the disadvantages in the static mode is the relatively long response time when microcantilevers are exposed to the target analytes.

In the dynamic mode, the microcantilever is excited into its resonance frequency. When the polymer coating absorb or adsorb the target molecules, a change in the mass of the sensing layer occurs, which will change the total mass of the vibrating microcantilever. Because of the change in the total mass, the change in the resonance frequency occurs. By measuring the change of the resonance frequency, the concentration of the target analyte can be determined.

Several types of mechanisms exist to excite a microcantilever into its resonance frequency including piezoelectric [36, 83-85], electrothermal [83-84], electromagnetic [84-85], electrostatic [70, 84-85] and optical [86]. The response signal is normally obtained by one of two methods. One method is to measure the tip deflection by optical

readout using a laser. In this case, a light from a laser diode is focused at the tip of the microcantilever and the reflected laser beam is detected by a position-sensitive detector (PSD) [74]. The output from the PSD is then related to the bending deflection and resonance frequency.

An alternative method is to measure the voltage difference of the piezoresistors, which are placed near the clamped end, on both sides of the microcantilever [57, 71, 80]. When the microcantilever is excited into its resonance, the electrical energy is converted into thermal energy through the thermoresistors, which are placed near the piezoresistors. The thermal energy will cause the temperature to increase locally [80]. Since the input signal is an AC signal, during a half period of cycle, the voltage is only applied to one of the two thermoresistors. In this case, the increasing temperature will cause one side of the microcantilever to expand. As the microcantilever bends toward one direction, the piezoresistors will detect the expansion in one side and compression in the other. This deflection-induced stress will cause the resistance of the piezoresistors to change. The change in the resistance will change the output voltage. As a result, the voltage change can be related to the deflection of the beam. The largest change of the voltage occurs at the maximum deflection of the beam, which occurs at the resonance frequency. By knowing the properties of the microcantilever and medium, the magnitude of the deflection can be investigated as a function of the exciting frequency. Using a network analyzer, the frequency spectrum of the vibrating microcantilever can be determined during the measurement.

Microcantilevers can be operated in three modes of vibration in the dynamic mode. They are described as the flexural mode [1, 5, 41, 47, 63, 64, 80, 87-89], torsional mode

[28, 67, 90-92], and longitudinal mode [29]. Specifically, the flexural mode consists of in-plane flexural mode and out-of-plane flexural mode [83, 93].

Microcantilevers excited into the out-of-plane flexural mode have been investigated both theoretically and experimentally [1, 5, 41, 47, 87, 89]. Microcantilevers vibrating in the out-of-plane flexural mode have been applied to a large variety of gas-phase detection applications due to their high mass sensitivity and frequency stability (the ability of an oscillator to maintain a desired operating frequency) [12-17]. However, for liquid phase detection, an additional liquid resistance coming from the surrounding liquid acts on the microcantilever and significantly decreases the frequency stability, which decreases its usefulness as an effective sensing platform. The liquid resistance consists of the effects of the inertia force associated with the liquid dragged along the microcantilever and the viscous force associated with the liquid damping. The inertia force acts like an additional mass added on the microcantilever, which decreases the resonance frequency [63, 80, 82]. Due to the viscosity of the liquid medium, the viscous force also decreases the resonance frequency.

The quality factor is another useful characteristic utilized as a measure of the frequency stability of an oscillatory system. Two possible definitions of the quality factor can be used when studying the dynamically operated microcantilevers [24, 94]. The first definition is 2π times the ratio of the maximum mechanical energy stored in the system to the amount of energy dissipated during one cycle. The other approach is to find the ratio of the resonance frequency to the half power or 3-dB bandwidth of the system. The 3-dB bandwidth definition enables one to obtain the quality factor by merely observing the frequency spectrum, while the energy definition provides a more precise way to calculate

the quality factor. However when the quality factor is much larger than 1, the two definitions are equivalent [24, 94].

In order to decrease the effect of the liquid on a dynamically driven microcantilever and increase the quality factor for liquid phase detection, other modes of vibration have been investigated. Microcantilevers excited in the in-plane flexural mode have been investigated theoretically and experimentally [63-64, 88]. Both theoretical and experimental results in Ref [63-64, 88] show that the in-plane mode of vibration significantly increases the quality factor by decreasing the liquid resistance acting on the microcantilever. However, the surface sensing area is limited by the geometry of the microcantilever and the shorter and wider beams make the microcantilever difficult to excite thermoelectrically near their base.

Torsional mode is another vibration mode that is being investigated for liquid phase detection [92, 95]. It is expected that the torsional mode of vibration will also reduce the liquid resistance acting on microcantilever due to the rotational motion compared to the out-of-plane mode. However, only few experimental investigations of the torsionally vibrating rectangular prismatic microcantilevers in liquids have been presented in the literatures. In Ref [29], the longitudinal mode has also been demonstrated to be useful in gas/liquid phase sensing applications, especially in highly viscous environments. In various fluids ranging from air to a Newtonian fluid of 300 cP viscosity, the measured quality factors for the first longitudinal mode range from 300 to 20 [29].

1.3 Methods to Improve the Characteristics of Laterally Vibrating Rectangular Prismatic Microcantilevers for Liquid Phase Sensing Applications

In order to improve the performance of laterally vibrating rectangular prismatic microcantilever-based chemical sensors in terms of the sensing characteristics, several methods have been proposed. First, higher order modes can be excited and used instead of the first order mode [96-99]. The quality factor achieved for higher order modes is larger than that of the same microcantilever operated in the fundamental mode [93]. However, some drawbacks of operating the microcantilever in the higher order modes include increase in the support loss and decrease in the magnitude of the deflection [99-102]. In microcantilever-based sensing applications, the magnitude of the deflection is an important measurand of the sensor's response. Operating the microcantilever in the higher order modes may decrease the performance of the sensor. Second, making the microcantilevers stiffer is known to increase the quality factor [47]. To make the microcantilevers stiffer, materials with higher Young's modulus can be chosen or the microcantilevers can simply be made shorter and wider. However, the materials selected for the microcantilever usually depend on the fabrication process. For practical chemical sensors applications in liquid environments, the materials have to be water proof and erosion proof. Shortening the length of microcantilevers will also decrease the effective sensing area and widening the width of the microcantilevers will make the microcantilevers harder to excite. As a result, besides changing the properties of rectangular microcantilevers with uniform cross-sections, various non-prismatic microcantilever (namely T-shape, inverse T-shape, V-shape and long- and short- based U-shape) have been investigated [59, 70-71], as indicated earlier. It is noted that the T-shape cantilever is also known as a rectangular hammerhead microcantilever.

A rectangular hammerhead microcantilever is a structure consists of a beam (also known as the stem) with an abrupt change in the width [60], as shown in Fig. 1-2. The stem, which is clamped at the support, has a length of L_1 and a smaller width, b_1; the head has a length of L_2 and a width, b_2, which is much larger than b_1. Compared to the conventional rectangular prismatic microcantilevers, the rectangular hammerhead microcantilevers significantly improve the effective sensing area due to the larger area of the head. As the hammerhead microcantilever with dimensions of [$L_1 \times b_1 \times h + L_2 \times b_2 \times h$] laterally vibrates in viscous liquids, the increase in the total stored mechanical energy in the system may be faster than the energy dissipated during one cycle, which may improve the quality factor compared to that of a prismatic beam with dimensions of [(L_1+ L_2)$\times b_1 \times h$]. To further improve the sensor characteristics, the mass center of the hammerhead can be shifted towards the clamped end of the stem. The hammerhead can also be designed into a circular shape with two finite gaps [71], as shown in Fig. 1-3.

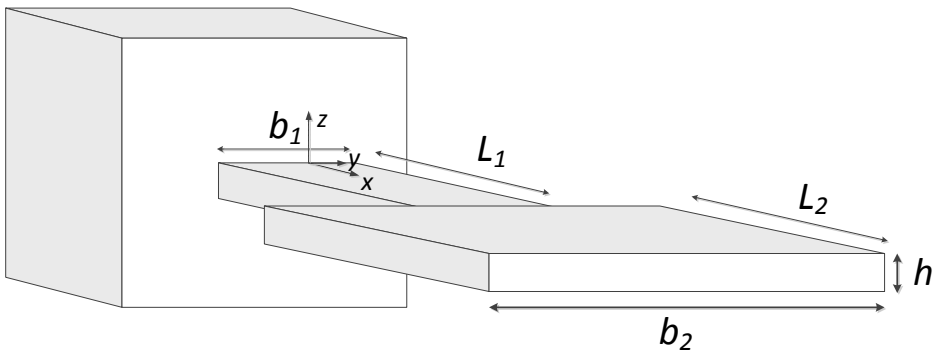

Figure 1-2: A rectangular hammerhead microcantilever with the length and width of the stem being L_1, b_1, respectively; the length and the width of the hammerhead are L_2, b_2, respectively and the thickness is h.

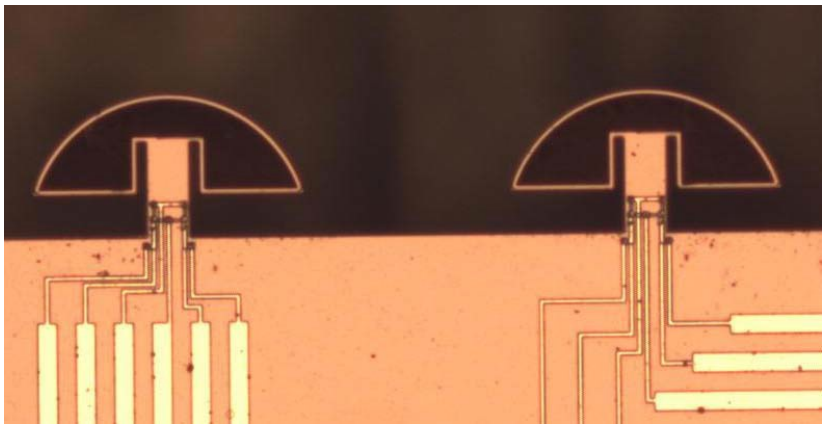

Figure 1-3: The shape of the hammerhead proposed in Ref 71

1.4 Modeling of Laterally Vibrating Prismatic/Non-prismatic Microcantilevers in a Viscous Liquid Medium

Euler-Bernoulli beam theory has been widely used to model laterally vibrating rectangular prismatic microcantilevers in a vacuum [63-64, 80]. However, when rectangular prismatic microcantilevers are immersed in a viscous liquid medium, the surrounding liquid will exert an additional force on the microcantilevers. Thus, the equation of motion in a vacuum must be modified. This additional force is defined by the hydrodynamic force [27].

The hydrodynamic force consists of a pressure force and a shear force. Due to the symmetry of the problem, the pressure and shear force acting on the laterally vibrating rectangular microcantilever in the direction perpendicular to its vibration cancel each other out, respectively. The hydrodynamic forces from the pressure acting on the leading and trailing edges of the microcantilever are equal. The hydrodynamic forces from the shear acting on the top and bottom of the microcantilever are equal. It has been found, as the thickness of the microcantilever becomes small enough compared to its width, the

microcantilever can be assumed to be a ribbon (infinitely thin) [24]. The hydrodynamic force coming from the pressure can then be neglected [80].

For a prismatic microcantilever with a rectangular cross section and a very small thickness compared to its width, the hydrodynamic force can be approximated by the steady-state solution of Stokes' second problem, which describes a semi-infinite domain of homogeneous incompressible liquid which occupies the space above an infinitely extend plate [103]. Stokes' solution states that the hydrodynamic force consists of two components. The imaginary part of the hydrodynamic function, which is in phase with velocity, is associated with the viscous damping; the real part of the hydrodynamic function is out of phase with the velocity, and is associated with the effective liquid mass. By knowing the velocity of any point along the length of the microcantilever, an estimate of the hydrodynamic force exerted on the microcantilever can be analytically calculated. However, as the thickness increases, the pressure force acting on the small surfaces of the beam cannot be neglected [63]. Furthermore, Stokes' second problem assumes an infinitely wide plate, so the stress singularities at the edges are ignored. However, for a beam with finite width, hydrodynamic forces near the edges of a finite surface are not uniform and the edge effect must be taken into account. As a result, it is necessary to find the hydrodynamic force considering both thickness and edge effects.

Several investigations have been conducted to find the hydrodynamic force with thickness and edge effects for laterally vibrating beams [27, 63-64]. In Ref [63], the hydrodynamic function, which is a normalized hydrodynamic force per unit length, is found for different Reynolds number, Re, and aspect ratio, h/b. Re is a dimensionless number that gives a measure of the ratio of inertia force to viscous force in a liquid and

consequently quantifies the relative importance of these two types of forces for a given flow condition [24]. However, the results were found for specific aspect ratios and liquid environment (*Re*) and no attempt was made to determine a general expression for the hydrodynamic forces. In Ref [64], semi-analytical expressions of the real and imaginary parts of the hydrodynamic function are determined as functions of *Re* and aspect ratio. The expressions are determined by multiplying the steady-state solution of Stokes' second problem by a set of correction factors. Thus, for any *Re* and aspect ratio within the investigated domain, the hydrodynamic force can be estimated based on these semi-analytical expressions.

In Ref 64, the correction factors were found by fitting the numerical results of the real and imaginary parts of the hydrodynamic function to the ones associated with Stokes' solution. The numerical results were found by modeling a laterally vibrating rigid cross-section in liquid domain using the FEA software ANSYS 11.0. After extracting the hydrodynamic force as a function of both the Reynolds number, and the aspect ratio of the beam (h/b), the results were validated in the limiting cases when the thickness approaches zero. Then the numerical results are compared with the results published in Ref [63]. Finally, the correction factors were found by fitting the numerical data to Stokes' solution. The hydrodynamic force with thickness and edge effects and the equation of motion for a laterally vibrating beam in viscous liquids were determined. With the appropriate boundary conditions, the equation of motion was solved and the frequency response was obtained.

While rectangular hammerhead microcantilevers have been mostly presented in the literature, it is understood that the head can be of any arbitrary symmetric shape, as

shown in Fig. 1-4. The stem, which is clamped at the support, has a smaller width, b_1, and the head has an abrupt change in the width, which is determined by a function, $2b_2(x)$. By abruptly increasing the width at the junction ($x=L_1$), the sensor characteristics may be significantly improved. As a result, it is necessary to investigate the laterally vibrating symmetric hammerhead microcantilevers in viscous liquids both theoretically and experimentally.

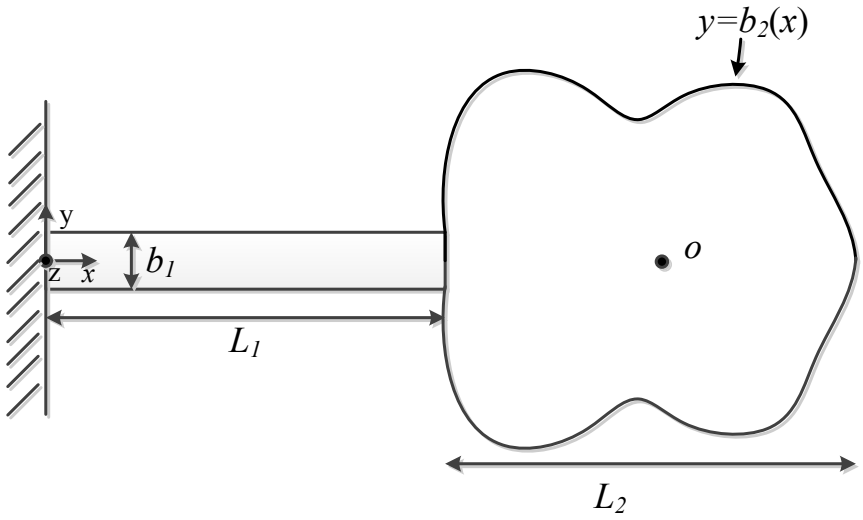

Figure 1-4: The top view of an arbitrary symmetric hammerhead microcantilever with a uniform thickness of h (z direction). The length and width of the stem are L_1 and b_1; the length and half width of the head are determined by L_2 and a function $2b_2$ (x), respectively.

There have been several attempts to theoretically model a transversely vibrating rectangular hammerhead microcantilever in a vacuum [22, 35-36, 60, 69, 104-109]. Initial modeling of a transversely vibrating rectangular hammerhead microcantilever treated the microcantilever as an elastic beam representing the stem and a point mass representing the head [60, 106]. Since there is no energy loss to the surrounding medium in a vacuum, the maximum kinetic energy equals the maximum potential energy of the microcantilever. Thus, using the Rayleigh Ritz method, an analytical expression for the

resonance frequency in a vacuum was obtained in a closed form [106]. In the case of lateral vibration, the analytical expression of the resonance frequency for a rectangular hammerhead microcantilever in a vacuum can be obtained as indicated in Ref [106]. In this case, it is noted that the second moment of area of cross-section for the stem, I_{stem}, is 1/12 multiplied by the width cubed and the thickness. However, this method loses its accuracy when the operating medium is a liquid environment, since, by assuming that the head is a point mass, one does not account for the additional liquid effects acting on the entire system. In a viscous liquid, the hydrodynamic load on a rectangular hammerhead microcantilever vibrating in the in-plane direction must be appropriately modeled. When the aspect ratio (thickness over width) increases, the thickness effect cannot be ignored [20-21]. Both liquid resistances coming from the large and small surfaces of the microcantilever must be taken into account. The hydrodynamic function on the microcantilever may not be modeled as a microcantilever vibrating in the out-of-plane direction with only the width and thickness dimensions switched [76].

Another method to model a laterally vibrating rectangular hammerhead microcantilever in a vacuum treated the stem and head as two Euler- Bernoulli beams with different widths [104]. In this case, two equations of motion representing the stem and head were presented. A total of eight boundary conditions were required. Four boundary conditions represent the physical conditions at the fixed end and free end. The other four boundary conditions represent the continuity conditions at the junction between the stem and head. By solving the two fourth-order differential equations, the analytical expressions of the resonance frequency are obtained in a vacuum. This model is more appropriate for the domain (geometries) where the width of the head is only

slightly larger than that of the stem. Such geometry is not of interest in the present investigation due to its relatively low quality factor.

In order to increase the effective surface sensing area for liquid phasing sensing applications, the width of the hammerhead should be much larger than the width of the stem. Then, the head tends to move rigidly without much deformation. Thus, a laterally vibrating symmetric hammerhead microcantilever can be modeled as an Euler-Bernoulli beam representing the stem, and a rigid body representing the head. In this case, the rotational effects coming from the head may be taken into account.

When the symmetric hammerhead microcantilever vibrates laterally in viscous liquids, the hydrodynamic forces acting on the stem and hammerhead are different. Since the symmetric head has a varying width, $2b_2(x)$, the hydrodynamic function along the head must be different. Since the cross-sections of the stem and head are rectangular, the analytical expressions of the real and imaginary parts of the hydrodynamic function presented in Ref [64] can be applied. However, the fitting accuracy from the numerical results to the obtained analytical expression in Ref [64] is relatively low. As a result, based on the numerical data presented in Ref [64], when analyzing the symmetric hammerhead microcantilever, it is necessary to find a new mathematical expression of the hydrodynamic function to improve the accuracy of the fitting.

1.5 Problem Statement and Objectives

Dynamically driven rectangular prismatic microcantilevers operating in the out-of-plane flexural mode have been widely investigated and used in gas phase sensing applications due to their large surface area-mass ratio, which allows ultrahigh mass detection sensitivity. However, in liquid phase sensing applications, the decreased quality

factor and sensitivity due to the additional liquid resistance significantly affect the performance of the device. As noted before, several methods have been attempted to improve the sensing characteristics of the device, including exciting the microcantilevers into different vibration modes (in-plane flexural mode, torsional mode or longitudinal mode) or higher order modes, increasing the stiffness of the microcantilever and optimizing the geometry of the microcantilevers. Operating the microcantilevers in the in-plane mode flexural significantly reduces the liquid resistance. However, when the microcantilever laterally vibrates in the higher order modes, the support loss will increase and the magnitude of the deflection, which is an important measurand, will decrease [99-102]. Furthermore, stiffening the rectangular prismatic microcantilever makes the microcantilever harder to excite. As a result, optimizing the geometry and driving the microcantilever in the in-plane flexural vibration mode may improve the effective sensing area and frequency stability. One method to possibly achieve this is to investigate laterally vibrating symmetric hammerhead microcantilevers with different geometries of the head (isosceles trapezoid, semi-circular, uniform rectangular and composite rectangular) to find an optimum geometry in terms of the sensing applications.

Symmetric hammerhead microcantilevers can be treated as non-prismatic microcantilevers with one end perfectly fixed and the other end free. The stem, which is clamped at the support, has a smaller width, and the head, which is perfectly connected to the stem, has a larger width. By attaching a larger head to the end of the stem, the sensing area is increased, while the resonance frequency is decreased, which makes the microcantilever easier to excite electrothermally than an equivalent rectangular cantilever

with a larger width. As a result, it is necessary to perform a complete theoretical analysis of such hammerhead microcantilevers in viscous liquids.

In order to perform a theoretically analysis of laterally vibrating symmetric hammerhead microcantilevers in viscous liquids, an idealized model must be set up according to the appropriate assumptions placed on the stem and head. In order to achieve a larger sensing area, the dimensions of the head must be much larger than those of the stem. In this case, the hammerhead microcantilever should be modeled as an elastic beam and a rigid body. The standard Euler-Bernoulli beam theory will be used to model the stem as an elastic beam. However, due to larger moment of inertia of the head, its rotational motion must be taken into account when analyzing the boundary conditions at the junction between the stem and the head.

After the theoretical model is set up, its validity must be determined. Three-dimensional numerical models, using FEA software Comsol 4.1, will be created to study the structure vibration in a vacuum. The first resonance frequencies corresponding to the lateral vibration will be extracted and compared to the ones from theoretical models. Thus, the domain (geometries) of the validity of the theoretical model can be found by analyzing the model in various limits (for example, by ignoring the hydrodynamic force acting on the hammerhead microcantilever ($g_{1,stem/head}$ and $g_{2,stem/head}$)) and comparing the results to those of the FEA model in a vacuum. This necessary step may provide reasonable confidence in applying the theoretical model to analyze the sensor characteristics in liquid environments.

In order to perform the above-mentioned theoretical analysis in liquid environments, the hydrodynamic forces on the stem and head must first be defined. The method to find

the hydrodynamic force on a symmetric hammerhead microcantilever with a varying head width will be analogous to that used to find the hydrodynamic force on a prismatic beam [64]. The hydrodynamic function, which is a normalized hydrodynamic force, proposed in Ref [64] cannot be directly used. The accuracy of the fitting from the numerical data to the analytical expression is relatively low. Thus, to improve the fitting accuracy, it is necessary to obtain an improved mathematical form of the analytical expression of the hydrodynamic function.

To further optimize the geometry of a simple rectangular hammerhead microcantilever, a composite head structure, as shown in Fig. 1-5, will be investigated to see if such geometry can improve sensing characteristics. By varying the dimensions of the gaps, as defined by b_4 and L_3, the characteristics of laterally vibrating hammerhead microcantilevers will be analyzed as a function of d_{os}, which represents the distance between the mass center and the tip of the stem.

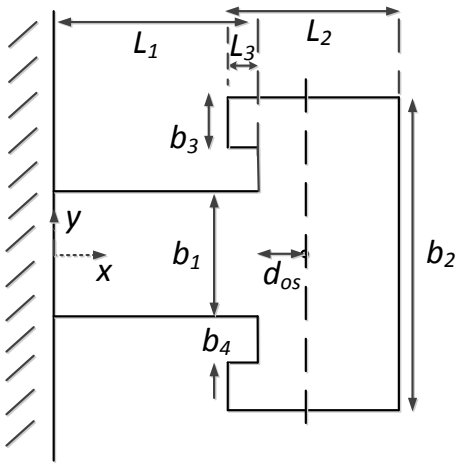

Figure 1-5: Top view of a composite rectangular hammerhead microcantilever with two finite rectangular gaps.

The primary objective of this work is to theoretically analyze the characteristics of the laterally vibrating symmetric hammerhead microcantilevers in viscous liquids. The characteristics such as the resonance frequency, quality factor, mass sensitivity and limit of detection of the microcantilever will be analyzed. By treating the head as a rigid body, the theoretical model will be setup and these characteristics will be obtained by solving the equation of motion of the stem with boundary conditions at the fixed end and at the junction between the stem and the head. In liquid phase, the hydrodynamic forces will exert an additional force on the microcantilever. This will result in changes in the equation of motion and the boundary conditions as presented in a vacuum. To further accurately calculate the hydrodynamic force, a new mathematical form of the analytical expression for the hydrodynamic function, will be proposed and applied in the theoretical investigation. After obtaining the characteristics of the laterally vibrating symmetric hammerhead microcantilevers with particularly the isosceles trapezoid, semi-circular, uniform rectangular and composite rectangular heads, the trend of the characteristics will be investigated as functions of the geometric parameters of the hammerhead microcantilever and the properties of the liquid medium to provide guidelines for the design of the microcantilever-based sensing platform.

1.6 Dissertation Organization

This dissertation is organized into five chapters. In chapter 2, a general model will be set up to investigate the characteristics of a laterally vibrating symmetric hammerhead microcantilever. The solutions for the symmetric hammerhead microcantilevers with the isosceles trapezoid, semi-circular, uniform rectangular and composite rectangular heads are presented. The equation of motion will be solved based on the appropriate boundary

conditions. The magnitude of the deflection at the end of the stem will be expressed as a function of the exciting frequency, which will be used to extract the resonance frequency. Then, a numerical analysis to validate the theoretical model (uniform rectangular head) is performed. In chapter 3, Different analytical expressions of the real and imaginary parts of the hydrodynamic function with thickness and edge effects will be proposed for a head with a varying width as a function of the position along the length of the microcantilever. The hydrodynamic functions on the stem and hammerhead with thickness and edge effects will be obtained. In chapter 4, using the proposed analytical expression of the hydrodynamic function with thickness and edge effects, the characteristics such as resonance frequency, quality factor, and mass sensitivity will be calculated. The quality factor obtained using the energy definition is compared with the quality factor obtained using the 3-dB definition. Trends of these characteristics as functions of the properties of the hammerhead microcantilever and the properties of the medium are found. Guidelines of the design of the sensing platform are provided. The characteristics of these symmetric hammerheads excited laterally are then compared and contrasted. Finally, chapter 5 gives a summary of the results and identifies areas of future research.

2. MODELING OF LATERALLY VIBRATING SYMMETRIC HAMMERHEAD MICROCANTILEVERS

2.1 Introduction

In this chapter, a theoretical model of a laterally vibrating symmetric hammerhead (of arbitrary shape) microcantilever in viscous liquid media will be explicitly presented. In order to study a laterally vibrating symmetric hammerhead microcantilever in viscous liquid media, it is necessary to set up an appropriate theoretical model. This model must first be analyzed in a vacuum and validated for various geometrical shapes and dimensions of interest. Then, the model will be investigated in the in-liquid case.

In sensor's applications, it is often necessary to improve sensors' characteristics and sensitivity of detection by increasing the dimensions of the head. Compared to the conventional rectangular prismatic microcantilevers, the rectangular hammerhead microcantilevers significantly improve the effective sensing area due to the larger area of the head. Since the dimensions of the head are much larger than those of the stem, the head will tend to move rigidly without much deformation.

Thus, in this investigation, it is proposed to model a vibrating symmetric hammerhead microcantilever by treating the stem as an elastic beam and the head as a rigid body.

Several different symmetric heads will be analyzed including the shapes of isosceles trapezoid, semi-circle, uniform and composite rectangle. These geometries will be investigated in both the in-vacuum and in-liquid cases.

To validate the general model which assumes the symmetric head as a rigid body in a vacuum, the uniform rectangular hammerhead microcantilevers are chosen as a

particular case. Three-dimensional (3-D) numerical models of laterally vibrating uniform rectangular hammerhead microcantilevers are also created for the in-vacuum case using an FEA package Comsol 4.1 for comparison purpose. The first natural frequency corresponding to the lateral vibration are simulated and recorded. By comparing the numerically and analytically obtained results, the domain of the validity associated with the analytical model will be determined.

Fig. 2-1 shows a typical symmetric, arbitrary shape hammerhead microcantilever with a uniform thickness of h. The length and width of the stem are L_1 and b_1; the length and half width of the head are determined by L_2 and a function $2b_2$ (x), respectively. The origin is located at the center of the stem-support interface with the x-axis, y-axis, and z-axis in the direction of the microcantilever's length, width, and thickness, respectively. O is noted as the mass center of the head. The hammerhead microcantilever is clamped at x=0 and free at $x=L_1+L_2$.

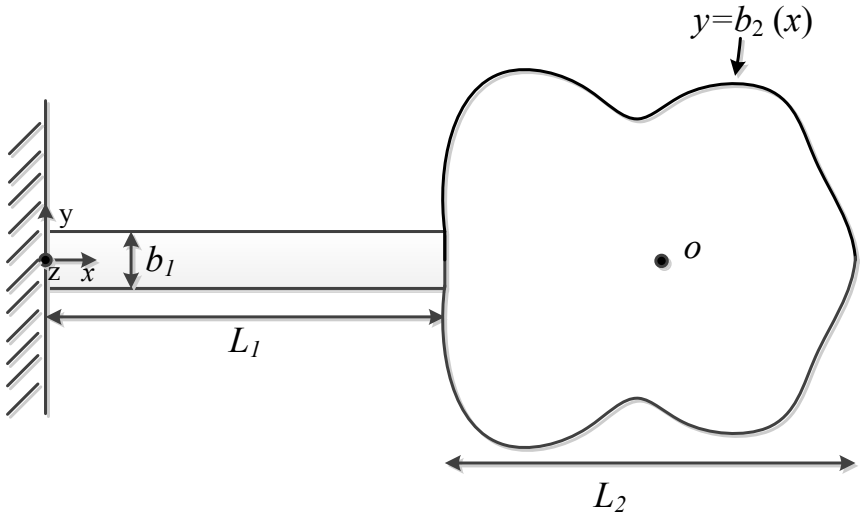

Figure 2-1: The top view of a typical symmetric hammerhead microcantilever with a uniform thickness of h (z direction). The length and width of the stem are L_1 and b_1; the length and half width of the head are determined by L_2 and a function $2b_2$ (x), respectively.

In order to set up the theoretical model for the problem, several assumptions are made throughout this work:

- The hammerhead microcantilever is assumed to be homogeneous and made of a material which is linear elastic and isotropic. (Silicon, often used as cantilever substrate, is an anisotropic material, thus, its Young's modulus is different in different crystalline directions, i.e. [100], [110] and [111]. In this investigation, the appropriate value of Young's modulus (169 GPa) in the [110] direction is used)
- The hammerhead microcantilever is perfectly fixed at the clamped end. (For a stem that is relative short and wide, the stem is very stiff relative to the support structure; and thus this assumption may be questionable due to support compliance [115])

- Only the first lateral mode is investigated and the other modes or mode couplings are not taken into account.
- Euler-Bernoulli beam theory is valid for the stem. i.e. $b_1 << L_1$, such that the shear deformation and rotational inertia of the stem are negligible [114].
- The in-plane flexural stiffness of the head in both the x and y direction are assumed to be much greater than the in-plane flexural stiffness of the stem in the y direction, thus, the head can be treated as a rigid body.
- The deflection and rotation of the stem and head are very small, so the displacement in the x direction is negligible.
- The forced vibration is assumed to be due to electrothermal excitation which is caused by two thermal resistors placed on the stem near the support end, as shown in Fig. 2-2. This is modeled by an equivalent support end rotation which is harmonic in time [80].
- The liquid is incompressible and Newtonian.
- The governing equations for the liquid domain are linearized Navier-Stokes' equations.
- The hydrodynamic forces on the stem and head are obtained from a two-dimensional numerical model which assumes rigid rectangular cross-sections for either part [110].

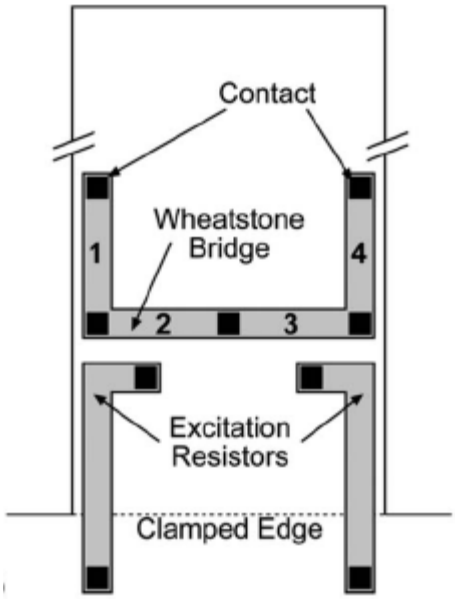

Figure 2-2: Schematic of the heating excitation resistors and the piezoresistive Wheatstone bridge for vibration detection [80].

2.2 Modeling the Stem as an Euler-Bernoulli Beam

In order to apply the standard Euler-Bernoulli beam theory on the stem, there are several assumptions that are placed on the stem:

- The cross-sectional area of the stem is uniform over the length of the stem.
- The length of the stem is much larger than the width of the stem. (It is noted in Ref 114 that if the length-to-width ratio of the beam is roughly 7 or higher, the Timoshenko beam effects may be considered negligible)
- The amplitude of the vibration of the stem is far smaller than any length scale of the stem.

By modeling the stem as an Euler-Bernoulli beam, the equations of motion (EOMs) for the stem in a vacuum and viscous liquid medium can be set up, respectively. To solve the EOMs for the in-vacuum and in-liquid cases, appropriate boundary conditions (BCs)

are used in either case, respectively. According to the assumptions made in Sec. 2.1, two BCs can be found at the fixed end ($x=0$), which will be discussed in Sec 2.2.1.

2.2.1 EOM and BCs at the Fixed End

In a vacuum, based on the standard Euler-Bernoulli beam theory, the EOM for the stem is presented as:

$$EI_{stem}\frac{\partial^4 v_{stem}(x,t)}{\partial x^4}+\rho_b b_1 h\frac{\partial^2 v_{stem}(x,t)}{\partial t^2}=0\,, \tag{2.1}$$

Eq. 2.1 is a fourth-order partial differential equation (PDE) that describes the in-vacuum motion of the stem in terms of its displacement (v_{stem}). E is the modulus of elasticity of the material. I_{stem} is the second moment of area of cross section corresponding to the stem. ρ_b is the density of the stem.

When laterally vibrating rectangular hammerhead microcantilevers are immersed in viscous liquid media, the surrounding liquid will impose hydrodynamic forces on the stem and head. As a result, the EOM for the stem is modified as:

$$EI_{stem}\frac{\partial^4 v_{stem}(x,t)}{\partial x^4}+\rho_b b_1 h\frac{\partial^2 v_{stem}(x,t)}{\partial t^2}=F_{stem,liquid}(x,t)\,. \tag{2.2}$$

The hydrodynamic force on the stem, $F_{stem.liquid}$, is a force per unit length, which is partially out-of-phase with the displacement and is given by [110]

$$F_{stem,liquid}(x,t)=-g_{1,stem}\frac{\partial v_{stem}(x,t)}{\partial t}-g_{2,stem}\frac{\partial^2 v_{stem}(x,t)}{\partial t^2}\,. \tag{2.3}$$

In Eq. 2.3, $g_{1,stem}$ is a coefficient associated with the viscous damping coming from the liquid and $g_{2,stem}$ is a coefficient associated with the effective mass coming from the liquid. Both $g_{1,stem}$ and $g_{2,stem}$ are time-independent coefficients and they are functions of

Re_{stem} and the aspect ratio, h/b_1. The expressions of $g_{1,stem}$ and $g_{2,stem}$ will be obtained and investigated in chapter 4.

It is shown in Eq. 2.1 and Eq.2.2 that the EOMs presented in a vacuum and viscous liquid are fourth-order PDEs. In order to solve a fourth-order PDE, a total of four BCs are needed. In a vacuum and viscous liquid medium, two BCs can be defined at the fixed end (x=0). One of them describes the zero deflection at the fixed end, and is given by

$$v_{stem}(0,t) = 0\,, \tag{2.4}$$

The other BC at the fixed end can be obtained differently according to the free vibration and forced vibration. For a free vibration, the bending slope (rotational angle) at the support end of the hammerhead microcantilever is expressed as:

$$\frac{\partial v_{stem}(x,t)}{\partial x}\Big|_{x=0} = 0\,, \tag{2.5}$$

For the forced vibration, since the exciting force is due to an equivalent, harmonic support rotation, the bending slope (rotational angle) of the support end of the hammerhead microcantilever is expressed as:

$$\frac{\partial v_{stem}(x,t)}{\partial x}\Big|_{x=0} = \theta_0 e^{j\omega t}\,. \tag{2.6}$$

In Eq. 2.6, θ_0 and ω are the amplitude and angular frequency of the effective support rotation [80]. This BC is originally inspired by a model of the electrothermal excitation that was first applied in another work [80].

The remaining two BCs, which describe the physical conditions at the junction between the stem and head (x=L_1), will be discussed in Sec. 2.3.1.

2.3 Modeling the Head as a Rigid Body

For a laterally vibrating hammerhead microcantilever, as the dimensions of the head become much larger than those of the stem, the head tends to move rigidly without any deformation in itself. This rigidity of the head causes two motions to occur: one is a translational motion and one is a rotational motion. The translational velocity of the mass center of the head is equal to the translational velocity at the tip of the stem plus the angular velocity at the end of the stem times the distance to the mass center. The angular velocity at any point on the head is the same as the angular velocity at the tip of the stem ($x=L_1$). In this work, the deflection and rotation of the head are assumed to be very small, so that the displacement in the x direction is negligible. By analyzing the motions of the head, the remaining two BCs can be found.

2.3.1 BCs at the Tip of the Stem

In a vacuum, to find the remaining two BCs, which describe the physical conditions at the junction ($x=L_1$), the forces and moments exerted at the boundary between the stem and head must be analyzed. A free body diagram of a laterally vibrating symmetric head in a vacuum is presented in Fig. 2-3, in which all the forces and moments are shown in their positive directions:

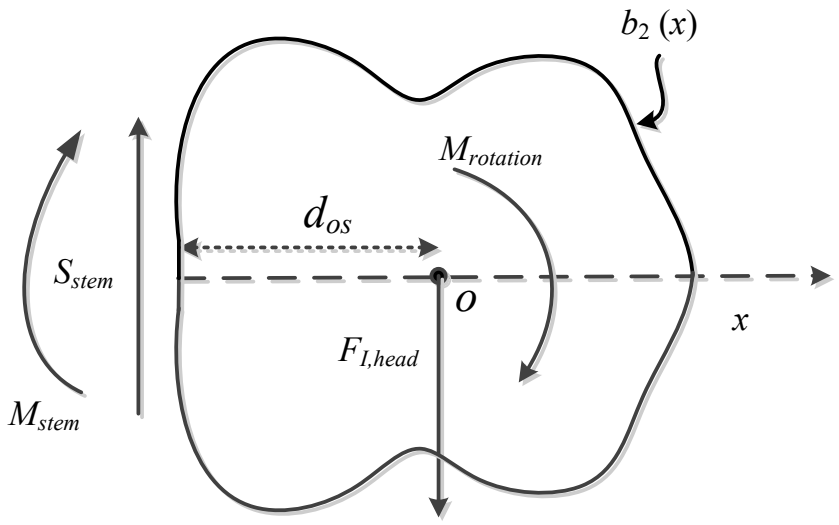

Figure 2-3: The free body diagram of the laterally vibrating symmetric hammerhead in a vacuum.

Based on the free body diagram presented in Fig. 2-2, the force and moment equilibrium at the junction ($x=L_1$) result in the following force and moment balance equations:

$$S_{stem} - F_{I,head} = 0\,, \tag{2.7}$$

$$M_{stem} + M_{I,head} + M_{rotation} = 0\,, \tag{2.8}$$

where

$$F_{I,head} = m_{head} \frac{\partial v^2{}_{head}(x,t)}{\partial t^2}\Big|_{x=L_1+d_{os}}\,, \tag{2.9}$$

$$M_{I,head} = F_{I,head} d_{os}\,, \tag{2.10}$$

$$M_{rotation} = J_{head} \frac{\partial^3 v_{stem}(x,t)}{\partial x \partial t^2}\Big|_{x=L_1}\,. \tag{2.11}$$

with m_{head}, the mass of the head, and J_{head}, the rotational inertia about the mass center of the head. In Eq. 2.7 and Eq. 2.8, S is noted as the shear force and M is noted as the

moment. $F_{I,head}$ is noted as the force due to the mass inertia of the head. Since the shape of the head is symmetric with respect to the x-axis, the mass of the head and the distance from the mass center of the head to the tip of the stem, d_{os}, can be found, respectively, as follows:

$$m_{head} = 2h\rho_b \int_{L_1}^{L_1+L_2} b_2(x)dx \tag{2.12}$$

$$d_{os} = \frac{\int_{L_1}^{L_1+L_2} xb_2(x)\,dx}{\int_{L_1}^{L_1+L_2} b_2(x)\,dx} - L_1, \tag{2.13}$$

$$J_{head} = J_z - m_{head} {d_{oz}}^2. \tag{2.14}$$

where

$$J_z = 2\rho_b h \int_{L_1}^{L_1+L_2} \left[x^2 b_2(x) + \frac{1}{3} {b_2}^3(x) \right] dx, \tag{2.15}$$

$$d_{oz} = L_1 + d_{os}, \tag{2.16}$$

In Eq. 2.12, $b_2(x)$ is noted as half width of the head. In Eq. 2.14, J_{head} is determined based on the parallel axis theorem. J_z is the rotational inertia of the head about the z-axis, and is given by Eq. 2.15. d_{oz} is the distance from the mass center of the head to the origin of the support, and can be found from Eq. 2.16.

Since the deflection and rotation of the hammerhead in the x direction are assumed to be negligible, only the deflection and rotation in the y direction are taken into account. As a result, the translational velocity at the mass center of the head is the translational velocity at the tip of the stem plus the angular velocity at the end of the stem times the distance to the mass center, and is given by:

$$\frac{\partial v_{head}(x,t)}{\partial t}\Big|_{x=L_1+d_{os}} = \left[\frac{\partial v_{stem}(x,t)}{\partial t} + d_{os}\frac{\partial^2 v_{stem}(x,t)}{\partial x \partial t}\right]\Big|_{x=L_1}, \tag{2.17}$$

The acceleration is the first derivative of the translational velocity with respect to time, and is given by

$$\frac{\partial^2 v_{head}(x,t)}{\partial t^2}\Big|_{x=L_1+d_{os}} = \left[\frac{\partial^2 v_{stem}(x,t)}{\partial t^2} + d_{os}\frac{\partial^3 v_{stem}(x,t)}{\partial x \partial t^2}\right]\Big|_{x=L_1}. \tag{2.18}$$

Applying Eq. 2.9 through Eq. 2.18 to Eq. 2.7 and Eq. 2.8, the expressions for the force and moment equilibrium, respectively, are as follows:

$$\left\{\begin{array}{l} m_{head}\left[\frac{\partial^2 v_{stem}(x,t)}{\partial t^2} + d_{os}\frac{\partial^3 v_{stem}}{\partial x \partial t^2}(x,t)\right]d_{os} \\ +EI_{stem}\frac{\partial^2 v_{stem}(x,t)}{\partial x^2} + J_{head}\frac{\partial^3 v_{stem}}{\partial x \partial t^2}(x,t) \end{array}\right\}\Big|_{x=L_1} = 0, \tag{2.19}$$

$$\left\{EI_{stem}\frac{\partial^3 v_{stem}(x,t)}{\partial x^3} - m_{head}\left[\frac{\partial^2 v_{stem}(x,t)}{\partial t^2} + d_{os}\frac{\partial^3 v_{stem}}{\partial x \partial t^2}(x,t)\right]\right\}\Big|_{x=L_1} = 0. \tag{2.20}$$

For convenience, the four BCs in a vacuum are rewritten as follows:

For the free vibration:

$$v_{stem}(0,t) = 0, \tag{2.21}$$

$$\frac{\partial v_{stem}(x,t)}{\partial x}\Big|_{x=0} = 0, \tag{2.22}$$

$$\left\{\begin{array}{l} m_{head}\left[\frac{\partial^2 v_{stem}(x,t)}{\partial t^2} + d_{os}\frac{\partial^3 v_{stem}}{\partial x \partial t^2}(x,t)\right]d_{os} \\ +EI_{stem}\frac{\partial^2 v_{stem}(x,t)}{\partial x^2} + J_{head}\frac{\partial^3 v_{stem}}{\partial x \partial t^2}(x,t) \end{array}\right\}\Big|_{x=L_1} = 0, \tag{2.23}$$

$$\left\{EI_{stem}\frac{\partial^3 v_{stem}(x,t)}{\partial x^3} - m_{head}\left[\frac{\partial^2 v_{stem}(x,t)}{\partial t^2} + d_{os}\frac{\partial^3 v_{stem}}{\partial x \partial t^2}(x,t)\right]\right\}\Big|_{x=L_1} = 0. \tag{2.24}$$

For the forced vibration which is due to an equivalent, harmonic support rotation, The BCs associated with the displacement at the fixed end, moment and shear equilibriums at the junction between the stem and head are the same. Only the BC corresponding to the bending slope of the support end of the microcantilever is different from the one by Eq. 2.22. For convenience, the four BCs are presented as:

$$v_{stem}(0,t)=0\,, \tag{2.25}$$

$$\frac{\partial v_{stem}(x,t)}{\partial x}\Big|_{x=0}=\theta_0 e^{j\omega t}\,. \tag{2.26}$$

$$\left\{\begin{array}{l} m_{head}\left[\dfrac{\partial^2 v_{stem}(x,t)}{\partial t^2}+d_{os}\dfrac{\partial^3 v_{stem}}{\partial x\partial t^2}(x,t)\right]d_{os} \\ +EI_{stem}\dfrac{\partial^2 v_{stem}(x,t)}{\partial x^2}+J_{head}\dfrac{\partial^3 v_{stem}}{\partial x\partial t^2}(x,t) \end{array}\right\}\Big|_{x=L_1}=0\,, \tag{2.27}$$

$$\left\{EI_{stem}\frac{\partial^3 v_{stem}(x,t)}{\partial x^3}-m_{head}\left[\frac{\partial^2 v_{stem}(x,t)}{\partial t^2}+d_{os}\frac{\partial^3 v_{stem}}{\partial x\partial t^2}(x,t)\right]\right\}\Big|_{x=L_1}=0\,. \tag{2.28}$$

In a viscous liquid medium, the remaining two BCs can be found at the junction between the stem and head ($x=L_1$). To obtain the force and moment equilibrium conditions at the junction, a free body diagram of a laterally vibrating symmetric hammerhead in viscous liquid media is presented in Fig. 2-4, in which all the forces and moments are shown in their positive directions:

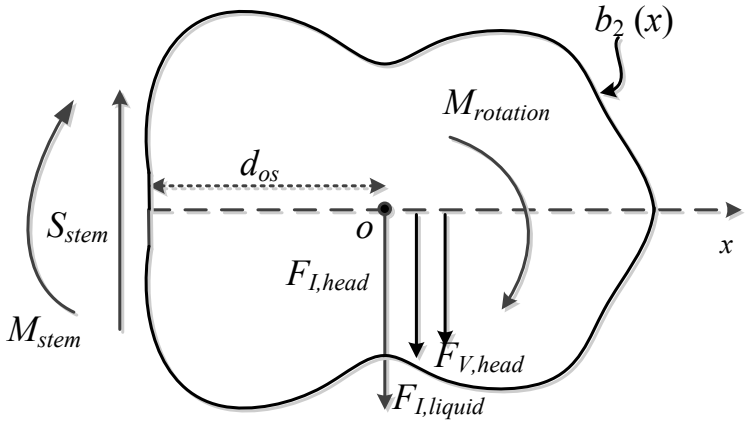

Figure 2-4: The free body diagram of a laterally vibrating symmetric hammerhead in viscous liquids.

In Fig. 2-4, the hydrodynamic force is separated into two effective forces and these forces result in corresponding moments. One effective force is the inertia force ($F_{I,liquid}$) coming from the effective mass and the other one is the damping force ($F_{V,liquid}$) coming from the liquid viscous damping. Then the force equilibrium and moment equilibrium are obtained as follows:

$$S_{stem} - F_{I,head} - F_{I,liquid} - F_{V,liquid} = 0\,. \tag{2.29}$$

$$M_{stem} + M_{I,head} + M_{I,liquid} + M_{V,liquid} + M_{rotation} = 0\,, \tag{2.30}$$

The inertia force ($F_{I,liquid}$) and viscous force ($F_{V,liquid}$) are proportional to the velocity and acceleration of the head, respectively. To find the total inertia, damping forces and resulting moments due to the liquid resistance, the force and moment acting on each differential element, *dx* (shown in Fig. 2-5), must be integrated from L_1 to L_1+L_2. Fig. 2-5 shows the inertia, damping forces and resulting moments due to viscous liquids on a differential element, *dx*, of a hammerhead.

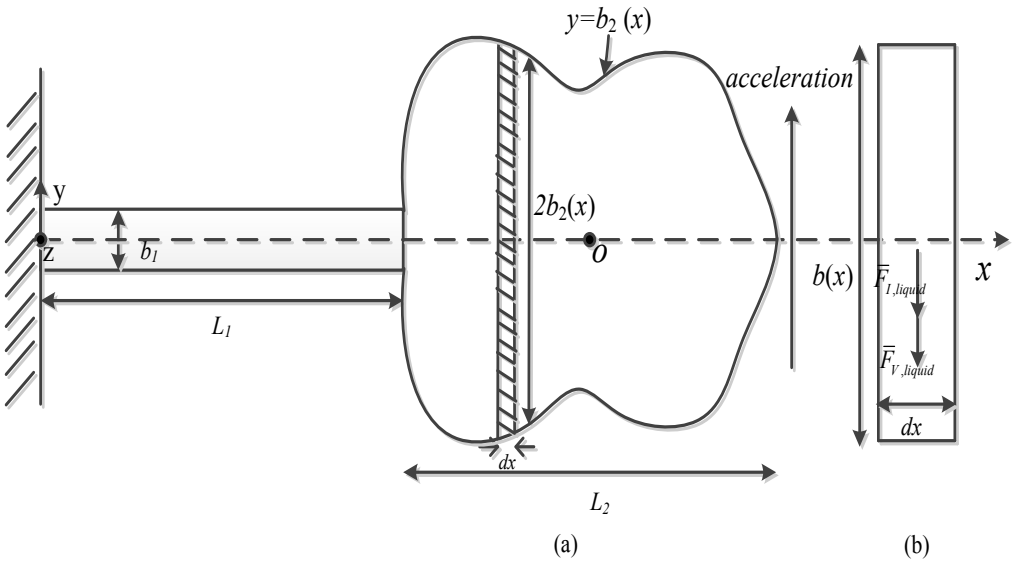

Figure 2-5: (a) A laterally vibrating hammerhead in a viscous liquid with its acceleration in positive y direction. (b) A differential element on the head with the hydrodynamic forces and resulting moments in their positive direction.

For each differential element, *dx*, the inertia/damping forces and resulting moments due to the liquid resistance are expressed as:

$$\bar{F}_{I,liquid} = g_{2,head}\frac{\partial^2 v_{head}(x,t)}{\partial t^2}, \tag{2.31}$$

$$\bar{F}_{V,liquid} = g_{1,head}\frac{\partial v_{head}(x,t)}{\partial t}, \tag{2.32}$$

$$\bar{M}_{I,liquid} = g_{2,head}(x-L_1)\frac{\partial^2 v_{head}(x,t)}{\partial t^2}, \tag{2.33}$$

$$\bar{M}_{V,liquid} = g_{1,head}(x-L_1)\frac{\partial v_{head}(x,t)}{\partial t}, \tag{2.34}$$

where

$$\frac{\partial v_{head}(x,t)}{\partial t} = \frac{\partial v_{stem}(x,t)}{\partial t}\Big|_{x=L_1} + (x-L_1)\left[\frac{\partial^2 v_{stem}(x,t)}{\partial x \partial t}\Big|_{x=L_1}\right], \tag{2.35}$$

$$\frac{\partial^2 v_{head}(x,t)}{\partial t^2} = \frac{\partial^2 v_{stem}(x,t)}{\partial t^2}\Big|_{x=L_1} + (x-L_1)\left[\frac{\partial^3 v_{stem}(x,t)}{\partial x \partial t^2}\Big|_{x=L_1}\right]. \tag{2.36}$$

The total inertia, damping forces and resulting moments due to the liquid resistance can be found by taking the integral from the tip of the stem ($x=L_1$) to the free end of the microcantilever ($x= L_1+L_2$) as:

$$F_{I/V,liquid} = \int_{L_1}^{L_1+L_2} \bar{F}_{I/V,liquid}\, dx\,, \tag{2.37}$$

$$M_{I/V,liquid} = \int_{L_1}^{L_1+L_2} \bar{M}_{I/V,liquid}\, dx\,. \tag{2.38}$$

Substituting Eq. 2.31 to Eq. 2.36 into Eq. 2.37 and Eq. 2.38, the specific expressions for the force and moment equilibrium can be obtained as follows:

$$\left\{\begin{array}{l} EI_{stem}\dfrac{\partial^2 v_{stem}(x,t)}{\partial x^2} + m_{head}\left[\dfrac{\partial^2 v_{stem}(x,t)}{\partial t^2} + d_{os}\dfrac{\partial^3 v_{stem}(x,t)}{\partial x \partial t^2}\right] d_{os} \\ + \displaystyle\int_{L_1}^{L_1+L_2} g_{2,head}(x-L_1)\left[\frac{\partial^2 v_{stem}(x,t)}{\partial t^2} + (x-L_1)\frac{\partial^3 v_{stem}(x,t)}{\partial x \partial t^2}\right] dx \\ + \displaystyle\int_{L_1}^{L_1+L_2} g_{1,head}(x-L_1)\left[\frac{\partial v_{stem}(x,t)}{\partial t} + (x-L_1)\frac{\partial^2 v_{stem}(x,t)}{\partial x \partial t}\right] dx \\ + J_{head}\dfrac{\partial^3 v_{stem}(x,t)}{\partial x \partial t^2} \end{array}\right\}\Big|_{x=L_1} = 0\,, \tag{2.39}$$

$$\left\{\begin{array}{l} EI_{stem}\dfrac{\partial^3 v_{stem}(x,t)}{\partial x^3} - m_{head}\left[\dfrac{\partial^2 v_{stem}(x,t)}{\partial t^2} + d_{os}\dfrac{\partial^3 v_{stem}(x,t)}{\partial x \partial t^2}\right] \\ - \displaystyle\int_{L_1}^{L_1+L_2} g_{2,head}\left[\frac{\partial^2 v_{stem}(x,t)}{\partial t^2} + (x-L_1)\frac{\partial^3 v_{stem}(x,t)}{\partial x \partial t^2}\right] dx \\ - \displaystyle\int_{L_1}^{L_1+L_2} g_{1,head}\left[\frac{\partial v_{stem}(x,t)}{\partial t} + (x-L_1)\frac{\partial^2 v_{stem}(x,t)}{\partial x \partial t}\right] dx \end{array}\right\}\Big|_{x=L_1} = 0\,. \tag{2.40}$$

For convenience, the four BCs in a viscous liquid medium are rewritten as follows:

$$v_{stem}(0,t) = 0\,, \tag{2.41}$$

$$\frac{\partial v_{stem}(x,t)}{\partial x}\Big|_{x=0} = \theta_0 e^{j\omega t} \ . \tag{2.42}$$

$$\left\{ \begin{aligned} & EI_{stem}\frac{\partial^2 v_{stem}(x,t)}{\partial x^2} + m_{head}\left[\frac{\partial^2 v_{stem}(x,t)}{\partial t^2} + d_{os}\frac{\partial^3 v_{stem}(x,t)}{\partial x \partial t^2}\right] d_{os} \\ & + \int_{L_1}^{L_1+L_2} g_{2,head}(x-L_1)\left[\frac{\partial^2 v_{stem}(x,t)}{\partial t^2} + (x-L_1)\frac{\partial^3 v_{stem}(x,t)}{\partial x \partial t^2}\right] dx \\ & + \int_{L_1}^{L_1+L_2} g_{1,head}(x-L_1)\left[\frac{\partial v_{stem}(x,t)}{\partial t} + (x-L_1)\frac{\partial^2 v_{stem}(x,t)}{\partial x \partial t}\right] dx \\ & + J_{head}\frac{\partial^3 v_{stem}(x,t)}{\partial x \partial t^2} \end{aligned} \right\}\Big|_{x=L_1} = 0 \ , \tag{2.43}$$

$$\left\{ \begin{aligned} & EI_{stem}\frac{\partial^3 v_{stem}(x,t)}{\partial x^3} - m_{head}\left[\frac{\partial^2 v_{stem}(x,t)}{\partial t^2} + d_{os}\frac{\partial^3 v_{stem}(x,t)}{\partial x \partial t^2}\right] \\ & - \int_{L_1}^{L_1+L_2} g_{2,head}\left[\frac{\partial^2 v_{stem}(x,t)}{\partial t^2} + (x-L_1)\frac{\partial^3 v_{stem}(x,t)}{\partial x \partial t^2}\right] dx \\ & - \int_{L_1}^{L_1+L_2} g_{1,head}\left[\frac{\partial v_{stem}(x,t)}{\partial t} + (x-L_1)\frac{\partial^2 v_{stem}(x,t)}{\partial x \partial t}\right] dx \end{aligned} \right\}\Big|_{x=L_1} = 0 \ . \tag{2.44}$$

It is noted that $g_{2,head}$ and $g_{1,head}$ are both functions of $Re(x)$ and the aspect ratio, $h/b(x)$ in this case. Since $g_{2,head}$ and $g_{1,head}$ are functions of the position x, these two terms must not be taken out of the integrals shown in Eq. 2.43 and Eq. 2.44. However, for a rectangular head, $b(x) = constant$, Eq. 2.43 and Eq. 2.44 can be further simplified. This particular case will be discussed in Sec 2.4.3 and Sec 2.4.4.

2.4 Solutions in a Vacuum and Viscous Liquid Medium

Solutions in a Vacuum: For the free vibration in a vacuum, the solution to Eq. 2.1 is sought by separation of time and space variables as follows:

$$v_{stem}(x,t) = X(x)e^{j\omega t} \ , \tag{2.45}$$

where $X(x)$ is the shape function of the vibrating stem. Substituting Eq. 2.45 into Eq. 2.1 gives:

$$\frac{d^4X(x)}{dx^4} - K^4X(x) = 0\,, \tag{2.46}$$

where

$$K = \left\{ \frac{\omega^2 \rho_b b_1 h}{EI_{stem}} \right\}^{1/4}\,. \tag{2.47}$$

The general solution of Eq. 2.46 is of the form:

$$X(x) = A_1 \cosh Kx + A_2 \sinh Kx + A_3 \cos Kx + A_4 \sin Kx\,. \tag{2.48}$$

where A_1-A_4 are coefficients associated with the geometrical and material properties of the hammerhead microcantilever in a vacuum.

Using Eq. 2.45, the BCs equations in Eq. 2.21 to Eq. 2.24 can be simplified as:

$$X(0) = 0\,, \tag{2.49}$$

$$\frac{dX(x)}{dx}\Big|_{x=0} = 0\,, \tag{2.50}$$

$$\left\{ \frac{\omega^2 d_{os}}{EI_{stem}} m_{head} \left[X(x) + d_{os} \frac{dX(x)}{dx} \right] + \frac{\omega^2 J_{head}}{EI_{stem}} \frac{dX(x)}{dx} - \frac{d^2X(x)}{dx^2} \right\}\Big|_{x=L_1} = 0\,, \tag{2.51}$$

$$\left\{ \frac{d^3X(x)}{dx^3} + \frac{\omega^2}{EI_{stem}} m_{head} \left[X(x) + d_{os} \frac{dX(x)}{dx} \right] \right\}\Big|_{x=L_1} = 0\,. \tag{2.52}$$

Imposing these four BCs (Eq. 2.49 to Eq. 2.52) on the general solution presented in Eq. 2.48, leads to the following algebraic system:

$$D(K, L_1, L_2, b_1, b_2) E(A_1, A_2, A_3, A_4) = 0\,, \tag{2.53}$$

where

$$D(K, L_1, L_2, b_1, b_2) = \{D_1, D_2, D_3, D_4\}\,, \tag{2.54}$$

$$D_1 = \begin{bmatrix} 1 \\ 0 \\ K^2 \cosh L_1 K - \alpha_1 \cosh L_1 K - \alpha_2 K \sinh L_1 K \\ K^3 \sinh L_1 K - \alpha_3 \cosh L_1 K - \alpha_4 K \sinh L_1 K \end{bmatrix}, \tag{2.55}$$

$$D_2 = \begin{bmatrix} 0 \\ 1 \\ K^2 \sinh L_1 K - \alpha_1 \sinh L_1 K - \alpha_2 K \cosh L_1 K \\ K^3 \cosh L_1 K - \alpha_3 \sinh L_1 K - \alpha_4 K \cosh L_1 K \end{bmatrix}, \tag{2.56}$$

$$D_3 = \begin{bmatrix} 1 \\ 0 \\ -K^2 \cos L_1 K - \alpha_1 \cos L_1 K + \alpha_2 K \sin L_1 K \\ K^3 \sin L_1 K - \alpha_3 \cos L_1 K + \alpha_4 K \sin L_1 K \end{bmatrix}, \tag{2.57}$$

$$D_4 = \begin{bmatrix} 0 \\ 1 \\ -K^2 \sin L_1 K - \alpha_1 \sin L_1 K - \alpha_2 K \cos L_1 K \\ -K^3 \cos L_1 K - \alpha_3 \sin L_1 K - \alpha_4 K \cos L_1 K \end{bmatrix}, \tag{2.58}$$

$$E\left(A_1, A_2, A_3, A_4\right) = \begin{bmatrix} A_1 \\ A_2 \\ A_3 \\ A_4 \end{bmatrix}, \tag{2.59}$$

$$\alpha_1 \equiv \frac{\omega^2 d_{os} m_{head}}{EI_{stem}}, \tag{2.60a}$$

$$\alpha_2 \equiv \frac{\omega^2 {d_{os}}^2 m_{head} + 3\omega^2 J_{head}}{EI_{stem}}, \tag{2.60b}$$

$$\alpha_3 \equiv \frac{-\omega^2 m_{head}}{EI_{stem}}, \tag{2.60c}$$

$$\alpha_4 \equiv \frac{-\omega^2 d_{os} m_{head}}{EI_{stem}}. \tag{2.60d}$$

For the solution of the resulting algebraic eigenvalue problem, the frequency equation is obtained by setting the determinant of the coefficient matrix equal to zero as:

$$D(K, L_1, L_2, b_1, b_2) = 0 . \tag{2.61}$$

As a result, the natural frequency of a laterally vibrating symmetric hammerhead microcantilever in a vacuum can be obtained by solving Eq. 2.61.

For the forced vibration in a vacuum due to an equivalent, harmonic support rotation which is mathematically expressed in Eq. 2.6, the BC presented in Eq. 2.50 associated with the bending slope of the support end of the microcantilever is modified as:

$$\frac{dX(x)}{dx}\Big|_{x=0} = \theta_0 . \tag{2.62}$$

Then, imposing the BCs (Eq. 2.49, Eq. 2.51, Eq. 2.52, and Eq. 2.62) on Eq. 2.48 gives the (complex) shape of the vibrating stem under an imposed (complex) harmonic rotation $\theta_0 e^{j\omega t}$:

$$X(x) = A_1(\cosh Kx - \cos Kx) + A_2(\sinh Kx - \sin Kx) + \frac{\theta_0}{K}\sin Kx , \tag{2.63}$$

where

$$A_1 = \frac{\Pi_3\Pi_5 - \Pi_6\Pi_2}{\Pi_1\Pi_5 - \Pi_4\Pi_2} , \quad A_2 = \frac{\Pi_3\Pi_4 - \Pi_6\Pi_1}{\Pi_2\Pi_4 - \Pi_1\Pi_5} , \tag{2.64}$$

with

$$\Pi_1 \equiv K^2(\cosh Kx + \cos Kx) - \alpha_1(\cosh Kx - \cos Kx) - \alpha_2 K(\sinh Kx + \sin Kx), \tag{2.65}$$

$$\Pi_2 \equiv K^2(\sinh Kx + \sin Kx) - \alpha_1(\sinh Kx - \sin Kx) - \alpha_2 K(\cosh Kx - \cos Kx), \tag{2.66}$$

$$\Pi_3 \equiv \frac{\theta_0}{K}\left[K^2 \sin Kx + \alpha_1 \sin Kx + \alpha_2 K \cos Kx\right], \tag{2.67}$$

$$\Pi_4 \equiv K^3(\sinh Kx - \sin Kx) - \alpha_3(\cosh Kx - \cos Kx) - \alpha_4 K(\sinh Kx + \sin Kx), \tag{2.68}$$

$$\Pi_5 \equiv K^3(\cosh Kx + \cos Kx) - \alpha_3(\sinh Kx - \sin Kx) - \alpha_4 K(\cosh Kx - \cos Kx), \tag{2.69}$$

$$\Pi_6 \equiv \frac{\theta_0}{K}\left[K^3 \cos Kx + \alpha_3 \sin Kx + \alpha_4 K \cos Kx\right]. \tag{2.70}$$

K, α_1, α_2, α_3 and α_4 remain the same as in Eq.2 47 and Eq. 2.60. Then, the amplitude of the deflection at the tip of the stem can be characterized as:

$$\left|\frac{X(L_1)}{L_1\theta_0}\right| = \left|\frac{A_1\left(\cosh KL_1 - \cos KL_1\right) + A_2\left(\sinh KL_1 - \sin KL_1\right) + \frac{\theta_0}{K}\sin KL_1}{L_1\theta_0}\right|. \quad (2.71)$$

In Eq. 2.71, the amplitude of the deflection at the tip of the stem is normalized by the maximum tip deflection corresponding to a slowly applied (quasistatic) harmonic support rotation. The magnitude in Eq. 2.71 reaches its maximum at the resonance frequency. Thus, from the frequency spectrum, the first resonance frequency of a laterally vibrating hammerhead microcantilever in a vacuum under a forced vibration can be easily determined.

Solution in Viscous Liquid Media: For a symmetric hammerhead microcantilever laterally vibrating in viscous liquid media, the procedure to obtain the frequency response at the tip of the stem is analogous to the procedure described above. The normalized amplitude of the deflection at the tip of the stem can be characterized by Eq. 2.71, in which the coefficients from Eq. 2 64 to Eq. 2.70 remain the same. However, Eq. 2.47 and Eq. 2.60 are modified due to the additional resistance coming from the viscous liquid media are now given as:

$$K = \left\{\frac{\omega^2\left[\rho_b h b_1 + g_{2,stem}\right] - j\omega g_{1,stem}}{EI_{stem}}\right\}^{1/4}, \quad (2.72)$$

$$\alpha_1 \equiv \frac{m_{head} d_{os} \omega^2}{EI_{stem}} + \frac{\int_{L_1}^{L_1+L_2} \omega^2 (x - L_1) g_{2,head} dx}{EI_{stem}} - \frac{j\int_{L_1}^{L_1+L_2} \omega (x - L_1) g_{1,head} dx}{EI_{stem}}, \quad (2.73a)$$

$$\alpha_2 \equiv \frac{m_{head} {d_{os}}^2 \omega^2}{EI_{stem}} + \frac{\int_{L_1}^{L_1+L_2} \omega^2 \left(x-L_1\right)^2 g_{2,head} dx}{EI_{stem}} - \frac{j\int_{L_1}^{L_1+L_2} \omega \left(x-L_1\right)^2 g_{1,head} dx}{EI_{stem}} + \frac{\omega^2 J_{head}}{EI_{stem}}, \tag{2.73b}$$

$$\alpha_3 \equiv -\frac{m_{head}\omega^2}{EI_{stem}} - \frac{\int_{L_1}^{L_1+L_2} \omega^2 g_{2,head} dx}{EI_{stem}} + \frac{j\int_{L_1}^{L_1+L_2} \omega g_{1,head} dx}{EI_{stem}}, \tag{2.73c}$$

$$\alpha_4 \equiv -\frac{m_{head} d_{os} \omega^2}{EI_{stem}} - \frac{\int_{L_1}^{L_1+L_2} \omega^2 \left(x-L_1\right) g_{2,head} dx}{EI_{stem}} + \frac{j\int_{L_1}^{L_1+L_2} \omega \left(x-L_1\right) g_{1,head} dx}{EI_{stem}}. \tag{2.73d}$$

As a result, Using Eq. 2.64 to Eq. 2.73, the resonance frequency can be extracted from the frequency spectrum of a laterally vibrating symmetric hammerhead microcantilever in viscous liquid media. Several cases of symmetric heads will be next investigated as particular cases of the general model in Sec. 2.4.1 to Sec 2.4.4.

2.4.1 Hammerhead Microcantilever with an Isosceles Trapezoid Head

The isosceles trapezoid-shaped hammerhead microcantilever is a particular case of the symmetric hammerhead microcantilever. Thus, the frequency response of a laterally vibrating isosceles trapezoid hammerhead microcantilever in a viscous liquid medium can be obtained based on the general model using Eq. 2.64 to Eq. 2.73. For convenience, Fig. 2-6 shows a typical hammerhead microcantilever with an isosceles trapezoid head.

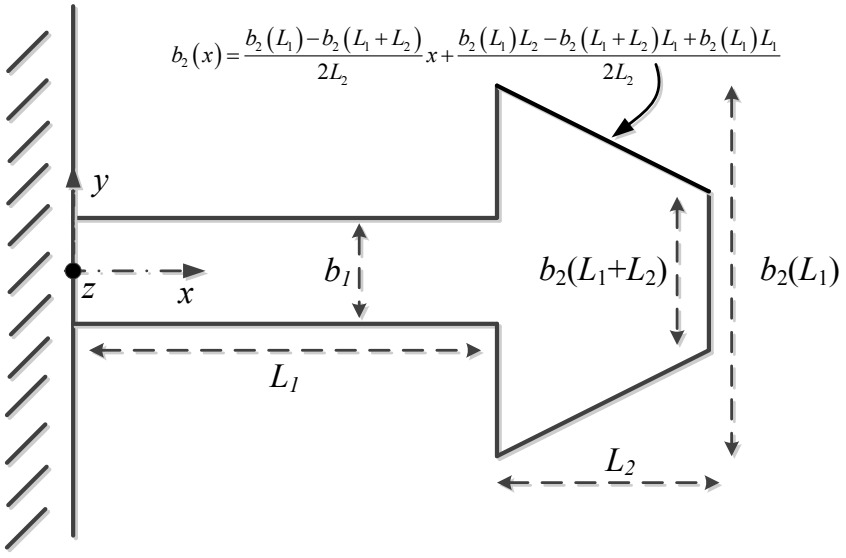

Figure 2-6: The top view of an isosceles trapezoid-shaped hammerhead microcantilever. The uniform thickness is h (z direction); the length and width of the stem are L_1 and b_1. The length of the head is L_2. The width of the head is determined by function $2b_2(x)$.

In Fig 2-6, one side of the isosceles trapezoid above the x-axis is determined by the function, $b_2(x)$, associated with the geometrical parameters of the isosceles trapezoid hammerhead microcantilever as. This function is given by:

$$b_2(x)=\frac{b_2(L_1)-b_2(L_1+L_2)}{2L_2}x+\frac{b_2(L_1)L_2-b_2(L_1+L_2)L_1+b_2(L_1)L_1}{2L_2}, \qquad (2.74)$$

For this geometry, the mass of the head, the distance from the mass center of the head to the tip of the stem and the rotational inertia of the head about its mass center are found, respectively, as:

$$m_{head}=\frac{\rho_b h L_2}{2}\left[b_2(L_1)-b_2(L_1+L_2)\right], \qquad (2.75)$$

$$d_{os}=\frac{L_2}{3}\left[\frac{b_2(L_1)+2b_2(L_1+L_2)}{b_2(L_1)+b_2(L_1+L_2)}\right], \qquad (2.76)$$

$$J_{head} = \frac{\rho_b h L_2 \left[4L_2{}^2 b_2 \left(L_1 + L_2 \right) b_2 \left(L_1 \right) + L_2{}^2 b_2{}^2 \left(L_1 \right) + L_2{}^2 b_2{}^2 \left(L_1 + L_2 \right) \right]}{36 \left[b_2 \left(L_1 \right) + b_2 \left(L_1 + L_2 \right) \right]}$$
$$+ \frac{\rho_b h L_2 \left[b_2{}^4 \left(L_1 + L_2 \right) + b_2{}^4 \left(L_1 \right) \right]}{48 \left[b_2 \left(L_1 \right) + b_2 \left(L_1 + L_2 \right) \right]} \tag{2.77}$$
$$+ \frac{\rho_b h L_2 \left[b_2{}^2 \left(L_1 + L_2 \right) b_2{}^2 \left(L_1 \right) + b_2{}^3 \left(L_1 + L_2 \right) b_2 \left(L_1 \right) + b_2 \left(L_1 + L_2 \right) b_2{}^3 \left(L_1 \right) \right]}{24 \left[b_2 \left(L_1 \right) + b_2 \left(L_1 + L_2 \right) \right]}$$

Substituting Eq. 2.74 to Eq. 2.77 into Eq. 2.73, the resonance frequency can be extracted from the frequency spectrum of a laterally vibrating isosceles trapezoid hammerhead microcantilever in viscous liquid media.

2.4.2 Hammerhead Microcantilever with a Semi-circular Head

The hammerhead microcantilever with a semi-circular head is another particular case of the symmetric hammerhead microcantilever. Thus, the frequency response of a laterally vibrating semi-circular hammerhead microcantilever in a viscous liquid medium can be obtained based on the general mode using Eq. 2.64 to Eq. 2.73. For convenience, Fig. 2-7 shows a typical semi-circular hammerhead microcantilever.

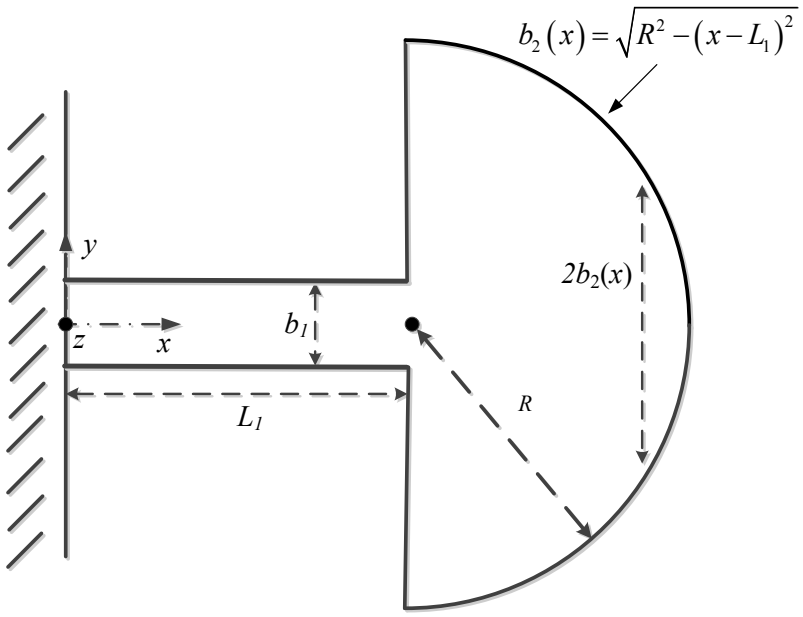

Figure 2-7: The top view of a semi-circular hammerhead microcantilever. The uniform thickness is h (z direction); the length and width of the stem are L_1 and b_1. The radius of the head is R. The width of the head is determined by a function $b(x) = 2b_2(x)$.

In Fig 2-7, the quarter-circle above the x-axis is determined by the function, $b_2(x)$, expressed as:

$$b_2(x) = \sqrt{R^2 - (x - L_1)^2}\ , \tag{2.78}$$

For this geometry, the mass of the head, the distance from the mass center of the head to the tip of the stem and the rotational inertia of the head about its mass center are found, respectively, as:

$$m_{head} = \frac{1}{2}\rho_b \pi R^2 h\ , \tag{2.79}$$

$$d_{os} = \frac{4R}{3\pi}, \tag{2.80}$$

$$J_{head} = \left(\frac{\pi}{4} - \frac{8}{9\pi} \right) \rho_b h R^4 \,. \tag{2.81}$$

Substituting Eq. 2.78 to Eq. 2.81 into Eq. 2.73, the resonance frequency can be extracted from the frequency spectrum of a laterally vibrating semi-circular hammerhead microcantilever in viscous liquid media.

2.4.3 Hammerhead Microcantilever with a Uniform Rectangular Head

The uniform rectangular hammerhead microcantilever is another particular case of the symmetric hammerhead microcantilever. Thus, the frequency response of a laterally vibrating uniform rectangular hammerhead microcantilever in a viscous liquid medium can be obtained based on the general mode using Eq. 2.64 to Eq. 2.73. For convenience, Fig. 2-8 shows a typical uniform rectangular hammerhead microcantilever.

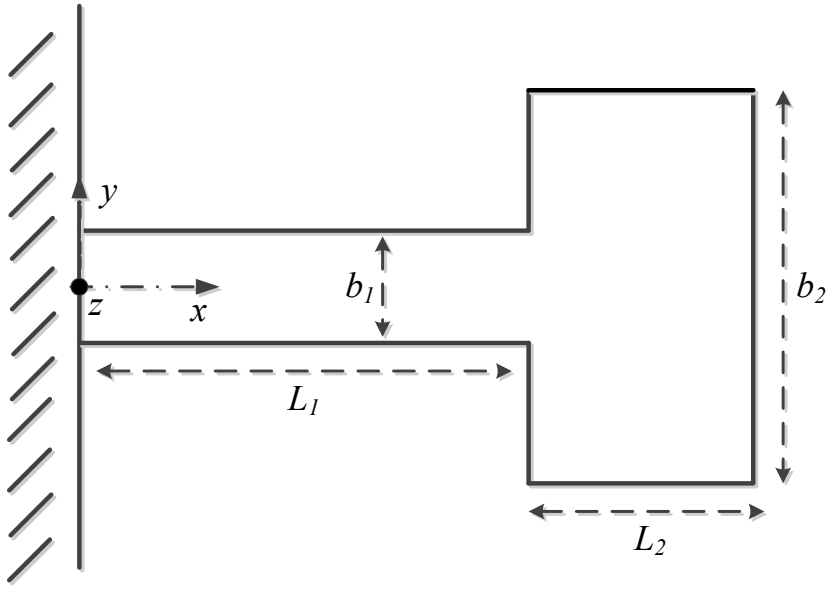

Figure 2-8: The top view of a uniform rectangular hammerhead microcantilever with a uniform thickness of h (z direction); the length and width of the stem are L_1 and b_1; the length and width of the head are L_2 and b_2, respectively.

For this geometry, the mass of the head, the distance from the mass center of the head to the tip of the stem and the rotational inertia of the head about its mass center are found, respectively, as:

$$m_{head} = \rho_b h L_2 b_2 \,, \tag{2.82}$$

$$d_{os} = \frac{L_2}{2} \,, \tag{2.83}$$

$$J_{head} = \frac{m_{head}(L_2{}^2 + b_2{}^2)}{12} \tag{2.84}$$

For a uniform rectangular head, the width of the head is a constant, $2b_2$. In this case, $g_{2,head}$ and $g_{1,head}$ are not functions of the position, x. Then, Eq. 2.73 can be further simplified by taking $g_{2,head}$ and $g_{1,head}$ out of the integrals as:

$$\alpha_1 \equiv \frac{\omega^2 L_2 \left[m_{head} + L_2 g_{2,head} \right] - j\omega L_2{}^2 g_{1,head}}{2EI_{stem}} \,, \tag{2.85a}$$

$$\alpha_2 \equiv \frac{3\omega^2 L_2{}^2 m_{head} + 4\omega^2 L_2{}^3 g_{2,head} + 12\omega^2 J_{head} - 4j\omega L_2{}^3 g_{2,head}}{12EI_{stem}} \,, \tag{2.85b}$$

$$\alpha_3 \equiv \frac{j\omega L_2 g_{1,head} - \omega^2 \left[m_{head} + L_2 g_{2,head} \right]}{EI_{stem}} \,, \tag{2.85c}$$

$$\alpha_4 \equiv \frac{j\omega L_2{}^2 g_{1,head} - \omega^2 L_2 \left[m_{head} + L_2 g_{2,head} \right]}{2EI_{stem}} \,. \tag{2.85d}$$

Substituting Eq. 2.82 to Eq. 2.85 into Eq. 2 85, the resonance frequency can be extracted from the frequency spectrum of a laterally vibrating uniform rectangular hammerhead microcantilever in viscous liquid media.

2.4.4 Hammerhead Microcantilever with a Composite Rectangular Head

In order to further increase sensing area and improve sensor characteristics, other geometrical shapes of the hammerhead microcantilever have been proposed [71]. An example of such geometries is shown in Fig. 2-9, where the shape of the head is a semi-circle. Near the tip of the stem, there are two rectangular gaps between the stem and the head. In the following investigation, a similar geometry but with a composite rectangular head is analyzed.

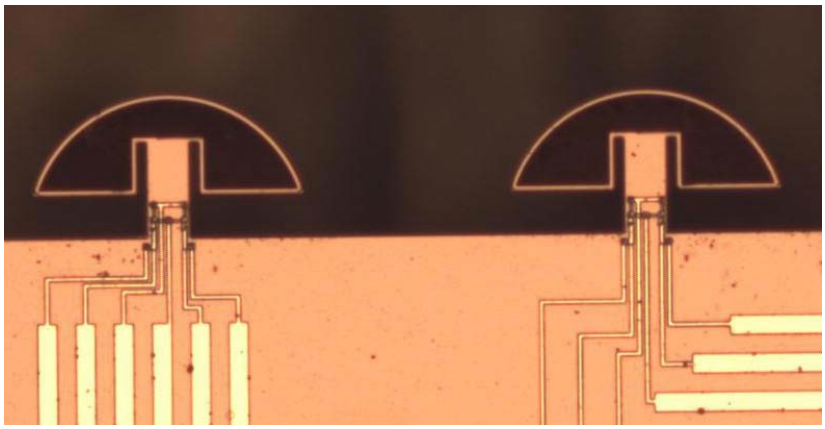

Figure 2-9: The proposed hammerhead microcantilevers, where the shape of the head is a half circle [71]

The geometry of the composite rectangular hammerhead microcantilever investigated in this work is shown in Fig. 2-10. This model can be considered as an extension of the model discussed in Sec. 2.4.3. By adding two small rectangular areas to the larger uniform rectangle, the sensing area is further improved and the mass center of the head is shifted towards the tip of the stem. This will affect the resonance frequency and further increase the quality factor, which is desired in liquid-phase chemical or

biochemical sensing applications. In order to perform the theoretical analysis of this composite rectangular hammerhead microcantilever laterally vibrating in viscous liquids, it is assumed that the gap effects are neglected, so the numerical results of the hydrodynamic function proposed in Ref 64 can be applied.

In Ref 64, it is assumed the liquid domain must be large enough to ensure the hydrodynamic force acting on the rigid oscillating rectangle to be independent on the domain size. Thus, the outer boundary of the liquid domain is set far away enough from the vibrating beam to neglect the squeezing and slide film effects. As a result, to apply the numerical results of the hydrodynamic function reported in Ref 64, the width of the gap must be large enough, so that the gap effects (squeezing and slide film effects due to the liquid trapped inside the gaps) can be neglected. Due to the composite rectangular hammerhead, a different method of finding the mass of the composite head, distance from the mass center of the head to the tip of the stem and the rotational inertia of the head about its mass center, is proposed.

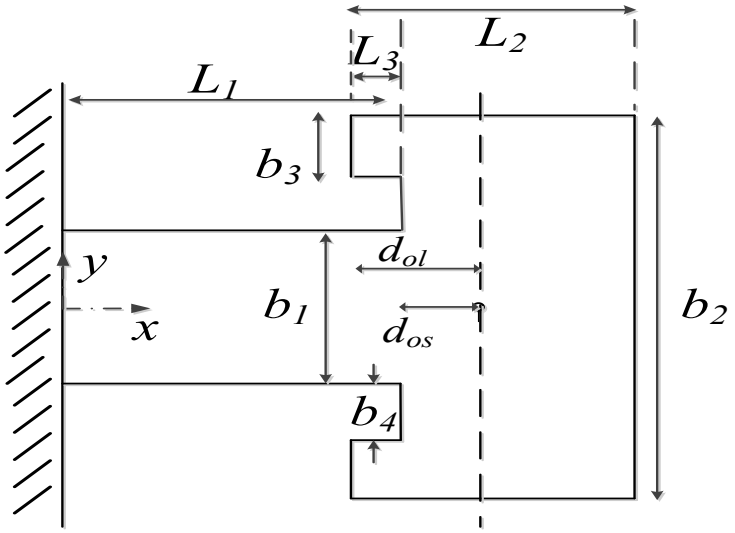

Figure 2-10: Top surface of a composite rectangular hammerhead microcantilever with two rectangular gaps.

In Fig. 2-10, the dimensions of the gap are determined by L_3 and b_4, respectively. Since the shape of the head is a composite rectangle, the previously defined width function $b(x)$ is directly replaced by b_2 for convenience. d_{ol} is an intermediate parameter, which represents the distance between the mass center of the head and the left side of the head, as shown in Fig. 2-9.

$$d_{ol} = \frac{L_2 b_2 \frac{L_2}{2} - L_3\left(b_1 + 2b_4\right)\frac{L_3}{2}}{L_2 b_2 - L_3\left(b_1 + 2b_4\right)}. \tag{2.86}$$

and

$$d_{os} = d_{ol} - L_3\,, \tag{2.87}$$

In Eq. 2.87, d_{os} can be a positive or negative value. When it is positive, it indicates that the mass center is on the head. When it is negative, it indicates that the mass center is on the stem. These two cases are described in Fig. 2-11:

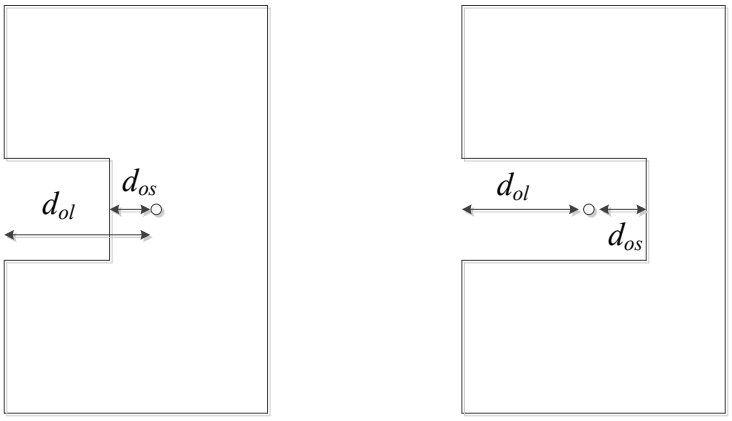

(a) (b)

Figure 2-11: Possible positions of the mass center of the head as the dimensions of the gaps vary

The mass of the composite rectangular head can be found as follows:

$$m_{head} = \rho_b h\left[L_2 b_2 - L_3(b_1 + 2b_4)\right]. \tag{2.88}$$

In order to find the rotational inertia of the head, the parallel axis theorem and superposition theorem will be applied. Based on the theorems, the mathematical expression for the rotational inertia about the mass center of the composite rectangular head can be found as:

$$J_{head} = (J_{rectangle,I} - J_{rectangle,II}), \tag{2.89}$$

where

$$J_{rectangle,I} = \rho_b L_2 b_2 h \frac{{L_2}^2 + {b_2}^2}{12} + \left(d_{ol} - \frac{L_2}{2}\right)^2 \left(\rho_b L_2 b_2 h\right), \tag{2.90}$$

and

$$J_{rectangle,II} = \rho_b L_3(b_1 + 2b_4)h \frac{{L_3}^2 + (b_1 + 2b_4)^2}{12} + \left(\frac{L_3}{2} + d_{os}\right)^2 \rho_b L_3(b_1 + 2b_4)h\,. \tag{2.91}$$

In Eq. 2.90 and Eq. 2.91, $J_{rectangle,I}$ and $J_{rectangle,II}$ represent the rotational inertia of the large and small rectangles about the mass center of the composite rectangular head, respectively, shown in Fig. 2-12. The circles in Fig. 2-12 represent the mass center of either rectangle.

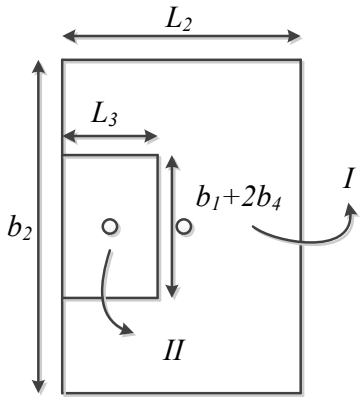

Figure 2-12: Geometry used in analyzing the rotational inertia of the composite rectangular hammerhead about its mass center.

Since the shape of the head is a composite rectangular, when analyzing the force and moment equilibrium at the junction (x=L_1), the head can be divided into three small rectangles for convenience, as shown in Fig 2-13. The procedure in finding the force and moment equilibrium is analogous to the procedure described in Sec 2.3.1.

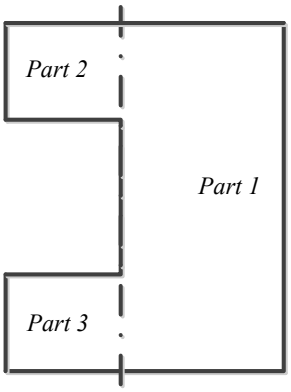

Figure 2-13: Geometry (three small rectangles make up a composite rectangle) used in finding the force and moment equilibrium in a viscous liquid medium

Due to the symmetry of the problem with respect to the *x*-axis, the total inertia, damping forces and resulting moments in Eq. 2.29 and Eq. 2.30 can be explicitly expressed as:

$$\begin{aligned} M_{I/V,liquid} &= M_{I/V,liquid,1} + M_{I/V,liquid,2} + M_{I/V,liquid,3} \\ &= M_{I/V,liquid,1} + 2M_{I/V,liquid,2} \,, \end{aligned} \tag{2.92}$$

$$\begin{aligned} F_{I/V,liquid} &= F_{I/V,liquid,1} + F_{I/V,liquid,2} + F_{I/V,liquid,3} \\ &= F_{I/V,liquid,1} + 2F_{I/V,liquid,2} \,, \end{aligned} \tag{2.93}$$

where

$$F_{I,liquid,1} = g_{2,head,1} \int_{L_1}^{L_1+L_2-L_3} \left[\begin{array}{l} \left. \dfrac{\partial^2 v_{stem}(x,t)}{\partial t^2} \right|_{x=L_1} \\ +(x-L_1) \left. \dfrac{\partial^3 v_{stem}(x,t)}{\partial x \partial t^2} \right|_{x=L_1} \end{array} \right] dx \,, \tag{2.94}$$

$$F_{I,liquid,2} = g_{2,head,2} \int_{L_1-L_3}^{L_1} \left[\begin{array}{l} \left. \dfrac{\partial^2 v_{stem}(x,t)}{\partial t^2} \right|_{x=L_1} \\ +(x-L_1) \left. \dfrac{\partial^3 v_{stem}(x,t)}{\partial x \partial t^2} \right|_{x=L_1} \end{array} \right] dx \,, \tag{2.95}$$

$$F_{V,liquid,1} = g_{1,head,1} \int_{L_1}^{L_1+L_2-L_3} \left[\begin{array}{l} \left. \frac{\partial v_{stem}(L_1,t)}{\partial t} \right|_{x=L_1} \\ +(x-L_1) \left. \frac{\partial^2 v_{stem}(L_1,t)}{\partial x \partial t} \right|_{x=L_1} \end{array} \right] dx \,, \tag{2.96}$$

$$F_{V,liquid,2} = g_{1,head,2} \int_{L_1-L_3}^{L_1} \left[\begin{array}{l} \left. \frac{\partial v_{stem}(L_1,t)}{\partial t} \right|_{x=L_1} \\ +(x-L_1) \left. \frac{\partial^2 v_{stem}(L_1,t)}{\partial x \partial t} \right|_{x=L_1} \end{array} \right] dx \,, \tag{2.97}$$

$$M_{I,liquid,1} = g_{2,head,1} \int_{L_1}^{L_1+L_2-L_3} (x-L_1) \left[\begin{array}{l} \left. \frac{\partial^2 v_{stem}(x,t)}{\partial t^2} \right|_{x=L_1} \\ +(x-L_1) \left. \frac{\partial^3 v_{stem}(x,t)}{\partial x \partial t^2} \right|_{x=L_1} \end{array} \right] dx \,, \tag{2.98}$$

$$M_{I,liquid,2} = g_{2,head,2} \int_{L_1-L_3}^{L_1} (x-L_1) \left[\begin{array}{l} \left. \frac{\partial^2 v_{stem}(x,t)}{\partial t^2} \right|_{x=L_1} \\ +(x-L_1) \left. \frac{\partial^3 v_{stem}(x,t)}{\partial x \partial t^2} \right|_{x=L_1} \end{array} \right] dx \,, \tag{2.99}$$

$$M_{V,liquid,1} = g_{1,head,1} \int_{L_1}^{L_1+L_2-L_3} (x-L_1) \left[\begin{array}{l} \left. \frac{\partial v_{stem}(L_1,t)}{\partial t} \right|_{x=L_1} \\ +(x-L_1) \left. \frac{\partial^2 v_{stem}(L_1,t)}{\partial x \partial t} \right|_{x=L_1} \end{array} \right] dx \,, \tag{2.100}$$

$$M_{V,liquid,2} = g_{1,head,2} \int_{L_1-L_3}^{L_1} (x-L_1) \left[\begin{array}{l} \left. \frac{\partial v_{stem}(L_1,t)}{\partial t} \right|_{x=L_1} \\ +(x-L_1) \left. \frac{\partial^2 v_{stem}(L_1,t)}{\partial x \partial t} \right|_{x=L_1} \end{array} \right] dx \,. \tag{2.101}$$

The subscript, *I/V, liquid, 1or2*, indicates the forces or moments due to the effective mass/viscous damping associated with rectangle *1* or *2*. Substituting Eq. 2.92 to Eq. 2.101 into Eq. 2.29 to Eq. 2.30, the BCs at the junction ($x=L_1$) are obtained as follows:

$$\left\{\begin{array}{l} EI_{stem}\dfrac{\partial^2 v_{stem}(x,t)}{\partial x^2}+J_{head}\dfrac{\partial^3 v_{stem}(x,t)}{\partial x\partial t^2} \\ +m_{head}\left[\dfrac{\partial^2 v_{stem}(x,t)}{\partial t^2}+d_{os}\dfrac{\partial^3 v_{stem}(x,t)}{\partial x\partial t^2}\right]d_{os} \\ +g_{2,head,1}\left[\dfrac{(L_2-L_3)^2}{2}\dfrac{\partial^2 v_{stem}(x,t)}{\partial t^2}+\dfrac{(L_2-L_3)^3}{3}\dfrac{\partial^3 v_{stem}(x,t)}{\partial x\partial t^2}\right] \\ +2g_{2,head,2}\left[\dfrac{L_3^3}{3}\dfrac{\partial^3 v_{stem}(x,t)}{\partial x\partial t^2}-\dfrac{L_3^2}{2}\dfrac{\partial^2 v_{stem}(x,t)}{\partial t^2}\right] \\ +g_{1,head,1}\left[\dfrac{(L_2-L_3)^2}{2}\dfrac{\partial v_{stem}(x,t)}{\partial t}+\dfrac{(L_2-L_3)^3}{3}\dfrac{\partial^2 v_{stem}(x,t)}{\partial x\partial t}\right] \\ +2g_{1,head,2}\left[\dfrac{L_3^3}{3}\dfrac{\partial^2 v_{stem}(x,t)}{\partial x\partial t}-\dfrac{L_3^2}{2}\dfrac{\partial v_{stem}(x,t)}{\partial t}\right] \end{array}\right\}\Big|_{x=L_1}=0, \tag{2.102}$$

$$\left\{\begin{array}{l} EI_{stem}\dfrac{\partial^3 v_{stem}(x,t)}{\partial x^3}-m_{head}\left[\dfrac{\partial^2 v_{stem}(x,t)}{\partial t^2}+d_{os}\dfrac{\partial^3 v_{stem}(x,t)}{\partial x\partial t^2}\right] \\ -g_{2,head,1}\left[(L_2-L_3)\dfrac{\partial^2 v_{stem}(x,t)}{\partial t^2}+\dfrac{(L_2-L_3)^2}{2}\dfrac{\partial^3 v_{stem}(x,t)}{\partial x\partial t^2}\right] \\ -2g_{2,head,2}\left[L_3\dfrac{\partial^2 v_{stem}(x,t)}{\partial t^2}-\dfrac{L_3^2}{2}\dfrac{\partial^3 v_{stem}(x,t)}{\partial x\partial t^2}\right] \\ -g_{1,head,1}\left[(L_2-L_3)\dfrac{\partial v_{stem}(x,t)}{\partial t}+\dfrac{(L_2-L_3)^2}{2}\dfrac{\partial^2 v_{stem}(x,t)}{\partial x\partial t}\right] \\ -2g_{1,head,2}\left[L_3\dfrac{\partial v_{stem}(x,t)}{\partial t}-\dfrac{L_3^2}{2}\dfrac{\partial^2 v_{stem}(x,t)}{\partial x\partial t}\right] \end{array}\right\}\Big|_{x=L_1}=0. \tag{2.103}$$

By applying the BCs (Eq. 2.4, Eq. 2.6, Eq.2.102 and Eq.2.103), the EOM presented in Eq. 2.2 can be solved. The procedure for finding the frequency response at the tip of the stem is analogous to the procedure described in Sec 2.4. The normalized amplitude of the deflection at the tip of the stem can be characterized by Eq. 2.71, in which the coefficients from Eq. 2.64 to Eq. 2.70 and Eq. 2.72 remain the same. Eq. 2.73 is simplified due to the composite rectangular head as:

$$\alpha_1 \equiv \frac{2\omega^2 d_{os} m_{head} + \omega^2 \left(L_2 - L_3\right)^2 g_{2,head,1}}{2EI_{stem}} - \frac{2\omega^2 L_3{}^2 g_{2,head,2} + j\omega\left(L_2 - L_3\right)^2 g_{1,head,1} - 2j\omega L_3{}^2 g_{1,head,2}}{2EI_{stem}}, \tag{2.104a}$$

$$\alpha_2 \equiv \frac{3\omega^2 d_{os}{}^2 m_{head} + \omega^2 \left(L_2 - L_3\right)^3 g_{2,head,1} + 3\omega^2 J_{head}}{3EI_{stem}} + \frac{2\omega^2 L_3{}^3 g_{2,head,2} - j\omega\left(L_2 - L_3\right)^3 g_{1,head,1} - 2j\omega L_3{}^3 g_{1,head,2}}{3EI_{stem}}, \tag{2.104b}$$

$$\alpha_3 \equiv \frac{j\omega\left(L_2 - L_3\right) g_{1,head,1} + 2j\omega L_3 g_{1,head,2}}{EI_{stem}} - \frac{\omega^2 m_{head} + \omega^2 \left(L_2 - L_3\right) g_{2,head,1} + 2\omega^2 L_3 g_{2,head,2}}{EI_{stem}}, \tag{2.104c}$$

$$\alpha_4 \equiv \frac{j\omega\left(L_2 - L_3\right)^2 g_{1,head,1} - 2j\omega L_3{}^2 g_{1,head,2}}{2EI_{stem}} - \frac{2\omega^2 d_{os} m_{head} + \omega^2 \left(L_2 - L_3\right)^2 g_{2,head,1} - 2\omega^2 L_3{}^2 g_{2,head,2}}{2EI_{stem}}. \tag{2.104d}$$

Substituting Eq. 2.87 to Eq. 2.89 into Eq. 2 104, the resonance frequency can be extracted from the frequency spectrum of a laterally vibrating composite rectangular hammerhead microcantilever in viscous liquid media.

2.5 Validation of the Theoretical Model in a Vacuum

The objective in this section is to validate the general theoretical model which assumes the hammerhead microcantilever as an elastic beam with a rigid body before further calculations of sensor's characteristics. It is convenient to validate the model in a vacuum, since the in-liquid theoretical model will reduce to the in-vacuum case if all the $g_{1,stem/head}$ and $g_{2,stem/head}$ are neglected. In this section, the theoretical model of a laterally vibrating uniform rectangular hammerhead microcantilever in a vacuum is carefully validated using numerical analysis. For other symmetric heads (shapes of isosceles

trapezoid, semi-circle and composite rectangle), the procedures of validation are analogous to the method used for a uniform rectangular hammerhead microcantilever. Thus, the validations of those geometries will not be repeated in this section.

To validate the model of a rectangular hammerhead microcantilever, the finite element analysis software COMSOL 4.1 is used to create 3-D structures of rectangular hammerhead microcantilevers in a vacuum and simulate the first natural frequencies corresponding to the in-plane vibration. Then the results obtained numerically are compared to those obtained from the analytical model. The domain of the validity of the theoretical model can be found. Conclusions are made and the ranges/domains of validity of the analytical model are given.

To model the problem numerically, a 3-D rectangular hammerhead microcantilever model is created in a vacuum and the material of the microcantilever is chosen. Then, the BCs are specified and the mesh density is determined so that the result is ensured to be convergent. Finally, the first natural frequency corresponding to the in-plane vibration is recorded. The above procedure is iterated for all the geometries of rectangular hammerhead microcantilevers that are of interest.

In this analysis, the space dimensions are selected as three dimensions, so that the numerical models are analogous to the physical microcantilevers. The hammerhead microcantilever model is set up in a vacuum and the physics in Comsol is chosen as Solid Mechanic. Then, the eigenfrequency is selected as the study type, so the frequencies will be directly recorded for all cases.

After the modeling environment is set up, a 3-D geometric model of a rectangular hammerhead microcantilever is created. In the material library, the material chosen for

the microcantilever is Si (silicon). The density and Young's modulus of the silicon must be consistent with the values used in the theoretical analysis ($\rho_b = 2330$ kg/m^3 and $E =$ 169 GPa). Then, it is specified that the displacements in all three directions (x, y and z) of the stem at the clamped end are zero and all of the other surfaces are set to be free.

After specifying the BCs, the mesh density must be tested to ensure that it is high enough to produce a good estimate of the natural frequencies. As the mesh density increases, the estimated natural frequencies should converge to a specific value. Physics-controlled meshing, which automatically creates meshes that are adapted to the physics in the model, is chosen in the mesh setting. In the setting, there are nine different meshing types which are predefined as "extremely coarse", "extra coarse", "coarser", "coarse", "normal", "fine", "finer", "extra fine", and "extreme fine". In this work, all of these physically controlled meshing types are tested for the rectangular hammerhead microcantilevers investigated as indicated in Table 2-1:

Stem Dimensions [um^2]	Length of the Hammerhead Microcantilever [μm]	Width of the Hammerhead Microcantilever [μm]	Thickness of the Hammerhead Microcantilever [μm]
150×45	50~300	60~300	1~15
200×45	50~300	60~300	1~15
250×45	50~300	60~300	1~15
300×45	50~300	60~300	1~15
400×45	50~300	60~300	1~15
600×45	50~300	60~300	1~15

Table 2-1: The dimensions of the rectangular hammerhead microcantilevers investigated in this work.

For all the investigated hammerhead microcantilever of the dimensions indicated in Table 2-1, the first natural frequencies corresponding to the lateral vibration are compared using all the predefined meshing types. It is found that the largest percent difference of the first natural frequencies between using the "extreme coarse" and "extreme fine" are less than 4%. It indicates that applying the "extreme coarse" meshing type will ensure the results to be convergent. In this work, the meshing type is chosen as "finer". In the domain of the analysis, the percent differences of the first natural frequencies corresponding to the lateral vibration between using "finer" and "extreme fine" meshing types are less than 0.2%. Thus, meshing the 3-D models using the predefined meshing type, "finer", will ensure the results to be convergent. Fig. 2-14 shows the "finer" mesh density of the hammerhead microcantilever of dimensions $[(200\times45\times12) + (300\times300\times12)]\ \mu m^3$.

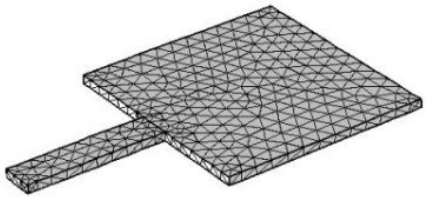

Figure 2-14: The "finer" mesh density of a rectangular hammerhead microcantilever of dimensions $[(200\times45\times12) + (300\times300\times12)]\ \mu m^3$.

Table 2-2 shows the first natural frequencies for a particular rectangular hammerhead of dimensions $[(200\times45\times12) + (300\times300\times12)]\ \mu m^3$ using different predefined meshing types. It is found that as the mesh density increases, the solutions to

the first natural frequencies converge. The same trend is also seen for all the investigated dimensions.

Element Size:	Extreme Coarse	Extra Coarse	Coarser	Coarse	Normal	Fine	Finer	Extra Fine	Extreme Fine
First natural frequency [Hz]	98527	97678	96927	96553	96504	96472	96352	96366	96245

Table 2-2: The first natural frequencies obtained by using different predefined element sizes.

To find the domain of the validity of the analytical model, the first natural frequencies corresponding to the lateral vibration obtained numerically and theoretically are compared. The percent difference of the first natural frequencies between the numerical and analytical results is defined as:

$$percent\ difference \equiv \frac{f_{na,theoretical\ result} - f_{na,numerical\ result}}{f_{na,numerical\ result}}. \qquad (2.105)$$

Using Eq. 2.105, the distribution of the percent differences can be found as a function of the dimensions of the head. The distribution can be used to predict the trend of the percent differences. For instance, the distribution for one particular stem of dimensions [200×45×12μm^3] is shown in Fig. 2-15:

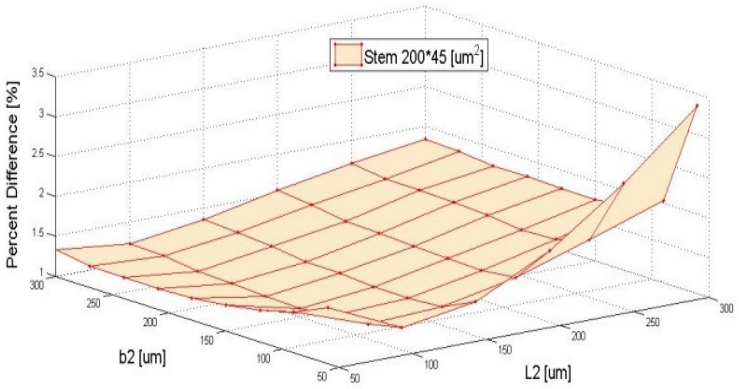

Figure 2-15: The distribution of the percent differences of the first natural frequencies corresponding to the lateral vibration for one particular stem of dimensions [200×45×12μm^3].

The percent differences of the first natural frequencies are calculated for the practical ranges of dimensions of the hammerhead microcantilevers. It is found that, the results obtained using Comsol are always smaller than those obtained using the theoretical model presented in this work. This is due to the stem being modeled using the standard Euler-Bernoulli beam theory which neglects shear deformation and rotatory inertia of the stem [114]. Among all the investigated cases, the largest percent difference is 5.8%. The largest difference is found for the rectangular hammerhead microcantilever with the shortest stem (L_1=150 μm, b_1= 45 μm), longest and narrowest head (L_2=300 μm, b_2= 60 μm), and smallest thickness (1μm). This is due to the limit of using the standard Euler-Bernoulli beam theory to model shorter and wider beams (Timoshenko beam effects) [114]. Furthermore, in the presented analysis, only the displacement in the y direction is taken into account, however, in the 3-D numerical analysis, as the microcantilever vibrates in the y direction, the material of the microcantilever will expand or compress in the *x* and *z* directions. Although the head is assumed to be

perfectly rigid in the analytical model, in the numerical analysis, as the microcantilever laterally vibrates, the head still slightly deforms due to its material property. The above reasons mainly contribute to the difference between the analytical and numerical results.

Stem [um^2]	600×45	400×45	300×45	250×45	200×45	150×45
PD_{max}	0.2%	0.7%	1.5%	2.2%	3.4%	5.5%
$PD_{average}$	0.1%	0.3%	0.7%	1.0%	1.7%	2.6%

Table 2-3: Maximum and average percent differences (PD) of the first natural frequencies for the investigated hammerhead microcantilevers of thickness 12 μm.

It is found, in the 3-D numerical analysis, that if only the thickness changes (1~15 μm), the percent differences will change by 0.2%~0.3%. Table 2-3 shows the maximum and average percent differences of the first natural frequencies for the investigated hammerhead microcantilevers of thickness 12 μm:

In Table 2-3, the maximum of the percent difference (5.5%) occurs at the shortest stem (L_1=150 μm, b_1= 45 μm), longest and narrowest head (L_2=300 μm, b_2= 60 μm). As the length of the stem increases, the standard Euler-Bernoulli beam theory becomes more appropriate in modeling longer beams and the largest and average percent differences decrease. For all the dimensions of the stems investigated in this study, as the width of the head becomes more than twice the width of the stem (b_2/b_1>2), the percent differences are always less than 4%.

Using the proposed analytical model, for the investigated ranges/domains, as the width ratio between the head and stem is larger than 4/3, the maximum percent difference is always less than 6%, which is acceptable in predicting the first natural frequency

corresponding to the lateral vibration. Although the investigated domain (geometries) of the rectangular hammerhead microcantilevers is limited in this study, as the dimensions of the head keep increasing, the analytical model is still valid. However, in practical fabrication and application, the dimensions of the head should not be too large compared to the dimensions of the stem.

Although this section mainly focuses on the model validation of uniform rectangular hammerhead microcantilevers in a vacuum, the method of validating other symmetric head (shapes of isosceles trapezoid, semi-circle and composite rectangle) are analogous to the method discussed in this section.

It is also found from the 3-D numerical simulations that, depending on the geometry and dimensions, the first natural frequency of in-plane mode may come after the second or third natural frequency associated with the out-of-plane or torsional mode. This often occurs when the hammerhead microcantilever becomes thinner and the head becomes larger. Such phenomenon can be further investigated to avoid mode coupling in design.

To obtain the characteristics of the laterally vibrating symmetric hammerhead microcantilevers in viscous liquids, Eq. 2.71 must be solved to obtain the frequency spectrum. The remaining unknown terms in Eq. 2.71 are $g_{1,stem}(Re_{stem}, h/b_1)$, $g_{2,stem}(Re_{stem}, h/b_1)$, $g_{1,head}[Re_{head}(x), h/b(x)]$ and $g_{2,head}[Re_{head}(x), h/b(x)]$. The analytical expressions of $g_{1,stem}(Re_{stem}, h/b_1)$, $g_{2,stem}(Re_{stem}, h/b_1)$, $g_{1,head}[Re_{head}(x), h/b(x)]$ and $g_{2,head}[Re_{head}(x), h/b(x)]$ will be discussed in chapter 3.

3. HYDRODYNAMIC FORCE ON LATERALLY VIBRATING SYMMETRIC HAMMERHEAD MICROCANTILEVERS IN VISCOUS LIQUID MEDIA

3.1 Introduction

In order to analyze the characteristics of laterally vibrating symmetric hammerhead microcantilevers in viscous liquid media, the hydrodynamic force acting on the microcantilevers must be found. The hydrodynamic force is defined by the resistance force acting on the microcantilever, when it is vibrating in liquid media. The hydrodynamic force acting on a laterally vibrating prismatic beam can be approximated by the steady-state solution of Stokes' second problem [80]. The solution provides a simpler analytical expression for the hydrodynamic function, which is a normalized hydrodynamic force per unit length. However, this analytical expression of the hydrodynamic function neglects the pressure force on the small surfaces of the microcantilever (thickness effects) and stress singularities on the edge of the microcantilever (edge effects) [64]. To consider the thickness and edge effects in the hydrodynamic force, a numerical analysis, which models a laterally vibrating rigid rectangular cross-section, has been first conducted [64]. In Ref 64, it is then proposed that the hydrodynamic function of a rectangular cantilever of finite dimensions can be obtained by multiplying Stokes' solution by a set of correction factors found from the numerical results to account for the thickness and edge effects. However, using the semi-analytical expression proposed in Ref 64, the differences between the hydrodynamic function obtained analytically and numerically are still high for some cases. This indicates that using the obtained semi-analytical expression for the hydrodynamic function would produce relatively high inaccuracy than directly using the numerical

results, especially for some range of aspect ratio, h/b, and Reynolds number, Re. To minimize the differences between the hydrodynamic functions obtained analytically and numerically for a wider range of the aspect ratio, h/b, and Reynolds number, Re, t is proposed to find a different analytical expression for the hydrodynamic function.

In this chapter, a different mathematical form of the analytical expression for the hydrodynamic function is proposed. Using this new approach, the differences between the analytical expression and numerical results of the hydrodynamic function for the investigated range of the aspect ratio, h/b, and Reynolds number, Re, are significantly minimized. Due to the composite shape of the hammerhead, a different method is proposed to find the total hydrodynamic force acting on the symmetric head. Then, using the semi-analytical expressions for the hydrodynamic force on the stem and head, respectively, the characteristics of the laterally vibrating symmetric hammerhead microcantilever can be calculated.

3.2 Review of the Hydrodynamic Function for a Laterally Vibrating Prismatic Beam

When a prismatic beam vibrates in an infinitely large liquid domain in the in-plane direction, the surrounding liquid will impose a resistance force on the beam. The resistance force is defined by the hydrodynamic force [27]. The hydrodynamic force, as shown in Fig. 3-1, consists of two components and is given by Eq. 3.1. One force is the pressure force which is perpendicular to the surface of the microcantilever; the other force is the shear force which is parallel to the surface of the microcantilever.

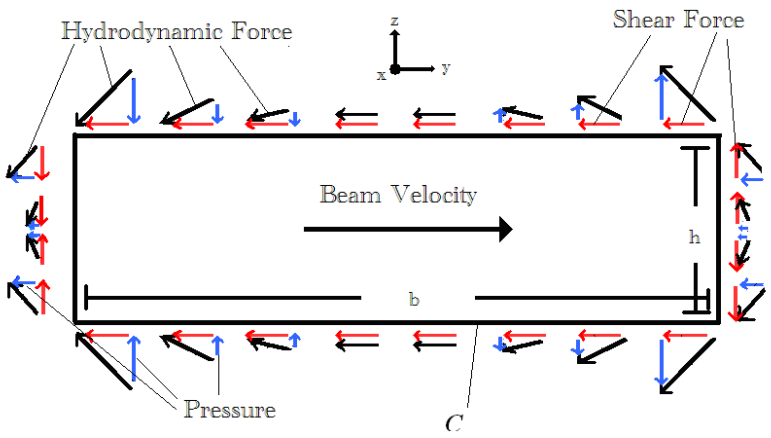

Figure 3-1: Hydrodynamic forces acting on the surfaces of a cross-section of a laterally vibrating microcantilever in fluid [64].

$$F_{medium,lat} = F_{pressure} + F_{shear} \tag{3.1}$$

As shown in Fig. 3-1, due to the symmetry of the problem, all pressure forces per unit length in the z direction cancel each other out while the pressure forces per unit length acting on the leading and trailing edges of the cross-section of the microcantilever are equal. Thus, the total remaining hydrodynamic force per unit length coming from the pressure is twice the pressure force acting on the leading or trailing edge:

$$F_{pressure}(x) = 2\int_{-h/2}^{h/2} P(b/2, z)\,dz \tag{3.2}$$

with P representing the pressure.

The remaining pressure force acting on the leading or trailing edges is partially out-of-phase with the velocity of the microcantilever. The component which is in-phase with the velocity is defined as the viscous damping while the component which is out-of-phase with the velocity is defined as the effective liquid mass of the system. Both the effective liquid mass and the viscous damping are functions of Re and the aspect ratio, h/b. As Re increases (or the viscosity decreases), the viscous damping becomes negligible. Then, the

pressure force only contributes to the effective liquid mass of the system. If the aspect ratio also approaches zero (or the thickness approaches zero), the pressure force becomes negligible for a laterally vibrating microcantilever.

In addition to the pressure force, the shear force is obtained by taking the shear stress over the entire contour of the cross-section of the microcantilever. The shear stress due to the liquid is defined as:

$$\tau = \eta \frac{du}{dn} \tag{3.3}$$

In Eq. 3.3, u is the velocity of the liquid in the vicinity of the beam-liquid interface and n is a coordinate in the direction normal to the surface [64]. It is shown that the shear stress is proportional to the dynamic viscosity, η. As noted before, the total shear force per unit length is obtained by taking the integral over the entire contour of the cross-section of the microcantilever as:

$$F_{shear} = \int_C \tau d\gamma \tag{3.4}$$

where C is the contour of the cross-section of the microcantilever.

Due to the symmetry of the problem, all shear forces in the z direction cancel each other out. The hydrodynamic forces from the shear acting on the top and bottom surfaces of the microcantilever are equal. Thus, the total remaining hydrodynamic force per unit length coming from the shear forces acting on the microcantilever is twice the shear force acting on the top or bottom surface of the microcantilever:

$$F_{shear}(x) = 2\int_{-b/2}^{b/2} \tau(y, h/2)\, dy \tag{3.5}$$

Utilizing Eq. 3.1, Eq. 3.2 and Eq. 3.5, the total hydrodynamic force per unit length on a laterally vibrating rectangular prismatic microcantilever in a viscous liquid medium

can be calculated. If the thickness of the microcantilever is small enough, the pressure force on the small surface can be neglected and only the shear force contributes to the hydrodynamic force. Then, the effective liquid mass and the viscous damping only come from the shear component. If *Re* also approaches infinity, the liquid medium becomes highly inviscid, and both the effective liquid mass and the damping from the shear component approach zero. The total hydrodynamic force acting on the beam is zero.

There have been several attempts to analytically express the hydrodynamic force acting on a laterally vibrating prismatic microcantilever [63, 80, 110, 64]. As indicated earlier, to account for the effects of thickness in viscous liquid environment, numerical analysis have been conducted as a first step to obtain a semi-analytical expression for the hydrodynamic function in terms of both *Re* and the aspect ratio of the beam, *h*/*b* [64]. Another relatively simpler expression is found by assuming that the thickness of the microcantilever is small enough compared to its width. Then the microcantilever is approximated as a laterally vibrating ribbon. The problem of a laterally vibrating ribbon reduces to the steady-state solution of Stokes' second problem if the width of the microcantilever is much wider compared to the boundary layer thickness of the liquid [80]. In this case, the hydrodynamic function can be obtained from the solution of Stokes' second problem and it is only a function of *Re*.

Stokes' second problem describes a semi-infinite domain of homogeneous incompressible liquid which occupies the space above an infinitely wide plate [103]. By solving the EOM for the liquid, the total hydrodynamic force per unit length can be found as:

$$F_{medium,lat,Stokes} = -\sqrt{\frac{2\eta\rho_f b^2}{\omega}}\frac{\partial^2 v(x,t)}{\partial t^2} - \sqrt{2\eta\rho_f b^2\omega}\frac{\partial v(x,t)}{\partial t} \tag{3.6}$$

Eq. 3.6 indicates that, when the thickness and edge effects are neglected, the total hydrodynamic force is 45° out of phase with the velocity of the beam and dependent on the exciting frequency, ω, the width, b, the square-root of the product of the dynamic viscosity, η, and liquid density, ρ_f. The real part of the hydrodynamic force per unit length is associated with the effective displacement mass (g_2); while the imaginary part of the hydrodynamic force per unit length is associated with the viscous damping (g_1):

$$g_{1,Stokes} = \sqrt{2\eta\rho_f b^2}\sqrt{\omega} \tag{3.7}$$

$$g_{2,Stokes} = \frac{\sqrt{2\eta\rho_f b^2}}{\sqrt{\omega}} \tag{3.8}$$

By normalizing the total hydrodynamic force per unit length, the hydrodynamic function can be found as

$$\Gamma_{lat,Stokes}(\mathrm{Re}) = \frac{F^*_{medium,lat,Stokes}}{j\pi\eta\,\mathrm{Re}\,U_0 e^{-j\omega t}} = \frac{2\sqrt{2}}{\pi\sqrt{\mathrm{Re}}}(1+j) \tag{3.9}$$

In Eq. 3.9, $F^*_{medium,lat,Stokes}$ is the complex conjugate of the hydrodynamic force obtained from Stokes' second problem. It is noted that, for the liquid resistance predicted by Stokes, the real and imaginary parts of the hydrodynamic function are numerically equal.

When the edge effects become negligible, Eq. 3.9 is good enough to give an approximation for the hydrodynamic function from the shear due to the liquid resistance. However, when the thickness is not small enough compared to the width and *Re* is not large enough, Eq. 3.9 fails to account for the thickness and edge effects. Thus, it is necessary to find a different analytical expression for the hydrodynamic function with these effects taken into account.

By fitting the numerical results to the hydrodynamic function presented in Eq. 3.9, a set of correction factors was found. Then, the real and imaginary parts of the hydrodynamic function with thickness and edge effects taken into account were obtained as [110]:

$$\Gamma_{real,lat}(\mathrm{Re},\frac{h}{b})=\frac{2\sqrt{2}}{\pi\sqrt{\mathrm{Re}}}\left[1.658\left(\frac{h}{b}\right)^{1.83}\sqrt{\mathrm{Re}}+3.08\left(\frac{h}{b}\right)^{0.85}+1\right] \tag{3.10}$$

$$\Gamma_{imag,lat}(\mathrm{Re},\frac{h}{b})=\frac{2\sqrt{2}}{\pi\sqrt{\mathrm{Re}}}\left[\left(2.56-1.321\left(\frac{h}{b}\right)\right)\frac{1}{\sqrt{\mathrm{Re}}}+3.108\left(\frac{h}{b}\right)^{0.85}+1\right] \tag{3.11}$$

It is noted that, the previously obtained numerical results of the hydrodynamic function are found for the range of aspect ratio, h/b, [0.02, 1] and the range of Re [10, 10000]; thus, calculations of the hydrodynamic function using Eq. 3.10 and Eq. 3.11 are mainly accurate in these ranges. In Ref 110, the analytically obtained hydrodynamic functions are also compared to the data in Ref 63. The maximum percent differences between the two methods for the real and imaginary parts of the hydrodynamic function are 5.88% and 9.85%, respectively, within the defined range of aspect ratio and Reynolds number. The average absolute percent differences between the two techniques for the real and imaginary parts are 1.37% and 3.8%, respectively. This provides the confidence in using the previously obtained numerical data to find a different mathematical form of the hydrodynamic function to further improve the fitting accuracy from the numerical data to the semi-analytical expression.

3.3 Hydrodynamic Function for a Symmetric Hammerhead Microcantilever Laterally Vibrating in Viscous Liquids

When a laterally vibrating symmetric hammerhead microcantilever is immersed in a viscous liquid medium, the liquid will impose hydrodynamic forces on the hammerhead

microcantilever (stem and head). To obtain the total hydrodynamic force acting on the stem and head, respectively, the hydrodynamic function for any cross-section of the microcantilever must be analyzed. Due to the difference in the dimensions of the stem and head, the hydrodynamic functions on the stem and head are different. Since the symmetric, arbitrary hammerhead microcantilever can be discretized into infinitely small rectangles, the hydrodynamic function for any cross-section (infinitely small rectangle) of the microcantilever can be obtained as a function of $Re(x)$ and $h/b(x)$. Since the rectangular stem has a constant width of b_1, the hydrodynamic function for any cross-section of the stem can be obtained as a function of Re_{stem} and h/b_1. Similarly, since the shape of the head is symmetric, the hydrodynamic function for each infinitely small rectangle of the head can be found as a function of $Re_{head}(x)$ and $h/[2b_2(x)]$. Thus, the general hydrodynamic force per unit length on the symmetric, arbitrary hammerhead microcantilever can be expressed as:

$$F_{liquid} = -g_1 \frac{\partial v}{\partial t} - g_2 \frac{\partial^2 v}{\partial t^2} \tag{3.12}$$

For the stem:

$$F_{stem,liquid} = -g_{1,stem} \frac{\partial v_{stem}}{\partial t} - g_{2,stem} \frac{\partial^2 v_{stem}}{\partial t^2} \tag{3.13}$$

where

$$g_{1,stem}\left(\mathrm{Re}_{stem}, \frac{h}{b_1}\right) = \frac{\pi}{4}\rho_f b_1^2 \Gamma_I \left(\mathrm{Re}_{stem}, \frac{h}{b_1}\right)\omega \tag{3.14}$$

$$g_{2,stem}\left(\mathrm{Re}_{stem}, \frac{h}{b_1}\right) = \frac{\pi}{4}\rho_f b_1^2 \Gamma_R \left(\mathrm{Re}_{stem}, \frac{h}{b_1}\right) \tag{3.15}$$

For the head:

$$F_{head,liquid} = -g_{1,head}\frac{\partial v_{head}}{\partial t} - g_{2,head}\frac{\partial^2 v_{head}}{\partial t^2} \tag{3.16}$$

where

$$g_{1,head}\left[\mathrm{Re}_{head}(x), \frac{h}{2b_2(x)}\right] = \frac{\pi}{4}\rho_f\left[2b_2(x)\right]^2\Gamma_I\left[\mathrm{Re}_{head}(x), \frac{h}{2b_2(x)}\right]\omega \tag{3.17}$$

$$g_{2,head}\left[\mathrm{Re}_{head}(x), \frac{h}{2b_2(x)}\right] = \frac{\pi}{4}\rho_f\left[2b_2(x)\right]^2\Gamma_R\left[\mathrm{Re}_{head}(x), \frac{h}{2b_2(x)}\right] \tag{3.18}$$

In the above equations:

$$\mathrm{Re}_{stem} = \frac{\rho_f \omega b_1^2}{4\eta} \quad \text{and} \quad \mathrm{Re}_{head}(x) = \frac{\rho_f \omega\left[2b_2(x)\right]^2}{4\eta} \tag{3.19}$$

The above equations define the hydrodynamic force per unit length on the stem and head. From these equations, the expressions for the real part (Γ_R) and imaginary part (Γ_I) of the hydrodynamic function can be obtained. The previously obtained semi-analytical expressions for the real and imaginary parts of the hydrodynamic function are provided in Eq. 3.10 and Eq. 3.11 [64]. However, the largest percent differences between the analytical expression and the numerical results for the real and imaginary parts are still relatively high, and are 20.5% and 5.7%, respectively. As a result, there is a need to find a more accurate expression for the hydrodynamic function.

To improve the fitting accuracy from the numerical data to the analytical expression for the hydrodynamic function, a different analytical expression is proposed. Each coefficient and power index for the analytical expression is determined simultaneously to obtain the optimum fitting results. The surface fitting tool in Matlab *R2011a* is used to fit the numerical data to the predefined mathematical form of the hydrodynamic function. The predefined mathematical forms of the real and imaginary parts of the hydrodynamic

function are proposed as a product of a function of *Re* and a function of the aspect ratio, *h*/*b*, as follows:

$$\Gamma\left(\mathrm{Re},\frac{h}{b}\right)=\Gamma_R\left(\mathrm{Re},\frac{h}{b}\right)+j\Gamma_I\left(\mathrm{Re},\frac{h}{b}\right) \tag{3.20}$$

where

$$\Gamma_R\left(\mathrm{Re},\frac{h}{b}\right)=\Gamma_{R1}(\mathrm{Re})\Gamma_{R2}\left(\frac{h}{b}\right) \text{ and } \Gamma_I\left(\mathrm{Re},\frac{h}{b}\right)=\Gamma_{I1}(\mathrm{Re})\Gamma_{I2}\left(\frac{h}{b}\right) \tag{3.21}$$

In Eq. 3.21, $\Gamma_{R1}(Re)$ or $\Gamma_{I1}(Re)$ are expected to depend on the boundary layer thickness [112].The boundary layer thickness is the thickness of the thin viscous layer surrounding the microcantilever, in which the velocity has dropped by a factor of 1/*e* [112]. Since the boundary layer thickness is associated with $Re^{-0.5}$, $\Gamma_{R1}(Re)$ or $\Gamma_{I1}(Re)$ are both expected to be functions in terms of $Re^{-0.5}$. $\Gamma_{R2}(h/b)$ or $\Gamma_{I2}(h/b)$ can be expanded into a summation of multiple *h*/*b* terms, which is similar to Taylor series expansion. The proposed real and imaginary parts of the hydrodynamic function are as follows:

$$\Gamma_R\left(\mathrm{Re},\frac{h}{b}\right)=\left[\frac{1}{\sqrt{\mathrm{Re}}}\sum_{m=0}^{m_{\max}}C_m\left(\frac{h}{b}\right)^{\frac{m}{2}}\right]+\left[\sum_{n=0}^{n_{\max}}D_n\left(\frac{h}{b}\right)^{\frac{n}{2}}\right] \tag{3.22}$$

$$\Gamma_I\left(\mathrm{Re},\frac{h}{b}\right)=\left[\frac{1}{\mathrm{Re}}\sum_{p=0}^{p_{\max}}E_p\left(\frac{h}{b}\right)^{\frac{p}{2}}\right]+\left[\frac{1}{\sqrt{\mathrm{Re}}}\sum_{q=0}^{q_{\max}}F_q\left(\frac{h}{b}\right)^{\frac{q}{2}}\right] \tag{3.23}$$

In Eq. 3.22 and Eq. 3.23, the coefficients (C_m, D_n, E_p, F_q) and power indices (m_{max}, n_{max}, p_{max}, q_{max}) are determined by Matlab to minimize the differences between the numerical data and the proposed analytical expression. Using the surface fitting, the power indices and coefficients are found as m_{max}=2, n_{max}=4, p_{max}=1, q_{max}=4, C_0=0.9003, C_1=0.6105, C_2=2.1722, D_0=0, D_1= -0.0021, D_2= -0.1459, D_3=0.8255, D_4= -1.3388, E_0=2.5758, E_1= -1.3388, F_0=0.9003, F_1= -0.7121, F_2=1.6845, F_3=0.8236 and F_4=0.4178.

It is noted that, a more complicated hydrodynamic function can be found by expanding the function of $\Gamma_{R2}(h/b)$ or $\Gamma_{I2}(h/b)$ with more terms to improve the fitting accuracy. However, the fitting results do not change significantly.

After obtaining the semi-analytical expression for the hydrodynamic function, the expressions for the real and imaginary parts are validated in the limiting cases. For instance, as h/b approaches zero, the analytical expression for the real part of the hydrodynamic function presented in Eq. 3.22 reduces to the hydrodynamic function corresponding to Stokes' solution [103]. The analytical expression for the imaginary part of hydrodynamic function presented in Eq. 3.23 will not exactly reduce to the hydrodynamic function corresponding to Stokes' solution due to edge effect [110]. Stokes' second problem assumes that the plate is infinitely wide such that the stress distribution along the contour of the beam cross section is uniform. However, in FEA model, the stress distribution is much denser near the edges compared to that in the middle of the plate. As the liquid medium becomes highly inviscid ($Re\rightarrow\infty$) and h/b approaches zero, which indicates that both the viscous damping and the effective mass approach zero, the real and imaginary parts of the hydrodynamic function approach zero. As the liquid medium becomes highly viscous ($Re\rightarrow 0$) and h/b approaches zero, both the real and imaginary parts of the hydrodynamic function approach infinity.

After validating the expressions in the limiting cases, the obtained semi-analytical expressions for the hydrodynamic functions are compared with the numerical data for different aspect ratios, h/b, and Reynolds number, Re. Fig. 3-2 shows the comparison of the expression and numerical results for the real and imaginary parts of the hydrodynamic function.

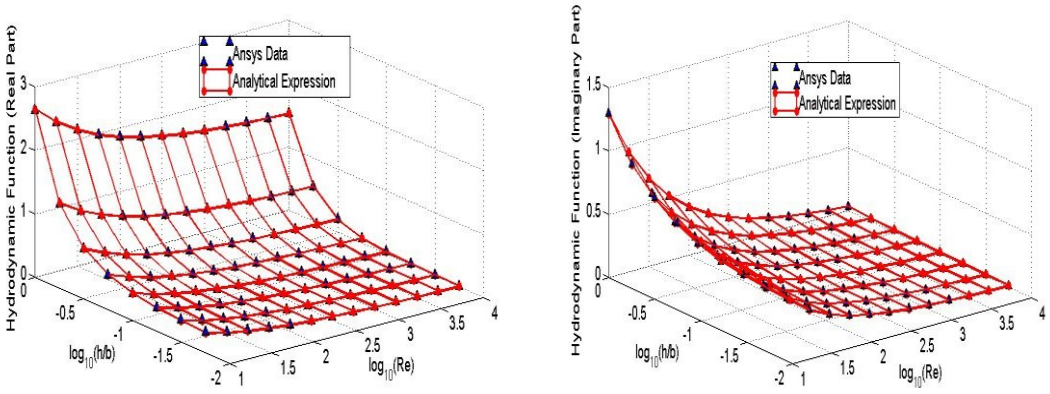

Figure 3-2: Comparison of the real and imaginary parts of the hydrodynamic function obtained numerically and analytically as functions of the aspect ratio, h/b and Reynolds number Re.

In the above figures, the percent difference between the hydrodynamic function obtained numerically and semi-analytically is defined as

$$percent\ difference = \frac{\Gamma_{analytical\ expression} - \Gamma_{numerical\ results}}{\Gamma_{numerical\ results}} \tag{3.24}$$

The results show that the differences between the semi-analytical expression and the numerical data are quite small. The ranges of the percent differences of the real and imaginary parts are [-3.8%, 6.1%] and [-2.0%, 2.8%], compared to [-5.9%, 20.6%] and [-5.7%, 2.4%] when using the originally proposed hydrodynamic function in Ref 110.

Compared with the results in Ref 63, the average percent differences of the real and imaginary parts are -0.56% and 4.22%, respectively. The ranges of the percent differences for the real and imaginary parts are [-3.34%, 1.28%] and [-1.7%, 13.23%]. The highest absolute percent differences for the real and imaginary parts of the hydrodynamic function, 3.34% and 13.23%, occur at Re =10 and h/b=0.02. This is because, at very small Re, the liquid becomes very viscous and the amount of liquid

excited by the beam increases, thus the thickness of the boundary layer increases. Furthermore, when h/b becomes smaller, the mesh density used in performing the numerical analysis increases. The above two conditions make it relatively difficult to achieve convergence in the numerical analysis of the hydrodynamic function, which results in the relatively high percent differences between the two methods.

After obtaining the analytical expressions for the hydrodynamic function, shown in Eq. 3.22 and Eq. 3.23, the hydrodynamic force on a laterally vibrating symmetric hammerhead microcantilever can be found by substituting the aspect ratio, $h/b(x)$, and Reynolds number, $Re(x)$, associated with the stem and head of the hammerhead microcantilever into Eq. 3.22 and Eq. 3.23. In this case, the width of the stem is constant, $b(x)=b_1$; the width of the head is defined by a function of $2b_2(x)$, as shown in Fig 2-1. The characteristics of the laterally vibrating symmetric hammerhead microcantilevers in viscous liquids will be analyzed in chapter 4.

4. CHARACTERISTICS OF LATERALLY VIBRATING SYMMETRIC HAMMERHEAD MICROCANTILEVERS IN VISCOUS LIQUIDS

4.1 Introduction

The characteristics of laterally vibrating symmetric hammerhead microcantilevers (isosceles trapezoid, semi-circle, uniform rectangle and composite rectangle) in viscous liquids are theoretically analyzed in this chapter. These four geometries are repeated and shown in Fig. 4-1 for convenience.

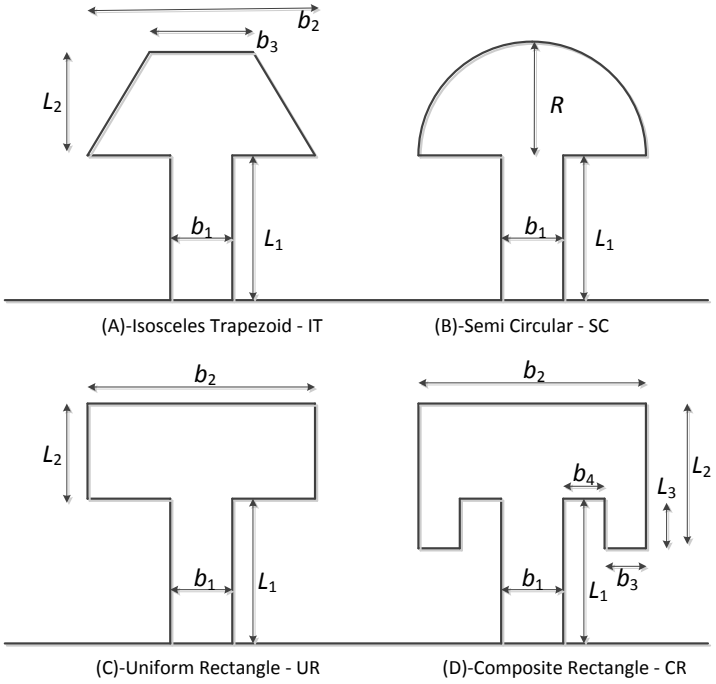

Figure 4-1: Four investigated symmetric hammerhead microcantilevers (isosceles trapezoid - IT, semi-circle - SC, uniform rectangle - UR and composite rectangle - CR)

To characterize and make relatively fair comparisons between these different head geometries, it is proposed to analyze microcantilevers with the same stems and head areas. In order to present the results conveniently, the investigated geometries in this work are

indicated in Table 4-1. From section 4.2 to section 4.4, these cases will be noted using their reference numbers, as indicated in Table 4-1. For example, for an isosceles trapezoid head shaped hammerhead microcantilever with a stem (surface dimensions of 150×45 um^2) and a head (surface area of 10000 um^2), the reference number is (A-1-a).

Geometry	Stem Surface Dimension [um^2]	Head Area [um^2]
(A)-Isosceles Trapezoid-IT	(1)-150×45	(a)-10000
		(b)-25000
		(c)-40000
	(2)-200×45	(a)-10000
		(b)-25000
		(c)-40000
	(3)-300×45	(a)-10000
		(b)-25000
		(c)-40000
(B)-Semi Circular-SC	(1)-150×45	(a)-10000
		(b)-25000
		(c)-40000
	(2)-200×45	(a)-10000
		(b)-25000
		(c)-40000
	(3)-300×45	(a)-10000
		(b)-25000
		(c)-40000
(C)-Uniform Rectangle-UR	(1)-150×45	(a)-10000
		(b)-25000
		(c)-40000
	(2)-200×45	(a)-10000
		(b)-25000
		(c)-40000
	(3)-300×45	(a)-10000
		(b)-25000
		(c)-40000
(D)-Composite Rectangle-CR	(1)-150×45	(a)-10000
		(b)-25000
		(c)-40000
	(2)-200×45	(a)-10000
		(b)-25000
		(c)-40000
	(3)-300×45	(a)-10000
		(b)-25000
		(c)-40000

Table 4-1: Investigated cases of different geometries in this work.

The characteristics investigated in this work include the resonance frequency, quality factor, and mass sensitivity of the microcantilever. These characteristics are evaluated based on the frequency response at the tip of the stem ($x=L_1$). The magnitude of the deflection occurs at the tip of the stem is obtained from the frequency spectrum of the system. It is recalled here that the head is considered as a rigid body in the analysis. The

results are analyzed as a function of the dimensions of the microcantilevers and the properties of the liquid media (density and viscosity). The quality factors are calculated and compared using two different methods which are based on the energy definition and the 3-dB bandwidth definition. The results of these symmetric hammerhead microcantilevers (isosceles trapezoid, semi-circle, uniform rectangle and composite rectangle) are achieved and compared.

4.2 Resonance Frequency

For a particular vibration mode, the resonance frequency is defined as the exciting frequency which maximizes the amplitude of the corresponding vibration. In microcantilever-based sensor applications, the changes in the resonance frequency of a dynamically driven microcantilever are used to detect the changes in the operational environment or molecules present in that environment. By coating a polymer layer on the surface of the substrate of the microcantilever, the sensing layer will absorb or adsorb the target molecules in the operational environment. Then, the resonance frequency will shift due to the change in the total mass of the microcantilever. By determining the resonance frequency and its shift due to the liquid environment (density and viscosity), other sensor characteristics including the quality factor, mass sensitivity and limit of detection can be obtained.

It is noted that, Eq. 2.71 is used to determine the maximum deflection which occurs at the junction between the stem and head. The displacement associated with the microcantilever at $x=L_1$ is a function of the exciting frequency, geometrical properties of the hammerhead microcantilever and the liquid medium. For convenience, a non-

dimensional model in viscous liquid media is developed by introducing the dimensionless parameters as follows:

$$\bar{v}_{stem} \equiv \frac{v_{stem}}{\theta_0 L_1}, \tag{4.1a}$$

$$\xi \equiv \frac{x}{L_1}, \tag{4.1b}$$

$$\tau \equiv \omega t \tag{4.1c}$$

In Eq. 4.1, $\bar{v}_{stem}$ is noted as the normalized deflection of the stem, ξ is noted as the normalized length and τ is noted as the normalized time.

The normalized frequency response at the tip of the stem can be obtained as follows:

$$\left|\bar{X}(1)\right| = \left|\bar{A}_1\left(\cosh\bar{K}\xi - \cos\bar{K}\xi\right) + \bar{A}_2\left(\sinh\bar{K}\xi - \sin\bar{K}\xi\right) + \frac{1}{\bar{K}}\sin\bar{K}\xi\right| \tag{4.2}$$

where

$$\bar{K} = \left\{\frac{\omega^2 L_1{}^4\left[\rho_b b_1 h + g_{2,stem}\right] - j\omega L_1{}^4 g_{1,stem}}{EI_{stem}}\right\}^{1/4} \tag{4.3}$$

$$\bar{A}_1 = \frac{\bar{\Pi}_3\bar{\Pi}_5 - \bar{\Pi}_6\bar{\Pi}_2}{\bar{\Pi}_1\bar{\Pi}_5 - \bar{\Pi}_4\bar{\Pi}_2} \quad \text{and} \quad \bar{A}_2 = \frac{\bar{\Pi}_3\bar{\Pi}_4 - \bar{\Pi}_6\bar{\Pi}_1}{\bar{\Pi}_2\bar{\Pi}_4 - \bar{\Pi}_1\bar{\Pi}_5} \tag{4.4}$$

$$\bar{\Pi}_1 \equiv \bar{K}^2\left(\cosh\bar{K}\xi + \cos\bar{K}\xi\right) - \bar{\alpha}_1\left(\cosh\bar{K}\xi - \cos\bar{K}\xi\right) - \bar{\alpha}_2\bar{K}\left(\sinh\bar{K}\xi + \sin\bar{K}\xi\right) \tag{4.5a}$$

$$\bar{\Pi}_2 \equiv \bar{K}^2\left(\sinh\bar{K}\xi + \sin\bar{K}\xi\right) - \bar{\alpha}_1\left(\sinh\bar{K}\xi - \sin\bar{K}\xi\right) - \bar{\alpha}_2\bar{K}\left(\cosh\bar{K}\xi - \cos\bar{K}\xi\right) \tag{4,5b}$$

$$\bar{\Pi}_3 \equiv \frac{1}{\bar{K}}\left[\bar{K}^2\sin\bar{K}\xi + \bar{\alpha}_1\sin\bar{K}\xi + \bar{\alpha}_2\bar{K}\cos\bar{K}\xi\right] \tag{4.5c}$$

$$\bar{\Pi}_4 \equiv \bar{K}^3\left(\sinh\bar{K}\xi - \sin\bar{K}\xi\right) - \bar{\alpha}_3\left(\cosh\bar{K}\xi - \cos\bar{K}\xi\right) - \bar{\alpha}_4\bar{K}\left(\sinh\bar{K}\xi + \sin\bar{K}\xi\right) \tag{4.5d}$$

$$\bar{\Pi}_5 \equiv \bar{K}^3\left(\cosh\bar{K}\xi + \cos\bar{K}\xi\right) - \bar{\alpha}_3\left(\sinh\bar{K}\xi - \sin\bar{K}\xi\right) - \bar{\alpha}_4\bar{K}\left(\cosh\bar{K}\xi - \cos\bar{K}\xi\right) \tag{4.5e}$$

$$\bar{\Pi}_6 \equiv \frac{1}{\bar{K}}\left[\bar{K}^3\cos\bar{K}\xi + \bar{\alpha}_3\sin\bar{K}\xi + \bar{\alpha}_4\bar{K}\cos\bar{K}\xi\right] \tag{4.5f}$$

with

$$\bar{\alpha}_1 \equiv \frac{m_{head} d_{os} \omega^2 L_1^{\,2}}{EI_{stem}} + \frac{\int_{L_1}^{L_1+L_2} \omega^2 L_1^{\,2} \left(x - L_1\right) g_{2,head} dx}{EI_{stem}} - \frac{j \int_{L_1}^{L_1+L_2} \omega L_1^{\,2} \left(x - L_1\right) g_{1,head} dx}{EI_{stem}}, \tag{4.6a}$$

$$\bar{\alpha}_2 \equiv \frac{m_{head} d_{os}^{\,2} \omega^2 L_1}{EI_{stem}} + \frac{\int_{L_1}^{L_1+L_2} \omega^2 L_1 \left(x - L_1\right)^2 g_{2,head} dx}{EI_{stem}} - \frac{j \int_{L_1}^{L_1+L_2} \omega L_1 \left(x - L_1\right)^2 g_{1,head} dx}{EI_{stem}} + \frac{\omega^2 L_1 J_{head}}{EI_{stem}}, \tag{4.6b}$$

$$\bar{\alpha}_3 \equiv -\frac{m_{head} \omega^2 L_1^{\,3}}{EI_{stem}} - \frac{\int_{L_1}^{L_1+L_2} \omega^2 L_1^{\,3} g_{2,head} dx}{EI_{stem}} + \frac{j \int_{L_1}^{L_1+L_2} \omega L_1^{\,3} g_{1,head} dx}{EI_{stem}}, \tag{4.6c}$$

$$\bar{\alpha}_4 \equiv -\frac{m_{head} d_{os} \omega^2 L_1^{\,2}}{EI_{stem}} - \frac{\int_{L_1}^{L_1+L_2} \omega^2 L_1^{\,2} \left(x - L_1\right) g_{2,head} dx}{EI_{stem}} + \frac{j \int_{L_1}^{L_1+L_2} \omega L_1^{\,2} \left(x - L_1\right) g_{1,head} dx}{EI_{stem}}. \tag{4.6d}$$

For a uniform rectangular hammerhead microcantilever (see Fig. 2-8), $\bar{\alpha}_1$, $\bar{\alpha}_2$, $\bar{\alpha}_3$ and $\bar{\alpha}_4$ are simplified as:

$$\bar{\alpha}_1 \equiv \frac{\omega^2 L_1^{\,2} L_2 \left[m_{head} + L_2 g_{2,head}\right] - j\omega L_1^{\,2} L_2^{\,2} g_{1,head}}{2EI_{stem}} \tag{4.7a}$$

$$\bar{\alpha}_2 \equiv \frac{3\omega^2 L_1 L_2^{\,2} m_{head} + 4\omega^2 L_1 L_2^{\,3} g_{2,head} + 12\omega^2 L_1 J_{head} - 4j\omega L_1 L_2^{\,3} g_{1,head}}{12EI_{stem}} \tag{4.7b}$$

$$\bar{\alpha}_3 \equiv \frac{j\omega L_1^{\,3} L_2 g_{1,head} - \omega^2 L_1^{\,3} \left[m_{head} + L_2 g_{2,head}\right]}{EI_{stem}} \tag{4.7c}$$

$$\bar{\alpha}_4 \equiv \frac{j\omega L_2^{\,2} g_{1,head} - \omega^2 L_2 \left[m_{head} + L_2 g_{2,head}\right]}{2EI_{stem}} \tag{4.7d}$$

For a composite rectangular hammerhead microcantilever (see Fig. 2-9), $\bar{\alpha}_1$, $\bar{\alpha}_2$, $\bar{\alpha}_3$ and $\bar{\alpha}_4$ are simplified as:

$$\bar{\alpha}_1 \equiv \frac{2\omega^2 L_1^{\,2} d_{os} m_{head} + \omega^2 L_1^{\,2}\left(L_2 - L_3\right)^2 g_{2,head,1}}{2EI_{stem}} - \frac{2\omega^2 L_1^{\,2} L_3^{\,2} g_{2,head,2} + j\omega L_1^{\,2}\left(L_2 - L_3\right)^2 g_{1,head,1} - 2j\omega L_1^{\,2} L_3^{\,2} g_{1,head,2}}{2EI_{stem}} \tag{4.8a}$$

$$\bar{\alpha}_2 \equiv \frac{3\omega^2 L_1 d_{os}^{\,2} m_{head} + \omega^2 L_1\left(L_2 - L_3\right)^3 g_{2,head,1} + 3\omega^2 L_1 J_{head}}{3EI_{stem}} + \frac{2\omega^2 L_1 L_3^{\,3} g_{2,head,2} - j\omega L_1\left(L_2 - L_3\right)^3 g_{1,head,1} - 2j\omega L_1 L_3^{\,3} g_{1,head,2}}{3EI_{stem}} \tag{4.8b}$$

$$\bar{\alpha}_3 \equiv \frac{j\omega L_1^{\,3}\left(L_2 - L_3\right) g_{1,head,1} + 2j\omega L_1^{\,3} L_3 g_{1,head,2}}{EI_{stem}} - \frac{\omega^2 L_1^{\,3}\left(L_2 - L_3\right) g_{2,head,1} + 2\omega^2 L_1^{\,3} L_3 g_{2,head,2}}{EI_{stem}} \tag{4.8c}$$

$$\bar{\alpha}_4 \equiv \frac{j\omega L_1^{\,2}\left(L_2 - L_3\right)^2 g_{1,head,1} - 2j\omega L_1^{\,2} L_3^{\,2} g_{1,head,2}}{2EI_{stem}} - \frac{2\omega^2 L_1^{\,2} d_{os} m_{head} + \omega^2 L_1^{\,2}\left(L_2 - L_3\right)^2 g_{2,head,1} - 2\omega^2 L_1^{\,2} L_3^{\,2} g_{2,head,2}}{2EI_{stem}} \tag{4.8d}$$

The normalized tip deflection of the stem is used to evaluate the frequency response of the symmetric hammerhead microcantilever, as given by Eq. 4.2. For a given hammerhead microcantilever, the dimensions of the structure are known, leaving only the unknown terms including the viscous damping and effective liquid mass per unit length associated with the stem ($g_{1,stem}$ and $g_{2,stem}$) and head ($g_{1,head}$ and $g_{2,head}$), respectively.

As is noted in chapter 3, the general expressions for the viscous damping and effective liquid mass are given by

For the stem:

$$g_{1,stem}\left(\mathrm{Re}_{stem}, h/b_1\right) = \frac{\pi}{4}\rho_f b_1^2 \Gamma_I\left(\mathrm{Re}_{stem}, h/b_1\right)\omega \tag{4.9}$$

$$g_{2,stem}\left(\mathrm{Re}_{stem}, h/b_1\right) = \frac{\pi}{4}\rho_f b_1^2 \Gamma_R\left(\mathrm{Re}_{stem}, h/b_1\right) \tag{4.10}$$

For the head:

$$g_{1,head}\left[\mathrm{Re}_{head}(x), \frac{h}{2b_2(x)}\right] = \frac{\pi}{4}\rho_f\left[2b_2(x)\right]^2 \Gamma_I\left[\mathrm{Re}_{head}(x), \frac{h}{2b_2(x)}\right]\omega \tag{4.11}$$

$$g_{2,head}\left[\mathrm{Re}_{head}(x), \frac{h}{2b_2(x)}\right] = \frac{\pi}{4}\rho_f\left[2b_2(x)\right]^2 \Gamma_R\left[\mathrm{Re}_{head}(x), \frac{h}{2b_2(x)}\right] \tag{4.12}$$

with *Re* given by

$$\mathrm{Re}_{stem} = \frac{\rho_f \omega b_1^2}{4\eta} \quad \text{and} \quad \mathrm{Re}_{head}(x) = \frac{\rho_f \omega\left[2b_2(x)\right]^2}{4\eta} \tag{4.13}$$

The real (Γ_R) and imaginary (Γ_I) parts of the hydrodynamic function are found as a function of the Reynolds number, *Re*, and the aspect ratio, *h*/*b*, corresponding to any cross-section of the microcantilever, and are given, respectively, by

$$\Gamma_R\left(\mathrm{Re}, \frac{h}{b}\right) = \left[\frac{1}{\sqrt{\mathrm{Re}}}\sum_{m=0}^{m_{\max}} C_m\left(\frac{h}{b}\right)^{\frac{m}{2}}\right] + \left[\sum_{n=0}^{n_{\max}} D_n\left(\frac{h}{b}\right)^{\frac{n}{2}}\right] \tag{4.14}$$

$$\Gamma_I\left(\mathrm{Re}, \frac{h}{b}\right) = \left[\frac{1}{\mathrm{Re}}\sum_{p=0}^{p_{\max}} E_p\left(\frac{h}{b}\right)^{\frac{p}{2}}\right] + \left[\frac{1}{\sqrt{\mathrm{Re}}}\sum_{q=0}^{q_{\max}} F_q\left(\frac{h}{b}\right)^{\frac{q}{2}}\right] \tag{4.15}$$

The power indices and coefficients are determined, and repeated here for convenience, as m_{max}=2, n_{max}=4, p_{max}=1, q_{max}=4 and C_0=0.9003, C_1=0.6105, C_2=2.1722 and D_0=0, D_1=-0.0021, D_2=-0.1459, D_3=0.8255, D_4=-1.3388 and E_0=2.5758, E_1=-1.3388 and F_0=0.9003, F_1=-0.7121, F_2=1.6845, F_3=0.8236, F_4=0.4178.

In this work, an assumed mass density of 2330 kg/m^3 and Young's modulus of 169 GPa for silicon will be utilized through the entire simulation. It is also assumed that the

density and viscosity of water are 1000 kg/m^3 and 1 cP at 20°C, respectively. The density and viscosity of air are assumed to be 1.205 kg/m^3 and 0.01827 cP for 20°C, respectively.

Fig. 4-2 shows the normalized maximum deflections at the tip of the stem when the symmetric hammerhead microcantilevers [isosceles trapezoid, semi-circle, uniform rectangle and composite rectangle] laterally vibrate in air and water. The geometrical parameters that are associated with the investigated geometries are indicated in Table 4-2 for convenience.

Surface Dimensions [um^2]	h [um]	L_2 (R) [um]	b_2 [um]	b_3 [um]	L_3=b_4 [um]	d_{os} [um]
A-2-c	12	200	30.77	369.23	N/A	71.7949
B-2-c	12	159.5769	N/A	N/A	N/A	67.7265
C-2-c	12	200	200	N/A	N/A	100
D-2-c	12	200	282	38.5	80	44.46

Table 4-2: The investigated geometries of hammerhead microcantilevers for the frequency spectra in Fig. 4-2.

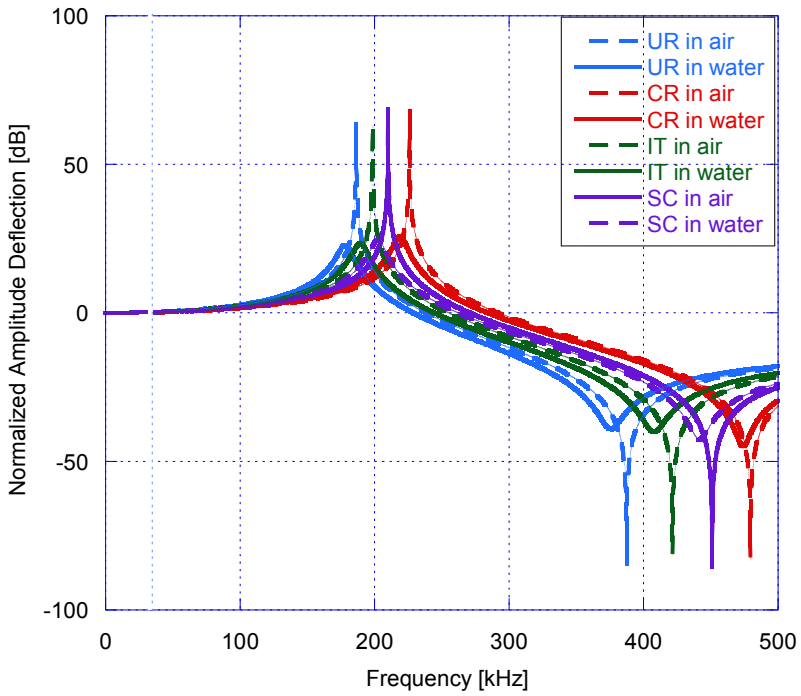

Figure 4-2: Calculated frequency spectra of four particular symmetric hammerhead microcantilevers, as indicated in Table 4-2, laterally vibrating in air and water.

It is shown in Fig. 4-2 that the resonance frequency for each laterally vibrating hammerhead microcantilever in water is always lower than that in air due to the additional liquid resistance. The liquid resistance comes from both the effective liquid mass and viscous damping. Due to the effect from the viscous damping, the frequency spectrum is broadened compared to the one in air. Since there are no analytical expressions for the resonance frequency in transverse and torsional modes in fluid (air and water), the undamped natural frequencies corresponding to the transverse and torsional modes in a vacuum are simulated using the numerical software (Comsol 4.1a). Since the differences between the resonance frequency in a vacuum and in air are very small, the resonance frequency in air can be approximated by that in a vacuum, for this group of geometries; the smallest difference of the resonance frequency between the first

torsional mode (in a vacuum) and first lateral mode (in air) is 17% for the rectangular hammerhead microcantilever. Thus, the hammerhead microcantilever geometry should be carefully designed to avoid the mode coupling issue. It is also found that the distance from the mass center of the uniform rectangular, isosceles trapezoid, semi-circular and composite rectangular head to the tip of each stem are 100 um, 71.7949 um, 67.7265um and 44.46 um, respectively. As the distance decreases, the resonance frequencies and quality factors increases for this particular studied group. However, this trend (for any particular head geometry) in the resonance frequency does not always hold true. The percent changes from air to water for the microcantilevers -uniform rectangle, isosceles trapezoid, semi-circle, and composite rectangle- are 4.4%, 4.56%, 3.62% and 3.14%, respectively. It is noted that the resonance frequency for the isosceles trapezoid hammerhead microcantilever is higher than that of the uniform rectangular hammerhead microcantilever in water; however, the percent difference from air to water for the isosceles trapezoid hammerhead microcantilever is slightly lower. This is due to the difference in the hydrodynamic force on the two different head geometries. As a result, further investigations regarding the trends of the sensor characteristics (resonance frequency, quality factor and mass sensitivity) as a function of the liquid properties and geometrical parameters are performed in the following sections.

To obtain these trends, a Matlab code is developed to determine the peak value corresponding to the frequency spectrum. This peak value also determines the resonance frequency of a laterally vibrating symmetrical hammerhead microcantilever. Then, the other sensor characteristics including resonance frequency, quality factor and mass sensitivity can be found.

4.2.1 Effects of the Liquid Properties on the Resonance Frequency

Effects of the density and viscosity of the liquids can be investigated individually by fixing one as a constant and varying the other property. However, these quantities are not associated with realistic examples of the operational liquid medium. For practical cases, different concentrations of glycerol-water and ethanol-water solution at 20°C are used to investigate the effects of liquid properties on the resonance frequencies for laterally vibrating symmetric hammerhead microcantilevers (isosceles trapezoid-shaped, semi-circular, uniform rectangular and composite rectangular head). The geometries of the microcantilevers studied in this section are those indicated in Table 4-2.

Table 4-3 indicates different concentrations of the glycerol-water solutions as well as the respective density and viscosity. It is shown in Fig. 4-3 that as the glycerol concentration in water increases, both density and viscosity will increase and the resonance frequency will decrease. It is due to the increase in the hydrodynamic force on the microcantilever (decrease in the Reynolds number) [110]. It is also noted that for most chemical sensors, the viscosity of operational liquid environment is lower than the high end of the glycerol-water solution.

Glycerol [%]	Density [kg/m^3]	Viscosity [cP]	Resonance Frequency [KHz]			
			IT	SC	UR	CR
0 (pure water)	1000	1.01	196.7	202.4	178.2	218.89
10	1022	1.31	195.7	201.6	177.3	218.08
20	1047	1.76	195.5	200.5	176.1	217.03
30	1073	2.50	192.9	198.9	174.5	215.59
40	1099	3.72	190.6	196.9	172.3	213.61
50	1126	6.00	187.2	193.7	169.0	210.61
60	1154	10.8	181.8	188.6	163.5	205.75
65	1168	15.2	177.7	184.8	159.6	202.18
70	1181	22.5	172.7	179.7	154.1	197.23
75	1195	35.5	164.1	172.2	146.3	190.09
80	1209	60.1	152.5	161.3	135.0	179.59
85	1222	109	135.6	145.6	119.2	164.24

Table 4-3: Calculated resonance frequencies of a particular group of symmetric hammerhead microcantilevers (microcantilever geometries as indicated in Table 4-2) laterally vibrating as a function of different concentrations of glycerol-water solutions at 20°C. Values of the density and viscosity of the glycerol-water solutions are from Ref 119.

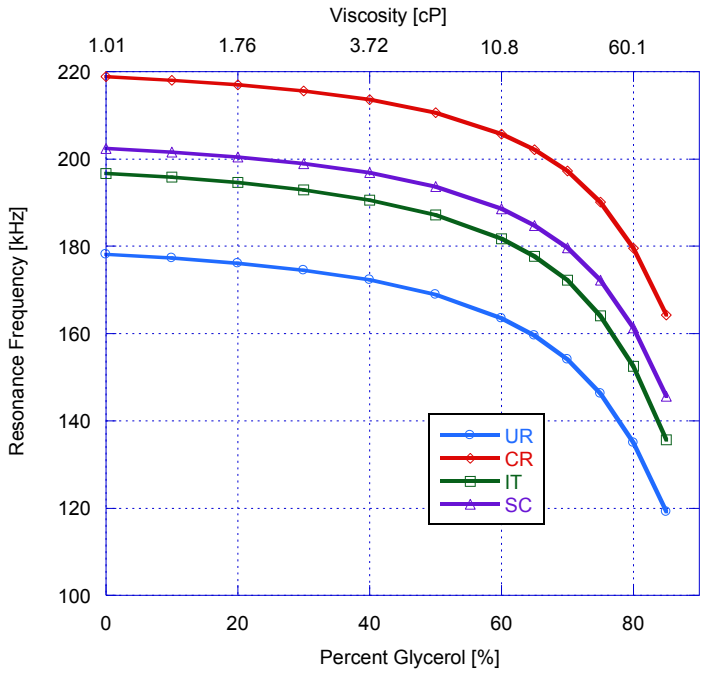

Figure 4-3: Trends of calculated resonance frequencies of a particular group of symmetric hammerhead microcantilevers (microcantilever geometries as indicated in Table 4-2) laterally vibrating as a function of different concentrations of glycerol-water solutions at 20°C.

Table 4-4 indicates different concentrations of the ethanol-water solutions as well as the respective density and viscosity. It is shown in Fig. 4-4 that as ethanol concentration in water increases, the density increases, however, the viscosity first increase then decrease. The resonance frequency first decreases then increases. This is due to the fact that the change in the resonance frequency mainly comes from the change in the change in the liquid medium's viscosity [110]. In Ref 110, it was also mentioned that, microcantilevers with higher Reynolds number would occasionally have lower resonance frequency due to the effect coming from the liquid density.

Ethanol [%]	Density [kg/m^3]	Viscosity [cP]	Resonance Frequency [KHz]			
			IT	SC	UR	CR
0 (pure water)	1000	1.01	196.7	202.4	178.2	218.89
10	984	1.54	195.5	201.3	177	217.78
20	970	2.18	194.3	200.1	175.8	216.7
30	956	2.71	193.4	199.4	175	215.95
40	937	2.91	193.3	199.2	174.8	215.8
50	915	2.87	193.5	199.4	175	215.98
60	893	2.67	194	199.8	175.5	216.4
70	869	2.37	194.7	200.5	176.2	217
80	845	2.01	195.6	201.2	176.9	217.72
90	819	1.61	196.5	202.1	177.9	218.56
100	791	1.2	197.6	203.1	179	219.46

Table 4-4: Calculated resonance frequencies of a particular group of symmetric hammerhead microcantilevers (microcantilever geometries as indicated in Table 4-2) laterally vibrating in different concentrations of ethanol-water solutions at 20°C. Values of the density and viscosity of the glycerol-water solutions are from Ref 119.

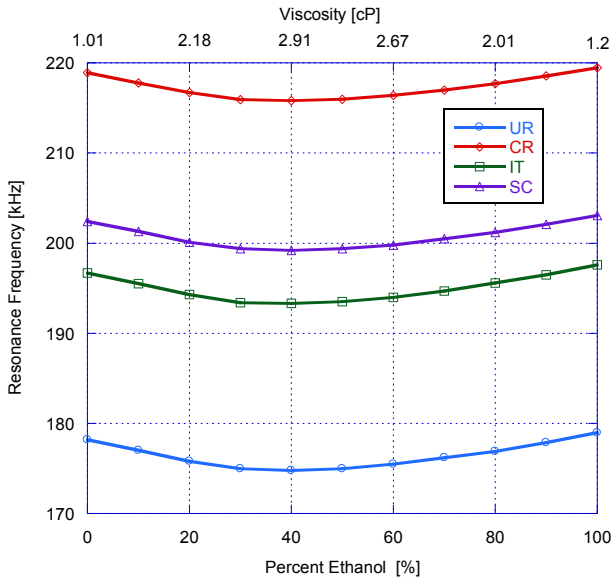

Figure 4-4: Trends of calculated resonance frequencies of a particular group of symmetric hammerhead microcantilevers (microcantilever geometries as indicated in Table 4-2) as a function of different concentrations of ethanol-water solutions at 20°C.

4.2.2 Effects of Dimensions of the Hammerhead Microcantilevers on the Resonance Frequency

In this section, the resonance frequency will be investigated as a function of the geometrical parameters of the hammerhead microcantilevers, indicated in Table 4-1. Due to the differences in the investigated head geometries, it is not trivial to find a general normalizing parameter which the resonance frequency depends on. Thus, the resonance frequency will be investigated in terms of the geometrical parameters for each case.

To solely study the effects of the thickness in the range of [2~15 (um)] on the resonance frequency, the geometries investigated are indicated in Table 4-5. It is shown in Fig. 4-5 that as the thickness increases, the resonance frequency will first increase at a high rate, then reaches a maximum and starts to slowly decrease. This trend was also noted for prismatic beams [110].

Surface Dimensions [um^2]	L_2 (R) [um]	b_3/ b_2	L_3=b_4 [um]	d_{os} [um]
A-2-c	200	1/12	N/A	71.7949
B-2-c	159.5769	N/A	N/A	67.7265
C-2-c	200	1	N/A	100
D-2-c	200	1	80	44.46

Table 4-5: Geometries of hammerhead microcantilevers used for the investigation of the effects of thickness on the resonance frequency.

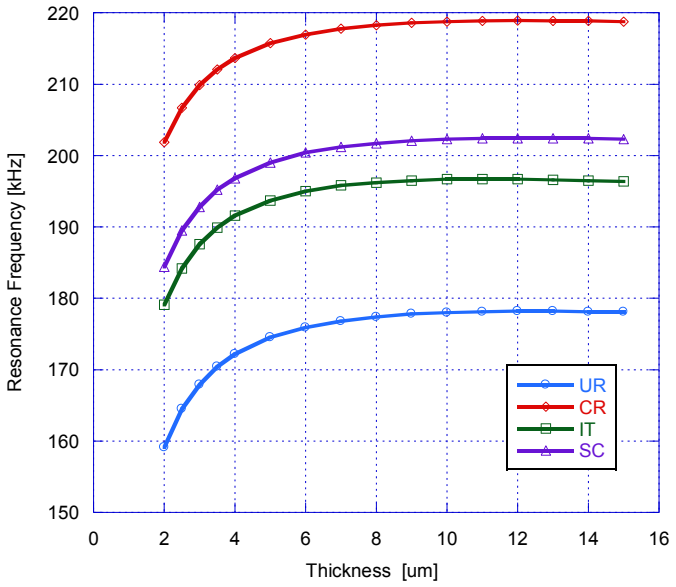

Figure 4-5: Trends of calculated resonance frequencies of a particular group of symmetric hammerhead microcantilevers, as indicated in Table 4-5, laterally vibrating in water with respect to different thicknesses.

Isosceles Trapezoid-shaped Hammerhead Microcantilever:

For an isosceles trapezoid-shaped hammerhead microcantilever [see Fig. 4-1 (A)] with a fixed stem and head, the parameters associated with its head include b_2, b_3 and L_2. For a constant surface head area, the change in these parameters will affect the distance

between the mass center of the head and the tip of the stem, d_{os}, which will change the resonance frequency. Thus, to investigate the effect of d_{os} on the resonance frequency, cases of [A-(1~3)-(a~c)], as indicated in Table 4-1, will be analyzed and the thicknesses of the microcantilevers will be fixed at 12 [um]. The ratio of b_3 and b_2 is constant and equal to 1/4. As the length of the head increases, in order to maintain the same surface area of the head, the length of b_2 and b_3 will decrease. It is shown in Fig.4-6, Fig. 4-7 and Fig. 4-8 that, for nine different cases, as L_2 increases, the distance between the mass center of the head and the tip of the stem will increase; the resonance frequency will first increase and then decrease.

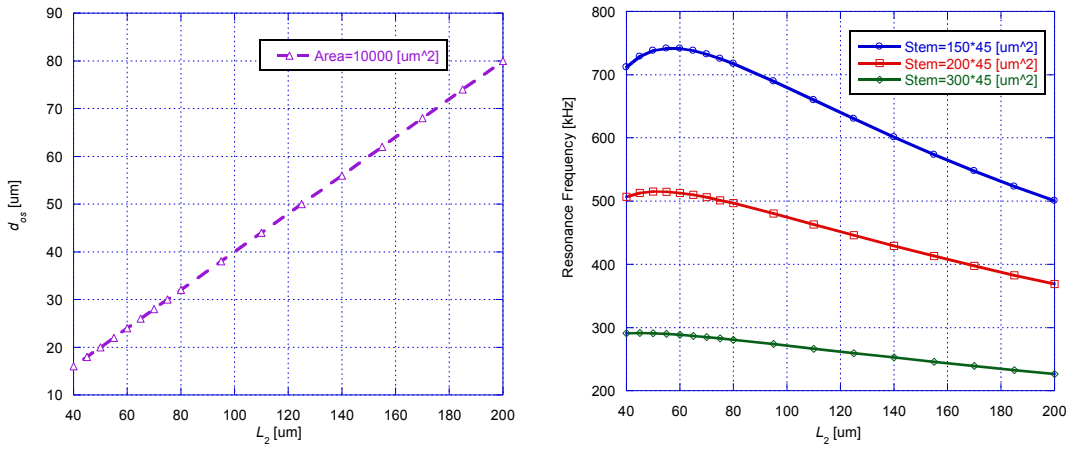

(a) (b)

Figure 4-6: (a) Distance between the mass center of the head and the tip of the stem and (b) calculated resonance frequency as a function of L_2 for three cases [A-(1~3)-a].

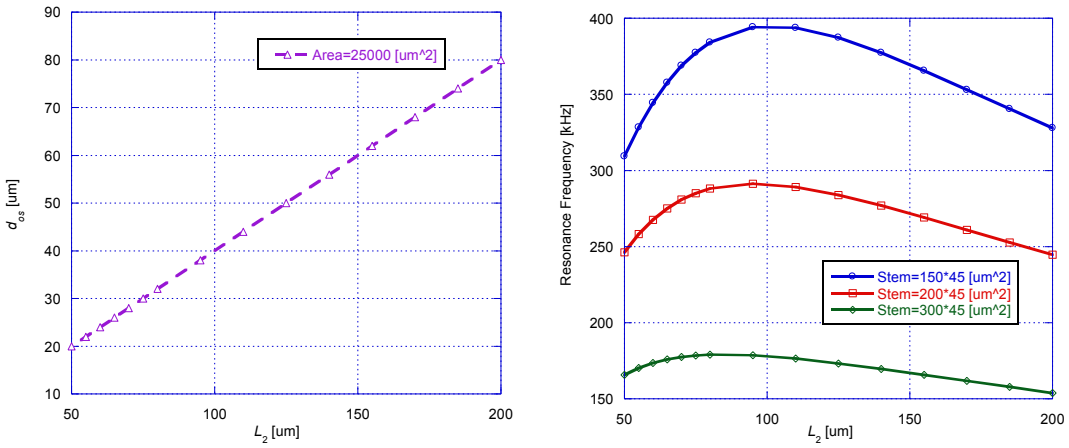

(a) (b)

Figure 4-7: (a) Distance between the mass center of the head and the tip of the stem and (b) calculated resonance frequency as a function of L_2 for three cases [A-(1~3)-b].

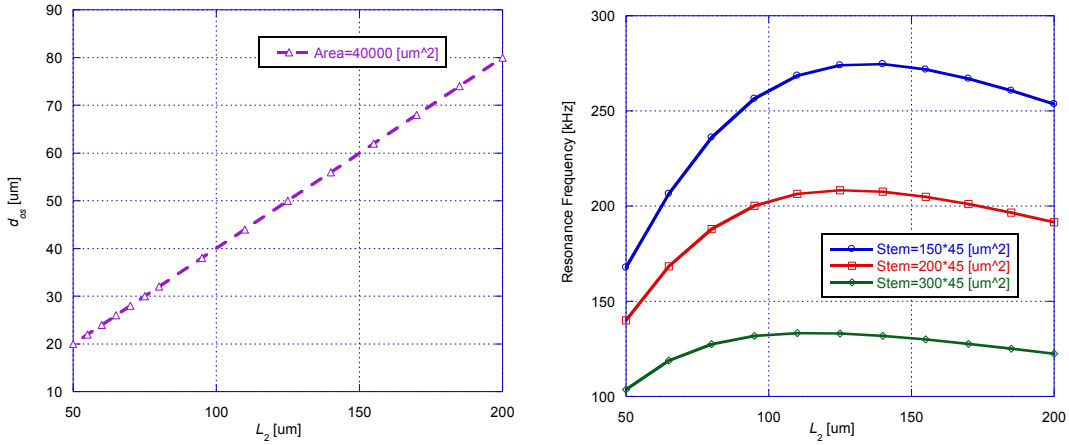

(a) (b)

Figure 4-8: (a) Distance between the mass center of the head and the tip of the stem and (b) calculated resonance frequency as a function of L_2 for three cases [A-(1~3)-c].

Semi-circular Hammerhead Microcantilever:

For semi-circular hammerhead microcantilevers [see Fig. 4-1 (B)], the radius of the head is determined for a fixed surface area of the head. Table 4-6 indicates the investigated cases [B-(1~3)-(a-c)]. It is found that, as the surface area of the semi-circular head increases, the radius of the semi-circular head and the distance between the mass center of the semi-circular head and the tip of the stem will increase, but the resonance frequency will decrease. This is due to the increase in the head mass.

Stem [um^3]	Resonance Frequency [KHz]		
	Head Area=10000 [um^2]	Head Area=25000 [um^2]	Head Area=40000 [um^2]
150×45×12	713	493.7	279.3
200×45×12	384.1	281.4	171.8
300×45×12	269.2	202.4	128.3

Table 4-6: Calculated resonance frequency for investigated cases [B-(1~3)-(a-c)].

Uniform Rectangular Hammerhead Microcantilever:

For a uniform rectangular hammerhead microcantilever [see Fig. 4-1 (C)] with a fixed stem and head, the change in b_2 or L_2 will affect the distance between the mass center of the head and the tip of the stem, d_{os}, which will change the resonance frequency. Thus, to investigate the effect of the position of the mass center of the head on the resonance frequency, cases of [C-(1~3)-(a~c)], as indicated in Table 4-1, will be analyzed and the thicknesses of the microcantilevers are fixed at 12 [um]. By varying the ratio between the width and length of the head (b_2/L_2), the distance between the mass center of the head and the tip of the stem and the resonance frequency can be found. As the length or width of the head increases, in order to maintain the same surface area of the head, the

width or length of the head will decrease, respectively. It is shown in Fig. 4-9, Fig 4-10 and Fig. 4-11 that, for nine different cases, as the ratio of b_2/L_2 increases, the mass center of the head will shift towards the tip of the stem; the resonance frequency will first increase and then decrease.

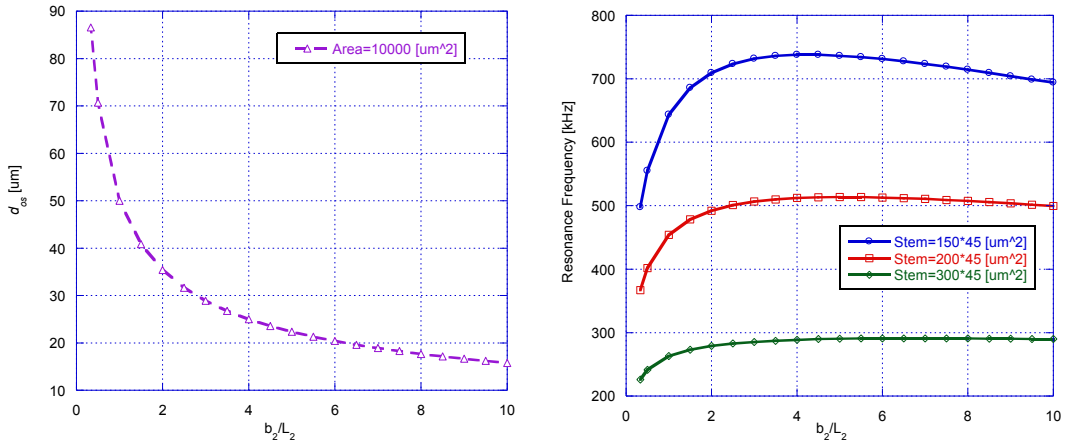

(a) (b)

Figure 4-9: (a) Distance between the mass center of the head and the tip of the stem and (b) calculated resonance frequency as a function of b_2/L_2 for three cases [C-(1~3)-a].

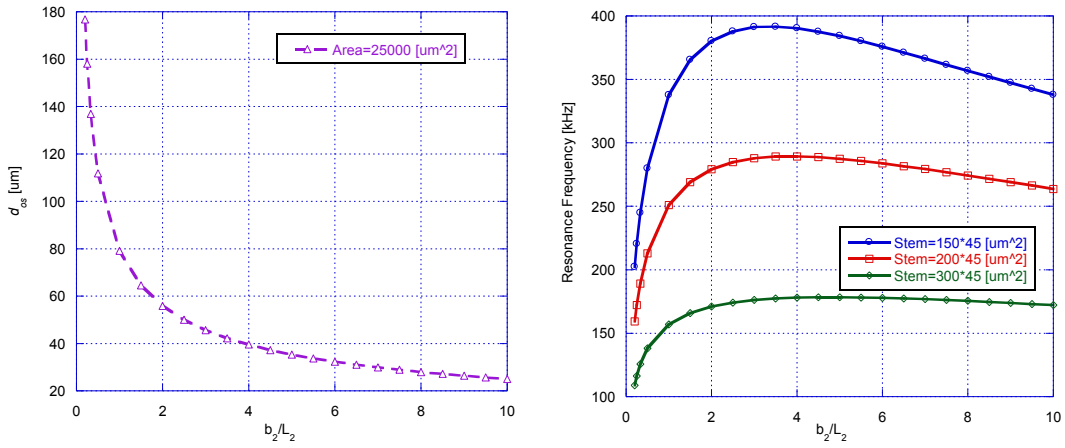

(a) (b)

Figure 4-10: (a) Distance between the mass center of the head and the tip of the stem and (b) calculated resonance frequency as a function of b_2/L_2 for three cases [C-(1~3)-b].

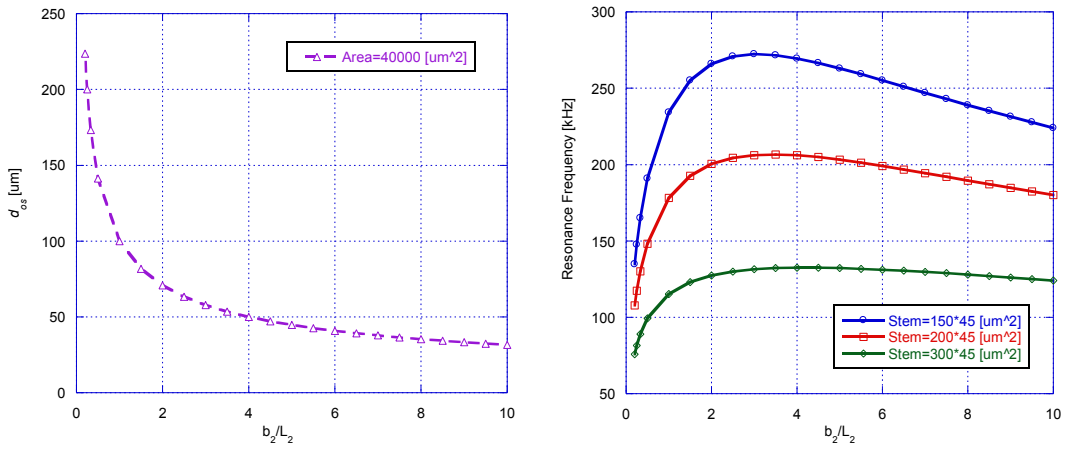

(a) (b)

Figure 4-11: (a) Distance between the mass center of the head and the tip of the stem and (b) calculated resonance frequency as a function of b_2/L_2 for three cases [C-(1~3)-c].

Composite Rectangular Hammerhead Microcantilever:

For a composite rectangular hammerhead microcantilever [see Fig. 4-1 (D)] with a fixed stem and head, the change in the dimensions of the gap ($b_4 \times L_3$) will affect the distance between the mass center of the head and the tip of the stem, d_{os}, which will change the resonance frequency. Thus, to investigate the effects of position of the mass center of the head on the resonance frequency, cases of [D-(1~3)-(a~c)], as indicated in Table 4-1, will be analyzed and the thicknesses of the microcantilevers are fixed at 12 [um]. By varying the dimensions of the gap (assuming $b_4=L_3$), the resonance frequency can be found as a function of the distance between the mass center of the head and the tip of the stem. As the dimensions of the gap increase, in order to maintain the same surface area of the head, the width the head (b_2) will increase for a head with a constant length (L_2). It is shown in Fig. 4-12, Fig 4-13 and Fig. 4-14 that, for nine different cases, as the dimensions of the gap increases, the mass center of the head will shift towards the support end of the stem; the resonance frequency will first increase and then decrease.

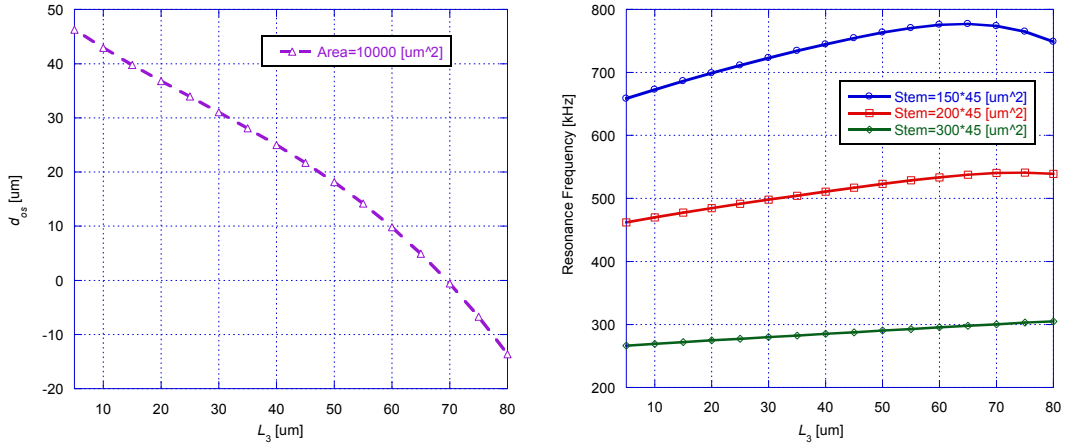

(a) (b)

Figure 4-12: (a) Distance between the mass center of the head and the tip of the stem and (b) calculated resonance frequency as a function of L_3 for three cases [D-(1~3)-b] and L_2=100 [um].

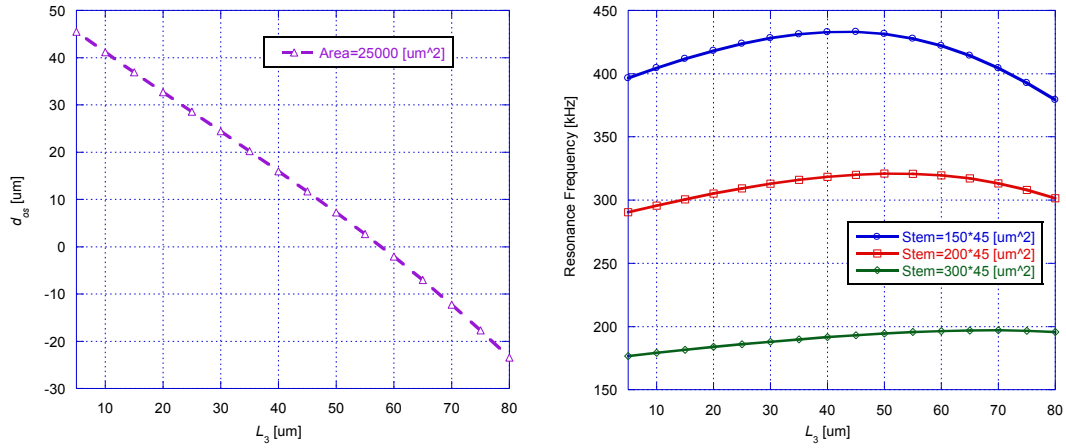

(a) (b)

Figure 4-13: (a) Distance between the mass center of the head and the tip of the stem and (b) calculated resonance frequency as a function of L_3 for three cases [D-(1~3)-a] and L_2=100 [um].

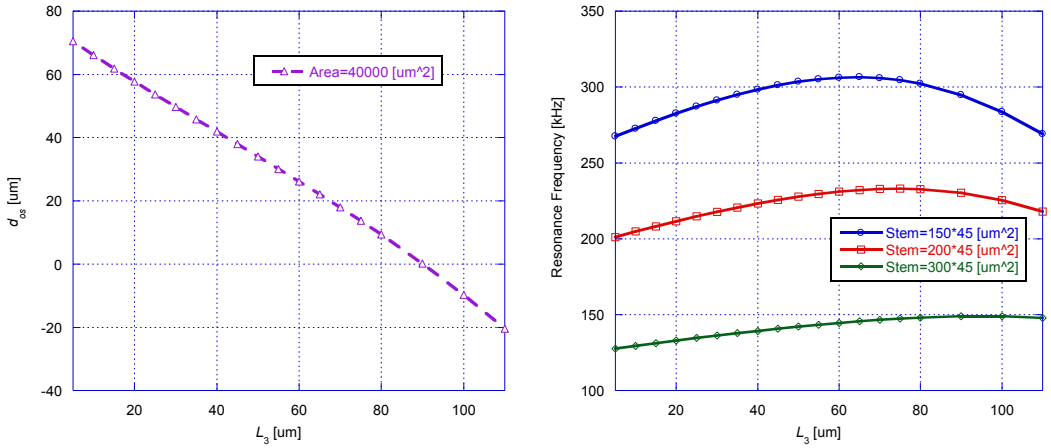

(a) (b)

Figure 4-14: (a) Distance between the mass center of the head and the tip of the stem and (b) calculated resonance frequency as a function of L_3 for three cases [D-(1~3)-c] and L_2=150 [um].

For the investigated cases including A-(1~3)-(a~c), C-(1~3)-(a~c) and D-(1~3)-(a~c), as the distance between the mass center of the head and the tip of the stem increases, the resonance frequency will first increase and then decrease. Such trend has been also found for the undamped case and confirmed using numerical analysis (Comsol 4.1a). This trend for the damped system may be explained based on the undamped system. For an undamped oscillating system, the resonance frequency is defined by the square root of the total potential energy divided by the total kinetic energy [60]. The total potential energy does not change due to a fixed stem. For a fixed head area, as d_{os} decreases, the change in the geometrical parameters of the head will cause the total kinetic energy to first decrease and then increase, which may yield the resonance frequency to first increase and then decrease. For example, for a uniform rectangular hammerhead microcantilever, the kinetic energy of the head consists of the translational kinetic energy and the rotational kinetic energy. As the mass center of the head moves towards the tip of the stem (ratio of b_2/L_2 increases), the translational kinetic energy of the head will keep decreasing (down to a constant value), but the rotational kinetic energy of the head will first decrease and then increase. Thus, the total kinetic energy of the head will first decrease and then increase, which means that the resonance frequency will first increase and then decrease. For the investigated cases [B-(1~3)-(a-c)], it is found that, as the surface area of the semi-circular head increases, the radius of the semi-circular head and the distance between the mass center of the semi-circular head and the tip of the stem will increase, but the resonance frequency will decrease. This is due to the increase in the head mass.

4.3 Quality Factor

For microcantilevers operated in a viscous liquid, the liquid resistance will decrease the performance of the microcantilevers. The increase in the viscous damping significantly broadens the frequency spectrum, hence causes the quality factor to decrease. There are two approaches used in defining the quality factor. The first definition is 2π times the ratio of the maximum mechanical energy stored in the system to the amount of energy dissipated in one cycle, and is given by Eq. 4.16. The second definition is the ratio of the resonance frequency to the 3dB bandwidth of the resonating system, and is given by Eq. 4.17.

$$Q_{energy} = 2\pi \frac{Maximum\ \ Mechanical\ Energy}{Energy\ Dissipated\ \ per\ Cycle} = 2\pi \frac{\left(U_{total} + T_{total}\right)_{\max}}{\Delta W} \tag{4.16}$$

$$Q_{3db} = \frac{f_{res}}{\Delta f_{3dB}} \tag{4.17}$$

In Eq. 4.16, U_{total} and T_{total} designate, respectively, the total potential energy and total kinetic energy of an arbitrary, symmetric hammerhead microcantilever. Since the head is assumed to be rigid, the total potential energy only comes from the potential energy of the stem. The total kinetic energy of the hammerhead microcantilever consists of the kinetic energy from the stem and head. Since the head has both translational motion and rotational motion, the kinetic energy of the head consists of the translational and rotational kinetic energy, and is given by Eq.4.18 and Eq. 4.19:

$$\begin{aligned} U_{total} &= U_{stem} + U_{head} \\ &= \frac{1}{2}\frac{EI_{stem}\theta_0^{\,2}}{L_1}\int_0^1 \left[\frac{\partial \overline{v}_{stem}^{\,2}\left(\xi,\tau\right)}{\partial \xi^2}\right]^2 d\xi \end{aligned} \tag{4.18}$$

$$
\begin{aligned}
T_{total} = {} & \frac{1}{2} m_{stem} \omega^2 L_1{}^2 \theta_0{}^2 \int_0^1 \left[\frac{\partial \overline{v}_{stem}(\xi,\tau)}{\partial \tau} \right]^2 d\xi + \frac{1}{2} m_{head} \omega^2 \theta_0{}^2 L_1{}^2 \left[\frac{\partial \overline{v}_{stem}(\xi,\tau)}{\partial \tau}\Big|_{\xi=1} \right]^2 \\
& + m_{head} \omega^2 \theta_0{}^2 L_1 d_{os} \left[\frac{\partial \overline{v}_{stem}(\xi,\tau)}{\partial \tau}\Big|_{\xi=1} \right] \left[\frac{\partial^2 \overline{v}_{stem}(\xi,\tau)}{\partial \xi \partial \tau}\Big|_{\xi=1} \right] \\
& + \frac{1}{2} m_{head} \omega^2 \theta_0{}^2 d_{os}{}^2 \left[\frac{\partial^2 \overline{v}_{stem}(\xi,\tau)}{\partial \xi \partial \tau}\Big|_{\xi=1} \right]^2 + \frac{1}{2} J_{head} \omega^2 \theta_0{}^2 \left[\frac{\partial^2 \overline{v}_{stem}(\xi,\tau)}{\partial \xi \partial \tau}\Big|_{\xi=1} \right]^2
\end{aligned} \tag{4.19}
$$

In practical applications, a real harmonic load of the equivalent support rotation, $\theta_0 cos\tau$ is considered, so the normalized displacement of the stem is given by [101]

$$
\overline{v}_{stem}(\xi,\tau) = real\left[\overline{X}(\xi) e^{j\tau} \right] \tag{4.20}
$$

In Eq. 4.20, $\overline{X}(\xi)$ is noted as the normalized shape function of the stem. Substituting Eq. 4.20 into Eq. 4.18 and Eq.4.19 gives the corresponding energies of the hammerhead microcantilever as follows:

$$
U_{stem} = \frac{1}{2} \frac{EI_{stem} \theta_0{}^2}{L_1} \left(\beta_1 \cos^2\tau + \beta_2 \sin^2\tau - 2\beta_3 \cos\tau \sin\tau \right) \tag{4.21}
$$

$$
T_{stem} = \frac{1}{2} m_{stem} L_1{}^2 \omega^2 \theta_0{}^2 \left(\beta_4 \sin^2\tau + \beta_5 \cos^2\tau + 2\beta_6 \sin\tau \cos\tau \right) \tag{4.22}
$$

$$
\begin{aligned}
T_{head} = {} & \frac{1}{2} m_{head} \omega^2 \theta_0{}^2 L_1{}^2 \left(\beta_7 \sin^2\tau + \beta_8 \cos^2\tau + 2\beta_9 \sin\tau \cos\tau \right) \\
& + m_{head} d_{os} \omega^2 \theta_0{}^2 L_1 \left(\beta_{10} \sin^2\tau + \beta_{11} \cos^2\tau + \beta_{12} \sin\tau \cos\tau \right) \\
& + \frac{1}{2} m_{head} d_{os}{}^2 \omega^2 \theta_0{}^2 \left(\beta_{13} \sin^2\tau + \beta_{14} \cos^2\tau + 2\beta_{15} \sin\tau \cos\tau \right) \\
& + \frac{1}{2} J_{head} \omega^2 \theta_0{}^2 \left(\beta_{16} \sin^2\tau + \beta_{17} \cos^2\tau + 2\beta_{18} \sin\tau \cos\tau \right)
\end{aligned} \tag{4.23}
$$

where

$$
\beta_1 = \int_0^1 \left\{ real\left[\frac{\partial^2 \overline{X}(\xi)}{\partial \xi^2} \right] \right\}^2 d\xi , \tag{4.24a}
$$

$$
\beta_2 = \int_0^1 \left\{ imag\left[\frac{\partial^2 \overline{X}(\xi)}{\partial \xi^2} \right] \right\}^2 d\xi , \tag{4.24b}
$$

$$\beta_3 \equiv \int_0^1 real\left[\frac{\partial^2 \bar{X}(\xi)}{\partial \xi^2}\right] imag\left[\frac{\partial^2 \bar{X}(\xi)}{\partial \xi^2}\right] d\xi \tag{4.24c}$$

$$\beta_4 = \int_0^1 \left\{real\left[\bar{X}(\xi)\right]\right\}^2 d\xi\,, \tag{4.24d}$$

$$\beta_5 = \int_0^1 \left\{imag\left[\bar{X}(\xi)\right]\right\}^2 d\xi\,, \tag{4.24e}$$

$$\beta_6 = \int_0^1 real\left[\bar{X}(\xi)\right] imag\left[\bar{X}(\xi)\right] d\xi \tag{4.24f}$$

$$\beta_7 = \left\{real\left[\bar{X}(1)\right]\right\}^2, \tag{4.24g}$$

$$\beta_8 = \left\{imag\left[\bar{X}(1)\right]\right\}^2, \tag{4.24h}$$

$$\beta_9 = real\left[\bar{X}(1)\right] imag\left[\bar{X}(1)\right] \tag{4.24i}$$

$$\beta_{10} = real\left[\bar{X}(1)\right] real\left[\frac{\partial \bar{X}'(\xi)}{\partial \xi}\Big|_{\xi=1}\right], \tag{4.24j}$$

$$\beta_{11} = imag\left[\bar{X}(1)\right] imag\left[\frac{\partial \bar{X}'(\xi)}{\partial \xi}\Big|_{\xi=1}\right] \tag{4.24k}$$

$$\beta_{12} = real\left[\bar{X}(1)\right] imag\left[\frac{\partial \bar{X}'(\xi)}{\partial \xi}\Big|_{\xi=1}\right] + real\left[\frac{\partial \bar{X}'(\xi)}{\partial \xi}\Big|_{\xi=1}\right] imag\left[\bar{X}(1)\right] \tag{4.24l}$$

$$\beta_{13} = \beta_{16} = \left\{real\left[\frac{\partial \bar{X}'(\xi)}{\partial \xi}\Big|_{\xi=1}\right]\right\}^2, \tag{4.24m}$$

$$\beta_{14} = \beta_{17} = \left\{imag\left[\frac{\partial \bar{X}'(\xi)}{\partial \xi}\Big|_{\xi=1}\right]\right\}^2 \tag{4.24n}$$

$$\beta_{15} = \beta_{18} = real\left[\frac{\partial \bar{X}'(\xi)}{\partial \xi}\Big|_{\xi=1}\right] imag\left[\frac{\partial \bar{X}'(\xi)}{\partial \xi}\Big|_{\xi=1}\right], \tag{4.24o}$$

Since the total mechanical energy of the hammerhead microcantilever does not change over one cycle in the steady state response, the energy lost due to the surrounding liquid per cycle is equal to the work done in imposing the support end rotation over one cycle, given by [101]:

$$\Delta W = \frac{EI_{stem}\theta_0^{\,2}}{L_1}\int_0^{2\pi}\left[\frac{\partial^2 \overline{v}_{stem}(\xi,\tau)}{\partial \xi^2}\Big|_{x=0}\right]\sin\tau d\tau = \beta_{19}\frac{\pi EI_{stem}\theta_0^{\,2}}{L_1}, \tag{4.25}$$

where

$$\beta_{19} = -imag\left[\frac{\partial^2 \overline{X}(\xi)}{\partial \xi^2}\Big|_{\xi=0}\right], \tag{4.26}$$

Substituting Eq. 4.18 - Eq. 4.26 into Eq. 4.16 yields the quality factor as follows:

$$Q(\tau) = \frac{\max\limits_{\tau}\left[F(\tau)\right]}{\beta_{19}}, \tag{4.27}$$

where

$$\begin{aligned} F(\tau) = {} & \beta_1\cos^2\tau + \beta_2\sin^2\tau - 2\beta_3\cos\tau\sin\tau \\ & + \frac{m_{stem}L_1^{\,3}\omega^2}{EI_{stem}}\left(\beta_5\cos^2\tau + \beta_5\sin^2\tau + 2\beta_6\cos\tau\sin\tau\right) \\ & + \frac{m_{head}L_1^{\,3}\omega^2}{EI_{stem}}\left(\beta_7\cos^2\tau + \beta_8\sin^2\tau + 2\beta_9\cos\tau\sin\tau\right) \\ & + \frac{2m_{head}L_1^{\,2}d_{os}\omega^2}{EI_{stem}}\left(\beta_{10}\cos^2\tau + \beta_{11}\sin^2\tau + 2\beta_{12}\cos\tau\sin\tau\right) \\ & + \frac{m_{head}L_1 d_{os}^{\,2}\omega^2}{EI_{stem}}\left(\beta_{13}\cos^2\tau + \beta_{14}\sin^2\tau + 2\beta_{15}\cos\tau\sin\tau\right) \\ & + \frac{J_{head}L_1\omega^2}{EI_{stem}}\left(\beta_{16}\cos^2\tau + \beta_{17}\sin^2\tau + 2\beta_{18}\cos\tau\sin\tau\right) \end{aligned}, \tag{4.28}$$

4.3.1 Effects of the Liquid Properties on the Quality Factor

In this section, the quality factor using the energy definition and 3-dB bandwidth definition are calculated and compared for different concentrations of glycerol-water and

ethanol-water solutions. A Matlab code is written to evaluate Eq. 4.27. The results of trend of the quality factor as a function of different concentrations of glycerol-water and ethanol-water solutions are shown in Fig. 4-15. The geometries of the hammerhead microcantilevers are the same as those investigated in Sec. 4.2.1.

It is shown in Fig. 4-15 that the range of the percent differences between the quality factors obtained using the two definitions is [0~29%]. It is found that the highest percent difference occurs at the highest viscosity (smallest quality factor). In this study, for the values of the quality factors which are greater than 10, the percent differences are always below 5%, which means either of these methods can be used to obtain the quality factors. For convenience, the 3-dB definition of quality factor will be applied in obtaining the quality factors in the following sections.

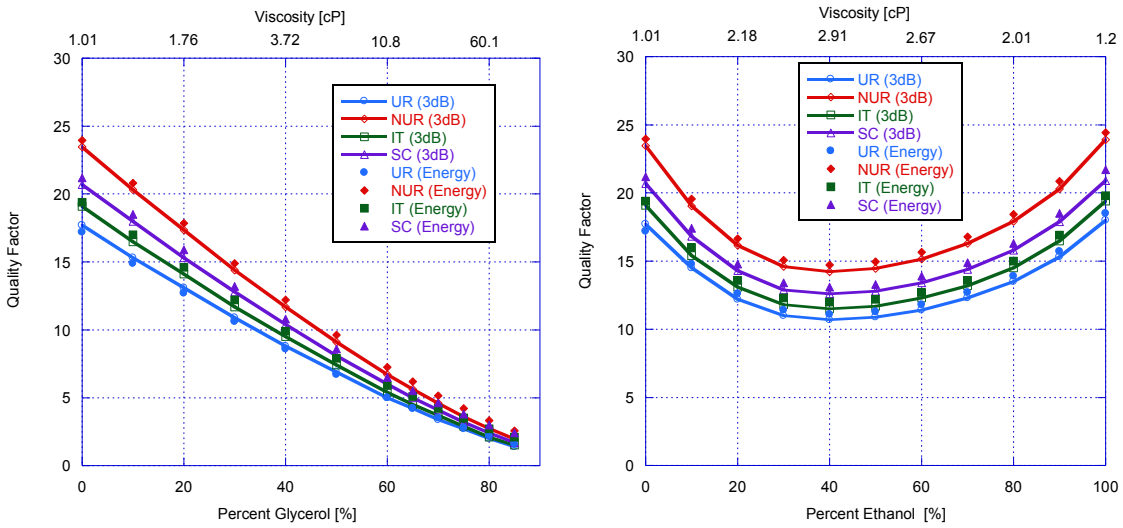

Figure 4-15: Trends of the calculated quality factors (two methods) of a particular group of symmetric hammerhead microcantilevers laterally vibrating in different concentrations of glycerol-water and ethanol-solutions at 20°C.

4.3.2 Effects of Dimensions of the Hammerhead Microcantilevers on the Quality Factor

In this section, the quality factor will be investigated as a function of the geometrical parameters of the hammerhead microcantilevers, as indicated in Table 4-1. To solely study the effects of the thickness in the range of [2~15 (um)] on the quality factor, the investigated geometries are indicated in Table 4-5. Fig. 4-16 shows that the quality factor appears to be linearly dependent on the thickness. In general, it is found that, when exciting a microcantilever laterally, shorter, thicker and wider beams will have higher quality factors [110].

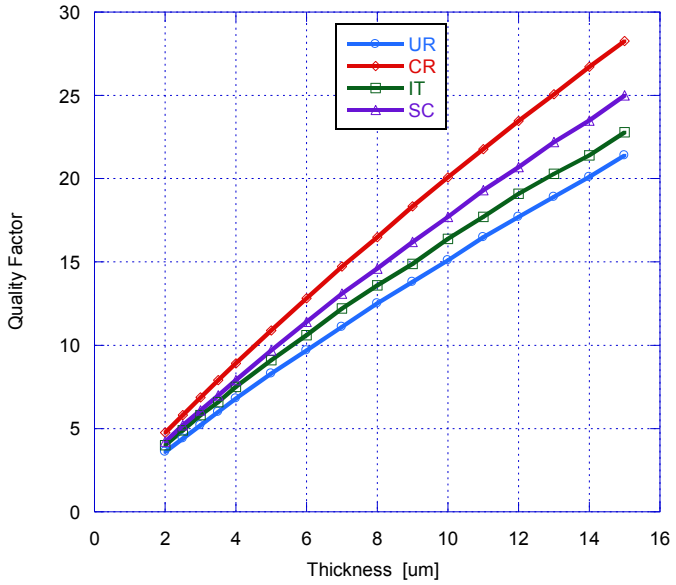

Figure 4-16: Trends of calculated quality factors for a particular group of symmetric hammerhead microcantilevers (geometries same as in Fig. 4-5) as a function of the thickness.

Isosceles Trapezoid-shaped Hammerhead Microcantilever:

The quality factor for an isosceles trapezoid-shaped hammerhead microcantilever will be investigated as a function of the distance between the mass center of the head and the tip of the stem in this part. The investigated cases of [A-(1~3)-(a~c)] are indicated in Table 4-1. The thicknesses of the microcantilevers are fixed at 12 [um] and the ratio of b_3 and b_2 is constant and equal to 1/4. It is shown in Fig.4-17, Fig. 4-18 and Fig. 4-19 that, for nine different cases, as L_2 increases, the distance between the mass center of the head and the tip of the stem will increase, but the quality factor will decrease.

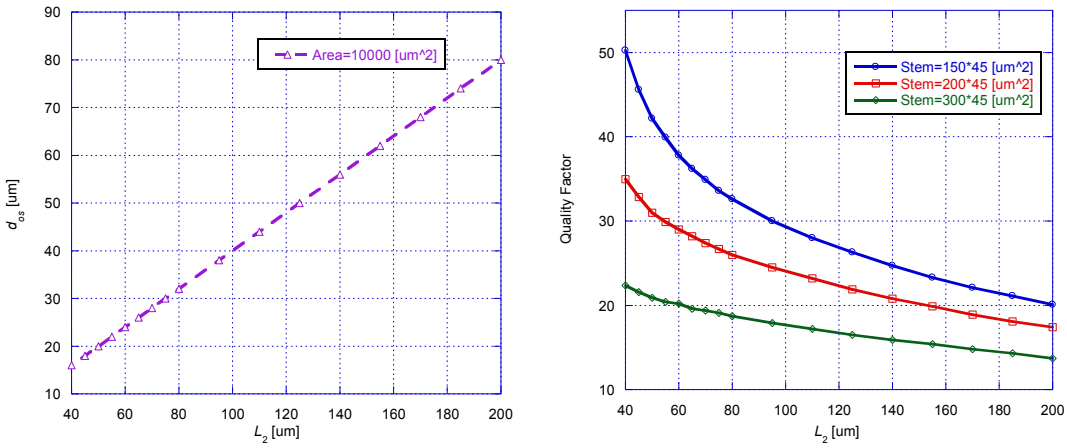

(a) (b)

Figure 4-17: (a) Distance between the mass center of the head and the tip of the stem and (b) calculated quality factor as a function of L_2 for three cases [A-(1~3)-a].

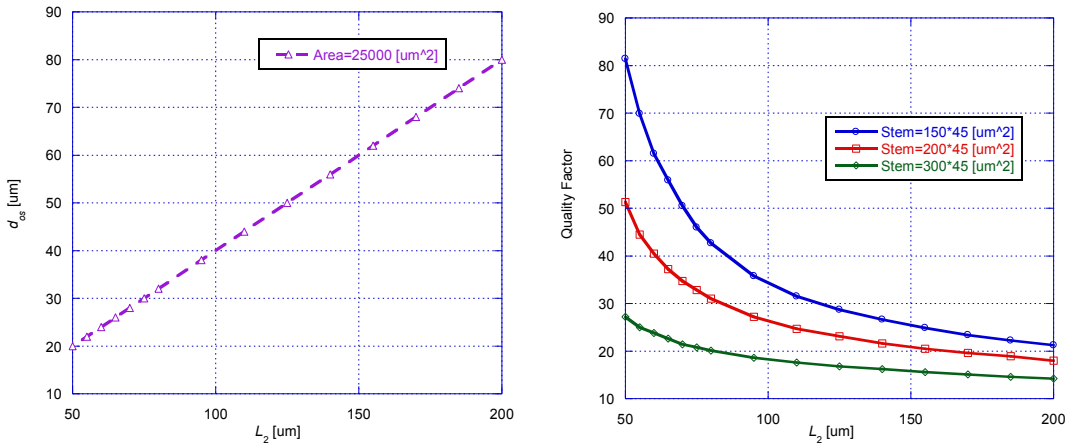

(a) (b)

Figure 4-18: (a) Distance between the mass center of the head and the tip of the stem and (b) calculated quality factor as a function of L_2 for three cases [A-(1~3)-a].

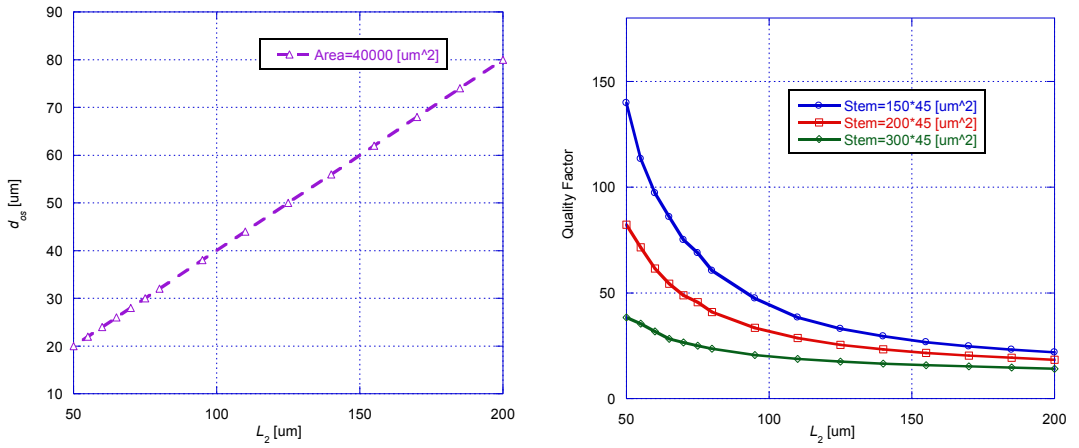

(a) (b)

Figure 4-19: (a) Distance between the mass center of the head and the tip of the stem and (b) calculated quality factor as a function of L_2 for three cases [A-(1~3)-a].

Semi-circular Hammerhead Microcantilever:

Table 4-7 indicates the investigated cases of [B-(1~3)-(a-c)] and their quality factors. It is found that, as the surface area of the semi-circular head increases, the radius of the

semi-circular head and will increase, but the quality factor will decrease. This is due to a more rapid decrease in the resonance frequency compared to the 3-dB bandwidth.

Stem [um^3]	Quality Factor		
	Area=10000 [um^2]	Area=25000 [um^2]	Area=40000 [um^2]
150×45×12	32.3	25.8	18.7
200×45×12	27.8	22.5	16.7
300×45×12	25.2	20.7	15.5

Table 4-7: Calculated quality factor for investigated cases [B-(1~3)-(a-c)].

Uniform Rectangular Hammerhead Microcantilever:

For a uniform rectangular hammerhead microcantilever [see Fig. 4-1 (C)] with a fixed stem and head, the change in b_2 or L_2 will affect the distance between the mass center of the head and the tip of the stem, d_{os}, which will change the quality factor. Thus, to investigate the effects of the position of the mass center of the head on the quality factor, cases of [C-(1~3)-(a~c)], as indicated in Table 4-1, will be analyzed and the thicknesses of the microcantilevers are fixed at 12 [um]. By varying the ratio between the width and length of the head (b_2/L_2), the distance between the mass center of the head and the tip of the stem and the quality factor can be found. It is shown in Fig. 4-20, Fig 4-21 and Fig. 4-22 that, for nine different cases, as the ratio of b_2/L_2 increases, the mass center of the head will shift towards the tip of the stem; the quality factor will increase.

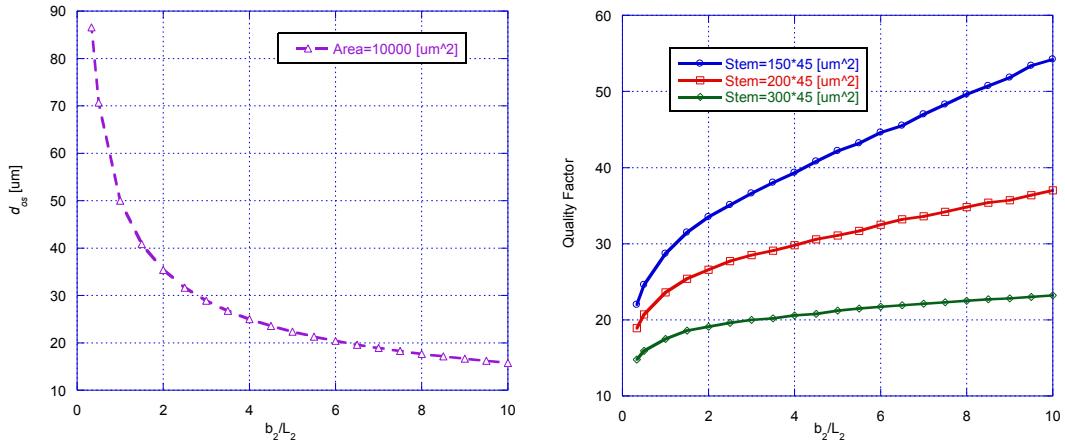

(a) (b)

Figure 4-20: (a) Distance between the mass center of the head and the tip of the stem and (b) calculated quality factor as a function of b_2/L_2 for three cases [C-(1~3)-a].

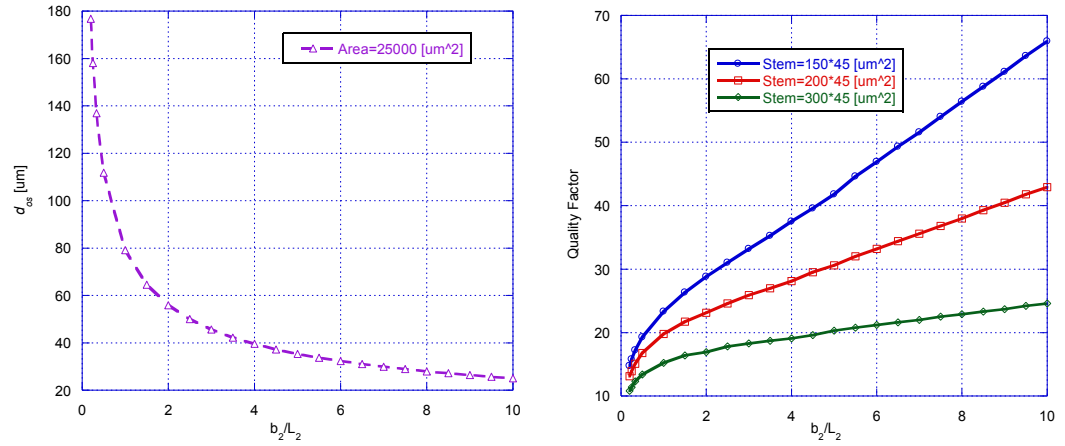

(a) (b)

Figure 4-21: (a) Distance between the mass center of the head and the tip of the stem and (b) calculated quality factor as a function of b_2/L_2 for three cases [C-(1~3)-b].

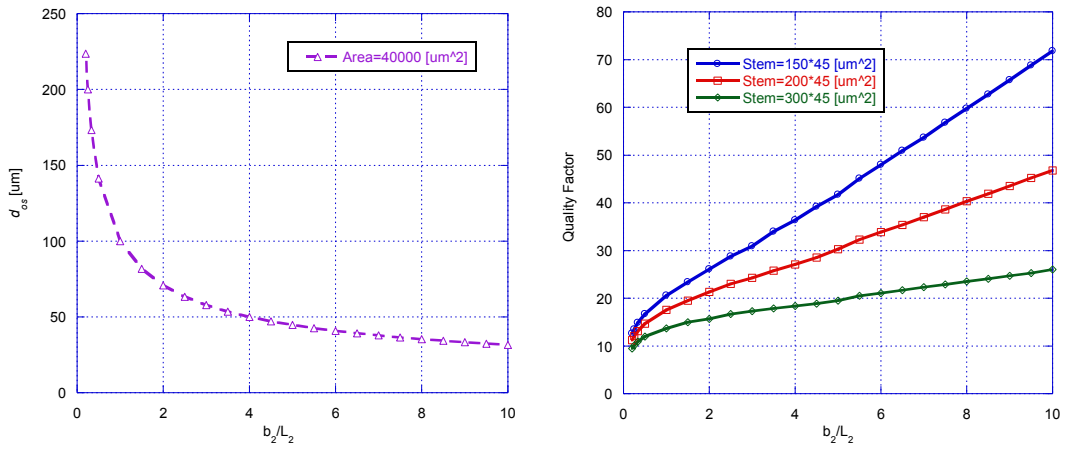

(a) (b)

Figure 4-22: (a) Distance between the mass center of the head and the tip of the stem and (b) calculated quality factor as a function of b_2/L_2 for three cases [C-(1~3)-c].

Composite Rectangular Hammerhead Microcantilever:

To investigate the effects of position of the mass center of the head on the quality factor for a composite rectangular hammerhead microcantilever [see Fig. 4-1 (D)], cases of [D-(1~3)-(a~c)], as indicated in Table 4-1, will be analyzed and the thicknesses of the microcantilevers are fixed at 12 [um]. By varying the dimensions of the gap (assuming b_4=L_3), the quality factor can be found as a function of the distance between the mass center of the head and the tip of the stem. It is shown in Fig. 4-23, Fig 4-24 and Fig. 4-25 that, for nine different cases, as the dimensions of the gap increases, the mass center of the head will shift towards the support end of the stem; the quality factor will keep increasing.

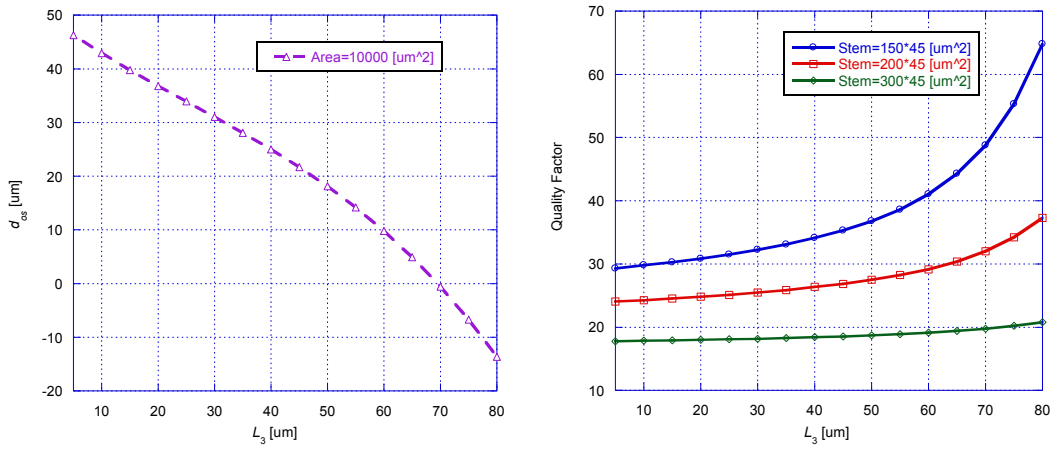

(a) (b)

Figure 4-23: (a) Distance between the mass center of the head and the tip of the stem and (b) calculated quality factor as a function of L_3 for three cases [D-(1~3)-a] and L_2=100 [um].

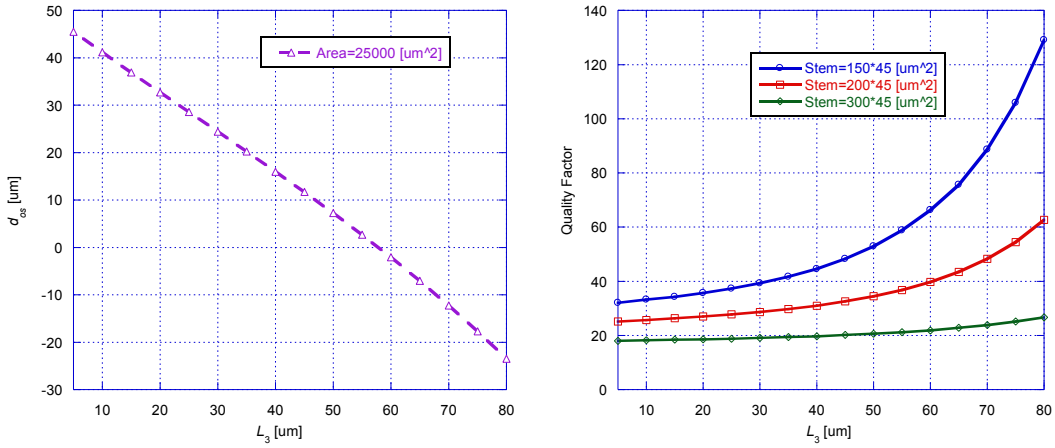

(a) (b)

Figure 4-24: (a) Distance between the mass center of the head and the tip of the stem and (b) calculated quality factor as a function of L_3 for three cases [D-(1~3)-b] and L_2=100 [um].

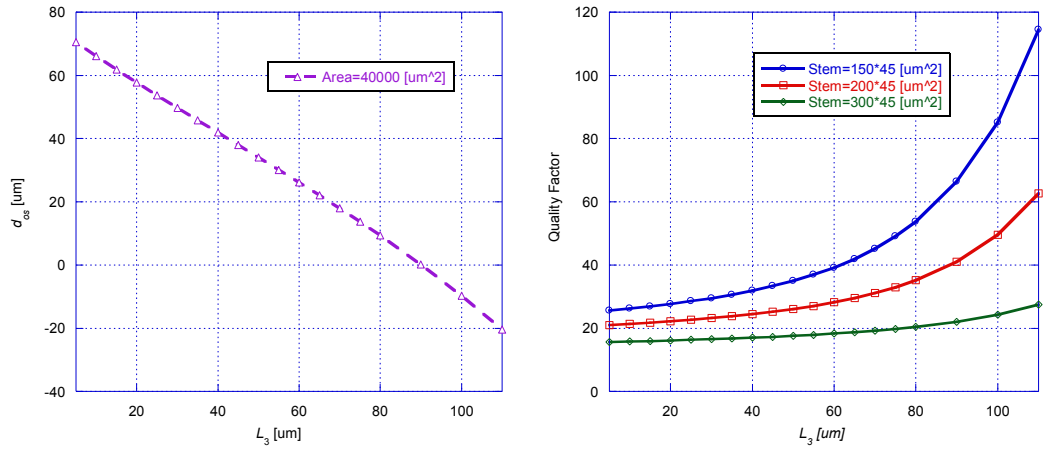

(a) (b)

Figure 4-25: (a) Distance between the mass center of the head and the tip of the stem and (b) calculated quality factor as a function of L_3 for three cases [D-(1~3)-c] and L_2=150 [um].

For the investigated cases [A-(1~3)-(a~c), C-(1~3)-(a~c) and D-(1~3)-(a~c)], as the distance between the mass center of the head and the tip of the stem decreases, the quality factor will keep increasing. Based on the energy definition, the increase of the quality factor may come from the increase of the total mechanical energy or the decrease in the energy dissipation. It is noted in Sec. 4.2 that, the kinetic energy of the head may first increase and then decrease. Thus, the total mechanical energy may first increase and then decrease. However, the dominating term in the quality factor may come from a more rapid decrease in the energy dissipation. The energy dissipation is proportional to the square of the translational velocity of the microcantilever. The translational velocity at the mass center of the head is equal to the translational velocity at the tip of the stem plus the angular velocity at the end of the stem times the distance to the mass center. As the distance between the mass center of the head and the tip of the stem decreases, the translational velocity at the mass center of the head will decrease and the energy

dissipation will decrease as well. It is also noted that, as the distance between the mass center of the head and the tip of the stem decreases, the Reynolds number associated with the hammerhead microcantilever will increase (*Re* is a function of the square of the cross section), which means that the hydrodynamic force (both real and imaginary parts) acting on the microcantilever will decrease. Thus, the quality factor will increase.

For composite hammerhead microcantilevers, as the dimensions of the gap keep increasing, the position of the mass center of the head will further move past the tip of the stem and towards the support end of the stem, which significantly increases the quality factor. Such trends can be used to optimize the performance of the device for chemical sensing applications in liquid environments.

For the investigated cases of [B-(1~3)-(a-c)], it is found that, as the surface area of the semi-circular head increases, the radius of the semi-circular head and will increase, but the quality factor will decrease. This is due to a more rapid decrease in the resonance frequency compared to the 3-dB bandwidth.

When applying this model, it should be noticed that, although the quality factor will keep increasing as the mass center moves towards the support end of the stem, the validity of the assumption (rigidity of the head) may not hold true as the length of the head becomes too small. For example, for a uniform rectangular hammerhead microcantilever with a large, constant head area, as the ratio of b_2/L_2 becomes too large (L_2 becomes too small), it is found in numerical analysis that, deformation of the head in the x-direction occurs.

4.4 Mass Sensitivity

In microcantilever-based sensor applications, a polymer coating on the surface of the substrate of the microcantilever absorbs or adsorbs the target molecules in the operational liquid environment. The absorbed or adsorbed molecules will increase the total mass of the microcantilever-based sensor device, which will change the resonance frequency. The sensitivity of the resonance frequency to the changes in the total mass of the microcantilever, or the mass sensitivity, is given by [110]

$$S_m = \frac{\Delta f_r}{\Delta m}, \tag{4.29}$$

In Eq. 4.29, Δf_r is the change in the resonance frequency due to the added mass in the polymer coating and Δm is the change in the total mass of the microcantilever.

It is assumed that the thickness of the polymer coating is very small ($h_{\text{polyer coating}} << h_{\text{microcantilever}}$). After absorption or adsorption, the total thickness of the microcantilever is still dominated by the thickness of the substrate. Thus, the only change considered in Δm is the change in the effective density of the microcantilever ($\Delta\rho_b$) in Eq. 4.29. Since the method in finding the resonance frequency shift is to exact two peak values corresponding to the frequency spectra using Eq. 4.2, an analytical expression for Δf_r is not necessarily required. Thus, the sensitivity of the resonance frequency (Δf) can be also found using Eq. 4.2.

Based on the above analysis, a Matlab code is developed to extract the mass sensitivity of the hammerhead microcantilever. Fig. 4-26 shows the change in the resonance frequency, Δf, for of a uniform rectangular hammerhead microcantilever with dimensions ($L_1 \times b_1 \times h + L_2 \times b_2 \times h$) of (200×45×12) +(50×200×12) [μm^3] due to added mass in the polymer coating.

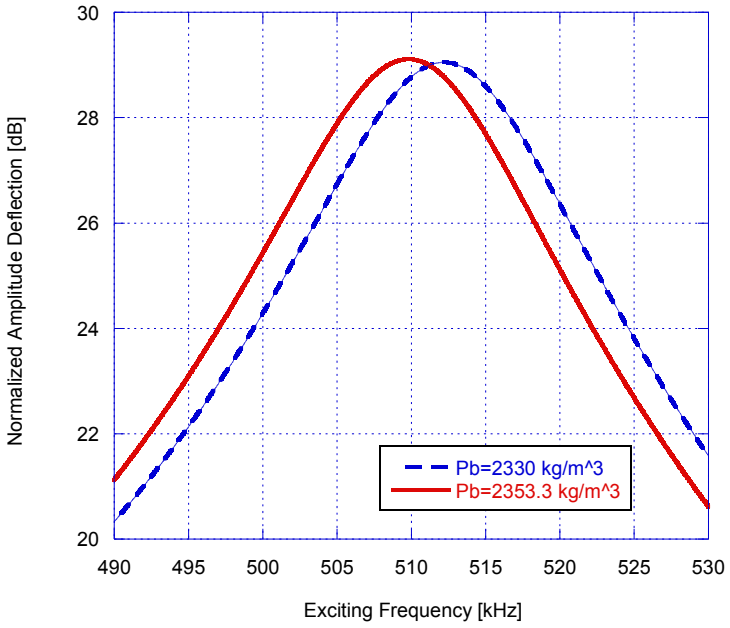

Figure 4-26: Calculated shift in the resonance frequency spectra of a uniform rectangular hammerhead microcantilever of dimensions (200×45×12)+(50×200×12) [μm^3] laterally vibrating in water, when the total mass of the microcantilever is uniformly increased by 1%.

For four different hammerhead microcantilevers [isosceles trapezoid-(A-2-c), semi-circle-(B-2-c), uniform rectangle-(C-2-c) and composite rectangle-(D-2-c)] with the same thickness of 12 um, Fig. 4-27 shows the change in the resonance frequency, Δf_{res}, as a function of Δm. The slope of Δf_{res} for each microcantilever is defined as the mass sensitivity. It is found that the composite rectangular hammerhead in this group of study has the highest mass sensitivity due to its highest resonance frequency.

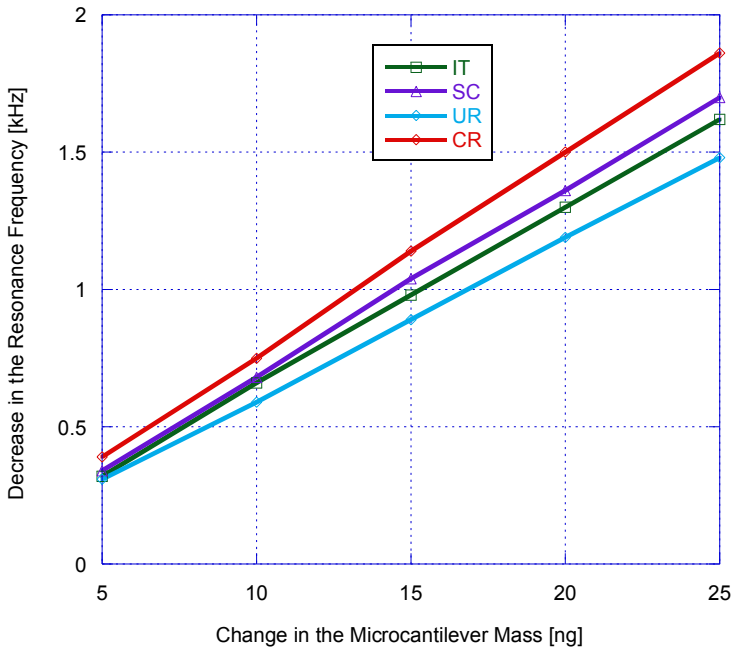

Figure 4-27: Calculated mass sensitivity as a function of Δm for four different hammerhead microcantilevers [isosceles trapezoid-(A-2-c), semi-circle-(B-2-c), uniform rectangle-(C-2-c) and composite rectangle-(D-2-c)]

Due to the additional mass attached at the end of the stem, the resonance frequency for the hammerhead microcantilever drastically decreases as the dimensions of the head become much larger. The change of the resonance frequency (Δf) is expected to decrease, correspondingly. Thus, the mass sensitivity for a hammerhead microcantilever [$L_1 \times b_1 \times h + L_2 \times b_2 \times h$] may be lower compared to that of a rectangular prismatic beam [$L_1 \times b_1 \times h$] without an additional mass attached to its end. In the following sections, the mass sensitivity will be investigated as a function of the dimensions of the hammerhead microcantilever.

4.4.1 Effects of Dimensions of the Hammerhead on the Mass Sensitivity

To solely study the effects of the thickness on the mass sensitivity, the geometries investigated are those indicated in Table 4-5. For the range of the thickness [2~15 (um)] considered, it is shown in Table 4-8 that as the thickness increases, the mass sensitivity will decrease, which is due to the microcantilever mass dominating over the liquid mass [110].

Thickness [um]	Mass Sensitivity [Hz/pg]			
	A-2-c	B-2-c	C-2-c	D-2-c
2	0.30	0.30	0.24	0.35
3	0.24	0.24	0.18	0.27
4	0.20	0.18	0.17	0.21
5	0.14	0.16	0.13	0.17
6	0.13	0.14	0.11	0.14
7	0.11	0.12	0.09	0.13
8	0.10	0.10	0.09	0.11
9	0.09	0.09	0.08	0.10
10	0.08	0.08	0.07	0.09
11	0.07	0.08	0.06	0.08
12	0.07	0.07	0.06	0.08
13	0.06	0.06	0.06	0.07
14	0.06	0.06	0.05	0.06
15	0.05	0.05	0.05	0.06

Table 4-8: Calculated mass sensitivity as a function of the thickness for investigated cases [A-2-c, B-2-c, C-2-c and D-2-c].

Isosceles Trapezoid Head Shaped Hammerhead Microcantilever:

The mass sensitivity for an isosceles trapezoid-shaped hammerhead microcantilever will be investigated as a function of L_2. The investigated cases of [A-(1~3)-(a~c)] are indicated in Table 4-1. The thicknesses of the microcantilevers are fixed at 12 [um] and the ratio of b_3 and b_2 is constant and equal to 1/4. It is shown in Table 4-9, Table 4-10 and Table 4-11 that, for nine different cases, as L_2 increases, the mass sensitivity will first increase and then decrease. Because the mass sensitivity depends on the change in the resonance frequency, the trend of the mass sensitivity is similar to that predicted for the resonance frequency. This trend is also more obvious for hammerhead microcantilevers with shorter stems due to their higher resonance frequencies.

Geometry [um^3]	Mass Sensitivity [Hz/pg]							
	L_2=50 [um^2]	L_2=60 [um^2]	L_2=70 [um^2]	L_2=80 [um^2]	L_2=110 [um^2]	L_2=140 [um^2]	L_2=170 [um^2]	L_2=200 [um^2]
A-1-b	0.171	0.186	0.202	0.210	0.210	0.194	0.179	0.163
A-2-b	0.123	0.131	0.145	0.145	0.145	0.131	0.123	0.116
A-3-b	0.077	0.077	0.077	0.077	0.077	0.070	0.064	0.058

Table 4-9: Calculated mass sensitivity as a function of L_2 for investigated cases [A-(1~3)-b].

Geometry [um^3]	Mass Sensitivity [Hz/pg]								
	L_2=40 [um^2]	L_2=45 [um^2]	L_2=50 [um^2]	L_2=60 [um^2]	L_2=80 [um^2]	L_2=110 [um^2]	L_2=140 [um^2]	L_2=170 [um^2]	L_2=200 [um^2]
A-1-a	0.722	0.728	0.751	0.736	0.692	0.618	0.545	0.486	0.442
A-2-a	0.445	0.452	0.454	0.441	0.415	0.389	0.337	0.311	0.285
A-3-a	0.200	0.201	0.210	0.199	0.189	0.178	0.157	0.147	0.147

Table 4-10: Calculated mass sensitivity as a function of L_2 for investigated cases [A-(1~3)-a].

Geometry [um^3]	Mass Sensitivity [Hz/pg]							
	L_2=50 [um^2]	L_2=60 [um^2]	L_2=70 [um^2]	L_2=80 [um^2]	L_2=110 [um^2]	L_2=140 [um^2]	L_2=170 [um^2]	L_2=200 [um^2]
A-1-c	0.063	0.074	0.084	0.09	0.095	0.100	0.095	0.090
A-2-c	0.050	0.060	0.065	0.065	0.075	0.071	0.070	0.065
A-3-c	0.032	0.037	0.040	0.041	0.041	0.041	0.041	0.037

Table 4-11: Calculated mass sensitivity as a function of L_2 for investigated cases [A-(1~3)-c].

Semi-circular Hammerhead Microcantilever:

Table 4-12 shows the investigated cases of [B-(1~3)-(a-c)] and their mass sensitivities. It is found that, as the surface area of the semi-circular head increases, the radius of the semi-circular head and will increase, but the mass sensitivity will decrease, due to a more rapid decrease in the resonance frequency.

Cases [um^3]	Mass Sensitivity [Hz/pg]		
	Area=10000 [um^2]	Area=25000 [um^2]	Area=40000 [um^2]
150×45×12	0.692	0.415	0.189
200×45×12	0.194	0.138	0.078
300×45×12	0.095	0.065	0.037

Table 4-12: Calculated mass sensitivity for investigated cases [B-(1~3)-(a-c)].

Uniform Rectangular Hammerhead Microcantilever:

For a uniform rectangular hammerhead microcantilever [see Fig. 4-1 (C)] with a fixed stem and head, the change in b_2/L_2 will change the mass sensitivity. Thus, to investigate the effects of the ratio of b_2/L_2 on the mass sensitivity, cases of [C-(1~3)-

(a~c)], as indicated in Table 4-1, will be analyzed and the thicknesses of the microcantilevers are fixed at 12 [um]. Table 4-13 shows that as the ratio of b_2/L_2 increases, the mass sensitivity will first increase and then decrease.

Geometry [um^3]	Mass Sensitivity [Hz/pg]							
	b_2/L_2=10	b_2/L_2=8	b_2/L_2=6	b_2/L_2=4	b_2/L_2=2	b_2/L_2=1	b_2/L_2=1/2	b_2/L_2=1/4
C-1-a	0.721	0.736	0.751	0.736	0.692	0.618	0.500	0.397
C-2-a	0.441	0.454	0.454	0.441	0.428	0.376	0.324	0.259
C-3-a	0.199	0.199	0.199	0.199	0.189	0.168	0.157	0.136
C-1-b	0.186	0.202	0.210	0.210	0.202	0.171	0.140	0.101
C-2-b	0.138	0.138	0.145	0.145	0.138	0.116	0.094	0.080
C-3-b	0.083	0.077	0.077	0.077	0.077	0.064	0.058	0.045
C-1-c	0.084	0.090	0.095	0.100	0.095	0.084	0.063	0.047
C-2-c	0.065	0.065	0.070	0.070	0.070	0.060	0.045	0.035
C-3-c	0.037	0.041	0.041	0.041	0.037	0.032	0.028	0.023

Table 4-13: Calculated mass sensitivity as a function of b_2/L_2 for investigated cases [C-(1~3)-(a~c)].

Composite Rectangular Hammerhead Microcantilever:

To investigate the dimensions of the gap on the mass sensitivity for a composite rectangular hammerhead microcantilever [see Fig. 4-1 (D)], cases of [D-(1~3)-(a~c)], as indicated in Table 4-1, will be analyzed and the thicknesses of the microcantilevers are fixed at 12 [um]. By varying the dimensions of the gap (assuming b_4=L_3), the mass sensitivity can be found as a function of L_3. It is shown in Table 4-14, Table 4-15 and Table 4-16 that, for nine different cases, as the dimensions of the gap increases, cases of [D-(1)-(a)], [D-(1~3)-b] and [D-(1~2)-c] show that the mass sensitivity will first increase

and then decrease. Cases of [D-(2~3)-(a)] and [D-3-c] show that the mass sensitivity starts to increase slowly after L_3 increases beyond 60 um. It is expected that the mass sensitivity will start to decrease if L_3 keeps increasing.

Geometry [um^3]	Mass Sensitivity [Hz/pg]							
	L_3=10	L_3=20	L_3=30	L_3=40	L_3=50	L_3=60	L_3=70	L_3=80
D-1-a	0.642	0.670	0.670	0.721	0.745	0.765	0.770	0.756
D-2-a	0.392	0.406	0.417	0.431	0.441	0.452	0.462	0.465
D-3-a	0.176	0.183	0.186	0.188	0.193	0.196	0.198	0.201

Table 4-14: Calculated mass sensitivity as a function of L_3 for investigated cases [D-(1~3)-a] and L_2=100 [um].

Geometry [um^3]	Mass Sensitivity [Hz/pg]							
	L_3=10	L_3=20	L_3=30	L_3=40	L_3=50	L_3=60	L_3=70	L_3=80
D-1-b	0.216	0.224	0.230	0.234	0.234	0.230	0.221	0.209
D-2-b	0.146	0.149	0.156	0.158	0.160	0.160	0.157	0.153
D-3-b	0.076	0.079	0.080	0.082	0.083	0.084	0.086	0.085

Table 4-15: Calculated mass sensitivity as a function of L_3 for investigated cases [D-(1~3)-b] and L_2=100 [um].

Geometry [um^3]	Mass Sensitivity [Hz/pg]							
	L_3=10	L_3=30	L_3=50	L_3=70	L_3=80	L_3=90	L_3=100	L_3=110
D-1-c	0.100	0.105	0.112	0.113	0.112	0.110	0.106	0.101
D-2-c	0.069	0.074	0.078	0.082	0.082	0.081	0.081	0.077
D-3-c	0.040	0.042	0.0438	0.046	0.046	0.046	0.046	0.046

Table 4-16: Calculated mass sensitivity as a function of L_3 for investigated cases [D-(1~3)-c] and L_2=150 [um].

For the investigated geometries [A-(1~3)-(a~c), C-(1~3)-(a~c) and D-(1~3)-(a~c)], as the distance between the mass center of the head and the tip of the stem decreases, the mass sensitivity will first increase and then decrease. For the investigated cases of [B-(1~3)-(a-c)], it is found that, as the surface area of the semi-circular head increases, the radius of the semi-circular head and will increase, but the mass sensitivity will decrease, due to a more rapid decrease in the resonance frequency. This trend is similar to that of the resonance frequency, which is due to the fact that the mass sensitivity is a function of the change in the resonance frequency. By attaching an additional mass to the tip of the stem, the resonance frequency of a hammerhead drops significantly, which decreases its mass sensitivity.

5. Summary, Conclusions and Future Work

5.1 Summary

The primary objective of this work is to theoretically analyze and compare the characteristics of laterally vibrating arbitrary, symmetric hammerhead microcantilever-based sensors for chemical or bio-chemical applications in viscous liquids. In particularly, various cases of different symmetric hammerhead geometries including isosceles trapezoid, semi-circle, uniform rectangle, composite rectangle were investigated and compared.

Dynamically driven prismatic rectangular microcantilevers excited in the in-plane direction have been investigated and used in liquid-phase sensing applications. However, in bio-chemical sensing applications, the performance of prismatic microcantilever-based sensors is restricted due to their limited surface sensing area. The increase in the surface area of hammerhead microcantilevers may also improve the sensing characteristics and make microcantilevers easier to excite due to lower frequency.

In order to perform the theoretically analysis of laterally vibrating symmetric hammerhead microcantilevers in viscous liquids, a model was set up based on the appropriate assumptions placed on the head. To achieve a larger sensing area, the dimensions of the head must be much larger than those of the stem. Thus, the symmetric hammerhead microcantilever was modeled as an elastic beam and a rigid body attached at the tip of the stem. The standard Euler-Bernoulli beam theory was used to model the stem as an elastic beam. Due to the rigidity of the head, negligible deformation occurs in the head and its translational and rotational motions were taken into account when analyzing the boundary conditions at the junction between the stem and the head.

After the theoretical model was set up, the validity of the model was determined for the ranges of dimensions considered, and also by reducing it to that of a uniform rectangular hammerhead microcantilever. Three-dimensional numerical models, using FEA software Comsol 4.1, were developed in a vacuum. The first resonance frequencies corresponding to the lateral vibration were extracted and compared to the ones from the theoretical models developed in this work. Then, the domain (range of parameters) of the validity of the model was found. This necessary step provided confidence in applying the theoretical model to analyze the sensor characteristics in liquid environments.

In order to perform the above-mentioned theoretical analysis in liquid environments, the analytical expressions for the hydrodynamic forces on the stem and head were derived. The method to find the hydrodynamic force on a rectangular hammerhead microcantilever was analogous to that used to find the hydrodynamic force on a prismatic beam [64]. The hydrodynamic function, which is a normalized hydrodynamic force, proposed in Ref [64] could be used. However, because the discrepancy between the analytical and numerical results is relatively large for small thicknesses and high Re, a new mathematical form of the analytical expression of the hydrodynamic function was proposed. Since the arbitrary, symmetric head has a varying width, $2b_2(x)$, the semi-analytical expression for the hydrodynamic function was obtained in terms of the Reynolds number, $Re(x)$, and aspect ratio, $h/[2b_2(x)]$.

Finally, the analytical expression for the frequency response at the tip of the stem was obtained as a function of the properties of hammerhead geometry and liquid media. The trends in the resonance frequency, quality factor and mass sensitivity were analyzed and the improvement in the sensing characteristics when using laterally vibrating

symmetric hammerhead microcantilevers was given, particularly for the four different head geometries (isosceles trapezoid, semi-circular, uniform rectangular, composite rectangular). Some design guidelines were provided for the hammerhead microcantilever geometries.

5.2 Conclusions

One of the major contributions in this work is the form of the theoretical model of a symmetric hammerhead microcantilever as an Euler-Bernoulli beam and a rigid body in viscous liquids. This modeling approach is more appropriate compared to merely treating the head as a point mass at the tip of the stem, especially when the hammerhead microcantilevers are immersed in viscous liquids and the surrounding liquid imposes hydrodynamic forces on the microcantilevers. It is noted that the hydrodynamic function for a hammerhead microcantilever is described in terms of its dimensional parameters.

The validity of the theoretical model for the range of dimensions considered was determined by also performing a numerical analysis of the vibrating devices. In particular, the first undamped natural frequency corresponding to the lateral vibration of uniform rectangular hammerhead microcantilevers was obtained in Comsol 4.1. Using the proposed analytical model, for the investigated ranges/domains, it is found that, as both length and width of the head increase, the maximum percent difference of the first natural frequency corresponding to the lateral vibration between the analytical and numerical result decreases; as the width ratio between the head and stem is larger than 4/3, the maximum percent difference is found to be always less than 6%, which indicates that it is appropriate to model a hammerhead microcantilever as an elastic beam and a rigid body. It is also found that from the 3-D numerical simulations, depending on the geometry and

dimensions, the first natural frequency of the in-plane mode may come after the second or third natural frequency associated with the out-of-plane or torsional mode. This often occurs as the thickness becomes smaller and the head becomes larger. This observation should be taken into account when choosing the dimensions of the hammerhead microcantilevers to avoid mode coupling issues.

The proposed hydrodynamic function for a laterally vibrating symmetric hammerhead microcantilever is another significant contribution from this work. Since the arbitrary head has a varying width, $2b_2(x)$, which is a function of the position along the length of the microcantilever, the proposed hydrodynamic function was found in terms of the Reynolds number, $Re(x)$ and the aspect ratio, $h/[2b_2(x)]$. Both terms depend on the function which defines the width of the stem and head. The new semi-analytical expressions for the real and imaginary part were found as a product of a function of $Re(x)$ and a function of $h/[2b_2(x)]$. The coefficients and indices associated with this hydrodynamic function were determined simultaneously to minimize the errors in the hydrodynamic functions obtained numerically and analytically. For the same ranges of the Reynolds number and the aspect ratio investigated in Ref 110, the ranges of the percent differences of the real and imaginary parts were found as [-3.8%, 6.1%] and [-2.0%, 2.8%], compared to [-5.9%, 20.6%] and [-5.7%, 2.4%] if using the originally proposed hydrodynamic function in Ref 110.

Analyzing the characteristics for laterally vibrating hammerhead microcantilevers (isosceles trapezoid-shaped head, semi-circular head, uniform rectangular head, composite rectangular head), it was found for a constant head surface area, that a change in the length or width of the head would cause the position of the mass center of the head

to change. The change in the position of the mass center of the head would cause the resonance frequency, quality factor and mass sensitivity to change. Such trends can be used to optimize the design of the microcantilever geometries and improve these characteristics. Based on the dimensions considered in this work, some conclusions regarding the sensing characteristics of different hammerhead microcantilevers are made as following:

Resonance Frequency

For a hammerhead microcantilever with a constant head area, it is found that, as the mass center of the head shifts towards the support end of the stem, the resonance frequency will first increase and then decrease. This is due to the kinetic energy of the system first decreasing and then increasing (effective mass first decreases and then increases). The resonance frequency is found to be slightly dependent on the thickness in the range of [2~15 (um)]. For thicknesses in the range of [2~12 (um)], as thickness increases, the resonance frequency will increase. This is due to the fact that the mass of the microcantilever being less than the effective mass of the viscous liquid. However, as the thickness keeps increasing in the range of [13~15 (um)], the resonance frequency will decrease slowly, which is due to the mass of the microcantilever being larger than the mass coming from the viscous liquid [110]. Such trends can be used to find the optimal thickness with respect to the resonance frequency, if the properties of the operational liquid are known.

Quality Factor

For a hammerhead microcantilever with a constant head area, it is found that, as the distance between the mass center of the head and the tip of the stem decreases, the quality

factor will keep increasing. For composite hammerhead microcantilevers, the position of the mass center of the head can further move past the tip of the stem and towards the support end of the stem, which significantly increases the quality factor. The quality factor is also found to be linearly dependent on the thickness in the range of [2~15 (um)]. As thickness increases, the quality factor will increase. It is also noticed that the hammerhead microcantilevers with shorter stems will have higher quality factors due to the higher stiffness. Such trends can be used to optimize the performance of the device for chemical sensing applications in liquid environments.

When applying this model, it should be noticed that, although the quality factor will keep increasing as the mass center moves towards the support end of the stem, the validity of the assumption (rigidity of the head) may not hold true as the length of the head becomes too small.

Mass Sensitivity

For a hammerhead microcantilever with a constant head area, it is found that, as the mass center of the head shifts towards the support end of the stem, the mass sensitivity will first increase and then decrease. This trend is similar to that of the resonance frequency, which is due to the fact that the mass sensitivity is a function of the change in the resonance frequency. By attaching an additional mass to the tip of the stem, the resonance frequency of a hammerhead drops significantly, which decreases its mass sensitivity. Such tradeoff must be considered when choosing the dimensions of the hammerhead microcantilever in terms of achieving a larger sensing head area or higher mass sensitivity.

5.3 Future Work

The work performed in this investigation can be expanded upon and further improved. Several improvements in the geometry of the head can be applied. For example, the thickness of the head can be made smaller than that of the stem. Thus, the sensing area will not be affected and the mass attached at the tip of the stem can be further minimized. The resonance frequency and the mass sensitivity will increase due to a smaller mass attached at the tip of the stem. The quality factor may also increase, as the rate of the increase in the resonance frequency may be faster than that of the 3-dB bandwidth. Since the area of the head is much larger than that of the stem, by merely putting the sensing layer on the head, the shift of the resonance frequency may be larger, which may further increase the mass sensitivity of the device.

Other geometries of the head can also be investigated theoretically to improve the sensing characteristics. For instance, the geometry of a composite semi-circular hammerhead microcantilever proposed in Ref 113 can be analyzed. By creating two large gaps between the head and the tip of the stem, the mass center of the head can be further shifted towards the support end of the stem and the sensing characteristics may be further improved. To theoretically model such geometries, the position of the mass center of the head and the rotational inertia about the mass center of the head must be found. Both of these quantities depend on the dimensions of the gaps. Then the characteristics of such microcantilevers can be found using Eq. 2.71, which determines the frequency response at the tip of the stem for an arbitrary, symmetric hammerhead microcantilever.

For hammerhead microcantilevers with two gaps between the head and the tip of the stem, as the dimensions of the gaps become smaller, the proposed hydrodynamic function

may not be appropriate due to the gap effects (squeezing and slide film effects due to the liquid trapped inside the gaps). Thus, the numerical analysis of the effects coming from the squeezing and slide films should be performed and the analytical expression for the hydrodynamic function may be found in terms of the Reynolds number, $Re(x)$, the aspect ratio, $h/[2b_2(x)]$ and the dimensions of the gaps.

Besides analyzing the characteristics of hammerhead microcantilevers in the in-plane mode, several attempts have been made in investigating the advantages in driving the hammerhead microcantilevers in the torsional model vibration. Most of the research merely focused on experimental analysis. Very few theoretical studies of the torsionally vibrating hammerhead microcantilevers in viscous liquids have been performed. The characteristics can be obtained as a function of the properties of the geometrical parameters and liquid media. Then, these characteristics can be compared with those of similar geometries operating in the in-plane direction.

For chemical sensing applications, it would be also necessary to investigate the effects of the coating thickness on the sensing characteristics due to the viscoelastic properties of the sensing layer. Since the amount of sorbed target molecules will affect the viscoelastic properties of the coating, the density and thickness of the polymer coating and its dynamic modulus must be taken into account when obtaining the frequency response. By performing the above theoretical analysis, the optimum thickness of the device can be found in terms of the sensing characteristics.

To further improve the sensing characteristics of hammerhead microcantilevers, the length of the stem can be made shorter and wider to increase its stiffness. In order to model such hammerhead microcantilevers with shorter and wider stems, it will be

appropriate to apply Timoshenko beam theory on the stem. Such analysis can be performed by incorporating the rotational inertia and shear deformation when setting up the equation of motion for the stem. The frequency response at the tip of the stem can then be found as a function of the properties of the hammerhead microcantilever geometry and the liquid media.

BIBLIOGRAPHY

[1] Lange, D., Hagleitner, C., Hierlemann, A., Brand, O., and Baltes, H., "Complementary Metal Oxide Semiconductor Cantilever Arrays on a Single Chip: Mass-Sensitive Detection of Volatile Organic Compounds" *Analytical Chemistry*, vol. 74, pp. 3084-3095, 2002

[2] Fadel, L., Lochon, F., Dufour, I., and Francais, O., "Chemical Sensing: Millimeter Size Resonant Microcantilever Performance" *Journal of Micromechanics and Microengeneering*, vol. 14, pp. S23–S30, 2004

[3] Pinnaduwage, L. A., Boiadjiev, V., Hawk, J. E., and Thundat, T., "Sensitive Detection of Plastic Explosives with Self-Assembled Monolayer-coated Microcantilevers," *Applied Physics Letters*, vol. 83, no. 7, p. 1471, 2003

[4] Calleja, M., Tamayo, J., Johansson, A., Rasmussen, P., Lechuga, L., and Boisena, A., "Polymeric Cantilever Arrays for Biosensing Applications," *Sensor Letters*, vol. 1, no. 1–5, 2003

[5] Pei, J., Tian, F. and Thundat, T., "Glucose Biosensor Based on the Microcantilever" *Analytical Chemistry*, vol. 76, no. 2, pp. 292-297, 2004

[6] Rogers, B., Manning, L., Jones, M., Sulchek, T., Murray, K., Beneschott, B., Adams, J.D., Hu, Z., Thundat, T., Cavazos, H., and Minne, S.C., "Mercury Vapor Detection with a Self-Sensing, Resonating Piezoelectric Cantilever" *Review of Scientific Instruments*, vol. 74, no. 11, pp. 4899-4901, 2003

[7] Thundat, T., Wachter, E.A., Sharp, S.L. and Warmack, S.J., "Detection of Mercury Vapor using Resonating Microcantilevers" *Applied Physics Letters*, vol. 66, iss. 13, pp. 1695-1697, 1995

[8] Kadam, A. R., Nordin, G. P., and George, M. A., "Use of Thermally Induced Higher Order Modes of a Microcantilever for Mercury Vapor Detection" *Journal of Applied Physics*, vol. 99, no. 094905, pp. 1-4, 2006

[9] Wachter, E. A., and Thundat, T., "Micromechanical Sensors for Chemical and Physical Measurements" *Review of Scientific Instruments*, vol. 66, no. 6, pp. 3662-3668, 1995

[10] Vancura, C., Li, Y., Lichtenberg, J., Kirstein, K.-U., Hierlemann, A., and Josse, F., "Liquid-Phase Chemical and Biochemical Detection Using Fully Integrated Magnetically Actuated Complementary Metal Oxide Semiconductor Resonant

Cantilever Sensor Systems" *Analytical Chemistry*, vol. 79, no. 4, pp. 1646-1654, January 2007

[11] Porter, T. L., Delinger, W., and Gunter, R. L., "Embedded Piezoresistive Microcantilever Sensors: Materials for Sensing Chemical and Biological Analytes" *Material Research Society Symposium Proceedings*, vol. 872, pp. 265-270, 2005

[12] Kapa, P., Liu, P., Bandhanadham, A., Ji, F., Varahramyan, K., Davis W., and Ji, H.-F., "Moisture Measurement Using Porous Aluminum Oxide Coated Microcantilevers" *Sensors and Actuators B*, vol. 134, no. 2, pp. 390-395, 2008

[13] Baselt, D. R., Fruhberger, B., Klaasen, E., Cemalovic, S., Britton Jr., C. L., Patel, S. V., Mlsna, T. E., McCorkle, D. and Warmack, B., "Design and Performance of a Microcantilever Based Hydrogen Sensor" *Sensors and Actuators B*, vol. 88, no. 2, pp. 120-131, 2003

[14] Goeders, K., Colton, J., and, Bottomley, L., "Microcantilevers: Sensing Chemical Interactions via Mechanical Motion" *Chemical Reviews*, vol. 108, no. 2, pp. 522-542, 2008

[15] Vancura, C., Ruegg, M., Li, Y., Lange, D., Hagleitner, C., Brand, O., Hierlemann, A., and Baltes, H., "Magnetically Actuated CMOS Resonant Cantilever Gas Sensor for Volatile Organic Compounds" *Transducers '03, 12th International Conference on Solid-State Sensors, Actuators and Microsystems,* vol. 2, pp. 1355-1358, 2003

[16] Neste, C. W. Van, Senesac, L. R., Yi, D., and Thundat, T., "Standoff Detection of Explosive Residues Using Photothermal Microcantilevers" *Applied Physics Letters*, vol. 92, no. 134102, pp. 1-3, 2008

[17] Plata, M. R., Hernando, J., Zougagh, M., Contento, A. M., Villasenor, M. J., Sanchez-Rojas, J. L., and Rios, A., "Characterization and Analytical Validation of a Microcantilever-Based Sensor for the Determination of Total Carbonate in Soil Samples" *Sensors and Actuators B*, vol. 134, no. 1, pp. 245-51, 2008

[18] Pinnaduwage, L. A., Boiadjiev, V., Hawk, J. E., and Thundat, T., "Sensitive Detection of Plastic Explosives with Self-Assembled Monolayer-coated Microcantilevers," *Applied Physics Letters*, vol. 83, no. 7, p. 1471, 2003

[19] Fu, L., Li, S., Zhang, K., Cheng, Z-Y., and Barbaree, J. M., "Detection of Bacillus Anthracis Spores in Water Using Biosensors Based on Magnetostrictive Microcantilever Coated with Phage" *Proceedings of the SPIE - The International Society for Optical Engineering*, vol. 6556, no. 1, pp. 655619-1-9, 2007

[20] Wu, G., Datar, R. H., Hansen, K. M., Thundat, T., Cote, R. J., and Majumdar, A., "Bioassay of Prostate-specific Antigen (PSA) using Microcantilevers" *Nature Biotechnology*, vol. 19, pp. 856-860, 2001

[21] Arntz, Y., Seelig, J. D., Zhang, J., Hunziker, P., Ramseyer, J. P., Meyer, E., Hegner, M., and Gerber, Ch., "Label-free Protein Assay based on a Nanomechanical Cantilever Array" *Nanotechnology*, vol. 14, pp. 86-90. 2003

[22] Vidhya, S., and Mathew, Lazar., "Design and Analysis of MEMS based Cantilever Sensor for Detection of Cardiac Markers in Acute Myocardial Infarction" *Proceedings of 23th in 13th International Conference on Biomedical Engineering*, pp. 810-812, 2009

[23] Subramanian, A., Oden, P. I., Kennel, S. J., Jacobson, K. B., Warmack, R. J., Thundat, T., and Doktycz, M. J., "Glucose Biosensing using an Enzyme-coated Microcantilever" *Applied Physics Letters*, vol. 81, pp. 385-387, 2002

[24] Sader, J. E., "Frequency Response of Cantilever Beams Immersed in Viscous Fluids with Applications to the Atomic Force Microscope" *Journal of Applied Physics*, vol. 84, pp. 64-76, 1998.

[25] Kirstein, S., Mertesdorf, M., and Schonhoff, M., "The Influence of a Viscous Fluid on the Vibration Dynamics of Scanning near-field Optical Microscopy Fiber Probes and Atomic Force Microscopy Cantilevers" *Journal of Applied Physics*, vol. 84, pp. 1782-1790, 1998.

[26] Abdelhamid, M., Cedric, H., Rodolphe, B., Cedric, J., Touria, C.-B., and Jean-Pierre, A., "Hydrodynamics of Oscillating Atomic Force Microscopy Cantilevers in Viscous Fluids" *Journal of Applied Physics*, vol. 97, p. 074907, 2005.

[27] Basak, S., Raman, A., and Garimella, S. V., "Hydrodynamic Loading of Microcantilevers Vibrating in Viscous Fluids" *Journal of Applied Physics*, vol. 99, pp. 114906-10, 06/01/ 2006.

[28] Reitsma, M.G., Gates, R.S., Cook, R.F., "Torsional Spring Constant Measurement of a T-shape Atomic Force Microscope Cantilever" *Proceedings of the SEM Annual Conference*, 2009

[29] Castille, C., Dufour, I., and Lucat, C., "Longitudinal Vibration Mode of Piezoelectric Thick-film Cantilever-based Sensors in Liquid Media" *Applied Physics Letters*, vol. 96, p. 154102, 2010.

[30] Kimber, M., and Garimella, S.V., "Measurement and Prediction of the Cooling Characteristics of a Generalized Vibrating Piezoelectric Fan" *International Journal of Heat and Mass Transfer*, vol. 52, p. 4470-80, September 2009.

[31] Shyy, W., Berg, M., and Ljungqvist, D., "Flapping and Flexible Wings for Biological and Micro Air Vehicles" *Progress in Aerospace Sciences*, vol. 35, p. 455-505, July 1999.

[32] Chen, Z., Shatara, S., and Tan, X., "Modeling of Biomimetic Robotic Fish Propelled by an Ionic Polymer-metal Composite Caudal Fin" *IEEE/ASME Transaction on Mechatronics*, vol. 13, p. 519-529, 2010.

[33] Aureli, M., Kopman, V., and Porfiri, M., "Free-locomotion of Underwater Vehicles Actuated by Ionic Polymer Metal Composites" *IEEE/ASME Transaction on Mechatronics*, vol. 15, p. 603-614, August 2010.

[34] Aureli, M., Prince, C., Porfiri, M., and Perterson, S.D., "Energy Harvesting from Base Excitation of Ionic polymer Metal Composites in Fluid Environments" *Smart Materials and Structures*, vol. 19, p. 015003, 2010.

[35] Jae, E.K., and Kim, Y.Y., "Analysis of Piezoelectric Energy Harvest of a Moderate Aspect Ratio with a Distributed Tip Mass" *Journal of Vibration and Acoustics*, vol. 133, pp. 041010-1-16, August 2011

[36] Aladwani, A., Arafa, M., Aldraihem, O., and Baz, A., "Cantilever Piezoelectric Energy Harvest with a Dynamic Maginifier" *Journal of Vibration and Acoustic*, vol. 134, pp 031004-1-10, June 2012

[37] Paci, D., Kirstein, K. U., Vancura, C., Lichtenberg, J., and Baltes, H., "A Behavioural Model of Resonant Cantilever for Chemical Sensing" *Analog Integrated Circuits and Signal Processing*, vol. 44, pp. 119-128, 2005

[38] Fletcher, P. C., Xu, Y., Gopinath, P., Williams, J., Alphenaar, B. W., Bradshaw R. D., and Keynton, R. S., "Piezoresistive Geometry for Maximizing Microcantilever Array Sensitivity" *Proceedings of IEEE Sensors 2008*, pp. 1580-1583, 2008

[39] Chatzandroulis, S., Tserepi, A., Goustouridis, D., Normand, P., and Tsoukalas, D., "Fabrication of Single Crystal Si Cantilevers using a Dry Release Process and Application in a Capacitive-Type Humidity Sensor" *Microelectronic Engineering,* vol. 61–62, pp. 995-961, 2002

[40] Gupta, A. , Denton, J. P., McNally, H., and Bashir, R., "Novel Fabrication Method for Surface Micromachined Thin Single-Crystal Silicon Cantilever Beams" *Journal of Microelectromechanical Systems*, vol. 12, no. 2, pp.1-7, 2003

[41] Hagleitner, C., Lange, D., Hierlemann, A., Brand, O., and Baltes, H., "CMOS Single-Chip Gas Detection System Comprising Capacitive, Calorimetric and

Mass-Sensitive Microsensors" *IEEE Journal of Solid-State Circuits*, vol. 37, no. 12, pp. 1867-1878, 2002

[42] Betts, T.A., Tipple, C.A., Sepaniak, M.J., and Datskos, P.G., "Selectivity of Chemical Sensors based on Micro-cantilevers coated with thin polymer films" *Analytica Chemica Acta*, vol. 422, pp. 89-99, 2000

[43] Keller, S.S., Gammelgaard, L., Jensen, M.P., Schmid, S., Davis, Z.J., and Boisen, A., "Deposition of biopolymer films on micromechanical sensors" *Microelectronic Engieering*, vol. 88, pp. 2297-2299, 2011

[44] Zhao, Y.-P., Fortin, J. B., Bonvallet, G., Wang, G.-C., and Lu, T.-M., "Kinetic Roughening in Polymer Film Growth by Vapor Deposition" *Physical Review Letters*, vol. 85, no. 15, pp. 3229-3233, October 2000

[45] Davis, Z.J., Abadal, G., Kuhn, O., Hansen, O., Grey, F., and Boisen, A., "Fabrication and Characterization of Nanoresonating Devices for Mass Detection" *Journal of Vacuum Science & Technology B*, vol. 18, no. 2, pp. 612-616, 2000

[46] Hosaka, S., Chiyoma, T., Ikeuchi, A., Okano, H., Sone, H., and Izumi, T., "Possibility of a Femtogram Mass Biosensor Using a Self-sensing Cantilever" *Second International Conference on Advanced Materials and Nanotechnology*, vol. 6, issue. 3, pp. 384-388, June 2006

[47] Cox, R., Josse, F., Wenzel, M. J., Heinrich, S. M., and Dufour, I., "Generalized Model of Resonant Polymer-Coated Microcantilevers in Viscous Liquid Media" *Analytical Chemistry*, vol. 80, no. 15, pp. 5760-5767, 2008

[48] Sampath, U., Heinrich, S. M., Josse, F., Lochon, F., Dufour, I. and Rebiere, D., "Study of Viscoelastic Effect on the Frequency Shift of Microcantilever Chemical Sensors" *IEEE Transactions on Ultrasonics, Ferroelectrics, and Frequency Control*, vol. 53, no. 11, 2006

[49] Oliviero, G., Bergese, P., Canavese, G., Chiari, M., Colombi, P., Cretich, M., Damin, F., Fiorilli, S., Marasso, S. L., Ricciardi, C., Rivolo, P., and Depero, L. E., "A Biofunctional Polymeric Coating for Microcantilever Molecular Recognition", *Analytica Chimica Acta,* vol. 630, pp. 161–167, 2008

[50] Zaromb, S. and Stetter, J. R., "Theoretical basis for identification and measurement of air contaminants using an array of sensors having partly overlapping selectivities," *Sensors and Actuators*, vol. 6, no. 4, pp. 225-243, Dec.1984.

[51] Ghatkesar, M., Barwich, V., Braun, T. Bredekamp, A., Drechsler, U., Despont, M., Lang, H., Hegner, M. and Gerber Ch., "Real-Time Mass Sensing by

Nanomechanical Resonators in Fluid", *Proceedings of IEEE Sensors 2004*, October, 2004

[52] Ji, H., and Thundat., "In Situ Detection of Calcium Ions with Chemically Modified Microcantilevers" *Biosensors & Bioelectronics*, vol. 17, pp. 337–343, 2002

[53] Boisen, A., and Thundat, T., "Design & Fabrication of Cantilever Array Biosensors" *Materials Today*, vol. 12, no. 9, pp. 32-38, 2009

[54] Wenzel, M., *Polymer-Coated and Polymer-Based Microcantilever Chemical Sensors: Analysis and Sensor Signal Processing*, Ph.D. Dissertation, August 2009, Marquette University, WI, USA

[55] Clague, D.S., Candy, J.V., Sinensky, A.K., Lee, C., Rudd, R.E., and Burnham, A.K., "Model-based Processing of Microcantilever Sensor Arrays" *Journal of Microelectromechanical*, vol. 15, iss. 5, pp. 1379-1391, 2006

[56] Obukhov, Y., Fong, K.C., Daughton, D., and Hammel, P.C., "Real Time Cantilever Signal Frequency Determination using Digital Signal Processing" *Journal of Applied Physics*, vol. 101, iss. 3, pp. 034315-1-5, 2007

[57] Lulec, S.Z. Sagiroglu, C., Mostafazadeh, A., Ermek, E., Timurdogan, E., Leblebici, Y., and Urey, H., "Simultaneous Self-sustained Actuation and Parallel Readout With MEMS Cantilever Sensor Array" *25th Conference on MEMS*, pp. 644-647, 2012

[58] Datskos, P. G., Thundat, T., Lavrik, and Nickolay V., "Micro and Nanocantilever Sensors" *Encyclopedia of Nanoscience and Nanotechnology*, vol. 10, pp. 1–10, 2004

[59] Siripon S., Dinesh K.S., and Gary R., "Geometric Optimisation of SU-8 Piezoresistive Cantilever Sensors for Biochemical Applications" *IEEE ISSNIP*, pp. 247-252, 2005

[60] Narducci, M., Figueras, E., Garcia, I., Fonseca, L., Santander, J., and Cane, C., "Modeling of T-shaped Microcantilever Resonators" *IEEE SENSOR Conference*, pp. 1127-1130, 2008

[61] Su, Y., Evans,A.G.R., Brunnschweiler, A., and Ensell, G., "Micromachined Flow Sensors Using a Piezoresistive Cantilever Paddle" *Proceeding of 26th of Solid State Device Research Conference in Europe*, pp. 717-720, September, 1996

[62] Park, K., Shim, J., Solovyeva, V., Corbin, E., Banerjee, S., and Bashir, R., "Hydrodynamic Loading and Viscous Damping of Patterned Perforations on

Microfabricated Resonant Structures" *Applied Physics Letter*, vol. 100 pp. 154107-1-5, 2012

[63] Brumley, D., Willcox, M., and Sader, J., "Oscillation of Cylinders of Rectangular Cross section Immersed in Fluid" *Physics of Fluids*, vol. 22, no. 052001, 2010

[64] Cox, R., Josse, F., Heinrich, S. M., Brand, O., and Dufour, I., "Characteristics of Laterally Vibrating Resonant Microcantilevers in Viscous Liquid Media" *Journal of Appl.Physics*, vol. 111, no. 1, 2012

[65] Vancura, C., Dufour, I., Heinrich, S. M., Josse, F., and Hierlemann, A., "Analysis of Resonating Microcantilevers Operating in a Viscous Liquid Environment" *Sensors and Actuators A*, vol. 141, pp. 43–51, 2008

[66] Plaza, J.A., Zinoviev, K., Villanueva, G., Alvarez, M., Tamayo., Dominguez, C., and Lechuga, L.M., "T-shaped Microcantilever Sensor with Reduced Deflection Offset" *Applied Physics Letter*, vol. 89, pp. 094109-1-3, 2006

[67] Jin, D., Li, X, Bao, H., Zhang, Z., Wang, Y., Yu, H., and Zuo, G., "Integrated Cantilever Sensors with a Torsional Resonance Mode for Ultraresoluble on-the-spot Bio/chemical Detection" *Applied Physics Letter*, vol. 90, pp. 041907-1-3, 2007

[68] Xia, X., Zhou, P., and Li ,X., "Effect of Resonance-mode on Mass-sensing Resolution of Microcantilever Sensors" *Sensors 2008 IEEE*, pp. 577-580,October, 2008

[69] Llic, B., Craighead, H.G., Krylov, S., Senaratne. W., Ober, C., and Neuzil, P., "Attogram Detection using Nanoelectromechanical oscillators" *Journal of Applied Physics*, vol. 98, pp. 3694-3703, April 2004

[70] Oyama, S., Okada, H., Makimoto, N., Tanaka, K., Itoh, T., and Maeda, R., "An Electrostatic Flied Sensor Driven by Self-excited Vibration of Sensor/actuator Integrated Piezoelectric Micro Cantilever" *25th Conference on MEMS*, pp. 527-530, 2012

[71] Beardslee, L.A., Truax, S., Lee, J.H., Pavlidis, S., Hesketh, P. , Hansen, K.M., Kramer, R., and Brand, O., "Selectivity Enhancement Strategy for Cantilever-based Gas-phase Voc Sensors through Use of Peptide-functionalized Carbon Nanotubes" *24th Conference on MEMS*, pp. 964-967, 2011

[72] Linden, J., and Oesterschuzle, E., "Improving the Quality Factor of Cantilever in Viscous Fluids by the Adaptation of their Interface" *Applied Physics Letter*, vol. 100, pp. 113511-1-2, 2012

[73] Finot, E., Passian, A., and Thundat, T., "Measurement of Mechanical Properties of Cantilever Shape" *Sensors*, vol. 8, issue 5, 2008

[74] Pinnaduwage, L.A., Wig, A., Hedden, D.L., Gehl, A., and Yi, D., "Detection of Trinitrotoluene via Deflagration on a Microcantilever" *Journal of Applied Physicis*, vol. 98, no. 10, pp. 5871-5875, 2004

[75] Hoof, S., Gosvami, N.N., and Hoogenboom, B.W., "Enhanced Quality Factors and Force Sensitivity by Attaching Magnetic Beads to Cantilevers for Atomic Force Microscopy in Liquid" *Journal of Applied Physics*, vol. 112, pp.114324-1-7, 2012

[76] Tao, Y., Li, X., Xu, T., Yu, H., Xu, P., Xiong, B., and Wei, C., "Resonant Cantilever Sensors Operated in a High-Q in-Plane Mode for Real-Time Bio/Chemical Detection in Liquids" *Sensors and Actuators B*, vol. 157, (606) 2011.

[77] Park, S.J., Doll, J.C., Rastegar, A.J., and Pruitt, B.L., "Piezoresistive Cantilever Performance –Part 2: Optimization" *Journal of Microelectromechanical Systems*, Vol. 19, iss. 1, pp. 149-161, 2010

[78] Pinnaduwage, L. A., Ji, H.-F., and Thundat, T., "Moore's Law in Homeland Defense: An Integrated Sensor Platform Based on Silicon Microcantilevers" *IEEE Sensors Journal*, vol. 5, no. 4, pp. 774-785, August 2005

[79] Chaudhary, M., and Gupta, A., "Microcantilever-Based Sensors" *Defence Science Journal*, vol.59, no.6, pp. 634-641, 2009

[80] Heinrich, S.M., Maharjan, R., Dufour, I. Josse, F., Beardslee, L. and Brand, O. "An analytical model of a thermally excited microcantilever vibrating laterally in a viscous fluid," *Proceedings IEEE Sensors 2010 Conference*, Waikoloa, Hawaii, pp. 1399-1404., 2010

[81] Timoshenko, S. P., "Analysis of Bi-Metal Thermostats" *Journal of the Optical Society of America,* vol. 11, iss. 3, pp. 233-255, 1925

[82] Heinrich, S.M., Wenzel, M.J., Josse, F., and Dufour, I., "An Analytical Model for Transient Deformation of Viscoelastically Coated Beams: Applications to Static-Mode Microcantilever Chemical Sensors," *Journal of Applied Physics*, vol. 105, no. 124903, pp. 1-36, 2009

[83] Beardslee, L., Addous, A. M., Heinrich, S. M., Josse, F., Dufour, I., and Brand, O., "Thermal Excitation and Piezoresistive Detection of Cantilever In-Plane Resonance Modes for Sensing Applications," *Journal of Microelectromechanical Systems*, vol. 19, no. 4, pp. 1015-1017, 2010

[84] Dufour, I., and Sarraute, E., "Analytical Modeling of Beam Behaviour Under Different Actuations: Profiles and Stress Expressions" *Journal of Modeling and Simulating of Microsystems*, vol. 1, no. 1, pp. 57-64, 1999

[85] Lobontiu, N., and Garcia, E., *Mechanics of Microelectromechanical Systems*, Kluwer Academic Publishers: New York, pp. 16-17, 66-114, and 182-262, 2005

[86] Wang, S., Wang, X., Liu, Y., and Huang, B., "Parameter Optimization of Microcantilevers Optically Excited by a Semiconductor Laser with Optical Feed Back" *Optik-International Journal for Light and Electron Optics*, vol. 120, Issue 13, pp. 676-682, 2009

[87] Dufour, I., and Fadel, L., "Resonant Microcantilever Type Chemical Sensors : Analytical Modeling in View of Optimization" *Sensors and Actuators B*, vol. 91, pp. 353–361, 2003

[88] Cox, R., Josse, F., Heinrich, S. M., Dufour, I., Brand, O., "Resonant Microcantilevers Vibrating Laterally in Viscous Liquid Media" *Proceedings of the 2010 IEEE International on Frequency Control Symposium (FCS)*, pp 85-90, 2010

[89] Lavrik, N. V., Sepaniak, M. J., and Datskos, P. G., "Cantilever Transducers as a Platform for Chemical and Biological Sensors" *Review of Scientific Instruments*, vol. 75, no. 7, pp. 2229-2253, July 2004

[90] Green, C. P., and Sader, J. E., "Torsional Frequency Response of Cantilever Beams Immersed in Viscous Fluids with Applications to the Atomic Force Microscope" *Journal of Applied Physics*, vol. 92, no. 10, 2002

[91] Xie, H., Vitard, J., Haliyo, S., and Régnier, S., "Enhanced Sensitivity of Mass Detection Using the First Torsional Mode of Microcantilevers" *Proceedings of the 2007 IEEE International Conference on Mechatronics and Automation*, pp. 39-44, 2007

[92] Cai, T., Josse, F., Dufour, I., Heinrich, S., Nigro, N., and Brand, O., "Resonant Characteristics of Rectangular Microcantilevers Vibrating Torsionally in Viscous Liquid Media" *Proceedings of the 2012 IEEE International on Frequency Control Symposium (FCS)*, pp 1-6, 2012

[93] Bargatin, I., Kozinsky, I., and Roukes, M. L., "Efficient Electrothermal Actuation of Multiple Modes of High-Frequency Nanoelectromechanical Resonators" *Applied Physics Letters*, vol. 90, no. 093116, pp. 1-3, 2007

[94] Razavi, B., "A Study of Phase Noise in CMOS Oscillators" *IEEE Journal of Solid-State Circuits*, vol. 31, no. 3, pp. 331-343, 1996

[95] Aureli, M., Pagano, C., and Porfiri, M., "Nonlinear Finite Amplitude Torsional Vibrations of Cantilevers in Viscous Fluids" *Journal of Applied Physics*, vol. 111, pp. 124915-1-16, 2012

[96] Eysden, C. A. Van, and Sader, J. E., "Frequency Response of Cantilever Beams Immersed in Viscous Fluids with Applications to the Atomic Force Microscope: Arbitrary Mode Order" *Journal of Applied Physics*, vol. 101, no. 044908, 2007

[97] Xia, X., Zhou, P., and Li, X., "Effect of Resonance-mode Order on Mass-sensing Resolution of Microcantilever Sensors" *Proceedings of IEEE Sensors 2008*, pp. 577-580, 2008

[98] Lochon, F., Dufour, I., and Rebiere, D., "An Alternative Solution to Improve Sensitivity of Resonant Microcantilever Chemical Sensors: Comparison Between Using High-Order Modes and Reducing Dimensions" *Sensors and Actuators B*, vol. 108, no. 1-2, p. 979–985, July 2005

[99] Hao, Z., Erbil, A., and Ayazi, F., "An Analytical Model for Support Loss in Micromachined Beam Resonators with In-plane Flexural Vibrations" *Sensors and Actuators A*, vol. 109, pp. 156–164, 2003

[100] Dufour, I., Heinrich, S., and Josse, F., "Theoretical Analysis of Strong-Axis Bending Mode Vibrations for Resonant Microcantilever (Bio)Chemical Sensors in Gas or Liquid Phase*" Journal of Microelectromechanical Systems*, vol.16, iss.1, pp. 44-49, Feb. 2007

[101] Heinrich, S.M., Maharjan, R., Beardslee, L. Brand, O., Dufour, I., and Josse, F. "An analytical model for in-plane flexural vibrations of thin cantilever-based sensors in viscous fluids: applications to chemical sensing in liquids," *Proceedings, International Workshop on Nanomechanical Cantilever Sensors*, Banff, Canada, pp. 2, 2010

[102] Naeli, K. and Brand, O., "Dimensional Considerations in Achieving Large Quality Factors for Resonant Silicon Cantilevers in Air" *Journal of Applied Physics* vol. 105, no. 014908, pp. 1-10, 2009

[103] Stokes, G., "On the Effects of the Internal Friction of Fluids on the Motion of Pendulums" *Transactions of the Cambridge Philosophical Society*, vol. 9, pp 8-106, 1851

[104] Bashash, H., Salehi-Khojin, A., and Jalili, N., "Forced Vibration Analysis of Flexible Euler-Bernoulli Beam with Geometrical Discontinuities" *American Control Conferences*, pp. 4029-4034, 2008

[105] Dufour, I. and Fadel, L., "Resonant Microcantilever Type Chemical Sensors: Analytical Modeling in View of Optimization" *Sensors and Actuators B*, vol. 91, pp. 353–361, 2003

[106] Chuang, W.-H., Luger, T., Fettig, R., and Ghodssi, R. "Mechanical Property Characterization of LPCVD Silicon Nitride Thin Films at Cryogenic Temperatures" *Journal of Microelectromechanical Systems*, vol. 13, no. 5, pp. 870-879, October 2004

[107] C.W.S To. "Vibration of a Cantilever Beam with a Base Excitation and Tip Mass" *Journal of Sound and Vibration*, vol. 83, iss. 4, pp. 445-460, August 1982

[108] Nieradka, K., Stegmann, H., and Gotszalk, T., "Focused Ion Beam Milling and Deposition Techniques in Validation of Mass Change Value and Position Determination Method for Micro and Nanomechanical Sensors" *Journal of Applied Physics*, vol. 112, iss. 11, (114509) 2012

[109] Hoof, S., Gosvami, N. N., and Hoogenboom, B. W., "Enhanced Quality Factors and Force Sensitivity by Attaching Magnetic Beads to Cantilever for Atomic Force Microscopy in Liquid" *Journal of Applied Physics*, vol. 112, iss. 11, (114324) 2012

[110] Cox, R., *Theoretical Analysis of Laterally Vibrating Microcantilever Sensors in Viscous Liquid Medium*, Ph.D. Dissertation, May 2011, Marquette University, WI, USA

[111] Wylie, C. Ray, Barrett, and Louis C., *Advanced Engineering Mathematics*, 6th edition, New York: McGraw-Hill, Inc, pp. 783-913, 1995

[112] Abdelhamid, M., Cedric, H., Rodolphe, B., Cedric, J., and Touria, C., "Hydrodynamics of oscillating atomic force microscopy cantilevers in viscous fluids" *Journal of Applied Physics*, iss. 97, pp. 074907-1-6, 2005

[113] Seo, J.H., and Brand, O., "High Q-factor In Plane-Mode Resonant Microsensor Platform for Gaseous/Liquid Environment" *JMEMS*, Vol. 17, iss. 2, pp. 483-497, 2008

[114] Schultz, J.A., *Lateral-Mode Vibration of Microcantilever-Based Sensors in Viscous Fluids Using Timoshenko Beam Theory* Doctoral Dissertation, December 2012, Marquette University, Wisconsin, USA.

[115] Maharjan, R., *Effect Support Compliance on the Resonant Behavior of Microcantilever-based Sensors in Viscous Fluids* Doctoral Dissertation, May 2013, Marquette University, Wisconsin, USA.

[116] Comsol Inc., *MEMS Module User's Guide*, Version 4.1& 4.2a

[117] Hibbeler, R.C., *Engineering Mechanics Dynamics*, 7th edition, 2007

[118] Hibbeler, R.C., *Mechanics of Materials*, 7th edition, 2007

[119] Weast, C. R., ed., *Handbook of Chemistry and Physics,* Ohio, 54th edition, 1973

APPENDIX A: MATLAB PROGRAM USED TO CALCULATE FREQUENCY SPECTRUM AND QUALITY FACTOR OF LATERALLY VIBRATING SYMMETRIC HAMMERHEAD MICROCANTILEVERS IN VISCOUS LIQUIDS

Case 1: Hammerhead Microcantilever with an Isosceles Trapezoid Head

```
ratio=1/4; % b3/b2
L1=300*10^-6; % length of the stem
L2=80*10^-6; % length of the head
stop=128*10^3; % Ending frequency
start=126*10^3; % Starting frequency
A=200*200*10^-12; % area of the head
b1=45*10^-6; % width of the stem
b2=(2*A)/(L2*(1+ratio)); % width of the head
b3=b2*ratio; % width of the head
h=12*10^-6; % thickness of the cantilever
E=169*10^9; % Young's Modulus
Pb=2330; % density of silicon
Pl=1000; % density of the fluid at 20C
%Pl=1.205; % density of the air at 20C
mm=Pb*L1*b1*h; % mass of the stem
mmbar=Pb*b1*h;
md=0.5*Pb*L2*(b2+b3)*h; % mass of the head
Im=(1/12)*h*(b1)^3; % moment of inertia of the stem
Jd=Pb*h*(144*b2+144*b3)^-
1*L2*(16*L2^2*b2*b3+4*L2^2*b2^2+4*L2^2*b3^2+3*b3^4+6*b3^2*b2^2+6*b3^3*b
2+6*b3*b2^3+3*b2^4); % moment of inertia
etal=0.001; % viscosity of the fluid 20C
%etal=0.00001827; % viscosity of the air 20C
step=10*2*pi;
% spectrum of the first lateral mode in air and water %
tol = 1e-20;
Lfreq = start*2*pi:step:stop*2*pi;
 start= start*2*pi;
for jfreq=1:length(Lfreq)
freq = start+step;
start=freq;
%%%%%%%%%%%%%%%%%%%% Finding spectrum in air %%%%%%%%%%%%%%%%%%
% denotes any point along the head
%Dsy= 2*((b3-b2)*x./(2*L2)+(b2*L2-b3*L1+b2*L1)/(2*L2)); % the length in
the y direction
Dsc=(L2/3)*(2*b3+b2)/(b3+b2); % distance of the mass center of the
headto the tip of the stem
%mdbar=Pb*h*2*2*((b3-b2)*x./(2*L2)+(b2*L2-b3*L1+b2*L1)/(2*L2));
Reym=(Pl*freq*b1^2)/(4*etal);
%fReyd= ((Pa*freq*(2*(b3-b2)*x./(2*L2)+(b2*L2-
b3*L1+b2*L1)/(2*L2)).^2)./(4*etaa));
Gammarm=Reym^-0.5*(0.9003+0.6105*(h/b1)^0.5+2.1722*(h/b1)^1)+(-
0.0021*(h/b1)^0.5-0.1459*(h/b1)^1+0.8255*(h/b1)^1.5+0.8144*(h/b1)^2);
Gammaim=Reym^-1*(2.5758-1.3388*(h/b1)^0.5)+Reym^-
0.5*(0.9003+0.7121*(h/b1)^0.5+1.6845*(h/b1)^1+0.8236*(h/b1)^1.5-
0.4178*(h/b1)^2);
```

```
%fGammard=(((Pa*freq*(2*(b3-b2)*x./(2*L2)+(b2*L2-
b3*L1+b2*L1)/(2*L2)).^2)./(4*etaa)).^-0.5*(0.9003+0.6105*(h./2*((b3-
b2)*x./(2*L2)+(b2*L2-b3*L1+b2*L1)/(2*L2))).^0.5+2.1722*(h./2*((b3-
b2)*x./(2*L2)+(b2*L2-b3*L1+b2*L1)/(2*L2))).^1)+(-0.0021*(h./2*((b3-
b2)*x./(2*L2)+(b2*L2-b3*L1+b2*L1)/(2*L2))).^0.5-0.1459*(h./2*((b3-
b2)*x./(2*L2)+(b2*L2-b3*L1+b2*L1)/(2*L2))).^1+0.8255*(h./2*((b3-
b2)*x./(2*L2)+(b2*L2-b3*L1+b2*L1)/(2*L2))).^1.5+0.8144*(h./2*((b3-
b2)*x./(2*L2)+(b2*L2-b3*L1+b2*L1)/(2*L2))).^2));
%fGammaid=(((Pa*freq*(2*(b3-b2)*x./(2*L2)+(b2*L2-
b3*L1+b2*L1)/(2*L2)).^2)./(4*etaa)).^-1*(2.5758-1.3388*(h./2*((b3-
b2)*x./(2*L2)+(b2*L2-b3*L1+b2*L1)/(2*L2))).^0.5)+((Pa*freq*(2*(b3-
b2)*x./(2*L2)+(b2*L2-b3*L1+b2*L1)/(2*L2)).^2)./(4*etaa)).^-
0.5*(0.9003+0.7121*(h./2*((b3-b2)*x./(2*L2)+(b2*L2-
b3*L1+b2*L1)/(2*L2))).^0.5+1.6845*(h./2*((b3-b2)*x./(2*L2)+(b2*L2-
b3*L1+b2*L1)/(2*L2))).^1+0.8236*(h./2*((b3-b2)*x./(2*L2)+(b2*L2-
b3*L1+b2*L1)/(2*L2))).^1.5-0.4178*(h./2*((b3-b2)*x./(2*L2)+(b2*L2-
b3*L1+b2*L1)/(2*L2))).^2));
%mfpmbar=0.25*pi*Pl*b1^2*Gammarm;
cfpmbar=0.25*pi*Pl*b1^2*Gammaim*freq;
%fmfpdbar= (0.25*pi*Pa*(2*(b3-b2)*x./(2*L2)+(b2*L2-
b3*L1+b2*L1)/(2*L2)).^2*(((Pa*freq*(2*(b3-b2)*x./(2*L2)+(b2*L2-
b3*L1+b2*L1)/(2*L2)).^2)./(4*etaa)).^-0.5*(0.9003+0.6105*(h./2*((b3-
b2)*x./(2*L2)+(b2*L2-b3*L1+b2*L1)/(2*L2))).^0.5+2.1722*(h./2*((b3-
b2)*x./(2*L2)+(b2*L2-b3*L1+b2*L1)/(2*L2))).^1)+(-0.0021*(h./2*((b3-
b2)*x./(2*L2)+(b2*L2-b3*L1+b2*L1)/(2*L2))).^0.5-0.1459*(h./2*((b3-
b2)*x./(2*L2)+(b2*L2-b3*L1+b2*L1)/(2*L2))).^1+0.8255*(h./2*((b3-
b2)*x./(2*L2)+(b2*L2-b3*L1+b2*L1)/(2*L2))).^1.5+0.8144*(h./2*((b3-
b2)*x./(2*L2)+(b2*L2-b3*L1+b2*L1)/(2*L2))).^2)));
%fcfpdbar= (0.25*pi*Pa*(2*(b3-b2)*x./(2*L2)+(b2*L2-
b3*L1+b2*L1)/(2*L2)).^2*(((Pa*freq*(2*(b3-b2)*x./(2*L2)+(b2*L2-
b3*L1+b2*L1)/(2*L2)).^2)./(4*etaa)).^-1*(2.5758-1.3388*(h./2*((b3-
b2)*x./(2*L2)+(b2*L2-b3*L1+b2*L1)/(2*L2))).^0.5)+((Pa*freq*(2*(b3-
b2)*x./(2*L2)+(b2*L2-b3*L1+b2*L1)/(2*L2)).^2)./(4*etaa)).^-
0.5*(0.9003+0.7121*(h./2*((b3-b2)*x./(2*L2)+(b2*L2-
b3*L1+b2*L1)/(2*L2))).^0.5+1.6845*(h./2*((b3-b2)*x./(2*L2)+(b2*L2-
b3*L1+b2*L1)/(2*L2))).^1+0.8236*(h./2*((b3-b2)*x./(2*L2)+(b2*L2-
b3*L1+b2*L1)/(2*L2))).^1.5-0.4178*(h./2*((b3-b2)*x./(2*L2)+(b2*L2-
b3*L1+b2*L1)/(2*L2))).^2))*freq);
Kp=L1*((freq.^2*(mmbar+mfpmbar)-1i*freq*cfpmbar)/(E*Im)).^0.25;
KKp=Kp;
Cfp=cosh(KKp);
Sfp=sinh(KKp);
sfp=sin(KKp);
cfp=cos(KKp);
F1 = @(x) (freq.^2.*L1.^2.*(x-L1).*(0.25.*pi.*Pl.*(2.*((b3-
b2).*x./(2.*L2)+(b2.*L2-
b3.*L1+b2.*L1)/(2.*L2))).^2.*(((Pl.*freq.*(2.*((b3-
b2).*x./(2.*L2)+(b2.*L2-b3.*L1+b2.*L1)/(2.*L2))).^2)./(4.*etal)).^-
0.5.*(0.9003+0.6105.*(h./(2.*((b3-b2).*x./(2.*L2)+(b2.*L2-
b3.*L1+b2.*L1)/(2.*L2)))).^0.5+2.1722.*(h./(2.*((b3-
b2).*x./(2.*L2)+(b2.*L2-b3.*L1+b2.*L1)/(2.*L2)))).^1)+(-
0.0021.*(h./(2.*((b3-b2).*x./(2.*L2)+(b2.*L2-
b3.*L1+b2.*L1)/(2.*L2)))).^0.5-0.1459.*(h./(2.*((b3-
b2).*x./(2.*L2)+(b2.*L2-
b3.*L1+b2.*L1)/(2.*L2)))).^1+0.8255.*(h./(2.*((b3-
b2).*x./(2.*L2)+(b2.*L2-
b3.*L1+b2.*L1)/(2.*L2)))).^1.5+0.8144.*(h./(2.*((b3-
```

```
b2).*x./(2.*L2)+(b2.*L2-b3.*L1+b2.*L1)/(2.*L2)))).^2))));
F2 = @(x) (freq.*L1.^2.*(x-L1).*(0.25.*pi.*Pl.*(2.*((b3-
b2).*x./(2.*L2)+(b2.*L2-
b3.*L1+b2.*L1)/(2.*L2))).^2.*(((Pl.*freq.*(2.*((b3-
b2).*x./(2.*L2)+(b2.*L2-b3.*L1+b2.*L1)/(2.*L2))).^2)./(4.*etal)).^-
1.*(2.5758-1.3388.*(h./(2.*((b3-b2).*x./(2.*L2)+(b2.*L2-
b3.*L1+b2.*L1)/(2.*L2)))).^0.5)+((Pl.*freq.*(2.*((b3-
b2).*x./(2.*L2)+(b2.*L2-b3.*L1+b2.*L1)/(2.*L2))).^2)./(4.*etal)).^-
0.5.*(0.9003+0.7121.*(h./(2.*((b3-b2).*x./(2.*L2)+(b2.*L2-
b3.*L1+b2.*L1)/(2.*L2)))).^0.5+1.6845.*(h./(2.*((b3-
b2).*x./(2.*L2)+(b2.*L2-
b3.*L1+b2.*L1)/(2.*L2)))).^1+0.8236.*(h./(2.*((b3-
b2).*x./(2.*L2)+(b2.*L2-b3.*L1+b2.*L1)/(2.*L2)))).^1.5-
0.4178.*(h./(2.*((b3-b2).*x./(2.*L2)+(b2.*L2-
b3.*L1+b2.*L1)/(2.*L2)))).^2)).*freq));
Gfp=(md*Dsc*freq^2*L1^2+quad( F1, L1, L1+L2, tol)-1i*quad(F2, L1,
L1+L2,tol))/(E*Im);
F3 = @(x) (freq.^2.*L1.*(x-L1).^2.*(0.25.*pi.*Pl.*(2.*((b3-
b2).*x./(2.*L2)+(b2.*L2-
b3.*L1+b2.*L1)/(2.*L2))).^2.*(((Pl.*freq.*(2.*((b3-
b2).*x./(2.*L2)+(b2.*L2-b3.*L1+b2.*L1)/(2.*L2))).^2)./(4.*etal)).^-
0.5.*(0.9003+0.6105.*(h./(2.*((b3-b2).*x./(2.*L2)+(b2.*L2-
b3.*L1+b2.*L1)/(2.*L2)))).^0.5+2.1722.*(h./(2.*((b3-
b2).*x./(2.*L2)+(b2.*L2-b3.*L1+b2.*L1)/(2.*L2)))).^1)+(-
0.0021.*(h./(2.*((b3-b2).*x./(2.*L2)+(b2.*L2-
b3.*L1+b2.*L1)/(2.*L2)))).^0.5-0.1459.*(h./(2.*((b3-
b2).*x./(2.*L2)+(b2.*L2-
b3.*L1+b2.*L1)/(2.*L2)))).^1+0.8255.*(h./(2.*((b3-
b2).*x./(2.*L2)+(b2.*L2-
b3.*L1+b2.*L1)/(2.*L2)))).^1.5+0.8144.*(h./(2.*((b3-
b2).*x./(2.*L2)+(b2.*L2-b3.*L1+b2.*L1)/(2.*L2)))).^2))));
F4 = @(x) (freq.*L1.*(x-L1).^2.*(0.25.*pi.*Pl.*(2.*((b3-
b2).*x./(2.*L2)+(b2.*L2-
b3.*L1+b2.*L1)/(2.*L2))).^2.*(((Pl.*freq.*(2.*((b3-
b2).*x./(2.*L2)+(b2.*L2-b3.*L1+b2.*L1)/(2.*L2))).^2)./(4.*etal)).^-
1.*(2.5758-1.3388.*(h./(2.*((b3-b2).*x./(2.*L2)+(b2.*L2-
b3.*L1+b2.*L1)/(2.*L2)))).^0.5)+((Pl.*freq.*(2.*((b3-
b2).*x./(2.*L2)+(b2.*L2-b3.*L1+b2.*L1)/(2.*L2))).^2)./(4.*etal)).^-
0.5.*(0.9003+0.7121.*(h./(2.*((b3-b2).*x./(2.*L2)+(b2.*L2-
b3.*L1+b2.*L1)/(2.*L2)))).^0.5+1.6845.*(h./(2.*((b3-
b2).*x./(2.*L2)+(b2.*L2-
b3.*L1+b2.*L1)/(2.*L2)))).^1+0.8236.*(h./(2.*((b3-
b2).*x./(2.*L2)+(b2.*L2-b3.*L1+b2.*L1)/(2.*L2)))).^1.5-
0.4178.*(h./(2.*((b3-b2).*x./(2.*L2)+(b2.*L2-
b3.*L1+b2.*L1)/(2.*L2)))).^2)).*freq));
Hfp=(md*Dsc^2*freq^2*L1+quad (F3, L1, L1+L2, tol)-1i*quad (F4,L1,
L1+L2,tol)+freq^2*L1*Jd)/(E*Im);
F5 = @(x) (freq.^2.*L1^3*(0.25.*pi.*Pl.*(2.*((b3-
b2).*x./(2.*L2)+(b2.*L2-
b3.*L1+b2.*L1)/(2.*L2))).^2.*(((Pl.*freq.*(2.*((b3-
b2).*x./(2.*L2)+(b2.*L2-b3.*L1+b2.*L1)/(2.*L2))).^2)./(4.*etal)).^-
0.5.*(0.9003+0.6105.*(h./(2.*((b3-b2).*x./(2.*L2)+(b2.*L2-
b3.*L1+b2.*L1)/(2.*L2)))).^0.5+2.1722.*(h./(2.*((b3-
b2).*x./(2.*L2)+(b2.*L2-b3.*L1+b2.*L1)/(2.*L2)))).^1)+(-
0.0021.*(h./(2.*((b3-b2).*x./(2.*L2)+(b2.*L2-
b3.*L1+b2.*L1)/(2.*L2)))).^0.5-0.1459.*(h./(2.*((b3-
b2).*x./(2.*L2)+(b2.*L2-
```

```
b3.*L1+b2.*L1)/(2.*L2)))).^1+0.8255.*(h./(2.*((b3-
b2).*x./(2.*L2)+(b2.*L2-
b3.*L1+b2.*L1)/(2.*L2)))).^1.5+0.8144.*(h./(2.*((b3-
b2).*x./(2.*L2)+(b2.*L2-b3.*L1+b2.*L1)/(2.*L2)))).^2))));
F6 = @(x) (freq.*L1^3*(0.25.*pi.*Pl.*(2.*((b3-b2).*x./(2.*L2)+(b2.*L2-
b3.*L1+b2.*L1)/(2.*L2))).^2.*(((Pl.*freq.*(2.*((b3-
b2).*x./(2.*L2)+(b2.*L2-b3.*L1+b2.*L1)/(2.*L2))).^2)./(4.*etal)).^-
1.*(2.5758-1.3388.*(h./(2.*((b3-b2).*x./(2.*L2)+(b2.*L2-
b3.*L1+b2.*L1)/(2.*L2)))).^0.5)+((Pl.*freq.*(2.*((b3-
b2).*x./(2.*L2)+(b2.*L2-b3.*L1+b2.*L1)/(2.*L2))).^2)./(4.*etal)).^-
0.5.*(0.9003+0.7121.*(h./(2.*((b3-b2).*x./(2.*L2)+(b2.*L2-
b3.*L1+b2.*L1)/(2.*L2)))).^0.5+1.6845.*(h./(2.*((b3-
b2).*x./(2.*L2)+(b2.*L2-
b3.*L1+b2.*L1)/(2.*L2)))).^1+0.8236.*(h./(2.*((b3-
b2).*x./(2.*L2)+(b2.*L2-b3.*L1+b2.*L1)/(2.*L2)))).^1.5-
0.4178.*(h./(2.*((b3-b2).*x./(2.*L2)+(b2.*L2-
b3.*L1+b2.*L1)/(2.*L2)))).^2)).*freq));
Ffp=(-md*freq^2*L1^3-quad (F5, L1, L1+L2, tol)+1i*quad (F6, L1,
L1+L2,tol))/(E*Im);
F7 = @(x) (freq.^2.*L1.^2.*(x-L1).*(0.25.*pi.*Pl.*(2.*((b3-
b2).*x./(2.*L2)+(b2.*L2-
b3.*L1+b2.*L1)/(2.*L2))).^2.*(((Pl.*freq.*(2.*((b3-
b2).*x./(2.*L2)+(b2.*L2-b3.*L1+b2.*L1)/(2.*L2))).^2)./(4.*etal)).^-
0.5.*(0.9003+0.6105.*(h./(2.*((b3-b2).*x./(2.*L2)+(b2.*L2-
b3.*L1+b2.*L1)/(2.*L2)))).^0.5+2.1722.*(h./(2.*((b3-
b2).*x./(2.*L2)+(b2.*L2-b3.*L1+b2.*L1)/(2.*L2)))).^1)+(-
0.0021.*(h./(2.*((b3-b2).*x./(2.*L2)+(b2.*L2-
b3.*L1+b2.*L1)/(2.*L2)))).^0.5-0.1459.*(h./(2.*((b3-
b2).*x./(2.*L2)+(b2.*L2-
b3.*L1+b2.*L1)/(2.*L2)))).^1+0.8255.*(h./(2.*((b3-
b2).*x./(2.*L2)+(b2.*L2-
b3.*L1+b2.*L1)/(2.*L2)))).^1.5+0.8144.*(h./(2.*((b3-
b2).*x./(2.*L2)+(b2.*L2-b3.*L1+b2.*L1)/(2.*L2)))).^2))));
F8 = @(x) (freq.*L1.^2.*(x-L1).*(0.25.*pi.*Pl.*(2.*((b3-
b2).*x./(2.*L2)+(b2.*L2-
b3.*L1+b2.*L1)/(2.*L2))).^2.*(((Pl.*freq.*(2.*((b3-
b2).*x./(2.*L2)+(b2.*L2-b3.*L1+b2.*L1)/(2.*L2))).^2)./(4.*etal)).^-
1.*(2.5758-1.3388.*(h./(2.*((b3-b2).*x./(2.*L2)+(b2.*L2-
b3.*L1+b2.*L1)/(2.*L2)))).^0.5)+((Pl.*freq.*(2.*((b3-
b2).*x./(2.*L2)+(b2.*L2-b3.*L1+b2.*L1)/(2.*L2))).^2)./(4.*etal)).^-
0.5.*(0.9003+0.7121.*(h./(2.*((b3-b2).*x./(2.*L2)+(b2.*L2-
b3.*L1+b2.*L1)/(2.*L2)))).^0.5+1.6845.*(h./(2.*((b3-
b2).*x./(2.*L2)+(b2.*L2-
b3.*L1+b2.*L1)/(2.*L2)))).^1+0.8236.*(h./(2.*((b3-
b2).*x./(2.*L2)+(b2.*L2-b3.*L1+b2.*L1)/(2.*L2)))).^1.5-
0.4178.*(h./(2.*((b3-b2).*x./(2.*L2)+(b2.*L2-
b3.*L1+b2.*L1)/(2.*L2)))).^2)).*freq));
Kfp=(-md*Dsc*freq^2*L1^2-quad (F7, L1, L1+L2, tol)+1i*quad (F8, L1,
L1+L2, tol))/(E*Im);
MMfp=KKp.^2.*(Cfp+cfp)-Gfp.*(Cfp-cfp)-Hfp.*KKp.*(Sfp+sfp);
NNfp=KKp.^2.*(Sfp+sfp)-Gfp.*(Sfp-sfp)-Hfp.*KKp.*(Cfp-cfp);
OOfp=KKp.^(-1).*(KKp.^2.*sfp+Gfp.*sfp+Hfp.*KKp.*cfp);
PPfp=KKp.^3.*(Sfp-sfp)-Ffp.*(Cfp-cfp)-Kfp.*KKp.*(Sfp+sfp);
QQfp=KKp.^3.*(Cfp+cfp)-Ffp.*(Sfp-sfp)-Kfp.*KKp.*(Cfp-cfp);
RRfp=KKp.^(-1).*(KKp.^3.*cfp+Ffp.*sfp+Kfp.*KKp.*cfp);
A1fp=(OOfp.*QQfp-RRfp.*NNfp)/(MMfp.*QQfp-PPfp.*NNfp);
A2fp=(OOfp.*PPfp-RRfp.*MMfp)/(NNfp.*PPfp-MMfp.*QQfp);
```

```
Dfpl=abs(A1fp.*(Cfp-cfp)+A2fp.*(Sfp-sfp)+KKp.^(-1).*sfp);
Rfreq(jfreq)=freq;
RDfpl(jfreq)=Dfpl;
end
[Amplitude, Location]=max(RDfpl);
resfl=Rfreq(Location);
for jfreq=1:length(Lfreq)
if(jfreq==1);
continue
else
if RDfpl(jfreq-1)<=Amplitude/sqrt(2);
%%%% if the above condition is not satisfied the loop
%%%% continues to next iteration
if(RDfpl(jfreq)>=(Amplitude/(sqrt(2))));
Dfpmagprevious=RDfpl(jfreq-1);
Dfpmagcurrent=RDfpl(jfreq);
Dfpmaglocal=[Dfpmagcurrent Dfpmagprevious];
 [Dfpmagmin,Iminlocal]=min(Dfpmaglocal);
%   Note that if Iminlocal equals 1, then the index
%   for Lamdbw is jlambda; if Iminlocal is 2, then the index
%   for Lamdbw is jlambda-1. So, in general, the index for
%   lambdabw may be written as jlambda+1-Iminlocal.
resfbw1=Rfreq(jfreq+1-Iminlocal);
end
end
if RDfpl(jfreq-1)>=Amplitude/sqrt(2);
if RDfpl(jfreq)<=Amplitude/sqrt(2);
Dfpmagprevious=RDfpl(jfreq-1);
Dfpmagcurrent=RDfpl(jfreq);
Dfpmaglocal=[Dfpmagcurrent Dfpmagprevious];
[Dfpmagmin,Iminlocal]=min(Dfpmaglocal);
%   Note that if Iminlocal equals 1, then the index
%   for lambdabw is jlambda; if Iminlocal is 2, then the index
%   for lambdabw is jlambda-1. So, in general, the index for
%   lambdabw may be written as jlambda+1-Iminlocal.
resfbw2=Rfreq(jfreq+1-Iminlocal);
end
end
end
end
%%%% Quality factor is given by lambdaresonant/bandwidth
resfl/(2*pi*10^3)
%Qp3db=resfl/(resfbw2-resfbw1)
```

Case 2: Hammerhead Microcantilever with a Semi-Circular Head

```
L1=150*10^-6; % length of the stem
stop=750*10^3;
start=730*10^3;
b1=45*10^-6; % width of the stem
A=200*50*10^-12;% area of the head
R=sqrt(2*A)/sqrt(pi); % Radium of the head
h=12*10^-6; % thickness of the cantilever
E=169*10^9; % Young's Modulus
%Pb=(2330*(200*45*12+200*200*12)*10^-18+0*10^-
12)/((200*45*12+200*200*12)*10^-18); % density of silicon for both
```

```
supporting beam and hammerhead
Pb=2330;
%Pl=1000; % density of the fluid at 20C
Pl=1.205; % density of the air at 20C
mm=Pb*L1*b1*h; % mass of the stem
mmbar=Pb*b1*h;
md=0.5*Pb*pi*R^2*h; % mass of the head
Im=(1/12)*h*(b1)^3; % moment of inertia of the stem
Jd=Pb*h*(pi/4-8/(9*pi))*R^4;
%etal=0.001; % viscosity of the fluid 20C
etal=0.00001827; % viscosity of the air 20C
step=30*2*pi;
% spectrum of the first lateral mode in air and water %
tol = 1e-20;
Lfreq = start*2*pi:step:stop*2*pi;
start= start*2*pi;
for jfreq=1:length(Lfreq)
freq = start+step;
start=freq;
%%%%%%%%%%%%%%%%%%%% Finding spectrum in air %%%%%%%%%%%%%%%%%%
% denotes any point along the head
%Dsy= 2*((b3-b2)*x./(2*R)+(b2*R-b3*L1+b2*L1)/(2*R)); % the length of
the isosceles trapezoid along y direction
Dsc=4*R/(3*pi); % distance of the mass center of the head to the tip of
the stem
%mdbar=Pb*h*2*2*((b3-b2)*x./(2*R)+(b2*R-
b3*L1+b2*L1)/(2*R));Reym=(Pl*freq*b1^2)/(4*etal);
%fReyd= ((Pa*freq*(2*(b3-b2)*x./(2*R)+(b2*R-
b3*L1+b2*L1)/(2*R)).^2)./(4*etaa));
Gammarm=Reym^-0.5*(0.9003+0.6105*(h/b1)^0.5+2.1722*(h/b1)^1)+(-
0.0021*(h/b1)^0.5-0.1459*(h/b1)^1+0.8255*(h/b1)^1.5+0.8144*(h/b1)^2);
           Gammaim=Reym^-1*(2.5758-1.3388*(h/b1)^0.5)+Reym^-
0.5*(0.9003+0.7121*(h/b1)^0.5+1.6845*(h/b1)^1+0.8236*(h/b1)^1.5-
0.4178*(h/b1)^2);
%            fGammard=(((Pa*freq*(2*(b3-b2)*x./(2*R)+(b2*R-
b3*L1+b2*L1)/(2*R)).^2)./(4*etaa)).^-0.5*(0.9003+0.6105*(h./2*((b3-
b2)*x./(2*R)+(b2*R-b3*L1+b2*L1)/(2*R))).^0.5+2.1722*(h./2*((b3-
b2)*x./(2*R)+(b2*R-b3*L1+b2*L1)/(2*R))).^1)+(-0.0021*(h./2*((b3-
b2)*x./(2*R)+(b2*R-b3*L1+b2*L1)/(2*R))).^0.5-0.1459*(h./2*((b3-
b2)*x./(2*R)+(b2*R-b3*L1+b2*L1)/(2*R))).^1+0.8255*(h./2*((b3-
b2)*x./(2*R)+(b2*R-b3*L1+b2*L1)/(2*R))).^1.5+0.8144*(h./2*((b3-
b2)*x./(2*R)+(b2*R-b3*L1+b2*L1)/(2*R))).^2));
%            fGammaid=(((Pa*freq*(2*(b3-b2)*x./(2*R)+(b2*R-
b3*L1+b2*L1)/(2*R)).^2)./(4*etaa)).^-1*(2.5758-1.3388*(h./2*((b3-
b2)*x./(2*R)+(b2*R-b3*L1+b2*L1)/(2*R))).^0.5)+((Pa*freq*(2*(b3-
b2)*x./(2*R)+(b2*R-b3*L1+b2*L1)/(2*R)).^2)./(4*etaa)).^-
0.5*(0.9003+0.7121*(h./2*((b3-b2)*x./(2*R)+(b2*R-
b3*L1+b2*L1)/(2*R))).^0.5+1.6845*(h./2*((b3-b2)*x./(2*R)+(b2*R-
b3*L1+b2*L1)/(2*R))).^1+0.8236*(h./2*((b3-b2)*x./(2*R)+(b2*R-
b3*L1+b2*L1)/(2*R))).^1.5-0.4178*(h./2*((b3-b2)*x./(2*R)+(b2*R-
b3*L1+b2*L1)/(2*R))).^2));
%mfpmbar=0.25*pi*Pl*b1^2*Gammarm;
cfpmbar=0.25*pi*Pl*b1^2*Gammaim*freq;
%fmfpdbar= (0.25*pi*Pa*(2*(b3-b2)*x./(2*R)+(b2*R-
b3*L1+b2*L1)/(2*R)).^2*(((Pa*freq*(2*(b3-b2)*x./(2*R)+(b2*R-
b3*L1+b2*L1)/(2*R)).^2)./(4*etaa)).^-0.5*(0.9003+0.6105*(h./2*((b3-
b2)*x./(2*R)+(b2*R-b3*L1+b2*L1)/(2*R))).^0.5+2.1722*(h./2*((b3-
```

```
b2)*x./(2*R)+(b2*R-b3*L1+b2*L1)/(2*R))).^1)+(-0.0021*(h./2*((b3-
b2)*x./(2*R)+(b2*R-b3*L1+b2*L1)/(2*R))).^0.5-0.1459*(h./2*((b3-
b2)*x./(2*R)+(b2*R-b3*L1+b2*L1)/(2*R))).^1+0.8255*(h./2*((b3-
b2)*x./(2*R)+(b2*R-b3*L1+b2*L1)/(2*R))).^1.5+0.8144*(h./2*((b3-
b2)*x./(2*R)+(b2*R-b3*L1+b2*L1)/(2*R))).^2)));
%fcfpdbar= (0.25*pi*Pa*(2*(b3-b2)*x./(2*R)+(b2*R-
b3*L1+b2*L1)/(2*R)).^2*(((Pa*freq*(2*(b3-b2)*x./(2*R)+(b2*R-
b3*L1+b2*L1)/(2*R)).^2)./(4*etaa)).^-1*(2.5758-1.3388*(h./2*((b3-
b2)*x./(2*R)+(b2*R-b3*L1+b2*L1)/(2*R))).^0.5)+((Pa*freq*(2*(b3-
b2)*x./(2*R)+(b2*R-b3*L1+b2*L1)/(2*R)).^2)./(4*etaa)).^-
0.5*(0.9003+0.7121*(h./2*((b3-b2)*x./(2*R)+(b2*R-
b3*L1+b2*L1)/(2*R))).^0.5+1.6845*(h./2*((b3-b2)*x./(2*R)+(b2*R-
b3*L1+b2*L1)/(2*R))).^1+0.8236*(h./2*((b3-b2)*x./(2*R)+(b2*R-
b3*L1+b2*L1)/(2*R))).^1.5-0.4178*(h./2*((b3-b2)*x./(2*R)+(b2*R-
b3*L1+b2*L1)/(2*R))).^2))*freq);
Kp=L1*((freq.^2*(mmbar+mfpmbar)-1i*freq*cfpmbar)/(E*Im)).^0.25;
KKp=Kp;
Cfp=cosh(KKp);
Sfp=sinh(KKp);
sfp=sin(KKp);
cfp=cos(KKp);
F1 = @(x) (freq.^2.*L1.^2.*(x-L1).*(0.25.*pi.*Pl.*(2.*(sqrt(R.^2-(x-
L1).^2))).^2.*(((Pl.*freq.*(2.*(sqrt(R.^2-(x-
L1).^2))).^2)./(4.*etal)).^-0.5.*(0.9003+0.6105.*(h./(2.*(sqrt(R.^2-(x-
L1).^2)))).^0.5+2.1722.*(h./(2.*(sqrt(R.^2-(x-L1).^2)))).^1)+(-
0.0021.*(h./(2.*(sqrt(R.^2-(x-L1).^2)))).^0.5-
0.1459.*(h./(2.*(sqrt(R.^2-(x-L1).^2)))).^1+0.8255.*(h./(2.*(sqrt(R.^2-
(x-L1).^2)))).^1.5+0.8144.*(h./(2.*(sqrt(R.^2-(x-L1).^2)))).^2))));
F2 = @(x) (freq.*L1.^2.*(x-L1).*(0.25.*pi.*Pl.*(2.*(sqrt(R.^2-(x-
L1).^2))).^2.*(((Pl.*freq.*(2.*(sqrt(R.^2-(x-
L1).^2))).^2)./(4.*etal)).^-1.*(2.5758-1.3388.*(h./(2.*(sqrt(R.^2-(x-
L1).^2)))).^0.5)+((Pl.*freq.*(2.*(sqrt(R.^2-(x-
L1).^2))).^2)./(4.*etal)).^-0.5.*(0.9003+0.7121.*(h./(2.*(sqrt(R.^2-(x-
L1).^2)))).^0.5+1.6845.*(h./(2.*(sqrt(R.^2-(x-
L1).^2)))).^1+0.8236.*(h./(2.*(sqrt(R.^2-(x-L1).^2)))).^1.5-
0.4178.*(h./(2.*(sqrt(R.^2-(x-L1).^2)))).^2).*freq));
Gfp=(md*Dsc*freq^2*L1^2+quad( F1, L1, L1+R, tol)-1i*quad(F2,L1, L1+R,
tol))/(E*Im);
F3 = @(x) (freq.^2.*L1.*(x-L1).^2.*(0.25.*pi.*Pl.*(2.*(sqrt(R.^2-(x-
L1).^2))).^2.*(((Pl.*freq.*(2.*(sqrt(R.^2-(x-
L1).^2))).^2)./(4.*etal)).^-0.5.*(0.9003+0.6105.*(h./(2.*(sqrt(R.^2-(x-
L1).^2)))).^0.5+2.1722.*(h./(2.*(sqrt(R.^2-(x-L1).^2)))).^1)+(-
0.0021.*(h./(2.*(sqrt(R.^2-(x-L1).^2)))).^0.5-
0.1459.*(h./(2.*(sqrt(R.^2-(x-L1).^2)))).^1+0.8255.*(h./(2.*(sqrt(R.^2-
(x-L1).^2)))).^1.5+0.8144.*(h./(2.*(sqrt(R.^2-(x-L1).^2)))).^2))));
F4 = @(x) (freq.*L1.*(x-L1).^2.*(0.25.*pi.*Pl.*(2.*(sqrt(R.^2-(x-
L1).^2))).^2.*(((Pl.*freq.*(2.*(sqrt(R.^2-(x-
L1).^2))).^2)./(4.*etal)).^-1.*(2.5758-1.3388.*(h./(2.*(sqrt(R.^2-(x-
L1).^2)))).^0.5)+((Pl.*freq.*(2.*(sqrt(R.^2-(x-
L1).^2))).^2)./(4.*etal)).^-0.5.*(0.9003+0.7121.*(h./(2.*(sqrt(R.^2-(x-
L1).^2)))).^0.5+1.6845.*(h./(2.*(sqrt(R.^2-(x-
L1).^2)))).^1+0.8236.*(h./(2.*(sqrt(R.^2-(x-L1).^2)))).^1.5-
0.4178.*(h./(2.*(sqrt(R.^2-(x-L1).^2)))).^2).*freq));
Hfp=(md*Dsc^2*freq^2*L1+quad (F3, L1, L1+R, tol)-1i*quad (F4,L1, L1+R,
tol)+freq^2*L1*Jd)/(E*Im);
F5 = @(x) (freq.^2.*L1^3*(0.25.*pi.*Pl.*(2.*(sqrt(R.^2-(x-
L1).^2))).^2.*(((Pl.*freq.*(2.*(sqrt(R.^2-(x-
```

```
L1).^2))).^2)./(4.*etal)).^-0.5.*(0.9003+0.6105.*(h./(2.*(sqrt(R.^2-(x-
L1).^2)))).^0.5+2.1722.*(h./(2.*(sqrt(R.^2-(x-L1).^2)))).^1)+(-
0.0021.*(h./(2.*(sqrt(R.^2-(x-L1).^2)))).^0.5-
0.1459.*(h./(2.*(sqrt(R.^2-(x-L1).^2)))).^1+0.8255.*(h./(2.*(sqrt(R.^2-
(x-L1).^2)))).^1.5+0.8144.*(h./(2.*(sqrt(R.^2-(x-L1).^2)))).^2))));
F6 = @(x) (freq.*L1^3*(0.25.*pi.*Pl.*(2.*(sqrt(R.^2-(x-
L1).^2))).^2.*(((Pl.*freq.*(2.*(sqrt(R.^2-(x-
L1).^2))).^2)./(4.*etal)).^-1.*(2.5758-1.3388.*(h./(2.*(sqrt(R.^2-(x-
L1).^2)))).^0.5)+((Pl.*freq.*(2.*(sqrt(R.^2-(x-
L1).^2))).^2)./(4.*etal)).^-0.5.*(0.9003+0.7121.*(h./(2.*(sqrt(R.^2-(x-
L1).^2)))).^0.5+1.6845.*(h./(2.*(sqrt(R.^2-(x-
L1).^2)))).^1+0.8236.*(h./(2.*(sqrt(R.^2-(x-L1).^2)))).^1.5-
0.4178.*(h./(2.*(sqrt(R.^2-(x-L1).^2)))).^2)).*freq));
Ffp=(-md*freq^2*L1^3-quad (F5, L1, L1+R, tol)+1i*quad (F6, L1, L1+R,
tol))/(E*Im);
F7 = @(x) (freq.^2.*L1.^2.*(x-L1).*(0.25.*pi.*Pl.*(2.*(sqrt(R.^2-(x-
L1).^2))).^2.*(((Pl.*freq.*(2.*(sqrt(R.^2-(x-
L1).^2))).^2)./(4.*etal)).^-0.5.*(0.9003+0.6105.*(h./(2.*(sqrt(R.^2-(x-
L1).^2)))).^0.5+2.1722.*(h./(2.*(sqrt(R.^2-(x-L1).^2)))).^1)+(-
0.0021.*(h./(2.*(sqrt(R.^2-(x-L1).^2)))).^0.5-
0.1459.*(h./(2.*(sqrt(R.^2-(x-L1).^2)))).^1+0.8255.*(h./(2.*(sqrt(R.^2-
(x-L1).^2)))).^1.5+0.8144.*(h./(2.*(sqrt(R.^2-(x-L1).^2)))).^2))));
F8 = @(x) (freq.*L1.^2.*(x-L1).*(0.25.*pi.*Pl.*(2.*(sqrt(R.^2-(x-
L1).^2))).^2.*(((Pl.*freq.*(2.*(sqrt(R.^2-(x-
L1).^2))).^2)./(4.*etal)).^-1.*(2.5758-1.3388.*(h./(2.*(sqrt(R.^2-(x-
L1).^2)))).^0.5)+((Pl.*freq.*(2.*(sqrt(R.^2-(x-
L1).^2))).^2)./(4.*etal)).^-0.5.*(0.9003+0.7121.*(h./(2.*(sqrt(R.^2-(x-
L1).^2)))).^0.5+1.6845.*(h./(2.*(sqrt(R.^2-(x-
L1).^2)))).^1+0.8236.*(h./(2.*(sqrt(R.^2-(x-L1).^2)))).^1.5-
0.4178.*(h./(2.*(sqrt(R.^2-(x-L1).^2)))).^2)).*freq));
Kfp=(-md*Dsc*freq^2*L1^2-quad (F7, L1, L1+R, tol)+1i*quad (F8, L1, L1+R,
tol))/(E*Im);
MMfp=KKp.^2.*(Cfp+cfp)-Gfp.*(Cfp-cfp)-Hfp.*KKp.*(Sfp+sfp);
NNfp=KKp.^2.*(Sfp+sfp)-Gfp.*(Sfp-sfp)-Hfp.*KKp.*(Cfp-cfp);
OOfp=KKp.^(-1).*(KKp.^2.*sfp+Gfp.*sfp+Hfp.*KKp.*cfp);
PPfp=KKp.^3.*(Sfp-sfp)-Ffp.*(Cfp-cfp)-Kfp.*KKp.*(Sfp+sfp);
QQfp=KKp.^3.*(Cfp+cfp)-Ffp.*(Sfp-sfp)-Kfp.*KKp.*(Cfp-cfp);
RRfp=KKp.^(-1).*(KKp.^3.*cfp+Ffp.*sfp+Kfp.*KKp.*cfp);
A1fp=(OOfp.*QQfp-RRfp.*NNfp)/(MMfp.*QQfp-PPfp.*NNfp);
A2fp=(OOfp.*PPfp-RRfp.*MMfp)/(NNfp.*PPfp-MMfp.*QQfp);
Dfpl=abs(A1fp.*(Cfp-cfp)+A2fp.*(Sfp-sfp)+KKp.^(-1).*sfp);
Rfreq(jfreq)=freq;
RDfpl(jfreq)=Dfpl;
end
[Amplitude, Location]=max(RDfpl);
resfl=Rfreq(Location);
resfl=resfl/(2*pi*1000)
for jfreq=1:length(Lfreq)
if(jfreq==1);
continue
else
if RDfpl(jfreq-1)<=Amplitude/sqrt(2);
%%%% if the above condition is not satisfied the loop
%%%% continues to next iteration
if(RDfpl(jfreq)>=(Amplitude/(sqrt(2))));
Dfpmagprevious=RDfpl(jfreq-1);
Dfpmagcurrent=RDfpl(jfreq);
```

```
Dfpmaglocal=[Dfpmagcurrent Dfpmagprevious];
 [Dfpmagmin,Iminlocal]=min(Dfpmaglocal);
%   Note that if Iminlocal equals 1, then the index         %   for
Lamdbw is jlambda; if Iminlocal is 2, then the index
%   for Lamdbw is jlambda-1. So, in general, the index for%   lambdabw
may be written as jlambda+1-Iminlocal.
resfbw1=Rfreq(jfreq+1-Iminlocal);
end
end
if RDfpl(jfreq-1)>=Amplitude/sqrt(2);
if RDfpl(jfreq)<=Amplitude/sqrt(2);
Dfpmagprevious=RDfpl(jfreq-1);
Dfpmagcurrent=RDfpl(jfreq);
Dfpmaglocal=[Dfpmagcurrent Dfpmagprevious];
 [Dfpmagmin,Iminlocal]=min(Dfpmaglocal);
%   Note that if Iminlocal equals 1, then the index
%   for lambdabw is jlambda; if Iminlocal is 2, then the index
%   for lambdabw is jlambda-1. So, in general, the index for
%   lambdabw may be written as jlambda+1-Iminlocal.
resfbw2=Rfreq(jfreq+1-Iminlocal);
end
end
end
end
%%%% Quality factor is given by lambdaresonant/bandwidth
Qp3db=resfl/(resfbw2-resfbw1)
```

Case 3: Hammerhead Microcantilever with a Uniform Rectangular Head

```
clear;
L1=200*10^-6; % length of the stem
b1=90*10^-6; % width of the stem
L2=100*10^-6 : 50*10^-6 : 100*10^-6; % length of the head
b2=300*10^-6 : 30*10^-6 : 300*10^-6; % width of the head
%eta=0.00001827:0.00001827:0.00001827; % viscosity of the fluid
eta=0.001:0.001:0.001; % viscosity of the fluid
h=12*10^-6; % thickness of the cantilever
E=169*10^9; % Young's Modulus
Pb=2353.3; % density of silicon for both supporting beam and hammerhead
%Pb=2330;
%Pf=1.205; % density of the fluid
Pf=1000; % density of the fluid
mm=Pb*L1*b1*h; % mass of the stem
mmbar=Pb*b1*h; % mass per unit length of stem
Im=(1/12)*h*(b1)^3; % moment of inertia of the stem
freq = 700000*2*pi:2*pi*1:800000*2*pi;
%%%%%%%%%%% Using Correction Factor %%%%%%%%%%%%%%
for jeta=1:length(eta);
  for jL2=1:length(L2);
    for jb2=1:length(b2)
        for jfreq=1:length(freq)
           md(jb2,jL2)=Pb*L2(jL2)*b2(jb2)*h; % mass of the head
           mdbar(jb2)=Pb*b2(jb2)*h; % mass per unit length of the head
           Jd(jb2,jL2)=(1/12)*md(jb2,jL2)*(L2(jL2)^2+b2(jb2)^2); %
moment of inertia
```

```
                            %%%%%%%%%%%%%%%%%%%%%%%%%%%%%%%%%%%%%%%%%%%
%%%%%%%%%%%%%%%%%%%%%%%%
                              %%%%%%%%%% Hydrodynamic function including
thickness correction %%%%%%%%%%
            Reym(jfreq,jeta)=(Pf*freq(jfreq)*b1^2)/(4*eta(jeta));
Reyd(jfreq,jb2,jeta)=(Pf*freq(jfreq)*b2(jb2)^2)/(4*eta(jeta));
                        Gammarm(jfreq,jeta)=Reym(jfreq,jeta)^-
0.5*(0.9003+0.6105*(h/b1)^0.5+2.1722*(h/b1)^1)+(-0.0021*(h/b1)^0.5-
0.1459*(h/b1)^1+0.8255*(h/b1)^1.5+0.8144*(h/b1)^2);
            Gammaim(jfreq,jeta)=Reym(jfreq,jeta)^-1*(2.5758-
1.3388*(h/b1)^0.5)+Reym(jfreq,jeta)^-
0.5*(0.9003+0.7121*(h/b1)^0.5+1.6845*(h/b1)^1+0.8236*(h/b1)^1.5-
0.4178*(h/b1)^2);
            Gammard(jfreq,jb2,jeta)=Reyd(jfreq,jb2,jeta)^-
0.5*(0.9003+0.6105*(h/b2(jb2))^0.5+2.1722*(h/b2(jb2))^1)+(-
0.0021*(h/b2(jb2))^0.5-
0.1459*(h/b2(jb2))^1+0.8255*(h/b2(jb2))^1.5+0.8144*(h/b2(jb2))^2);
            Gammaid(jfreq,jb2,jeta)=Reyd(jfreq,jb2,jeta)^-1*(2.5758-
1.3388*(h/b2(jb2))^0.5)+Reyd(jfreq,jb2,jeta)^-
0.5*(0.9003+0.7121*(h/b2(jb2))^0.5+1.6845*(h/b2(jb2))^1+0.8236*(h/b2(jb
2))^1.5-0.4178*(h/b2(jb2))^2);
            mfpmbar(jfreq,jeta)=0.25*pi*Pf*b1^2*Gammarm(jfreq,jeta);
cfpmbar(jfreq,jeta)=0.25*pi*Pf*b1^2*Gammaim(jfreq,jeta)*freq(jfreq);
mfpdbar(jfreq,jb2,jeta)=0.25*pi*Pf*b2(jb2)^2*Gammard(jfreq,jb2,jeta);
cfpdbar(jfreq,jb2,jeta)=0.25*pi*Pf*b2(jb2)^2*Gammaid(jfreq,jb2,jeta)*fr
eq(jfreq);
Kp(jfreq,jeta)=L1*((freq(jfreq)^2*(mmbar+mfpmbar(jfreq,jeta))-
1i*freq(jfreq)*cfpmbar(jfreq,jeta))/(E*Im))^0.25;
            KKp=Kp(jfreq,jeta);
            Cfp=cosh(KKp);
            Sfp=sinh(KKp);
            sfp=sin(KKp);
            cfp=cos(KKp);
                        Gfp(jfreq,jb2,jL2,jeta)=0.5*(E*Im)^(-
1)*(freq(jfreq)^2*L1^2*L2(jL2)*(md(jb2,jL2)+L2(jL2)*mfpdbar(jfreq,jb2,j
eta))-j*freq(jfreq)*L1^2*L2(jL2)^2*cfpdbar(jfreq,jb2,jeta));
            Hfp(jfreq,jb2,jL2,jeta)=(12*E*Im)^(-
1)*(3*freq(jfreq)^2*L1*L2(jL2)^2*md(jb2,jL2)+4*freq(jfreq)^2*L1*L2(jL2)
^3*mfpdbar(jfreq,jb2,jeta)+12*freq(jfreq)^2*L1*Jd(jb2,jL2)-
4*j*freq(jfreq)*L1*L2(jL2)^3*cfpdbar(jfreq,jb2,jeta));
            Ffp(jfreq,jb2,jL2,jeta)=(E*Im)^(-
1)*(j*freq(jfreq)*L1^3*L2(jL2)*cfpdbar(jfreq,jb2,jeta)-
freq(jfreq)^2*L1^3*(md(jb2,jL2)+L2(jL2)*mfpdbar(jfreq,jb2,jeta)));
        Kfp(jfreq,jb2,jL2,jeta)=0.5*(E*Im)^(-
1)*(j*freq(jfreq)*L1^2*L2(jL2)^2*cfpdbar(jfreq,jb2,jeta)-
freq(jfreq)^2*L1^2*L2(jL2)*(md(jb2,jL2)+L2(jL2)*mfpdbar(jfreq,jb2,jeta)
));
            MMfp(jfreq,jb2,jL2,jeta)=KKp^2*(Cfp+cfp)-
Gfp(jfreq,jb2,jL2,jeta)*(Cfp-cfp)-
Hfp(jfreq,jb2,jL2,jeta)*KKp*(Sfp+sfp);NNfp(jfreq,jb2,jL2,jeta)=KKp^2*(S
fp+sfp)-Gfp(jfreq,jb2,jL2,jeta)*(Sfp-sfp)-
Hfp(jfreq,jb2,jL2,jeta)*KKp*(Cfp-cfp);
            OOfp(jfreq,jb2,jL2,jeta)=KKp^(-
1)*(KKp^2*sfp+Gfp(jfreq,jb2,jL2,jeta)*sfp+Hfp(jfreq,jb2,jL2,jeta)*KKp*c
fp);
            PPfp(jfreq,jb2,jL2,jeta)=KKp^3*(Sfp-sfp)-
Ffp(jfreq,jb2,jL2,jeta)*(Cfp-cfp)-
```

```
Kfp(jfreq,jb2,jL2,jeta)*KKp*(Sfp+sfp);QQfp(jfreq,jb2,jL2,jeta)=KKp^3*(C
fp+cfp)-Ffp(jfreq,jb2,jL2,jeta)*(Sfp-sfp)-
Kfp(jfreq,jb2,jL2,jeta)*KKp*(Cfp-cfp);
          RRfp(jfreq,jb2,jL2,jeta)=KKp^(-
1)*(KKp^3*cfp+Ffp(jfreq,jb2,jL2,jeta)*sfp+Kfp(jfreq,jb2,jL2,jeta)*KKp*c
fp);
A1fp(jfreq,jb2,jL2,jeta)=(OOfp(jfreq,jb2,jL2,jeta)*QQfp(jfreq,jb2,jL2,j
eta)-
RRfp(jfreq,jb2,jL2,jeta)*NNfp(jfreq,jb2,jL2,jeta))/(MMfp(jfreq,jb2,jL2,
jeta)*QQfp(jfreq,jb2,jL2,jeta)-
PPfp(jfreq,jb2,jL2,jeta)*NNfp(jfreq,jb2,jL2,jeta));
A2fp(jfreq,jb2,jL2,jeta)=(OOfp(jfreq,jb2,jL2,jeta)*PPfp(jfreq,jb2,jL2,j
eta)-
RRfp(jfreq,jb2,jL2,jeta)*MMfp(jfreq,jb2,jL2,jeta))/(NNfp(jfreq,jb2,jL2,
jeta)*PPfp(jfreq,jb2,jL2,jeta)-
MMfp(jfreq,jb2,jL2,jeta)*QQfp(jfreq,jb2,jL2,jeta));
          Dfp(jfreq,jb2,jL2,jeta)=abs(A1fp(jfreq,jb2,jL2,jeta)*(Cfp-
cfp)+A2fp(jfreq,jb2,jL2,jeta)*(Sfp-sfp)+KKp^(-1)*sfp);
        end
          Dfpmax(jb2,jL2,jeta)=max(Dfp(:,jb2,jL2,jeta));
          Dfpmaxsqrt2(jb2,jL2,jeta)=Dfpmax(jb2,jL2,jeta)/sqrt(2);
    end
  end
end
%%%% find resonant frequency%%%
for jeta=1:length(eta);
  for  jL2=1:length(L2);
      for jb2=1:length(b2);
          for jfreq=1:length(freq);
                   %LLamd(jfreq) =
((mmbar*L1^4*(freq(jfreq))^2)/(E*Im))^0.25;
           if(Dfp(jfreq,jb2,jL2,jeta)==Dfpmax(jb2,jL2,jeta));
              resf(jb2,jL2,jeta)=freq(jfreq);
ReymR(jb2,jL2,jeta)=(Pf*resf(jb2,jL2,jeta)*b1^2)/(4*eta(jeta));
ReydR(jb2,jL2,jeta)=(Pf*resf(jb2,jL2,jeta)*b2(jb2)^2)/(4*eta(jeta));end
      end
   end
  end
end
% calculating Q using 3db method %
resfbw1=zeros(length(b2),length(L2),length(eta));
resfbw2=zeros(length(b2),length(L2),length(eta));
for jeta=1:length(eta);
  for jL2=1:length(L2);
    for jb2=1:length(b2)
        for jfreq=1:length(freq)
        if(jfreq==1);
             continue
        else
              if (Dfp(jfreq-
1,jb2,jL2,jeta)<=(Dfpmaxsqrt2(jb2,jL2,jeta)));
                %%%% if the above condition is not satisfied the loop
                %%%% continues to next iteration
if(Dfp(jfreq,jb2,jL2,jeta)>=(Dfpmaxsqrt2(jb2,jL2,jeta)));
      Dfpmagprevious=Dfp(jfreq-1,jb2,jL2,jeta);
                   Dfpmagcurrent=Dfp(jfreq,jb2,jL2,jeta);
                   Dfpmaglocal=[Dfpmagcurrent Dfpmagprevious];
```

```
                    [Dfpmagmin,Iminlocal]=min(Dfpmaglocal);
                    %   Note that if Iminlocal equals 1, then the index
                    %   for Lamdbw is jlambda; if Iminlocal is 2, then
the index
                    %   for Lamdbw is jlambda-1. So, in general, the
index for
                    %   lambdabw may be written as jlambda+1-Iminlocal.
                    resfbw1(jb2,jL2,jeta)=freq(jfreq+1-Iminlocal);
                end
            end
                if(Dfp(jfreq-
1,jb2,jL2,jeta)>=Dfpmaxsqrt2(jb2,jL2,jeta));
if(Dfp(jfreq,jb2,jL2,jeta)<=Dfpmaxsqrt2(jb2,jL2,jeta));
                    Dfpmagprevious=Dfp(jfreq-1,jb2,jL2,jeta);
                    Dfpmagcurrent=Dfp(jfreq,jb2,jL2,jeta);
                    Dfpmaglocal=[Dfpmagcurrent Dfpmagprevious];
                    [Dfpmagmin,Iminlocal]=min(Dfpmaglocal);
                    %   Note that if Iminlocal equals 1, then the index
  %   for lambdabw is jlambda; if Iminlocal is 2, then the index
     %   for lambdabw is jlambda-1. So, in general, the index for
                    %   lambdabw may be written as jlambda+1-Iminlocal.
                    resfbw2(jb2,jL2,jeta)=freq(jfreq+1-Iminlocal);
                  end
              end
        end
        end
            %%%% Quality factor is given by lambdaresonant/bandwidth
      Qp3db(jb2,jL2,jeta)=resf(jb2,jL2,jeta)/(resfbw2(jb2,jL2,jeta)-
resfbw1(jb2,jL2,jeta));
  end
  end
end
```

Case 4: Hammerhead Microcantilever with a Composite Rectangular Head

```
clear;
L1=300*10^-6; % length of the stem
b1=45*10^-6; % width of the stem
A=200*125*10^-12;
L2=100*10^-6; % length of the head
%b2=200*10^-6; % width of the head
LLL3=70;
L3=LLL3*10^-6 : 15*10^-6 : LLL3*10^-6; % length of the gap
b4=L3;
%b4=10*10^-6 : 1*10^-6 : 10*10^-6; % width of the gap
%eta=0.00001827:0.00001827:0.00001827; % viscosity of the fluid
Pf=1000; % density of he fluid
eta=0.001:0.0012:0.001; % viscosity of the fluid
h=12*10^-6; % thickness of the cantilever
E=169*10^9; % Young's Modulus
%Pb=(2330*(200*45*12+200*200*12)*10^-18+0*10^-
12)/((200*45*12+200*200*12)*10^-18); % density of silicon for both
supporting beam and hammerhead
Pb=2363.8;
%Pf=1.205; % density of the fluid
```

```
mm=Pb*L1*b1*h; % mass of the stem
mmbar=Pb*b1*h; % mass per unit length of stem
Im=(1/12)*h*(b1)^3; % moment of inertia of the stem
freq = 190000*2*pi :30*2*pi: 200000*2*pi;
for jeta=1:length(eta);
  for jL3=1:length(L3);
    for jb4=1:length(b4);
        for jfreq=1:length(freq)
        b2(jb4,jL3)=(A+L3(jL3)*(b1+2*b4(jb4)))/L2;
        b3(jb4,jL3)=0.5*(b2(jb4,jL3)-b1-2*b4(jb4));
        dc(jb4,jL3)=(0.5*L2*b2(jb4,jL3)*L2-
0.5*L3(jL3)*(b1+2*b4(jb4))*L3(jL3))/(L2*b2(jb4,jL3)-
L3(jL3)*(b1+2*b4(jb4))); % distance of the mass center to the end of
the HH rectangle
        ds(jb4,jL3)=(0.5*L2*b2(jb4,jL3)*L2-
0.5*L3(jL3)*(b1+2*b4(jb4))*L3(jL3))/(L2*b2(jb4,jL3)-
L3(jL3)*(b1+2*b4(jb4)))-L3(jL3); % distance of the mass center to the
end of the stem
        dc2(jb4,jL3)=(0.5*L2*b2(jb4,jL3)*L2-0.5*L3(jL3)*(b2(jb4,jL3)-
2*b3(jb4,jL3))*L3(jL3))/(L2*b2(jb4,jL3)-L3(jL3)*(b2(jb4,jL3)-2*b3)); %
distance of the mass center to the end of the HH rectangle
        ds2(jb4,jL3)=(0.5*L2*b2(jb4,jL3)*L2-0.5*L3(jL3)*(b2(jb4,jL3)-
2*b3(jb4,jL3))*L3(jL3))/(L2*b2(jb4,jL3)-L3(jL3)*(b2(jb4,jL3)-2*b3))-
L3(jL3); % distance of the mass center to the end of the stem
Jd(jb4,jL3)=(1/12)*Pb*L2*b2(jb4,jL3)*h*(L2^2+b2(jb4,jL3)^2)+(dc(jb4,jL3
)-0.5*L2)^2*Pb*L2*b2(jb4,jL3)*h-
((1/12)*Pb*L3(jL3)*(b1+2*b4(jb4))*h*(L3(jL3)^2+(b1+2*b4(jb4))^2)+(ds(jb
4,jL3)+0.5*L3(jL3))^2*Pb*L3(jL3)*(b1+2*b4(jb4))*h); % moment of inertia
due to rotation
        md(jb4,jL3)=Pb*h*(L2*b2(jb4,jL3)-L3(jL3)*(b1+2*b4(jb4))); %
mass of the HH
        %%%%%%%%%%%%%%%%%%%%%%%%%%%%%%%%%%%%%%%%%%%%%%%%%%%%%%%%%%%%%%%%%%%%
%%%%%%%%
        %%%%%%%%%% Hydrodynamic function including thickness
correction %%%%%%%%%%
            Reym(jfreq,jeta)=(Pf*freq(jfreq)*b1^2)/(4*eta(jeta));
Reyd1(jfreq,jb4,jL3,jeta)=(Pf*freq(jfreq)*b2(jb4,jL3)^2)/(4*eta(jeta));
Reyd2(jfreq,jb4,jL3,jeta)=(Pf*freq(jfreq)*b3(jb4,jL3)^2)/(4*eta(jeta));
            Gammarm(jfreq,jeta)=Reym(jfreq,jeta)^-
0.5*(0.9003+0.6105*(h/b1)^0.5+2.1722*(h/b1)^1)+(-0.0021*(h/b1)^0.5-
0.1459*(h/b1)^1+0.8255*(h/b1)^1.5+0.8144*(h/b1)^2);
            Gammaim(jfreq,jeta)=Reym(jfreq,jeta)^-1*(2.5758-
1.3388*(h/b1)^0.5)+Reym(jfreq,jeta)^-
0.5*(0.9003+0.7121*(h/b1)^0.5+1.6845*(h/b1)^1+0.8236*(h/b1)^1.5-
0.4178*(h/b1)^2);
            Gammard1(jfreq,jb4,jL3,jeta)=Reyd1(jfreq,jb4,jL3,jeta)^-
0.5*(0.9003+0.6105*(h/b2(jb4,jL3))^0.5+2.1722*(h/b2(jb4,jL3))^1)+(-
0.0021*(h/b2(jb4,jL3))^0.5-
0.1459*(h/b2(jb4,jL3))^1+0.8255*(h/b2(jb4,jL3))^1.5+0.8144*(h/b2(jb4,jL
3))^2);
            Gammaid1(jfreq,jb4,jL3,jeta)=Reyd1(jfreq,jb4,jL3,jeta)^-
1*(2.5758-1.3388*(h/b2(jb4,jL3))^0.5)+Reyd1(jfreq,jb4,jL3,jeta)^-
0.5*(0.9003+0.7121*(h/b2(jb4,jL3))^0.5+1.6845*(h/b2(jb4,jL3))^1+0.8236*
(h/b2(jb4,jL3))^1.5-0.4178*(h/b2(jb4,jL3))^2);

            Gammard2(jfreq,jb4,jL3,jeta)=Reyd2(jfreq,jb4,jL3,jeta)^-
0.5*(0.9003+0.6105*(h/b3(jb4,jL3))^0.5+2.1722*(h/b3(jb4,jL3))^1)+(-
```

```
0.0021*(h/b3(jb4,jL3))^0.5-
0.1459*(h/b3(jb4,jL3))^1+0.8255*(h/b3(jb4,jL3))^1.5+0.8144*(h/b3(jb4,jL
3))^2);
          Gammaid2(jfreq,jb4,jL3,jeta)=Reyd2(jfreq,jb4,jL3,jeta)^-
1*(2.5758-1.3388*(h/b3(jb4,jL3))^0.5)+Reyd2(jfreq,jb4,jL3,jeta)^-
0.5*(0.9003+0.7121*(h/b3(jb4,jL3))^0.5+1.6845*(h/b3(jb4,jL3))^1+0.8236*
(h/b3(jb4,jL3))^1.5-0.4178*(h/b3(jb4,jL3))^2);
          mfpmbar(jfreq,jeta)=0.25*pi*Pf*b1^2*Gammarm(jfreq,jeta);
cfpmbar(jfreq,jeta)=0.25*pi*Pf*b1^2*Gammaim(jfreq,jeta)*freq(jfreq);
mfpdbar1(jfreq,jb4,jL3,jeta)=0.25*pi*Pf*b2(jb4,jL3)^2*Gammard1(jfreq,jb
4,jL3,jeta);
cfpdbar1(jfreq,jb4,jL3,jeta)=0.25*pi*Pf*b2(jb4,jL3)^2*Gammaid1(jfreq,jb
4,jL3,jeta)*freq(jfreq);
mfpdbar2(jfreq,jb4,jL3,jeta)=0.25*pi*Pf*b3(jb4,jL3)^2*Gammard2(jfreq,jb
4,jL3,jeta);
cfpdbar2(jfreq,jb4,jL3,jeta)=0.25*pi*Pf*b3(jb4,jL3)^2*Gammaid2(jfreq,jb
4,jL3,jeta)*freq(jfreq);
Kp(jfreq,jeta)=L1*((freq(jfreq)^2*(mmbar+mfpmbar(jfreq,jeta))-
1i*freq(jfreq)*cfpmbar(jfreq,jeta))/(E*Im))^0.25;
          KKp=Kp(jfreq,jeta);
          Cfp=cosh(KKp);
          Sfp=sinh(KKp);
          sfp=sin(KKp);
          cfp=cos(KKp);
       Gfp(jfreq,jb4,jL3,jeta)=0.5*(E*Im)^(-
1)*(2*freq(jfreq)^2*L1^2*ds(jb4,jL3)*md(jb4,jL3)+freq(jfreq)^2*L1^2*(L2
-L3(jL3))^2*mfpdbar1(jfreq,jb4,jL3,jeta)-
2*freq(jfreq)^2*L1^2*L3(jL3)^2*mfpdbar2(jfreq,jb4,jL3,jeta)-
j*freq(jfreq)*L1^2*(L2-
L3(jL3))^2*cfpdbar1(jfreq,jb4,jL3,jeta)+2*j*freq(jfreq)*L1^2*L3(jL3)^2*
cfpdbar2(jfreq,jb4,jL3,jeta));
          Hfp(jfreq,jb4,jL3,jeta)=(3*E*Im)^(-
1)*(3*freq(jfreq)^2*L1*ds(jb4,jL3)^2*md(jb4,jL3)+freq(jfreq)^2*L1*(L2-
L3(jL3))^3*mfpdbar1(jfreq,jb4,jL3,jeta)+2*freq(jfreq)^2*L1*L3(jL3)^3*mf
pdbar2(jfreq,jb4,jL3,jeta)+3*freq(jfreq)^2*L1*Jd(jb4,jL3)-
j*freq(jfreq)*L1*(L2-L3(jL3))^3*cfpdbar1(jfreq,jb4,jL3,jeta)-
2*j*freq(jfreq)*L1*L3(jL3)^3*cfpdbar2(jfreq,jb4,jL3,jeta));
          Ffp(jfreq,jb4,jL3,jeta)=(E*Im)^(-1)*(-
freq(jfreq)^2*L1^3*md(jb4,jL3)-freq(jfreq)^2*L1^3*(L2-
L3(jL3))*mfpdbar1(jfreq,jb4,jL3,jeta)-
2*freq(jfreq)^2*L1^3*L3(jL3)*mfpdbar2(jfreq,jb4,jL3,jeta)+j*freq(jfreq)
*L1^3*(L2-
L3(jL3))*cfpdbar1(jfreq,jb4,jL3,jeta)+2*j*freq(jfreq)*L1^3*L3(jL3)*cfpd
bar2(jfreq,jb4,jL3,jeta));
          Kfp(jfreq,jb4,jL3,jeta)=0.5*(E*Im)^(-1)*(-
2*freq(jfreq)^2*L1^2*ds(jb4,jL3)*md(jb4,jL3)-freq(jfreq)^2*L1^2*(L2-
L3(jL3))^2*mfpdbar1(jfreq,jb4,jL3,jeta)+2*freq(jfreq)^2*L1^2*L3(jL3)^2*
mfpdbar2(jfreq,jb4,jL3,jeta)+j*freq(jfreq)*L1^2*(L2-
L3(jL3))^2*cfpdbar1(jfreq,jb4,jL3,jeta)-
2*j*freq(jfreq)*L1^2*L3(jL3)^2*cfpdbar2(jfreq,jb4,jL3,jeta));
          MMfp(jfreq,jb4,jL3,jeta)=KKp^2*(Cfp+cfp)-
Gfp(jfreq,jb4,jL3,jeta)*(Cfp-cfp)-
Hfp(jfreq,jb4,jL3,jeta)*KKp*(Sfp+sfp);NNfp(jfreq,jb4,jL3,jeta)=KKp^2*(S
fp+sfp)-Gfp(jfreq,jb4,jL3,jeta)*(Sfp-sfp)-
Hfp(jfreq,jb4,jL3,jeta)*KKp*(Cfp-cfp);
          OOfp(jfreq,jb4,jL3,jeta)=KKp^(-
1)*(KKp^2*sfp+Gfp(jfreq,jb4,jL3,jeta)*sfp+Hfp(jfreq,jb4,jL3,jeta)*KKp*c
```

```
fp);
          PPfp(jfreq,jb4,jL3,jeta)=KKp^3*(Sfp-sfp)-
Ffp(jfreq,jb4,jL3,jeta)*(Cfp-cfp)-
Kfp(jfreq,jb4,jL3,jeta)*KKp*(Sfp+sfp);QQfp(jfreq,jb4,jL3,jeta)=KKp^3*(C
fp+cfp)-Ffp(jfreq,jb4,jL3,jeta)*(Sfp-sfp)-
Kfp(jfreq,jb4,jL3,jeta)*KKp*(Cfp-cfp);
          RRfp(jfreq,jb4,jL3,jeta)=KKp^(-
1)*(KKp^3*cfp+Ffp(jfreq,jb4,jL3,jeta)*sfp+Kfp(jfreq,jb4,jL3,jeta)*KKp*c
fp);
A1fp(jfreq,jb4,jL3,jeta)=(OOfp(jfreq,jb4,jL3,jeta)*QQfp(jfreq,jb4,jL3,j
eta)-
RRfp(jfreq,jb4,jL3,jeta)*NNfp(jfreq,jb4,jL3,jeta))/(MMfp(jfreq,jb4,jL3,
jeta)*QQfp(jfreq,jb4,jL3,jeta)-
PPfp(jfreq,jb4,jL3,jeta)*NNfp(jfreq,jb4,jL3,jeta));

A2fp(jfreq,jb4,jL3,jeta)=(OOfp(jfreq,jb4,jL3,jeta)*PPfp(jfreq,jb4,jL3,j
eta)-
RRfp(jfreq,jb4,jL3,jeta)*MMfp(jfreq,jb4,jL3,jeta))/(NNfp(jfreq,jb4,jL3,
jeta)*PPfp(jfreq,jb4,jL3,jeta)-
MMfp(jfreq,jb4,jL3,jeta)*QQfp(jfreq,jb4,jL3,jeta));
          Dfp(jfreq,jb4,jL3,jeta)=abs(A1fp(jfreq,jb4,jL3,jeta)*(Cfp-
cfp)+A2fp(jfreq,jb4,jL3,jeta)*(Sfp-sfp)+KKp^(-1)*sfp);
        end
          Dfpmax(jb4,jL3,jeta)=max(Dfp(:,jb4,jL3,jeta));
          Dfpmaxsqrt2(jb4,jL3,jeta)=Dfpmax(jb4,jL3,jeta)/sqrt(2);
    end
  end
end
%%%% find resonant frequency%%%
for jeta=1:length(eta);
  for  jL3=1:length(L3);
      for jb4=1:length(b4);
           for jfreq=1:length(freq);
            %LLamd(jfreq) =
((mmbar*L1^4*(freq(jfreq))^2)/(E*Im))^0.25;if(Dfp(jfreq,jb4,jL3,jeta)==
Dfpmax(jb4,jL3,jeta));
               resf(jb4,jL3,jeta)=freq(jfreq);
            end
      end
   end
  end
end
% calculating Q using 3db method %
resfbw1=zeros(length(b4),length(L3),length(eta));
resfbw2=zeros(length(b4),length(L3),length(eta));
for jeta=1:length(eta);
  for jL3=1:length(L3);
    for jb4=1:length(b4)
        for jfreq=1:length(freq)
        if(jfreq==1);
             continue
        else
              if (Dfp(jfreq-
1,jb4,jL3,jeta)<=(Dfpmaxsqrt2(jb4,jL3,jeta)));
                %%%% if the above condition is not satisfied the loop
                %%%% continues to next iteration
if(Dfp(jfreq,jb4,jL3,jeta)>=(Dfpmaxsqrt2(jb4,jL3,jeta)));
```

```
                    Dfpmagprevious=Dfp(jfreq-1,jb4,jL3,jeta);
                    Dfpmagcurrent=Dfp(jfreq,jb4,jL3,jeta);
                    Dfpmaglocal=[Dfpmagcurrent Dfpmagprevious];
                    [Dfpmagmin,Iminlocal]=min(Dfpmaglocal);
                    %   Note that if Iminlocal equals 1, then the index
                    %   for Lamdbw is jlambda; if Iminlocal is 2, then
the index
                    %   for Lamdbw is jlambda-1. So, in general, the
index for
                    %   lambdabw may be written as jlambda+1-Iminlocal.
                    resfbw1(jb4,jL3,jeta)=freq(jfreq+1-Iminlocal);
                end

            end
                if(Dfp(jfreq-
1,jb4,jL3,jeta)>=Dfpmaxsqrt2(jb4,jL3,jeta));

if(Dfp(jfreq,jb4,jL3,jeta)<=Dfpmaxsqrt2(jb4,jL3,jeta));

                    Dfpmagprevious=Dfp(jfreq-1,jb4,jL3,jeta);
                    Dfpmagcurrent=Dfp(jfreq,jb4,jL3,jeta);
                    Dfpmaglocal=[Dfpmagcurrent Dfpmagprevious];
                    [Dfpmagmin,Iminlocal]=min(Dfpmaglocal);
                    %   Note that if Iminlocal equals 1, then the index
                    %   for lambdabw is jlambda; if Iminlocal is 2,
then the index
                    %   for lambdabw is jlambda-1. So, in general, the
index for
                    %   lambdabw may be written as jlambda+1-
Iminlocal.resfbw2(jb4,jL3,jeta)=freq(jfreq+1-Iminlocal); end
        end
        end
            %%%% Quality factor is given by lambdaresonant/bandwidth
      Qp3db(jb4,jL3,jeta)=resf(jb4,jL3,jeta)/(resfbw2(jb4,jL3,jeta)-
resfbw1(jb4,jL3,jeta));
  end
  end
end
```

APPENDIX B: MATLAB PROGRAM USED TO CALCULATE QUALITY FACTOR (ENERGY DEFINATION) OF LATERALLY VIBRATING SYMMETRIC HAMMERHEAD MICROCANTILEVERS IN VISCOUS LIQUIDS

Case 1: Hammerhead Microcantilever with an Isosceles Trapezoid-shaped Head

```
ratio=1/12; % b3/b2
L1=200*10^-6; % length of the stem
L2=200*10^-6; % length of the head
A=200*200*10^-12; % area of the head
b1=45*10^-6; % width of the stem
b2=(2*A)/(L2*(1+ratio)); % width of the head
b3=b2*ratio; % width of the head
h=12*10^-6; % thickness of the cantilever
E=169*10^9; % Young's Modulus
Pb=2330; % density of silicon for both supporting beam and hammerhead
Pl=1022; % density of the fluid at 20C
Pa=1.205; % density of the air at 20C
mm=Pb*L1*b1*h; % mass of the stem
mmbar=Pb*b1*h;
md=0.5*Pb*L2*(b2+b3)*h; % mass of the head
Im=(1/12)*h*(b1)^3; % moment of inertia of the stem
Jd=Pb*h*(144*b2+144*b3)^-
1*L2*(16*L2^2*b2*b3+4*L2^2*b2^2+4*L2^2*b3^2+3*b3^4+6*b3^2*b2^2+6*b3^3*b
2+6*b3*b2^3+3*b2^4); % moment of inertia
etal=0.00131; % viscosity of the fluid 20C
etaa=0.00001827; % viscosity of the air 20C
step=100*2*pi;
% spectrum of the first lateral mode in air and water %
tol = 1e-20;
Lfreq = 80000*2*pi:step:150000*2*pi;
Ltau = 0:0.5:6;
start= 80000*2*pi;
for jfreq=1:length(Lfreq)
          freq = start+step;
          start=freq;
%%%%%%%%%%%%%%%%%%%% Finding spectrum in air %%%%%%%%%%%%%%%%%%%
           % denotes any point along the head
           %Dsy= 2*((b3-b2)*x./(2*L2)+(b2*L2-b3*L1+b2*L1)/(2*L2)); %
the length of the isosceles trapezoid along y direction
           Dsc=(L2/3)*(2*b3+b2)/(b3+b2); % distance of the mass center
of the head to the tip of the stem
%            mdbar=Pb*h*2*2*((b3-b2)*x./(2*L2)+(b2*L2-
b3*L1+b2*L1)/(2*L2));
           Reym=(Pl*freq*b1^2)/(4*etal);
           %fReyd= ((Pa*freq*(2*(b3-b2)*x./(2*L2)+(b2*L2-
b3*L1+b2*L1)/(2*L2)).^2)./(4*etaa));
           Gammarm=Reym^-
0.5*(0.9003+0.6105*(h/b1)^0.5+2.1722*(h/b1)^1)+(-0.0021*(h/b1)^0.5-
0.1459*(h/b1)^1+0.8255*(h/b1)^1.5+0.8144*(h/b1)^2);
           Gammaim=Reym^-1*(2.5758-1.3388*(h/b1)^0.5)+Reym^-
```

```
0.5*(0.9003+0.7121*(h/b1)^0.5+1.6845*(h/b1)^1+0.8236*(h/b1)^1.5-
0.4178*(h/b1)^2);
%            fGammard=(((Pa*freq*(2*(b3-b2)*x./(2*L2)+(b2*L2-
b3*L1+b2*L1)/(2*L2)).^2)./(4*etaa)).^-0.5*(0.9003+0.6105*(h./2*((b3-
b2)*x./(2*L2)+(b2*L2-b3*L1+b2*L1)/(2*L2))).^0.5+2.1722*(h./2*((b3-
b2)*x./(2*L2)+(b2*L2-b3*L1+b2*L1)/(2*L2))).^1)+(-0.0021*(h./2*((b3-
b2)*x./(2*L2)+(b2*L2-b3*L1+b2*L1)/(2*L2))).^0.5-0.1459*(h./2*((b3-
b2)*x./(2*L2)+(b2*L2-b3*L1+b2*L1)/(2*L2))).^1+0.8255*(h./2*((b3-
b2)*x./(2*L2)+(b2*L2-b3*L1+b2*L1)/(2*L2))).^1.5+0.8144*(h./2*((b3-
b2)*x./(2*L2)+(b2*L2-b3*L1+b2*L1)/(2*L2))).^2));
%            fGammaid=(((Pa*freq*(2*(b3-b2)*x./(2*L2)+(b2*L2-
b3*L1+b2*L1)/(2*L2)).^2)./(4*etaa)).^-1*(2.5758-1.3388*(h./2*((b3-
b2)*x./(2*L2)+(b2*L2-b3*L1+b2*L1)/(2*L2))).^0.5)+((Pa*freq*(2*(b3-
b2)*x./(2*L2)+(b2*L2-b3*L1+b2*L1)/(2*L2)).^2)./(4*etaa)).^-
0.5*(0.9003+0.7121*(h./2*((b3-b2)*x./(2*L2)+(b2*L2-
b3*L1+b2*L1)/(2*L2))).^0.5+1.6845*(h./2*((b3-b2)*x./(2*L2)+(b2*L2-
b3*L1+b2*L1)/(2*L2))).^1+0.8236*(h./2*((b3-b2)*x./(2*L2)+(b2*L2-
b3*L1+b2*L1)/(2*L2))).^1.5-0.4178*(h./2*((b3-b2)*x./(2*L2)+(b2*L2-
b3*L1+b2*L1)/(2*L2))).^2));
%  mfpmbar=0.25*pi*Pl*b1^2*Gammarm;
  cfpmbar=0.25*pi*Pl*b1^2*Gammaim*freq;
%            fmfpdbar= (0.25*pi*Pa*(2*(b3-b2)*x./(2*L2)+(b2*L2-
b3*L1+b2*L1)/(2*L2)).^2*(((Pa*freq*(2*(b3-b2)*x./(2*L2)+(b2*L2-
b3*L1+b2*L1)/(2*L2)).^2)./(4*etaa)).^-0.5*(0.9003+0.6105*(h./2*((b3-
b2)*x./(2*L2)+(b2*L2-b3*L1+b2*L1)/(2*L2))).^0.5+2.1722*(h./2*((b3-
b2)*x./(2*L2)+(b2*L2-b3*L1+b2*L1)/(2*L2))).^1)+(-0.0021*(h./2*((b3-
b2)*x./(2*L2)+(b2*L2-b3*L1+b2*L1)/(2*L2))).^0.5-0.1459*(h./2*((b3-
b2)*x./(2*L2)+(b2*L2-b3*L1+b2*L1)/(2*L2))).^1+0.8255*(h./2*((b3-
b2)*x./(2*L2)+(b2*L2-b3*L1+b2*L1)/(2*L2))).^1.5+0.8144*(h./2*((b3-
b2)*x./(2*L2)+(b2*L2-b3*L1+b2*L1)/(2*L2))).^2)));
%            fcfpdbar= (0.25*pi*Pa*(2*(b3-b2)*x./(2*L2)+(b2*L2-
b3*L1+b2*L1)/(2*L2)).^2*(((Pa*freq*(2*(b3-b2)*x./(2*L2)+(b2*L2-
b3*L1+b2*L1)/(2*L2)).^2)./(4*etaa)).^-1*(2.5758-1.3388*(h./2*((b3-
b2)*x./(2*L2)+(b2*L2-b3*L1+b2*L1)/(2*L2))).^0.5)+((Pa*freq*(2*(b3-
b2)*x./(2*L2)+(b2*L2-b3*L1+b2*L1)/(2*L2)).^2)./(4*etaa)).^-
0.5*(0.9003+0.7121*(h./2*((b3-b2)*x./(2*L2)+(b2*L2-
b3*L1+b2*L1)/(2*L2))).^0.5+1.6845*(h./2*((b3-b2)*x./(2*L2)+(b2*L2-
b3*L1+b2*L1)/(2*L2))).^1+0.8236*(h./2*((b3-b2)*x./(2*L2)+(b2*L2-
b3*L1+b2*L1)/(2*L2))).^1.5-0.4178*(h./2*((b3-b2)*x./(2*L2)+(b2*L2-
b3*L1+b2*L1)/(2*L2))).^2))*freq);
   Kp=L1*((freq.^2*(mmbar+mfpmbar)-1i*freq*cfpmbar)/(E*Im)).^0.25;
           KKp=Kp;
           Cfp=cosh(KKp);
           Sfp=sinh(KKp);
           sfp=sin(KKp);
           cfp=cos(KKp);
F1 = @(x) (freq.^2.*L1.^2.*(x-L1).*(0.25.*pi.*Pl.*(2.*((b3-
b2).*x./(2.*L2)+(b2.*L2-
b3.*L1+b2.*L1)/(2.*L2))).^2.*(((Pl.*freq.*(2.*((b3-
b2).*x./(2.*L2)+(b2.*L2-b3.*L1+b2.*L1)/(2.*L2))).^2)./(4.*etal)).^-
0.5.*(0.9003+0.6105.*(h./(2.*((b3-b2).*x./(2.*L2)+(b2.*L2-
b3.*L1+b2.*L1)/(2.*L2)))).^0.5+2.1722.*(h./(2.*((b3-
b2).*x./(2.*L2)+(b2.*L2-b3.*L1+b2.*L1)/(2.*L2)))).^1)+(-
0.0021.*(h./(2.*((b3-b2).*x./(2.*L2)+(b2.*L2-
b3.*L1+b2.*L1)/(2.*L2)))).^0.5-0.1459.*(h./(2.*((b3-
b2).*x./(2.*L2)+(b2.*L2-
b3.*L1+b2.*L1)/(2.*L2)))).^1+0.8255.*(h./(2.*((b3-
```

```
b2).*x./(2.*L2)+(b2.*L2-
b3.*L1+b2.*L1)/(2.*L2)))).^1.5+0.8144.*(h./(2.*((b3-
b2).*x./(2.*L2)+(b2.*L2-b3.*L1+b2.*L1)/(2.*L2)))).^2))));
  F2 = @(x) (freq.*L1.^2.*(x-L1).*(0.25.*pi.*Pl.*(2.*((b3-
b2).*x./(2.*L2)+(b2.*L2-
b3.*L1+b2.*L1)/(2.*L2))).^2.*(((Pl.*freq.*(2.*((b3-
b2).*x./(2.*L2)+(b2.*L2-b3.*L1+b2.*L1)/(2.*L2))).^2)./(4.*etal)).^-
1.*(2.5758-1.3388.*(h./(2.*((b3-b2).*x./(2.*L2)+(b2.*L2-
b3.*L1+b2.*L1)/(2.*L2)))).^0.5)+((Pl.*freq.*(2.*((b3-
b2).*x./(2.*L2)+(b2.*L2-b3.*L1+b2.*L1)/(2.*L2))).^2)./(4.*etal)).^-
0.5.*(0.9003+0.7121.*(h./(2.*((b3-b2).*x./(2.*L2)+(b2.*L2-
b3.*L1+b2.*L1)/(2.*L2)))).^0.5+1.6845.*(h./(2.*((b3-
b2).*x./(2.*L2)+(b2.*L2-
b3.*L1+b2.*L1)/(2.*L2)))).^1+0.8236.*(h./(2.*((b3-
b2).*x./(2.*L2)+(b2.*L2-b3.*L1+b2.*L1)/(2.*L2)))).^1.5-
0.4178.*(h./(2.*((b3-b2).*x./(2.*L2)+(b2.*L2-
b3.*L1+b2.*L1)/(2.*L2)))).^2)).*freq));
  Gfp=(md*Dsc*freq^2*L1^2+quad( F1, L1, L1+L2, tol)-1i*quad(F2, L1,
L1+L2, tol))/(E*Im);
F3 = @(x) (freq.^2.*L1.*(x-L1).^2.*(0.25.*pi.*Pl.*(2.*((b3-
b2).*x./(2.*L2)+(b2.*L2-
b3.*L1+b2.*L1)/(2.*L2))).^2.*(((Pl.*freq.*(2.*((b3-
b2).*x./(2.*L2)+(b2.*L2-b3.*L1+b2.*L1)/(2.*L2))).^2)./(4.*etal)).^-
0.5.*(0.9003+0.6105.*(h./(2.*((b3-b2).*x./(2.*L2)+(b2.*L2-
b3.*L1+b2.*L1)/(2.*L2)))).^0.5+2.1722.*(h./(2.*((b3-
b2).*x./(2.*L2)+(b2.*L2-b3.*L1+b2.*L1)/(2.*L2)))).^1)+(-
0.0021.*(h./(2.*((b3-b2).*x./(2.*L2)+(b2.*L2-
b3.*L1+b2.*L1)/(2.*L2)))).^0.5-0.1459.*(h./(2.*((b3-
b2).*x./(2.*L2)+(b2.*L2-
b3.*L1+b2.*L1)/(2.*L2)))).^1+0.8255.*(h./(2.*((b3-
b2).*x./(2.*L2)+(b2.*L2-
b3.*L1+b2.*L1)/(2.*L2)))).^1.5+0.8144.*(h./(2.*((b3-
b2).*x./(2.*L2)+(b2.*L2-b3.*L1+b2.*L1)/(2.*L2)))).^2))));
  F4 = @(x) (freq.*L1.*(x-L1).^2.*(0.25.*pi.*Pl.*(2.*((b3-
b2).*x./(2.*L2)+(b2.*L2-
b3.*L1+b2.*L1)/(2.*L2))).^2.*(((Pl.*freq.*(2.*((b3-
b2).*x./(2.*L2)+(b2.*L2-b3.*L1+b2.*L1)/(2.*L2))).^2)./(4.*etal)).^-
1.*(2.5758-1.3388.*(h./(2.*((b3-b2).*x./(2.*L2)+(b2.*L2-
b3.*L1+b2.*L1)/(2.*L2)))).^0.5)+((Pl.*freq.*(2.*((b3-
b2).*x./(2.*L2)+(b2.*L2-b3.*L1+b2.*L1)/(2.*L2))).^2)./(4.*etal)).^-
0.5.*(0.9003+0.7121.*(h./(2.*((b3-b2).*x./(2.*L2)+(b2.*L2-
b3.*L1+b2.*L1)/(2.*L2)))).^0.5+1.6845.*(h./(2.*((b3-
b2).*x./(2.*L2)+(b2.*L2-
b3.*L1+b2.*L1)/(2.*L2)))).^1+0.8236.*(h./(2.*((b3-
b2).*x./(2.*L2)+(b2.*L2-b3.*L1+b2.*L1)/(2.*L2)))).^1.5-
0.4178.*(h./(2.*((b3-b2).*x./(2.*L2)+(b2.*L2-
b3.*L1+b2.*L1)/(2.*L2)))).^2)).*freq));
Hfp=(md*Dsc^2*freq^2*L1+quad (F3, L1, L1+L2, tol)-1i*quad (F4,L1,
L1+L2,tol)+freq^2*L1*Jd)/(E*Im);
   F5 = @(x) (freq.^2.*L1^3*(0.25.*pi.*Pl.*(2.*((b3-
b2).*x./(2.*L2)+(b2.*L2-
b3.*L1+b2.*L1)/(2.*L2))).^2.*(((Pl.*freq.*(2.*((b3-
b2).*x./(2.*L2)+(b2.*L2-b3.*L1+b2.*L1)/(2.*L2))).^2)./(4.*etal)).^-
0.5.*(0.9003+0.6105.*(h./(2.*((b3-b2).*x./(2.*L2)+(b2.*L2-
b3.*L1+b2.*L1)/(2.*L2)))).^0.5+2.1722.*(h./(2.*((b3-
b2).*x./(2.*L2)+(b2.*L2-b3.*L1+b2.*L1)/(2.*L2)))).^1)+(-
0.0021.*(h./(2.*((b3-b2).*x./(2.*L2)+(b2.*L2-
```

```
b3.*L1+b2.*L1)/(2.*L2)))).^0.5-0.1459.*(h./(2.*((b3-
b2).*x./(2.*L2)+(b2.*L2-
b3.*L1+b2.*L1)/(2.*L2)))).^1+0.8255.*(h./(2.*((b3-
b2).*x./(2.*L2)+(b2.*L2-
b3.*L1+b2.*L1)/(2.*L2)))).^1.5+0.8144.*(h./(2.*((b3-
b2).*x./(2.*L2)+(b2.*L2-b3.*L1+b2.*L1)/(2.*L2)))).^2))));
  F6 = @(x) (freq.*L1^3*(0.25.*pi.*Pl.*(2.*((b3-
b2).*x./(2.*L2)+(b2.*L2-
b3.*L1+b2.*L1)/(2.*L2))).^2.*(((Pl.*freq.*(2.*((b3-
b2).*x./(2.*L2)+(b2.*L2-b3.*L1+b2.*L1)/(2.*L2))).^2)./(4.*etal)).^-
1.*(2.5758-1.3388.*(h./(2.*((b3-b2).*x./(2.*L2)+(b2.*L2-
b3.*L1+b2.*L1)/(2.*L2)))).^0.5)+((Pl.*freq.*(2.*((b3-
b2).*x./(2.*L2)+(b2.*L2-b3.*L1+b2.*L1)/(2.*L2))).^2)./(4.*etal)).^-
0.5.*(0.9003+0.7121.*(h./(2.*((b3-b2).*x./(2.*L2)+(b2.*L2-
b3.*L1+b2.*L1)/(2.*L2)))).^0.5+1.6845.*(h./(2.*((b3-
b2).*x./(2.*L2)+(b2.*L2-
b3.*L1+b2.*L1)/(2.*L2)))).^1+0.8236.*(h./(2.*((b3-
b2).*x./(2.*L2)+(b2.*L2-b3.*L1+b2.*L1)/(2.*L2)))).^1.5-
0.4178.*(h./(2.*((b3-b2).*x./(2.*L2)+(b2.*L2-
b3.*L1+b2.*L1)/(2.*L2)))).^2)).*freq));
  Ffp=(-md*freq^2*L1^3-quad (F5, L1, L1+L2, tol)+1i*quad (F6, L1,
L1+L2,tol))/(E*Im);
F7 = @(x) (freq.^2.*L1.^2.*(x-L1).*(0.25.*pi.*Pl.*(2.*((b3-
b2).*x./(2.*L2)+(b2.*L2-
b3.*L1+b2.*L1)/(2.*L2))).^2.*(((Pl.*freq.*(2.*((b3-
b2).*x./(2.*L2)+(b2.*L2-b3.*L1+b2.*L1)/(2.*L2))).^2)./(4.*etal)).^-
0.5.*(0.9003+0.6105.*(h./(2.*((b3-b2).*x./(2.*L2)+(b2.*L2-
b3.*L1+b2.*L1)/(2.*L2)))).^0.5+2.1722.*(h./(2.*((b3-
b2).*x./(2.*L2)+(b2.*L2-b3.*L1+b2.*L1)/(2.*L2)))).^1)+(-
0.0021.*(h./(2.*((b3-b2).*x./(2.*L2)+(b2.*L2-
b3.*L1+b2.*L1)/(2.*L2)))).^0.5-0.1459.*(h./(2.*((b3-
b2).*x./(2.*L2)+(b2.*L2-
b3.*L1+b2.*L1)/(2.*L2)))).^1+0.8255.*(h./(2.*((b3-
b2).*x./(2.*L2)+(b2.*L2-
b3.*L1+b2.*L1)/(2.*L2)))).^1.5+0.8144.*(h./(2.*((b3-
b2).*x./(2.*L2)+(b2.*L2-b3.*L1+b2.*L1)/(2.*L2)))).^2))));
F8 = @(x) (freq.*L1.^2.*(x-L1).*(0.25.*pi.*Pl.*(2.*((b3-
b2).*x./(2.*L2)+(b2.*L2-
b3.*L1+b2.*L1)/(2.*L2))).^2.*(((Pl.*freq.*(2.*((b3-
b2).*x./(2.*L2)+(b2.*L2-b3.*L1+b2.*L1)/(2.*L2))).^2)./(4.*etal)).^-
1.*(2.5758-1.3388.*(h./(2.*((b3-b2).*x./(2.*L2)+(b2.*L2-
b3.*L1+b2.*L1)/(2.*L2)))).^0.5)+((Pl.*freq.*(2.*((b3-
b2).*x./(2.*L2)+(b2.*L2-b3.*L1+b2.*L1)/(2.*L2))).^2)./(4.*etal)).^-
0.5.*(0.9003+0.7121.*(h./(2.*((b3-b2).*x./(2.*L2)+(b2.*L2-
b3.*L1+b2.*L1)/(2.*L2)))).^0.5+1.6845.*(h./(2.*((b3-
b2).*x./(2.*L2)+(b2.*L2-
b3.*L1+b2.*L1)/(2.*L2)))).^1+0.8236.*(h./(2.*((b3-
b2).*x./(2.*L2)+(b2.*L2-b3.*L1+b2.*L1)/(2.*L2)))).^1.5-
0.4178.*(h./(2.*((b3-b2).*x./(2.*L2)+(b2.*L2-
b3.*L1+b2.*L1)/(2.*L2)))).^2)).*freq));
Kfp=(-md*Dsc*freq^2*L1^2-quad (F7, L1, L1+L2, tol)+1i*quad (F8, L1,
L1+L2, tol))/(E*Im);
MMfp=KKp.^2.*(Cfp+cfp)-Gfp.*(Cfp-cfp)-Hfp.*KKp.*(Sfp+sfp);
NNfp=KKp.^2.*(Sfp+sfp)-Gfp.*(Sfp-sfp)-Hfp.*KKp.*(Cfp-cfp);
  OOfp=KKp.^(-1).*(KKp.^2.*sfp+Gfp.*sfp+Hfp.*KKp.*cfp);
  PPfp=KKp.^3.*(Sfp-sfp)-Ffp.*(Cfp-cfp)-Kfp.*KKp.*(Sfp+sfp);
  QQfp=KKp.^3.*(Cfp+cfp)-Ffp.*(Sfp-sfp)-Kfp.*KKp.*(Cfp-cfp);
```

```
RRfp=KKp.^(-1).*(KKp.^3.*cfp+Ffp.*sfp+Kfp.*KKp.*cfp);
A1fp=(OOfp.*QQfp-RRfp.*NNfp)/(MMfp.*QQfp-PPfp.*NNfp);
A2fp=(OOfp.*PPfp-RRfp.*MMfp)/(NNfp.*PPfp-MMfp.*QQfp);
Dfpl=abs(A1fp.*(Cfp-cfp)+A2fp.*(Sfp-sfp)+KKp.^(-1).*sfp);
Rfreq(jfreq)=freq;
RDfpl(jfreq)=Dfpl;
end
 [Amplitude, Location]=max(RDfpl);
resfl=Rfreq(Location);
for jfreq=1:length(Lfreq)
if(jfreq==1);
continue
else
if RDfpl(jfreq-1)<=Amplitude/sqrt(2);
                %%%% if the above condition is not satisfied the loop
                %%%% continues to next iteration
                if(RDfpl(jfreq)>=(Amplitude/(sqrt(2))));

                    Dfpmagprevious=RDfpl(jfreq-1);
                    Dfpmagcurrent=RDfpl(jfreq);
                    Dfpmaglocal=[Dfpmagcurrent Dfpmagprevious];
                    [Dfpmagmin,Iminlocal]=min(Dfpmaglocal);
                    %   Note that if Iminlocal equals 1, then the index
    %   for Lamdbw is jlambda; if Iminlocal is 2, then the index
    %   for Lamdbw is jlambda-1. So, in general, the index for
        %   lambdabw may be written as jlambda+1-Iminlocal.
    resfbw1=Rfreq(jfreq+1-Iminlocal);
                end
            end
                if RDfpl(jfreq-1)>=Amplitude/sqrt(2);
                  if RDfpl(jfreq)<=Amplitude/sqrt(2);
                    Dfpmagprevious=RDfpl(jfreq-1);
                    Dfpmagcurrent=RDfpl(jfreq);
                    Dfpmaglocal=[Dfpmagcurrent Dfpmagprevious];
                    [Dfpmagmin,Iminlocal]=min(Dfpmaglocal);
                    %   Note that if Iminlocal equals 1, then the index
  %   for lambdabw is jlambda; if Iminlocal is 2, then the index
   %   for lambdabw is jlambda-1. So, in general, the index for
  %   lambdabw may be written as jlambda+1-Iminlocal.
  resfbw2=Rfreq(jfreq+1-Iminlocal);
                  end
              end
        end
        end
            %%%% Quality factor is given by lambdaresonant/bandwidth
            resfl/(2*pi*10^3)
            Qp3db=resfl/(resfbw2-resfbw1)
%%%% energy method %%%%
resfl=196.7*10^3*2*pi;
%%%%%%%%%%%%%%%%%%%% Finding spectrum in air %%%%%%%%%%%%%%%%%%
            % denotes any point along the head
           %Dsy= 2*((b3-b2)*x./(2*L2)+(b2*L2-b3*L1+b2*L1)/(2*L2)); %
the length of the isosceles trapezoid along y direction
          Dsc=(L2/3)*(2*b3+b2)/(b3+b2); % distance of the mass center
of the head to the tip of the stem
%            mdbar=Pb*h*2*2*((b3-b2)*x./(2*L2)+(b2*L2-
b3*L1+b2*L1)/(2*L2));
```

```
          Reym=(Pl*resfl*b1^2)/(4*etal);
          %fReyd= ((Pa*freq*(2*(b3-b2)*x./(2*L2)+(b2*L2-
b3*L1+b2*L1)/(2*L2)).^2)./(4*etaa));
          Gammarm=Reym^-
0.5*(0.9003+0.6105*(h/b1)^0.5+2.1722*(h/b1)^1)+(-0.0021*(h/b1)^0.5-
0.1459*(h/b1)^1+0.8255*(h/b1)^1.5+0.8144*(h/b1)^2);
          Gammaim=Reym^-1*(2.5758-1.3388*(h/b1)^0.5)+Reym^-
0.5*(0.9003+0.7121*(h/b1)^0.5+1.6845*(h/b1)^1+0.8236*(h/b1)^1.5-
0.4178*(h/b1)^2);
%           fGammard=(((Pa*freq*(2*(b3-b2)*x./(2*L2)+(b2*L2-
b3*L1+b2*L1)/(2*L2)).^2)./(4*etaa)).^-0.5*(0.9003+0.6105*(h./2*((b3-
b2)*x./(2*L2)+(b2*L2-b3*L1+b2*L1)/(2*L2))).^0.5+2.1722*(h./2*((b3-
b2)*x./(2*L2)+(b2*L2-b3*L1+b2*L1)/(2*L2))).^1)+(-0.0021*(h./2*((b3-
b2)*x./(2*L2)+(b2*L2-b3*L1+b2*L1)/(2*L2))).^0.5-0.1459*(h./2*((b3-
b2)*x./(2*L2)+(b2*L2-b3*L1+b2*L1)/(2*L2))).^1+0.8255*(h./2*((b3-
b2)*x./(2*L2)+(b2*L2-b3*L1+b2*L1)/(2*L2))).^1.5+0.8144*(h./2*((b3-
b2)*x./(2*L2)+(b2*L2-b3*L1+b2*L1)/(2*L2))).^2));
%           fGammaid=(((Pa*freq*(2*(b3-b2)*x./(2*L2)+(b2*L2-
b3*L1+b2*L1)/(2*L2)).^2)./(4*etaa)).^-1*(2.5758-1.3388*(h./2*((b3-
b2)*x./(2*L2)+(b2*L2-b3*L1+b2*L1)/(2*L2))).^0.5)+((Pa*freq*(2*(b3-
b2)*x./(2*L2)+(b2*L2-b3*L1+b2*L1)/(2*L2)).^2)./(4*etaa)).^-
0.5*(0.9003+0.7121*(h./2*((b3-b2)*x./(2*L2)+(b2*L2-
b3*L1+b2*L1)/(2*L2))).^0.5+1.6845*(h./2*((b3-b2)*x./(2*L2)+(b2*L2-
b3*L1+b2*L1)/(2*L2))).^1+0.8236*(h./2*((b3-b2)*x./(2*L2)+(b2*L2-
b3*L1+b2*L1)/(2*L2))).^1.5-0.4178*(h./2*((b3-b2)*x./(2*L2)+(b2*L2-
b3*L1+b2*L1)/(2*L2))).^2));
%           mfpmbar=0.25*pi*Pl*b1^2*Gammarm;
cfpmbar=0.25*pi*Pl*b1^2*Gammaim*resfl;
%           fmfpdbar= (0.25*pi*Pa*(2*(b3-b2)*x./(2*L2)+(b2*L2-
b3*L1+b2*L1)/(2*L2)).^2*(((Pa*freq*(2*(b3-b2)*x./(2*L2)+(b2*L2-
b3*L1+b2*L1)/(2*L2)).^2)./(4*etaa)).^-0.5*(0.9003+0.6105*(h./2*((b3-
b2)*x./(2*L2)+(b2*L2-b3*L1+b2*L1)/(2*L2))).^0.5+2.1722*(h./2*((b3-
b2)*x./(2*L2)+(b2*L2-b3*L1+b2*L1)/(2*L2))).^1)+(-0.0021*(h./2*((b3-
b2)*x./(2*L2)+(b2*L2-b3*L1+b2*L1)/(2*L2))).^0.5-0.1459*(h./2*((b3-
b2)*x./(2*L2)+(b2*L2-b3*L1+b2*L1)/(2*L2))).^1+0.8255*(h./2*((b3-
b2)*x./(2*L2)+(b2*L2-b3*L1+b2*L1)/(2*L2))).^1.5+0.8144*(h./2*((b3-
b2)*x./(2*L2)+(b2*L2-b3*L1+b2*L1)/(2*L2))).^2)));
%           fcfpdbar= (0.25*pi*Pa*(2*(b3-b2)*x./(2*L2)+(b2*L2-
b3*L1+b2*L1)/(2*L2)).^2*(((Pa*freq*(2*(b3-b2)*x./(2*L2)+(b2*L2-
b3*L1+b2*L1)/(2*L2)).^2)./(4*etaa)).^-1*(2.5758-1.3388*(h./2*((b3-
b2)*x./(2*L2)+(b2*L2-b3*L1+b2*L1)/(2*L2))).^0.5)+((Pa*freq*(2*(b3-
b2)*x./(2*L2)+(b2*L2-b3*L1+b2*L1)/(2*L2)).^2)./(4*etaa)).^-
0.5*(0.9003+0.7121*(h./2*((b3-b2)*x./(2*L2)+(b2*L2-
b3*L1+b2*L1)/(2*L2))).^0.5+1.6845*(h./2*((b3-b2)*x./(2*L2)+(b2*L2-
b3*L1+b2*L1)/(2*L2))).^1+0.8236*(h./2*((b3-b2)*x./(2*L2)+(b2*L2-
b3*L1+b2*L1)/(2*L2))).^1.5-0.4178*(h./2*((b3-b2)*x./(2*L2)+(b2*L2-
b3*L1+b2*L1)/(2*L2))).^2))*freq);
  Kp=L1*((resfl.^2*(mmbar+mfpmbar)-1i*resfl*cfpmbar)/(E*Im)).^0.25;
          KKp=Kp;
          Cfp=cosh(KKp);
          Sfp=sinh(KKp);
          sfp=sin(KKp);
          cfp=cos(KKp);
    F1 = @(x) (resfl.^2.*L1.^2.*(x-L1).*(0.25.*pi.*Pl.*(2.*((b3-
b2).*x./(2.*L2)+(b2.*L2-
b3.*L1+b2.*L1)/(2.*L2))).^2.*(((Pl.*resfl.*(2.*((b3-
b2).*x./(2.*L2)+(b2.*L2-b3.*L1+b2.*L1)/(2.*L2))).^2)./(4.*etal)).^-
```

```
0.5.*(0.9003+0.6105.*(h./(2.*((b3-b2).*x./(2.*L2)+(b2.*L2-
b3.*L1+b2.*L1)/(2.*L2)))).^0.5+2.1722.*(h./(2.*((b3-
b2).*x./(2.*L2)+(b2.*L2-b3.*L1+b2.*L1)/(2.*L2)))).^1)+(-
0.0021.*(h./(2.*((b3-b2).*x./(2.*L2)+(b2.*L2-
b3.*L1+b2.*L1)/(2.*L2)))).^0.5-0.1459.*(h./(2.*((b3-
b2).*x./(2.*L2)+(b2.*L2-
b3.*L1+b2.*L1)/(2.*L2)))).^1+0.8255.*(h./(2.*((b3-
b2).*x./(2.*L2)+(b2.*L2-
b3.*L1+b2.*L1)/(2.*L2)))).^1.5+0.8144.*(h./(2.*((b3-
b2).*x./(2.*L2)+(b2.*L2-b3.*L1+b2.*L1)/(2.*L2)))).^2))));
             F2 = @(x) (resfl.*L1.^2.*(x-L1).*(0.25.*pi.*Pl.*(2.*((b3-
b2).*x./(2.*L2)+(b2.*L2-
b3.*L1+b2.*L1)/(2.*L2))).^2.*(((Pl.*resfl.*(2.*((b3-
b2).*x./(2.*L2)+(b2.*L2-b3.*L1+b2.*L1)/(2.*L2))).^2)./(4.*etal)).^-
1.*(2.5758-1.3388.*(h./(2.*((b3-b2).*x./(2.*L2)+(b2.*L2-
b3.*L1+b2.*L1)/(2.*L2)))).^0.5)+((Pl.*resfl.*(2.*((b3-
b2).*x./(2.*L2)+(b2.*L2-b3.*L1+b2.*L1)/(2.*L2))).^2)./(4.*etal)).^-
0.5.*(0.9003+0.7121.*(h./(2.*((b3-b2).*x./(2.*L2)+(b2.*L2-
b3.*L1+b2.*L1)/(2.*L2)))).^0.5+1.6845.*(h./(2.*((b3-
b2).*x./(2.*L2)+(b2.*L2-
b3.*L1+b2.*L1)/(2.*L2)))).^1+0.8236.*(h./(2.*((b3-
b2).*x./(2.*L2)+(b2.*L2-b3.*L1+b2.*L1)/(2.*L2)))).^1.5-
0.4178.*(h./(2.*((b3-b2).*x./(2.*L2)+(b2.*L2-
b3.*L1+b2.*L1)/(2.*L2)))).^2)).*resfl));
          Gfp=(md*Dsc*resfl^2*L1^2+quad( F1, L1, L1+L2, tol)-
1i*quad(F2, L1, L1+L2, tol))/(E*Im);
             F3 = @(x) (resfl.^2.*L1.*(x-
L1).^2.*(0.25.*pi.*Pl.*(2.*((b3-b2).*x./(2.*L2)+(b2.*L2-
b3.*L1+b2.*L1)/(2.*L2))).^2.*(((Pl.*resfl.*(2.*((b3-
b2).*x./(2.*L2)+(b2.*L2-b3.*L1+b2.*L1)/(2.*L2))).^2)./(4.*etal)).^-
0.5.*(0.9003+0.6105.*(h./(2.*((b3-b2).*x./(2.*L2)+(b2.*L2-
b3.*L1+b2.*L1)/(2.*L2)))).^0.5+2.1722.*(h./(2.*((b3-
b2).*x./(2.*L2)+(b2.*L2-b3.*L1+b2.*L1)/(2.*L2)))).^1)+(-
0.0021.*(h./(2.*((b3-b2).*x./(2.*L2)+(b2.*L2-
b3.*L1+b2.*L1)/(2.*L2)))).^0.5-0.1459.*(h./(2.*((b3-
b2).*x./(2.*L2)+(b2.*L2-
b3.*L1+b2.*L1)/(2.*L2)))).^1+0.8255.*(h./(2.*((b3-
b2).*x./(2.*L2)+(b2.*L2-
b3.*L1+b2.*L1)/(2.*L2)))).^1.5+0.8144.*(h./(2.*((b3-
b2).*x./(2.*L2)+(b2.*L2-b3.*L1+b2.*L1)/(2.*L2)))).^2))));
             F4 = @(x) (resfl.*L1.*(x-L1).^2.*(0.25.*pi.*Pl.*(2.*((b3-
b2).*x./(2.*L2)+(b2.*L2-
b3.*L1+b2.*L1)/(2.*L2))).^2.*(((Pl.*resfl.*(2.*((b3-
b2).*x./(2.*L2)+(b2.*L2-b3.*L1+b2.*L1)/(2.*L2))).^2)./(4.*etal)).^-
1.*(2.5758-1.3388.*(h./(2.*((b3-b2).*x./(2.*L2)+(b2.*L2-
b3.*L1+b2.*L1)/(2.*L2)))).^0.5)+((Pl.*resfl.*(2.*((b3-
b2).*x./(2.*L2)+(b2.*L2-b3.*L1+b2.*L1)/(2.*L2))).^2)./(4.*etal)).^-
0.5.*(0.9003+0.7121.*(h./(2.*((b3-b2).*x./(2.*L2)+(b2.*L2-
b3.*L1+b2.*L1)/(2.*L2)))).^0.5+1.6845.*(h./(2.*((b3-
b2).*x./(2.*L2)+(b2.*L2-
b3.*L1+b2.*L1)/(2.*L2)))).^1+0.8236.*(h./(2.*((b3-
b2).*x./(2.*L2)+(b2.*L2-b3.*L1+b2.*L1)/(2.*L2)))).^1.5-
0.4178.*(h./(2.*((b3-b2).*x./(2.*L2)+(b2.*L2-
b3.*L1+b2.*L1)/(2.*L2)))).^2)).*resfl));
    Hfp=(md*Dsc^2*resfl^2*L1+quad (F3, L1, L1+L2, tol)-1i*quad (F4,L1,
L1+L2, tol)+resfl^2*L1*Jd)/(E*Im);
```

```
F5 = @(x) (resfl.^2.*L1^3*(0.25.*pi.*Pl.*(2.*((b3-
b2).*x./(2.*L2)+(b2.*L2-
b3.*L1+b2.*L1)/(2.*L2))).^2.*(((Pl.*resfl.*(2.*((b3-
b2).*x./(2.*L2)+(b2.*L2-b3.*L1+b2.*L1)/(2.*L2))).^2)./(4.*etal)).^-
0.5.*(0.9003+0.6105.*(h./(2.*((b3-b2).*x./(2.*L2)+(b2.*L2-
b3.*L1+b2.*L1)/(2.*L2)))).^0.5+2.1722.*(h./(2.*((b3-
b2).*x./(2.*L2)+(b2.*L2-b3.*L1+b2.*L1)/(2.*L2)))).^1)+(-
0.0021.*(h./(2.*((b3-b2).*x./(2.*L2)+(b2.*L2-
b3.*L1+b2.*L1)/(2.*L2)))).^0.5-0.1459.*(h./(2.*((b3-
b2).*x./(2.*L2)+(b2.*L2-
b3.*L1+b2.*L1)/(2.*L2)))).^1+0.8255.*(h./(2.*((b3-
b2).*x./(2.*L2)+(b2.*L2-
b3.*L1+b2.*L1)/(2.*L2)))).^1.5+0.8144.*(h./(2.*((b3-
b2).*x./(2.*L2)+(b2.*L2-b3.*L1+b2.*L1)/(2.*L2)))).^2))));
             F6 = @(x) (resfl.*L1^3*(0.25.*pi.*Pl.*(2.*((b3-
b2).*x./(2.*L2)+(b2.*L2-
b3.*L1+b2.*L1)/(2.*L2))).^2.*(((Pl.*resfl.*(2.*((b3-
b2).*x./(2.*L2)+(b2.*L2-b3.*L1+b2.*L1)/(2.*L2))).^2)./(4.*etal)).^-
1.*(2.5758-1.3388.*(h./(2.*((b3-b2).*x./(2.*L2)+(b2.*L2-
b3.*L1+b2.*L1)/(2.*L2)))).^0.5)+((Pl.*resfl.*(2.*((b3-
b2).*x./(2.*L2)+(b2.*L2-b3.*L1+b2.*L1)/(2.*L2))).^2)./(4.*etal)).^-
0.5.*(0.9003+0.7121.*(h./(2.*((b3-b2).*x./(2.*L2)+(b2.*L2-
b3.*L1+b2.*L1)/(2.*L2)))).^0.5+1.6845.*(h./(2.*((b3-
b2).*x./(2.*L2)+(b2.*L2-
b3.*L1+b2.*L1)/(2.*L2)))).^1+0.8236.*(h./(2.*((b3-
b2).*x./(2.*L2)+(b2.*L2-b3.*L1+b2.*L1)/(2.*L2)))).^1.5-
0.4178.*(h./(2.*((b3-b2).*x./(2.*L2)+(b2.*L2-
b3.*L1+b2.*L1)/(2.*L2)))).^2)).*resfl));
   Ffp=(-md*resfl^2*L1^3-quad (F5, L1, L1+L2, tol)+1i*quad (F6, L1,
L1+L2, tol))/(E*Im);
   F7 = @(x) (resfl.^2.*L1.^2.*(x-L1).*(0.25.*pi.*Pl.*(2.*((b3-
b2).*x./(2.*L2)+(b2.*L2-
b3.*L1+b2.*L1)/(2.*L2))).^2.*(((Pl.*resfl.*(2.*((b3-
b2).*x./(2.*L2)+(b2.*L2-b3.*L1+b2.*L1)/(2.*L2))).^2)./(4.*etal)).^-
0.5.*(0.9003+0.6105.*(h./(2.*((b3-b2).*x./(2.*L2)+(b2.*L2-
b3.*L1+b2.*L1)/(2.*L2)))).^0.5+2.1722.*(h./(2.*((b3-
b2).*x./(2.*L2)+(b2.*L2-b3.*L1+b2.*L1)/(2.*L2)))).^1)+(-
0.0021.*(h./(2.*((b3-b2).*x./(2.*L2)+(b2.*L2-
b3.*L1+b2.*L1)/(2.*L2)))).^0.5-0.1459.*(h./(2.*((b3-
b2).*x./(2.*L2)+(b2.*L2-
b3.*L1+b2.*L1)/(2.*L2)))).^1+0.8255.*(h./(2.*((b3-
b2).*x./(2.*L2)+(b2.*L2-
b3.*L1+b2.*L1)/(2.*L2)))).^1.5+0.8144.*(h./(2.*((b3-
b2).*x./(2.*L2)+(b2.*L2-b3.*L1+b2.*L1)/(2.*L2)))).^2))));
  F8 = @(x) (resfl.*L1.^2.*(x-L1).*(0.25.*pi.*Pl.*(2.*((b3-
b2).*x./(2.*L2)+(b2.*L2-
b3.*L1+b2.*L1)/(2.*L2))).^2.*(((Pl.*resfl.*(2.*((b3-
b2).*x./(2.*L2)+(b2.*L2-b3.*L1+b2.*L1)/(2.*L2))).^2)./(4.*etal)).^-
1.*(2.5758-1.3388.*(h./(2.*((b3-b2).*x./(2.*L2)+(b2.*L2-
b3.*L1+b2.*L1)/(2.*L2)))).^0.5)+((Pl.*resfl.*(2.*((b3-
b2).*x./(2.*L2)+(b2.*L2-b3.*L1+b2.*L1)/(2.*L2))).^2)./(4.*etal)).^-
0.5.*(0.9003+0.7121.*(h./(2.*((b3-b2).*x./(2.*L2)+(b2.*L2-
b3.*L1+b2.*L1)/(2.*L2)))).^0.5+1.6845.*(h./(2.*((b3-
b2).*x./(2.*L2)+(b2.*L2-
b3.*L1+b2.*L1)/(2.*L2)))).^1+0.8236.*(h./(2.*((b3-
b2).*x./(2.*L2)+(b2.*L2-b3.*L1+b2.*L1)/(2.*L2)))).^1.5-
0.4178.*(h./(2.*((b3-b2).*x./(2.*L2)+(b2.*L2-
```

```
b3.*L1+b2.*L1)/(2.*L2)))).^2)).*resfl));
  Kfp=(-md*Dsc*resfl^2*L1^2-quad (F7, L1, L1+L2, tol)+1i*quad (F8, L1,
L1+L2, tol))/(E*Im);
           MMfp=KKp.^2.*(Cfp+cfp)-Gfp.*(Cfp-cfp)-Hfp.*KKp.*(Sfp+sfp);
           NNfp=KKp.^2.*(Sfp+sfp)-Gfp.*(Sfp-sfp)-Hfp.*KKp.*(Cfp-cfp);
           OOfp=KKp.^(-1).*(KKp.^2.*sfp+Gfp.*sfp+Hfp.*KKp.*cfp);
           PPfp=KKp.^3.*(Sfp-sfp)-Ffp.*(Cfp-cfp)-Kfp.*KKp.*(Sfp+sfp);
           QQfp=KKp.^3.*(Cfp+cfp)-Ffp.*(Sfp-sfp)-Kfp.*KKp.*(Cfp-cfp);
           RRfp=KKp.^(-1).*(KKp.^3.*cfp+Ffp.*sfp+Kfp.*KKp.*cfp);
           A1fp=(OOfp.*QQfp-RRfp.*NNfp)/(MMfp.*QQfp-PPfp.*NNfp);
           A2fp=(OOfp.*PPfp-RRfp.*MMfp)/(NNfp.*PPfp-MMfp.*QQfp);
           xi=sym('xi','real'); % denotes x/L1
           X=A1fp*(cosh(KKp*xi)-cos(KKp*xi))+A2fp*(sinh(KKp*xi)-
sin(KKp*xi))+KKp^(-1)*sin(KKp*xi); % normalized shape function
           Xp=KKp*(A1fp*(sinh(KKp*xi)+sin(KKp*xi))+A2fp*(cosh(KKp*xi)-
cos(KKp*xi))+KKp^(-1)*cos(KKp*xi)); % first derivative of normalized
deflection measns X'
Xpp=KKp^2*(A1fp*(cosh(KKp*xi)+cos(KKp*xi))+A2fp*(sinh(KKp*xi)+sin(KKp*x
i))-KKp^(-1)*sin(KKp*xi)); % second derivative of normalized deflection
measns X''
            BB1=int((real(Xpp))^2, xi, 0, 1);
            BB2=int((imag(Xpp))^2, xi, 0, 1);
            BB3=int((real(Xpp))*(imag(Xpp)), xi, 0, 1);
            BB4=int((real(X))^2, xi, 0, 1);
            BB5=int((imag(X))^2, xi, 0, 1);
            BB6=int((real(X))*(imag(X)), xi, 0, 1);
            BB7=(real(A1fp*(cosh(KKp)-cos(KKp))+A2fp*(sinh(KKp)-
sin(KKp))+KKp^(-1)*sin(KKp)))^2;
            BB8=(imag(A1fp*(cosh(KKp)-cos(KKp))+A2fp*(sinh(KKp)-
sin(KKp))+KKp^(-1)*sin(KKp)))^2;
            BB9=(real(A1fp*(cosh(KKp)-cos(KKp))+A2fp*(sinh(KKp)-
sin(KKp))+KKp^(-1)*sin(KKp)))*(imag(A1fp*(cosh(KKp)-
cos(KKp))+A2fp*(sinh(KKp)-sin(KKp))+KKp^(-1)*sin(KKp)));
            BB13=(real(KKp*(A1fp*(sinh(KKp)+sin(KKp))+A2fp*(cosh(KKp)-
cos(KKp))+KKp^(-1)*cos(KKp))))^2;
            BB14=(imag(KKp*(A1fp*(sinh(KKp)+sin(KKp))+A2fp*(cosh(KKp)-
cos(KKp))+KKp^(-1)*cos(KKp))))^2;
            BB15=(real(KKp*(A1fp*(sinh(KKp)+sin(KKp))+A2fp*(cosh(KKp)-
cos(KKp))+KKp^(-
1)*cos(KKp))))*(imag(KKp*(A1fp*(sinh(KKp)+sin(KKp))+A2fp*(cosh(KKp)-
cos(KKp))+KKp^(-1)*cos(KKp))));
            BB10=sqrt(BB7)*sqrt(BB13);
            BB11=sqrt(BB8)*sqrt(BB14);
            BB12=sqrt(BB7)*sqrt(BB14)+sqrt(BB13)*sqrt(BB8);
            BB16=BB13;
            BB17=BB14;
            BB18=BB15;
            BB19=-imag(2*A1fp*KKp^2);
for jtau=1:length(Ltau)
          F(jtau)=BB1*(cos(jtau))^2+BB2*(sin(jtau))^2-
2*BB3*(cos(jtau))*(sin(jtau))+(L1^4*mmbar*resfl^2*(E*Im)^(-
1))*(BB4*(sin(jtau))^2+BB5*(cos(jtau))^2+2*BB6*(cos(jtau))*(sin(jtau)))
+(md*L1^3*resfl^2*(E*Im)^(-
1))*(BB7*(sin(jtau))^2+BB8*(cos(jtau))^2+2*BB9*(cos(jtau))*(sin(jtau)))
+(2*md*L1^2*Dsc*resfl^2*(E*Im)^(-
1))*(BB10*(sin(jtau))^2+BB11*(cos(jtau))^2+BB12*(cos(jtau))*(sin(jtau))
)+(md*L1*Dsc^2*resfl^2*(E*Im)^(-
```

```
1))*(BB13*(sin(jtau))^2+BB14*(cos(jtau))^2+2*BB15*(cos(jtau))*(sin(jtau
)))+(Jd*L1*resfl^2*(E*Im)^(-
1))*(BB16*(sin(jtau))^2+BB17*(cos(jtau))^2+2*BB18*(cos(jtau))*(sin(jtau
)));
Qua(jtau)=F(jtau)/BB19;
end
Quaactual=max (double(Qua(:)))
```

Case 2: Hammerhead Microcantilever with a Semi-circular Head

```
L1=200*10^-6; % length of the stem
b1=45*10^-6; % width of the stem
A=200*200*10^-12;% area of the head
R=sqrt(2*A)/sqrt(pi); % radius of the head
h=12*10^-6; % thickness of the cantilever
E=169*10^9; % Young's Modulus
Pb=2330; % density of silicon for both supporting beam and hammerhead
Pl=1222; % density of the fluid at 20C
Pa=1.205; % density of the air at 20C
mm=Pb*L1*b1*h; % mass of the stem
mmbar=Pb*b1*h;
md=0.5*Pb*pi*R^2*h; % mass of the head
Im=(1/12)*h*(b1)^3; % moment of inertia of the stem
Jd=Pb*h*(pi/4-8/(9*pi))*R^4;
etal=0.106; % viscosity of the fluid 20C
etaa=0.00001827; % viscosity of the air 20C
step=20*2*pi;
% spectrum of the first lateral mode in air and water %
tol = 1e-20;
Lresfl = 190000*2*pi:step:200000*2*pi;
Ltau = 0:0.5:6;
resfl= 145.6*1000*2*pi;
%%%%%%%%%%%%%%%%%%%% Finding spectrum in air %%%%%%%%%%%%%%%%%%
           % denotes any point along the head
           %Dsy= 2*((b3-b2)*x./(2*R)+(b2*R-b3*L1+b2*L1)/(2*R)); % the
length of the isosceles trapezoid along y direction
           Dsc=4*R/(3*pi); % distance of the mass center of the head to
the tip of the stem
%            mdbar=Pb*h*2*2*((b3-b2)*x./(2*R)+(b2*R-b3*L1+b2*L1)
/(2*R));
           Reym=(Pl*resfl*b1^2)/(4*etal);
           %fReyd= ((Pa*resfl*(2*(b3-b2)*x./(2*R)+(b2*R-
b3*L1+b2*L1)/(2*R)).^2)./(4*etaa));
           Gammarm=Reym^-
0.5*(0.9003+0.6105*(h/b1)^0.5+2.1722*(h/b1)^1)+(-0.0021*(h/b1)^0.5-
0.1459*(h/b1)^1+0.8255*(h/b1)^1.5+0.8144*(h/b1)^2);
           Gammaim=Reym^-1*(2.5758-1.3388*(h/b1)^0.5)+Reym^-
0.5*(0.9003+0.7121*(h/b1)^0.5+1.6845*(h/b1)^1+0.8236*(h/b1)^1.5-
0.4178*(h/b1)^2);
%            fGammard=(((Pa*resfl*(2*(b3-b2)*x./(2*R)+(b2*R-
b3*L1+b2*L1)/(2*R)).^2)./(4*etaa)).^-0.5*(0.9003+0.6105*(h./2*((b3-
b2)*x./(2*R)+(b2*R-b3*L1+b2*L1)/(2*R))).^0.5+2.1722*(h./2*((b3-
b2)*x./(2*R)+(b2*R-b3*L1+b2*L1)/(2*R))).^1)+(-0.0021*(h./2*((b3-
b2)*x./(2*R)+(b2*R-b3*L1+b2*L1)/(2*R))).^0.5-0.1459*(h./2*((b3-
b2)*x./(2*R)+(b2*R-b3*L1+b2*L1)/(2*R))).^1+0.8255*(h./2*((b3-
```

```
b2)*x./(2*R)+(b2*R-b3*L1+b2*L1)/(2*R))).^1.5+0.8144*(h./2*((b3-
b2)*x./(2*R)+(b2*R-b3*L1+b2*L1)/(2*R))).^2));
%            fGammaid=(((Pa*resfl*(2*(b3-b2)*x./(2*R)+(b2*R-
b3*L1+b2*L1)/(2*R)).^2)./(4*etaa)).^-1*(2.5758-1.3388*(h./2*((b3-
b2)*x./(2*R)+(b2*R-b3*L1+b2*L1)/(2*R))).^0.5)+((Pa*resfl*(2*(b3-
b2)*x./(2*R)+(b2*R-b3*L1+b2*L1)/(2*R)).^2)./(4*etaa)).^-
0.5*(0.9003+0.7121*(h./2*((b3-b2)*x./(2*R)+(b2*R-
b3*L1+b2*L1)/(2*R))).^0.5+1.6845*(h./2*((b3-b2)*x./(2*R)+(b2*R-
b3*L1+b2*L1)/(2*R))).^1+0.8236*(h./2*((b3-b2)*x./(2*R)+(b2*R-
b3*L1+b2*L1)/(2*R))).^1.5-0.4178*(h./2*((b3-b2)*x./(2*R)+(b2*R-
b3*L1+b2*L1)/(2*R))).^2));
%            mfpmbar=0.25*pi*Pl*b1^2*Gammarm;
cfpmbar=0.25*pi*Pl*b1^2*Gammaim*resfl;
%            fmfpdbar= (0.25*pi*Pa*(2*(b3-b2)*x./(2*R)+(b2*R-
b3*L1+b2*L1)/(2*R)).^2*(((Pa*resfl*(2*(b3-b2)*x./(2*R)+(b2*R-
b3*L1+b2*L1)/(2*R)).^2)./(4*etaa)).^-0.5*(0.9003+0.6105*(h./2*((b3-
b2)*x./(2*R)+(b2*R-b3*L1+b2*L1)/(2*R))).^0.5+2.1722*(h./2*((b3-
b2)*x./(2*R)+(b2*R-b3*L1+b2*L1)/(2*R))).^1)+(-0.0021*(h./2*((b3-
b2)*x./(2*R)+(b2*R-b3*L1+b2*L1)/(2*R))).^0.5-0.1459*(h./2*((b3-
b2)*x./(2*R)+(b2*R-b3*L1+b2*L1)/(2*R))).^1+0.8255*(h./2*((b3-
b2)*x./(2*R)+(b2*R-b3*L1+b2*L1)/(2*R))).^1.5+0.8144*(h./2*((b3-
b2)*x./(2*R)+(b2*R-b3*L1+b2*L1)/(2*R))).^2)));
%            fcfpdbar= (0.25*pi*Pa*(2*(b3-b2)*x./(2*R)+(b2*R-
b3*L1+b2*L1)/(2*R)).^2*(((Pa*resfl*(2*(b3-b2)*x./(2*R)+(b2*R-
b3*L1+b2*L1)/(2*R)).^2)./(4*etaa)).^-1*(2.5758-1.3388*(h./2*((b3-
b2)*x./(2*R)+(b2*R-b3*L1+b2*L1)/(2*R))).^0.5)+((Pa*resfl*(2*(b3-
b2)*x./(2*R)+(b2*R-b3*L1+b2*L1)/(2*R)).^2)./(4*etaa)).^-
0.5*(0.9003+0.7121*(h./2*((b3-b2)*x./(2*R)+(b2*R-
b3*L1+b2*L1)/(2*R))).^0.5+1.6845*(h./2*((b3-b2)*x./(2*R)+(b2*R-
b3*L1+b2*L1)/(2*R))).^1+0.8236*(h./2*((b3-b2)*x./(2*R)+(b2*R-
b3*L1+b2*L1)/(2*R))).^1.5-0.4178*(h./2*((b3-b2)*x./(2*R)+(b2*R-
b3*L1+b2*L1)/(2*R))).^2))*resfl);
                  Kp=L1*((resfl.^2*(mmbar+mfpmbar)-
1i*resfl*cfpmbar)/(E*Im)).^0.25;
           KKp=Kp;
           Cfp=cosh(KKp);
           Sfp=sinh(KKp);
           sfp=sin(KKp);
           cfp=cos(KKp);
             F1 = @(x) (resfl.^2.*L1.^2.*(x-
L1).*(0.25.*pi.*Pl.*(2.*(sqrt(R.^2-(x-
L1).^2))).^2.*(((Pl.*resfl.*(2.*(sqrt(R.^2-(x-
L1).^2))).^2)./(4.*etal)).^-0.5.*(0.9003+0.6105.*(h./(2.*(sqrt(R.^2-(x-
L1).^2)))).^0.5+2.1722.*(h./(2.*(sqrt(R.^2-(x-L1).^2)))).^1)+(-
0.0021.*(h./(2.*(sqrt(R.^2-(x-L1).^2)))).^0.5-
0.1459.*(h./(2.*(sqrt(R.^2-(x-L1).^2)))).^1+0.8255.*(h./(2.*(sqrt(R.^2-
(x-L1).^2)))).^1.5+0.8144.*(h./(2.*(sqrt(R.^2-(x-L1).^2)))).^2))));
             F2 = @(x) (resfl.*L1.^2.*(x-
L1).*(0.25.*pi.*Pl.*(2.*(sqrt(R.^2-(x-
L1).^2))).^2.*(((Pl.*resfl.*(2.*(sqrt(R.^2-(x-
L1).^2))).^2)./(4.*etal)).^-1.*(2.5758-1.3388.*(h./(2.*(sqrt(R.^2-(x-
L1).^2)))).^0.5)+((Pl.*resfl.*(2.*(sqrt(R.^2-(x-
L1).^2))).^2)./(4.*etal)).^-0.5.*(0.9003+0.7121.*(h./(2.*(sqrt(R.^2-(x-
L1).^2)))).^0.5+1.6845.*(h./(2.*(sqrt(R.^2-(x-
L1).^2)))).^1+0.8236.*(h./(2.*(sqrt(R.^2-(x-L1).^2)))).^1.5-
0.4178.*(h./(2.*(sqrt(R.^2-(x-L1).^2)))).^2)).*resfl));
           Gfp=(md*Dsc*resfl^2*L1^2+quad( F1, L1, L1+R, tol)-
```

```
1i*quad(F2,L1, L1+R, tol))/(E*Im);
             F3 = @(x) (resfl.^2.*L1.*(x-
L1).^2.*(0.25.*pi.*Pl.*(2.*(sqrt(R.^2-(x-
L1).^2))).^2.*(((Pl.*resfl.*(2.*(sqrt(R.^2-(x-
L1).^2))).^2)./(4.*etal)).^-0.5.*(0.9003+0.6105.*(h./(2.*(sqrt(R.^2-(x-
L1).^2)))).^0.5+2.1722.*(h./(2.*(sqrt(R.^2-(x-L1).^2)))).^1)+(-
0.0021.*(h./(2.*(sqrt(R.^2-(x-L1).^2)))).^0.5-
0.1459.*(h./(2.*(sqrt(R.^2-(x-L1).^2)))).^1+0.8255.*(h./(2.*(sqrt(R.^2-
(x-L1).^2)))).^1.5+0.8144.*(h./(2.*(sqrt(R.^2-(x-L1).^2)))).^2))));
             F4 = @(x) (resfl.*L1.*(x-
L1).^2.*(0.25.*pi.*Pl.*(2.*(sqrt(R.^2-(x-
L1).^2))).^2.*(((Pl.*resfl.*(2.*(sqrt(R.^2-(x-
L1).^2))).^2)./(4.*etal)).^-1.*(2.5758-1.3388.*(h./(2.*(sqrt(R.^2-(x-
L1).^2)))).^0.5)+((Pl.*resfl.*(2.*(sqrt(R.^2-(x-
L1).^2))).^2)./(4.*etal)).^-0.5.*(0.9003+0.7121.*(h./(2.*(sqrt(R.^2-(x-
L1).^2)))).^0.5+1.6845.*(h./(2.*(sqrt(R.^2-(x-
L1).^2)))).^1+0.8236.*(h./(2.*(sqrt(R.^2-(x-L1).^2)))).^1.5-
0.4178.*(h./(2.*(sqrt(R.^2-(x-L1).^2)))).^2)).*resfl));
          Hfp=(md*Dsc^2*resfl^2*L1+quad (F3, L1, L1+R, tol)-1i*quad
(F4,L1, L1+R, tol)+resfl^2*L1*Jd)/(E*Im);
             F5 = @(x) (resfl.^2.*L1^3*(0.25.*pi.*Pl.*(2.*(sqrt(R.^2-
(x-L1).^2))).^2.*(((Pl.*resfl.*(2.*(sqrt(R.^2-(x-
L1).^2))).^2)./(4.*etal)).^-0.5.*(0.9003+0.6105.*(h./(2.*(sqrt(R.^2-(x-
L1).^2)))).^0.5+2.1722.*(h./(2.*(sqrt(R.^2-(x-L1).^2)))).^1)+(-
0.0021.*(h./(2.*(sqrt(R.^2-(x-L1).^2)))).^0.5-
0.1459.*(h./(2.*(sqrt(R.^2-(x-L1).^2)))).^1+0.8255.*(h./(2.*(sqrt(R.^2-
(x-L1).^2)))).^1.5+0.8144.*(h./(2.*(sqrt(R.^2-(x-L1).^2)))).^2))));
             F6 = @(x) (resfl.*L1^3*(0.25.*pi.*Pl.*(2.*(sqrt(R.^2-(x-
L1).^2))).^2.*(((Pl.*resfl.*(2.*(sqrt(R.^2-(x-
L1).^2))).^2)./(4.*etal)).^-1.*(2.5758-1.3388.*(h./(2.*(sqrt(R.^2-(x-
L1).^2)))).^0.5)+((Pl.*resfl.*(2.*(sqrt(R.^2-(x-
L1).^2))).^2)./(4.*etal)).^-0.5.*(0.9003+0.7121.*(h./(2.*(sqrt(R.^2-(x-
L1).^2)))).^0.5+1.6845.*(h./(2.*(sqrt(R.^2-(x-
L1).^2)))).^1+0.8236.*(h./(2.*(sqrt(R.^2-(x-L1).^2)))).^1.5-
0.4178.*(h./(2.*(sqrt(R.^2-(x-L1).^2)))).^2)).*resfl));
      Ffp=(-md*resfl^2*L1^3-quad (F5, L1, L1+R, tol)+1i*quad (F6, L1,
L1+R, tol))/(E*Im);
  F7 = @(x) (resfl.^2.*L1.^2.*(x-L1).*(0.25.*pi.*Pl.*(2.*(sqrt(R.^2-(x-
L1).^2))).^2.*(((Pl.*resfl.*(2.*(sqrt(R.^2-(x-
L1).^2))).^2)./(4.*etal)).^-0.5.*(0.9003+0.6105.*(h./(2.*(sqrt(R.^2-(x-
L1).^2)))).^0.5+2.1722.*(h./(2.*(sqrt(R.^2-(x-L1).^2)))).^1)+(-
0.0021.*(h./(2.*(sqrt(R.^2-(x-L1).^2)))).^0.5-
0.1459.*(h./(2.*(sqrt(R.^2-(x-L1).^2)))).^1+0.8255.*(h./(2.*(sqrt(R.^2-
(x-L1).^2)))).^1.5+0.8144.*(h./(2.*(sqrt(R.^2-(x-L1).^2)))).^2))));
             F8 = @(x) (resfl.*L1.^2.*(x-
L1).*(0.25.*pi.*Pl.*(2.*(sqrt(R.^2-(x-
L1).^2))).^2.*(((Pl.*resfl.*(2.*(sqrt(R.^2-(x-
L1).^2))).^2)./(4.*etal)).^-1.*(2.5758-1.3388.*(h./(2.*(sqrt(R.^2-(x-
L1).^2)))).^0.5)+((Pl.*resfl.*(2.*(sqrt(R.^2-(x-
L1).^2))).^2)./(4.*etal)).^-0.5.*(0.9003+0.7121.*(h./(2.*(sqrt(R.^2-(x-
L1).^2)))).^0.5+1.6845.*(h./(2.*(sqrt(R.^2-(x-
L1).^2)))).^1+0.8236.*(h./(2.*(sqrt(R.^2-(x-L1).^2)))).^1.5-
0.4178.*(h./(2.*(sqrt(R.^2-(x-L1).^2)))).^2)).*resfl));
  Kfp=(-md*Dsc*resfl^2*L1^2-quad (F7, L1, L1+R, tol)+1i*quad (F8, L1,
L1+R, tol))/(E*Im);
       MMfp=KKp.^2.*(Cfp+cfp)-Gfp.*(Cfp-cfp)-Hfp.*KKp.*(Sfp+sfp);
           NNfp=KKp.^2.*(Sfp+sfp)-Gfp.*(Sfp-sfp)-Hfp.*KKp.*(Cfp-cfp);
```

```
           OOfp=KKp.^(-1).*(KKp.^2.*sfp+Gfp.*sfp+Hfp.*KKp.*cfp);
           PPfp=KKp.^3.*(Sfp-sfp)-Ffp.*(Cfp-cfp)-Kfp.*KKp.*(Sfp+sfp);
           QQfp=KKp.^3.*(Cfp+cfp)-Ffp.*(Sfp-sfp)-Kfp.*KKp.*(Cfp-cfp);
           RRfp=KKp.^(-1).*(KKp.^3.*cfp+Ffp.*sfp+Kfp.*KKp.*cfp);
           A1fp=(OOfp.*QQfp-RRfp.*NNfp)/(MMfp.*QQfp-PPfp.*NNfp);
           A2fp=(OOfp.*PPfp-RRfp.*MMfp)/(NNfp.*PPfp-MMfp.*QQfp);
          xi=sym('xi','real'); % denotes x/L1
           X=A1fp*(cosh(KKp*xi)-cos(KKp*xi))+A2fp*(sinh(KKp*xi)-
sin(KKp*xi))+KKp^(-1)*sin(KKp*xi); % normalized shape function
           Xp=KKp*(A1fp*(sinh(KKp*xi)+sin(KKp*xi))+A2fp*(cosh(KKp*xi)-
cos(KKp*xi))+KKp^(-1)*cos(KKp*xi)); % first derivative of normalized
deflection measns X'
Xpp=KKp^2*(A1fp*(cosh(KKp*xi)+cos(KKp*xi))+A2fp*(sinh(KKp*xi)+sin(KKp*x
i))-KKp^(-1)*sin(KKp*xi)); % second derivative of normalized deflection
measns X''
            BB1=int((real(Xpp))^2, xi, 0, 1);
            BB2=int((imag(Xpp))^2, xi, 0, 1);
            BB3=int((real(Xpp))*(imag(Xpp)), xi, 0, 1);
            BB4=int((real(X))^2, xi, 0, 1);
            BB5=int((imag(X))^2, xi, 0, 1);
            BB6=int((real(X))*(imag(X)), xi, 0, 1);
            BB7=(real(A1fp*(cosh(KKp)-cos(KKp))+A2fp*(sinh(KKp)-
sin(KKp))+KKp^(-1)*sin(KKp)))^2;
            BB8=(imag(A1fp*(cosh(KKp)-cos(KKp))+A2fp*(sinh(KKp)-
sin(KKp))+KKp^(-1)*sin(KKp)))^2;
            BB9=(real(A1fp*(cosh(KKp)-cos(KKp))+A2fp*(sinh(KKp)-
sin(KKp))+KKp^(-1)*sin(KKp)))*(imag(A1fp*(cosh(KKp)-
cos(KKp))+A2fp*(sinh(KKp)-sin(KKp))+KKp^(-1)*sin(KKp)));
            BB13=(real(KKp*(A1fp*(sinh(KKp)+sin(KKp))+A2fp*(cosh(KKp)-
cos(KKp))+KKp^(-1)*cos(KKp))))^2;
            BB14=(imag(KKp*(A1fp*(sinh(KKp)+sin(KKp))+A2fp*(cosh(KKp)-
cos(KKp))+KKp^(-1)*cos(KKp))))^2;
            BB15=(real(KKp*(A1fp*(sinh(KKp)+sin(KKp))+A2fp*(cosh(KKp)-
cos(KKp))+KKp^(-
1)*cos(KKp))))*(imag(KKp*(A1fp*(sinh(KKp)+sin(KKp))+A2fp*(cosh(KKp)-
cos(KKp))+KKp^(-1)*cos(KKp))));
            BB10=sqrt(BB7)*sqrt(BB13);
            BB11=sqrt(BB8)*sqrt(BB14);
            BB12=sqrt(BB7)*sqrt(BB14)+sqrt(BB13)*sqrt(BB8);
            BB16=BB13;
            BB17=BB14;
            BB18=BB15;
            BB19=-imag(2*A1fp*KKp^2);
for jtau=1:length(Ltau)
          F(jtau)=BB1*(cos(jtau))^2+BB2*(sin(jtau))^2-
2*BB3*(cos(jtau))*(sin(jtau))+(L1^4*mmbar*resfl^2*(E*Im)^(-
1))*(BB4*(sin(jtau))^2+BB5*(cos(jtau))^2+2*BB6*(cos(jtau))*(sin(jtau)))
+(md*L1^3*resfl^2*(E*Im)^(-
1))*(BB7*(sin(jtau))^2+BB8*(cos(jtau))^2+2*BB9*(cos(jtau))*(sin(jtau)))
+(2*md*L1^2*Dsc*resfl^2*(E*Im)^(-
1))*(BB10*(sin(jtau))^2+BB11*(cos(jtau))^2+BB12*(cos(jtau))*(sin(jtau))
)+(md*L1*Dsc^2*resfl^2*(E*Im)^(-
1))*(BB13*(sin(jtau))^2+BB14*(cos(jtau))^2+2*BB15*(cos(jtau))*(sin(jtau
)))+(Jd*L1*resfl^2*(E*Im)^(-
1))*(BB16*(sin(jtau))^2+BB17*(cos(jtau))^2+2*BB18*(cos(jtau))*(sin(jtau
)));
   Qua(jtau)=F(jtau)/BB19;
```

```
end
 Quaactual=max (double(Qua(:)))
```

Case 3: Hammerhead Microcantilever with a Uniform Rectangular Head

```
clear;
L1=200*10^-6; % length of the stem
b1=45*10^-6; % width of the stem
L2=200*10^-6 : 200*10^-6 : 200*10^-6; % length of the head
b2=200*10^-6 : 200*10^-6 : 200*10^-6; % width of the head
eta=0.001:0.001:0.050; % viscosity of the fluid
h=12*10^-6; % thickness of the cantilever
E=169*10^9; % Young's Modulus
Pb=2330; % density of silicon for both supporting beam and hammerhead
Pf=1000; % density of the fluid
mm=Pb*L1*b1*h; % mass of the stem
mmbar=Pb*b1*h; % mass per unit length of stem
Im=(1/12)*h*(b1)^3; % moment of inertia of the stem
tau = 0:1:6;
freq = 800000:100:1200000;
%%%%%%%%%%% Using Correction Factor %%%%%%%%%%%%%
for jeta=1:length(eta);
  for jL2=1:length(L2);
    for jb2=1:length(b2)
        for jfreq=1:length(freq)
           md(jb2,jL2)=Pb*L2(jL2)*b2(jb2)*h; % mass of the head
           mdbar(jb2)=Pb*b2(jb2)*h; % mass per unit length of the head
           Jd(jb2,jL2)=(1/12)*md(jb2,jL2)*(L2(jL2)^2+b2(jb2)^2); %
moment of inertia
           %%%%%%%%%% Hydrodynamic function including thickness
correction %%%%%%%%%%
           Reym(jfreq,jeta)=(Pf*freq(jfreq)*b1^2)/(4*eta(jeta));
Reyd(jfreq,jb2,jeta)=(Pf*freq(jfreq)*b2(jb2)^2)/(4*eta(jeta));
           Gammarm(jfreq,jeta)=Reym(jfreq,jeta)^-
0.5*(0.9003+0.6105*(h/b1)^0.5+2.1722*(h/b1)^1)+(-0.0021*(h/b1)^0.5-
0.1459*(h/b1)^1+0.8255*(h/b1)^1.5+0.8144*(h/b1)^2);
           Gammaim(jfreq,jeta)=Reym(jfreq,jeta)^-1*(2.5758-
1.3388*(h/b1)^0.5)+Reym(jfreq,jeta)^-
0.5*(0.9003+0.7121*(h/b1)^0.5+1.6845*(h/b1)^1+0.8236*(h/b1)^1.5-
0.4178*(h/b1)^2);
           Gammard(jfreq,jb2,jeta)=Reyd(jfreq,jb2,jeta)^-
0.5*(0.9003+0.6105*(h/b2(jb2))^0.5+2.1722*(h/b2(jb2))^1)+(-
0.0021*(h/b2(jb2))^0.5-
0.1459*(h/b2(jb2))^1+0.8255*(h/b2(jb2))^1.5+0.8144*(h/b2(jb2))^2);
           Gammaid(jfreq,jb2,jeta)=Reyd(jfreq,jb2,jeta)^-1*(2.5758-
1.3388*(h/b2(jb2))^0.5)+Reyd(jfreq,jb2,jeta)^-
0.5*(0.9003+0.7121*(h/b2(jb2))^0.5+1.6845*(h/b2(jb2))^1+0.8236*(h/b2(jb
2))^1.5-0.4178*(h/b2(jb2))^2);
           mfpmbar(jfreq,jeta)=0.25*pi*Pf*b1^2*Gammarm(jfreq,jeta);
cfpmbar(jfreq,jeta)=0.25*pi*Pf*b1^2*Gammaim(jfreq,jeta)*freq(jfreq);
mfpdbar(jfreq,jb2,jeta)=0.25*pi*Pf*b2(jb2)^2*Gammard(jfreq,jb2,jeta);
cfpdbar(jfreq,jb2,jeta)=0.25*pi*Pf*b2(jb2)^2*Gammaid(jfreq,jb2,jeta)*fr
eq(jfreq);
Kp(jfreq,jb2,jeta)=L1*((freq(jfreq)^2*(mmbar+mfpmbar(jfreq,jeta))-
1i*freq(jfreq)*cfpmbar(jfreq,jeta))/(E*Im))^0.25;
```

```
            KKp=Kp(jfreq,jb2,jeta);
            Cfp=cosh(KKp);
            Sfp=sinh(KKp);
            sfp=sin(KKp);
            cfp=cos(KKp);
            Gfp(jfreq,jb2,jL2,jeta)=0.5*(E*Im)^(-
1)*(freq(jfreq)^2*L1^2*L2(jL2)*(md(jb2,jL2)+L2(jL2)*mfpdbar(jfreq,jb2,j
eta))-j*freq(jfreq)*L1^2*L2(jL2)^2*cfpdbar(jfreq,jb2,jeta));
            Hfp(jfreq,jb2,jL2,jeta)=(12*E*Im)^(-
1)*(3*freq(jfreq)^2*L1*L2(jL2)^2*md(jb2,jL2)+4*freq(jfreq)^2*L1*L2(jL2)
^3*mfpdbar(jfreq,jb2,jeta)+12*freq(jfreq)^2*L1*Jd(jb2,jL2)-
4*j*freq(jfreq)*L1*L2(jL2)^3*cfpdbar(jfreq,jb2,jeta));
            Ffp(jfreq,jb2,jL2,jeta)=(E*Im)^(-
1)*(j*freq(jfreq)*L1^3*L2(jL2)*cfpdbar(jfreq,jb2,jeta)-
freq(jfreq)^2*L1^3*(md(jb2,jL2)+L2(jL2)*mfpdbar(jfreq,jb2,jeta)));
            Kfp(jfreq,jb2,jL2,jeta)=0.5*(E*Im)^(-
1)*(j*freq(jfreq)*L1^2*L2(jL2)^2*cfpdbar(jfreq,jb2,jeta)-
freq(jfreq)^2*L1^2*L2(jL2)*(md(jb2,jL2)+L2(jL2)*mfpdbar(jfreq,jb2,jeta)
));
            MMfp(jfreq,jb2,jL2,jeta)=KKp^2*(Cfp+cfp)-
Gfp(jfreq,jb2,jL2,jeta)*(Cfp-cfp)-
Hfp(jfreq,jb2,jL2,jeta)*KKp*(Sfp+sfp);NNfp(jfreq,jb2,jL2,jeta)=KKp^2*(S
fp+sfp)-Gfp(jfreq,jb2,jL2,jeta)*(Sfp-sfp)-
Hfp(jfreq,jb2,jL2,jeta)*KKp*(Cfp-cfp);
            OOfp(jfreq,jb2,jL2,jeta)=KKp^(-
1)*(KKp^2*sfp+Gfp(jfreq,jb2,jL2,jeta)*sfp+Hfp(jfreq,jb2,jL2,jeta)*KKp*c
fp);
            PPfp(jfreq,jb2,jL2,jeta)=KKp^3*(Sfp-sfp)-
Ffp(jfreq,jb2,jL2,jeta)*(Cfp-cfp)-
Kfp(jfreq,jb2,jL2,jeta)*KKp*(Sfp+sfp);QQfp(jfreq,jb2,jL2,jeta)=KKp^3*(C
fp+cfp)-Ffp(jfreq,jb2,jL2,jeta)*(Sfp-sfp)-
Kfp(jfreq,jb2,jL2,jeta)*KKp*(Cfp-cfp);
            RRfp(jfreq,jb2,jL2,jeta)=KKp^(-
1)*(KKp^3*cfp+Ffp(jfreq,jb2,jL2,jeta)*sfp+Kfp(jfreq,jb2,jL2,jeta)*KKp*c
fp);
A1fp(jfreq,jb2,jL2,jeta)=(OOfp(jfreq,jb2,jL2,jeta)*QQfp(jfreq,jb2,jL2,j
eta)-
RRfp(jfreq,jb2,jL2,jeta)*NNfp(jfreq,jb2,jL2,jeta))/(MMfp(jfreq,jb2,jL2,
jeta)*QQfp(jfreq,jb2,jL2,jeta)-
PPfp(jfreq,jb2,jL2,jeta)*NNfp(jfreq,jb2,jL2,jeta));
A2fp(jfreq,jb2,jL2,jeta)=(OOfp(jfreq,jb2,jL2,jeta)*PPfp(jfreq,jb2,jL2,j
eta)-
RRfp(jfreq,jb2,jL2,jeta)*MMfp(jfreq,jb2,jL2,jeta))/(NNfp(jfreq,jb2,jL2,
jeta)*PPfp(jfreq,jb2,jL2,jeta)-
MMfp(jfreq,jb2,jL2,jeta)*QQfp(jfreq,jb2,jL2,jeta));
            Dfp(jfreq,jb2,jL2,jeta)=abs(A1fp(jfreq,jb2,jL2,jeta)*(Cfp-
cfp)+A2fp(jfreq,jb2,jL2,jeta)*(Sfp-sfp)+KKp^(-1)*sfp);
        end
          Dfpmax(jb2,jL2,jeta)=max(Dfp(:,jb2,jL2,jeta));
          Dfpmaxsqrt2(jb2,jL2,jeta)=Dfpmax(jb2,jL2,jeta)/sqrt(2);
    end
  end
end
%%%% find resonant frequency%%%
for jeta=1:length(eta);
  for  jL2=1:length(L2);
      for jb2=1:length(b2);
```

```
           for jfreq=1:length(freq);

            %LLamd(jfreq) =
((mmbar*L1^4*(freq(jfreq))^2)/(E*Im))^0.25;if(Dfp(jfreq,jb2,jL2,jeta)==
Dfpmax(jb2,jL2,jeta));
      resf(jb2,jL2,jeta)=freq(jfreq);
    end
      end
   end
  end
end
for jeta=1:length(eta);
  for jL2=1:length(L2);
    for jb2=1:length(b2)
            md(jb2,jL2)=Pb*L2(jL2)*b2(jb2)*h; % mass of the head
            mdbar(jb2)=Pb*b2(jb2)*h; % mass per unit length of the
headJd(jb2,jL2)=(1/12)*md(jb2,jL2)*(L2(jL2)^2+b2(jb2)^2); % moment of
inertia
                          %%%%%%%%%% Hydrodynamic function including
thickness correction %%%%%%%%%%
Reym(jb2,jL2,jeta)=(Pf*resf(jb2,jL2,jeta)*b1^2)/(4*eta(jeta));
Reyd(jb2,jL2,jeta)=(Pf*resf(jb2,jL2,jeta)*b2(jb2)^2)/(4*eta(jeta));
  Gammarm(jb2,jL2,jeta)=Reym(jb2,jL2,jeta)^-
0.5*(0.9003+0.6105*(h/b1)^0.5+2.1722*(h/b1)^1)+(-0.0021*(h/b1)^0.5-
0.1459*(h/b1)^1+0.8255*(h/b1)^1.5+0.8144*(h/b1)^2);
  Gammaim(jb2,jL2,jeta)=Reym(jb2,jL2,jeta)^-1*(2.5758-
1.3388*(h/b1)^0.5)+Reym(jb2,jL2,jeta)^-
0.5*(0.9003+0.7121*(h/b1)^0.5+1.6845*(h/b1)^1+0.8236*(h/b1)^1.5-
0.4178*(h/b1)^2);
  Gammard(jb2,jL2,jeta)=Reyd(jb2,jL2,jeta)^-
0.5*(0.9003+0.6105*(h/b2(jb2))^0.5+2.1722*(h/b2(jb2))^1)+(-
0.0021*(h/b2(jb2))^0.5-
0.1459*(h/b2(jb2))^1+0.8255*(h/b2(jb2))^1.5+0.8144*(h/b2(jb2))^2);
           Gammaid(jb2,jL2,jeta)=Reyd(jb2,jL2,jeta)^-1*(2.5758-
1.3388*(h/b2(jb2))^0.5)+Reyd(jb2,jL2,jeta)^-
0.5*(0.9003+0.7121*(h/b2(jb2))^0.5+1.6845*(h/b2(jb2))^1+0.8236*(h/b2(jb
2))^1.5-0.4178*(h/b2(jb2))^2);

mfpmbar(jb2,jL2,jeta)=0.25*pi*Pf*b1^2*Gammarm(jb2,jL2,jeta);cfpmbar(jb2
,jL2,jeta)=0.25*pi*Pf*b1^2*Gammaim(jb2,jL2,jeta)*resf(jb2,jL2,jeta);
mfpdbar(jb2,jL2,jeta)=0.25*pi*Pf*b2(jb2)^2*Gammard(jb2,jL2,jeta);
cfpdbar(jb2,jL2,jeta)=0.25*pi*Pf*b2(jb2)^2*Gammaid(jb2,jL2,jeta)*resf(j
b2,jL2,jeta);
Kp(jb2,jL2,jeta)=L1*((resf(jb2,jL2,jeta)^2*(mmbar+mfpmbar(jb2,jL2,jeta)
)-1i*resf(jb2,jL2,jeta)*cfpmbar(jb2,jL2,jeta))/(E*Im))^0.25;
           KKp=Kp(jb2,jL2,jeta);
           Cfp=cosh(KKp);
           Sfp=sinh(KKp);
           sfp=sin(KKp);
           cfp=cos(KKp);
           Gfp(jb2,jL2,jeta)=0.5*(E*Im)^(-
1)*(resf(jb2,jL2,jeta)^2*L1^2*L2(jL2)*(md(jb2,jL2)+L2(jL2)*mfpdbar(jfre
q,jb2,jeta))-
j*resf(jb2,jL2,jeta)*L1^2*L2(jL2)^2*cfpdbar(jfreq,jb2,jeta));
           Hfp(jb2,jL2,jeta)=(12*E*Im)^(-
1)*(3*resf(jb2,jL2,jeta)^2*L1*L2(jL2)^2*md(jb2,jL2)+4*resf(jb2,jL2,jeta
)^2*L1*L2(jL2)^3*mfpdbar(jfreq,jb2,jeta)+12*resf(jb2,jL2,jeta)^2*L1*Jd(
```

```
jb2,jL2)-4*j*resf(jb2,jL2,jeta)*L1*L2(jL2)^3*cfpdbar(jfreq,jb2,jeta));
          Ffp(jb2,jL2,jeta)=(E*Im)^(-
1)*(j*resf(jb2,jL2,jeta)*L1^3*L2(jL2)*cfpdbar(jfreq,jb2,jeta)-
resf(jb2,jL2,jeta)^2*L1^3*(md(jb2,jL2)+L2(jL2)*mfpdbar(jfreq,jb2,jeta))
);
          Kfp(jb2,jL2,jeta)=0.5*(E*Im)^(-
1)*(j*resf(jb2,jL2,jeta)*L1^2*L2(jL2)^2*cfpdbar(jfreq,jb2,jeta)-
resf(jb2,jL2,jeta)^2*L1^2*L2(jL2)*(md(jb2,jL2)+L2(jL2)*mfpdbar(jfreq,jb
2,jeta)));
          MMfp(jb2,jL2,jeta)=KKp^2*(Cfp+cfp)-Gfp(jb2,jL2,jeta)*(Cfp-
cfp)-Hfp(jb2,jL2,jeta)*KKp*(Sfp+sfp);
          NNfp(jb2,jL2,jeta)=KKp^2*(Sfp+sfp)-Gfp(jb2,jL2,jeta)*(Sfp-
sfp)-Hfp(jb2,jL2,jeta)*KKp*(Cfp-cfp);
          OOfp(jb2,jL2,jeta)=KKp^(-
1)*(KKp^2*sfp+Gfp(jb2,jL2,jeta)*sfp+Hfp(jb2,jL2,jeta)*KKp*cfp);
          PPfp(jb2,jL2,jeta)=KKp^3*(Sfp-sfp)-Ffp(jb2,jL2,jeta)*(Cfp-
cfp)-Kfp(jb2,jL2,jeta)*KKp*(Sfp+sfp);
          QQfp(jb2,jL2,jeta)=KKp^3*(Cfp+cfp)-Ffp(jb2,jL2,jeta)*(Sfp-
sfp)-Kfp(jb2,jL2,jeta)*KKp*(Cfp-cfp);
          RRfp(jb2,jL2,jeta)=KKp^(-
1)*(KKp^3*cfp+Ffp(jb2,jL2,jeta)*sfp+Kfp(jb2,jL2,jeta)*KKp*cfp);
          A1fp(jb2,jL2,jeta)=(OOfp(jb2,jL2,jeta)*QQfp(jb2,jL2,jeta)-
RRfp(jb2,jL2,jeta)*NNfp(jb2,jL2,jeta))/(MMfp(jb2,jL2,jeta)*QQfp(jb2,jL2
,jeta)-PPfp(jb2,jL2,jeta)*NNfp(jb2,jL2,jeta));
          A2fp(jb2,jL2,jeta)=(OOfp(jb2,jL2,jeta)*PPfp(jb2,jL2,jeta)-
RRfp(jb2,jL2,jeta)*MMfp(jb2,jL2,jeta))/(NNfp(jb2,jL2,jeta)*PPfp(jb2,jL2
,jeta)-MMfp(jb2,jL2,jeta)*QQfp(jb2,jL2,jeta));
          xi=sym('xi','real'); % denotes x/L1
          X(jb2,jL2,jeta)=A1fp(jb2,jL2,jeta)*(cosh(KKp*xi)-
cos(KKp*xi))+A2fp(jb2,jL2,jeta)*(sinh(KKp*xi)-sin(KKp*xi))+KKp^(-
1)*sin(KKp*xi); % normalized shape function
Xp(jb2,jL2,jeta)=KKp*(A1fp(jb2,jL2,jeta)*(sinh(KKp*xi)+sin(KKp*xi))+A2f
p(jb2,jL2,jeta)*(cosh(KKp*xi)-cos(KKp*xi))+KKp^(-1)*cos(KKp*xi)); %
first derivative of normalized deflection measns X'
Xpp(jb2,jL2,jeta)=KKp^2*(A1fp(jb2,jL2,jeta)*(cosh(KKp*xi)+cos(KKp*xi))+
A2fp(jb2,jL2,jeta)*(sinh(KKp*xi)+sin(KKp*xi))-KKp^(-1)*sin(KKp*xi)); %
second derivative of normalized deflection measns X''
   BB1(jb2,jL2,jeta)=int((real(Xpp(jb2,jL2,jeta)))^2, xi, 0, 1);
   BB2(jb2,jL2,jeta)=int((imag(Xpp(jb2,jL2,jeta)))^2, xi, 0, 1);
BB3(jb2,jL2,jeta)=int((real(Xpp(jb2,jL2,jeta)))*(imag(Xpp(jb2,jL2,jeta)
)), xi, 0, 1);
BB4(jb2,jL2,jeta)=int((real(X(jb2,jL2,jeta)))^2, xi, 0, 1);
  BB5(jb2,jL2,jeta)=int((imag(X(jb2,jL2,jeta)))^2, xi, 0, 1);
BB6(jb2,jL2,jeta)=int((real(X(jb2,jL2,jeta)))*(imag(X(jb2,jL2,jeta))),x
i, 0, 1);
BB7(jb2,jL2,jeta)=(real(A1fp(jb2,jL2,jeta)*(cosh(KKp)-
cos(KKp))+A2fp(jb2,jL2,jeta)*(sinh(KKp)-sin(KKp))+KKp^(-
1)*sin(KKp)))^2;BB8(jb2,jL2,jeta)=(imag(A1fp(jb2,jL2,jeta)*(cosh(KKp)-
cos(KKp))+A2fp(jb2,jL2,jeta)*(sinh(KKp)-sin(KKp))+KKp^(-
1)*sin(KKp)))^2;BB9(jb2,jL2,jeta)=(real(A1fp(jb2,jL2,jeta)*(cosh(KKp)-
cos(KKp))+A2fp(jb2,jL2,jeta)*(sinh(KKp)-sin(KKp))+KKp^(-
1)*sin(KKp)))*(imag(A1fp(jb2,jL2,jeta)*(cosh(KKp)-
cos(KKp))+A2fp(jb2,jL2,jeta)*(sinh(KKp)-sin(KKp))+KKp^(-1)*sin(KKp)));
BB13(jb2,jL2,jeta)=(real(KKp*(A1fp(jb2,jL2,jeta)*(sinh(KKp)+sin(KKp))+A
2fp(jb2,jL2,jeta)*(cosh(KKp)-cos(KKp))+KKp^(-1)*cos(KKp))))^2;
BB14(jb2,jL2,jeta)=(imag(KKp*(A1fp(jb2,jL2,jeta)*(sinh(KKp)+sin(KKp))+A
2fp(jb2,jL2,jeta)*(cosh(KKp)-cos(KKp))+KKp^(-1)*cos(KKp))))^2;
```

```
BB15(jb2,jL2,jeta)=(real(KKp*(A1fp(jb2,jL2,jeta)*(sinh(KKp)+sin(KKp))+A
2fp(jb2,jL2,jeta)*(cosh(KKp)-cos(KKp))+KKp^(-
1)*cos(KKp))))*(imag(KKp*(A1fp(jb2,jL2,jeta)*(sinh(KKp)+sin(KKp))+A2fp(
jb2,jL2,jeta)*(cosh(KKp)-cos(KKp))+KKp^(-1)*cos(KKp))));
BB10(jb2,jL2,jeta)=sqrt(BB7(jb2,jL2,jeta))*sqrt(BB13(jb2,jL2,jeta));
BB11(jb2,jL2,jeta)=sqrt(BB8(jb2,jL2,jeta))*sqrt(BB14(jb2,jL2,jeta));
BB12(jb2,jL2,jeta)=sqrt(BB7(jb2,jL2,jeta))*sqrt(BB14(jb2,jL2,jeta))+sqr
t(BB13(jb2,jL2,jeta))*sqrt(BB8(jb2,jL2,jeta));
BB16(jb2,jL2,jeta)=BB13(jb2,jL2,jeta);
   BB17(jb2,jL2,jeta)=BB14(jb2,jL2,jeta);
  BB18(jb2,jL2,jeta)=BB15(jb2,jL2,jeta);
  BB19(jb2,jL2,jeta)=-imag(2*A1fp(jb2,jL2,jeta)*KKp^2);
  for jtau=1:length(tau)
F(jtau,jb2,jL2,jeta)=BB1(jb2,jL2,jeta)*(cos(jtau))^2+BB2(jb2,jL2,jeta)*
(sin(jtau))^2-
2*BB3(jb2,jL2,jeta)*(cos(jtau))*(sin(jtau))+(L1^4*mmbar*resf(jb2,jL2,je
ta)^2*(E*Im)^(-
1))*(BB4(jb2,jL2,jeta)*(sin(jtau))^2+BB5(jb2,jL2,jeta)*(cos(jtau))^2+2*
BB6(jb2,jL2,jeta)*(cos(jtau))*(sin(jtau)))+(mdbar(jb2)*L1^3*L2(jL2)*res
f(jb2,jL2,jeta)^2*(E*Im)^(-
1))*(BB7(jb2,jL2,jeta)*(sin(jtau))^2+BB8(jb2,jL2,jeta)*(cos(jtau))^2+2*
BB9(jb2,jL2,jeta)*(cos(jtau))*(sin(jtau)))+(mdbar(jb2)*L1^2*L2(jL2)^2*r
esf(jb2,jL2,jeta)^2*(E*Im)^(-
1))*(BB10(jb2,jL2,jeta)*(sin(jtau))^2+BB11(jb2,jL2,jeta)*(cos(jtau))^2+
BB12(jb2,jL2,jeta)*(cos(jtau))*(sin(jtau)))+(1/3)*(mdbar(jb2)*L1*L2(jL2
)^3*resf(jb2,jL2,jeta)^2*(E*Im)^(-
1))*(BB13(jb2,jL2,jeta)*(sin(jtau))^2+BB14(jb2,jL2,jeta)*(cos(jtau))^2+
2*BB15(jb2,jL2,jeta)*(cos(jtau))*(sin(jtau)))+(1/12)*(mdbar(jb2)*L1*L2(
jL2)*b2(jb2)^2*resf(jb2,jL2,jeta)^2*(E*Im)^(-
1))*(BB16(jb2,jL2,jeta)*(sin(jtau))^2+BB17(jb2,jL2,jeta)*(cos(jtau))^2+
2*BB18(jb2,jL2,jeta)*(cos(jtau))*(sin(jtau)));
Qua(jtau,jb2,jL2,jeta)=F(jtau,jb2,jL2,jeta)/BB19(jb2,jL2,jeta);
  end
  end
  end
end
for jeta=1:length(eta);
  for jL2=1:length(L2);
    for jb2=1:length(b2)
    Quaactual(jb2,jL2,jeta)=max(double(Qua(:,jb2,jL2,jeta)))
    end
  end
end
```

Case 4: Hammerhead Microcantilever with a Composite Rectangular Head

```
clear;
L1=200*10^-6; % length of the stem
b1=45*10^-6; % width of the stem
 L2=100*10^-6 : 100*10^-6 : 100*10^-6; % length of the head
b2=100*10^-6 : 100*10^-6 : 100*10^-6; % width of the head
 L3=30*10^-6 : 30*10^-6 : 30*10^-6; % length of the gap
b4=30*10^-6 : 30*10^-6 : 30*10^-6; % width of the gap
 eta=0.001:0.001:0.05; % viscosity of the fluid
 h=12*10^-6; % thickness of the cantilever
```

```
E=169*10^9; % Young's Modulus
Pb=2330; % density of silicon for both supporting beam and hammerhead
Pf=1000; % density of the fluid
mm=Pb*L1*b1*h; % mass of the stem
mmbar=Pb*b1*h; % mass per unit length of stem
Im=(1/12)*h*(b1)^3; % moment of inertia of the stem
 tau = 0:0.5:6;
freq = 950000:100:1400000;
for jeta=1:length(eta);
      for jL2=1:length(L2);
         for jb2=1:length(b2);
           for jL3=1:length(L3);
              for jb4=1:length(b4);
                 for jfreq=1:length(freq)
        b3(jb4,jb2)=0.5*(b2(jb2)-b1-2*b4(jb4));
        dc(jb4,jL3,jb2,jL2)=(0.5*L2(jL2)*b2(jb2)*L2(jL2)-
0.5*L3(jL3)*(b1+2*b4(jb4))*L3(jL3))/(L2(jL2)*b2(jb2)-
L3(jL3)*(b1+2*b4(jb4))); % distance of the mass center to the end of
the HH rectangle using L2,L3,b1,b4
        ds(jb4,jL3,jb2,jL2)=(0.5*L2(jL2)*b2(jb2)*L2(jL2)-
0.5*L3(jL3)*(b1+2*b4(jb4))*L3(jL3))/(L2(jL2)*b2(jb2)-
L3(jL3)*(b1+2*b4(jb4)))-L3(jL3); % distance of the mass center to the
end of the stem using L2,L3,b1,b4
        dc2(jb4,jL3,jb2,jL2)=(0.5*L2(jL2)*b2(jb2)*L2(jL2)-
0.5*L3(jL3)*(b2(jb2)-2*b3(jb4,jb2))*L3(jL3))/(L2(jL2)*b2(jb2)-
L3(jL3)*(b2(jb2)-2*b3(jb4,jb2))); % distance of the mass center to the
end of the HH rectangle using L2,L3,b2,b3
        ds2(jb4,jL3,jb2,jL2)=(0.5*L2(jL2)*b2(jb2)*L2(jL2)-
0.5*L3(jL3)*(b2(jb2)-2*b3(jb4,jb2))*L3(jL3))/(L2(jL2)*b2(jb2)-
L3(jL3)*(b2(jb2)-2*b3(jb4,jb2)))-L3(jL3); % distance of the mass center
to the end of the stem using L2,L3,b2,b3
Jd(jb4,jL3,jb2,jL2)=(1/12)*Pb*L2(jL2)*b2(jb2)*h*(L2(jL2)^2+b2(jb2)^2)+(
dc(jb4,jL3,jb2,jL2)-0.5*L2(jL2))^2*Pb*L2(jL2)*b2(jb2)*h-
((1/12)*Pb*L3(jL3)*(b1+2*b4(jb4))*h*(L3(jL3)^2+(b1+2*b4(jb4))^2)+(ds(jb
4,jL3,jb2,jL2)+0.5*L3(jL3))^2*Pb*L3(jL3)*(b1+2*b4(jb4))*h); % moment of
inertia due to rotation
        md(jb4,jL3,jb2,jL2)=Pb*h*(L2(jL2)*b2(jb2)-
L3(jL3)*(b1+2*b4(jb4))); % mass of the HH
        %%%%%%%%%% Hydrodynamic function including thickness
correction %%%%%%%%%%
           Reym(jfreq,jeta)=(Pf*freq(jfreq)*b1^2)/(4*eta(jeta));

eyd1(jfreq,jb2,jeta)=(Pf*freq(jfreq)*b2(jb2)^2)/(4*eta(jeta));
Reyd2(jfreq,jb4,jb2,jeta)=(Pf*freq(jfreq)*b3(jb4,jb2)^2)/(4*eta(jeta));
Gammarm(jfreq,jeta)=Reym(jfreq,jeta)^-
0.5*(0.9003+0.6105*(h/b1)^0.5+2.1722*(h/b1)^1)+(-0.0021*(h/b1)^0.5-
0.1459*(h/b1)^1+0.8255*(h/b1)^1.5+0.8144*(h/b1)^2);
           Gammaim(jfreq,jeta)=Reym(jfreq,jeta)^-1*(2.5758-
1.3388*(h/b1)^0.5)+Reym(jfreq,jeta)^-
0.5*(0.9003+0.7121*(h/b1)^0.5+1.6845*(h/b1)^1+0.8236*(h/b1)^1.5-
0.4178*(h/b1)^2);
           Gammard1(jfreq,jb2,jeta)=Reyd1(jfreq,jb2,jeta)^-
0.5*(0.9003+0.6105*(h/b2(jb2))^0.5+2.1722*(h/b2(jb2))^1)+(-
0.0021*(h/b2(jb2))^0.5-
0.1459*(h/b2(jb2))^1+0.8255*(h/b2(jb2))^1.5+0.8144*(h/b2(jb2))^2);
           Gammaid1(jfreq,jb2,jeta)=Reyd1(jfreq,jb2,jeta)^-1*(2.5758-
1.3388*(h/b2(jb2))^0.5)+Reyd1(jfreq,jb2,jeta)^-
```

```
0.5*(0.9003+0.7121*(h/b2(jb2))^0.5+1.6845*(h/b2(jb2))^1+0.8236*(h/b2(jb
2))^1.5-0.4178*(h/b2(jb2))^2);
          Gammard2(jfreq,jb4,jb2,jeta)=Reyd2(jfreq,jb4,jb2,jeta)^-
0.5*(0.9003+0.6105*(h/b3(jb4,jb2))^0.5+2.1722*(h/b3(jb4,jb2))^1)+(-
0.0021*(h/b3(jb4,jb2))^0.5-
0.1459*(h/b3(jb4,jb2))^1+0.8255*(h/b3(jb4,jb2))^1.5+0.8144*(h/b3(jb4,jb
2))^2);
Gammaid2(jfreq,jb4,jb2,jeta)=Reyd2(jfreq,jb4,jb2,jeta)^-1*(2.5758-
1.3388*(h/b3(jb4,jb2))^0.5)+Reyd2(jfreq,jb4,jb2,jeta)^-
0.5*(0.9003+0.7121*(h/b3(jb4,jb2))^0.5+1.6845*(h/b3(jb4,jb2))^1+0.8236*
(h/b3(jb4,jb2))^1.5-0.4178*(h/b3(jb4,jb2))^2);
          mfpmbar(jfreq,jeta)=0.25*pi*Pf*b1^2*Gammarm(jfreq,jeta);
cfpmbar(jfreq,jeta)=0.25*pi*Pf*b1^2*Gammaim(jfreq,jeta)*freq(jfreq);
mfpdbar1(jfreq,jb2,jeta)=0.25*pi*Pf*b2(jb2)^2*Gammard1(jfreq,jb2,jeta);
cfpdbar1(jfreq,jb2,jeta)=0.25*pi*Pf*b2(jb2)^2*Gammaid1(jfreq,jb2,jeta)*
freq(jfreq);
mfpdbar2(jfreq,jb4,jb2,jeta)=0.25*pi*Pf*b3(jb4,jb2)^2*Gammard2(jfreq,jb
4,jb2,jeta);
cfpdbar2(jfreq,jb4,jb2,jeta)=0.25*pi*Pf*b3(jb4,jb2)^2*Gammaid2(jfreq,jb
4,jb2,jeta)*freq(jfreq);
Kp(jfreq,jeta)=L1*((freq(jfreq)^2*(mmbar+mfpmbar(jfreq,jeta))-
1i*freq(jfreq)*cfpmbar(jfreq,jeta))/(E*Im))^0.25;
          KKp=Kp(jfreq,jeta);
          Cfp=cosh(KKp);
          Sfp=sinh(KKp);
          sfp=sin(KKp);
          cfp=cos(KKp);
          Gfp(jfreq,jb4,jL3,jb2,jL2,jeta)=0.5*(E*Im)^(-
1)*(2*freq(jfreq)^2*L1^2*ds(jb4,jL3,jb2,jL2)*md(jb4,jL3,jb2,jL2)+freq(j
freq)^2*L1^2*(L2(jL2)-L3(jL3))^2*mfpdbar1(jfreq,jb2,jeta)-
2*freq(jfreq)^2*L1^2*L3(jL3)^2*mfpdbar2(jfreq,jb4,jb2,jeta)-
j*freq(jfreq)*L1^2*(L2(jL2)-
L3(jL3))^2*cfpdbar1(jfreq,jb2,jeta)+2*j*freq(jfreq)*L1^2*L3(jL3)^2*cfpd
bar2(jfreq,jb4,jb2,jeta));
          Hfp(jfreq,jb4,jL3,jb2,jL2,jeta)=(3*E*Im)^(-
1)*(3*freq(jfreq)^2*L1*ds(jb4,jL3,jb2,jL2)^2*md(jb4,jL3,jb2,jL2)+freq(j
freq)^2*L1*(L2(jL2)-
L3(jL3))^3*mfpdbar1(jfreq,jb2,jeta)+2*freq(jfreq)^2*L1*L3(jL3)^3*mfpdba
r2(jfreq,jb4,jb2,jeta)+3*freq(jfreq)^2*L1*Jd(jb4,jL3,jb2,jL2)-
j*freq(jfreq)*L1*(L2(jL2)-L3(jL3))^3*cfpdbar1(jfreq,jb2,jeta)-
2*j*freq(jfreq)*L1*L3(jL3)^3*cfpdbar2(jfreq,jb4,jb2,jeta));
          Ffp(jfreq,jb4,jL3,jb2,jL2,jeta)=(E*Im)^(-1)*(-
freq(jfreq)^2*L1^3*md(jb4,jL3,jb2,jL2)-freq(jfreq)^2*L1^3*(L2(jL2)-
L3(jL3))*mfpdbar1(jfreq,jb2,jeta)-
2*freq(jfreq)^2*L1^3*L3(jL3)*mfpdbar2(jfreq,jb4,jb2,jeta)+j*freq(jfreq)
*L1^3*(L2(jL2)-
L3(jL3))*cfpdbar1(jfreq,jb2,jeta)+2*j*freq(jfreq)*L1^3*L3(jL3)*cfpdbar2
(jfreq,jb4,jb2,jeta));
          Kfp(jfreq,jb4,jL3,jb2,jL2,jeta)=0.5*(E*Im)^(-1)*(-
2*freq(jfreq)^2*L1^2*ds(jb4,jL3,jb2,jL2)*md(jb4,jL3,jb2,jL2)-
freq(jfreq)^2*L1^2*(L2(jL2)-
L3(jL3))^2*mfpdbar1(jfreq,jb2,jeta)+2*freq(jfreq)^2*L1^2*L3(jL3)^2*mfpd
bar2(jfreq,jb4,jb2,jeta)+j*freq(jfreq)*L1^2*(L2(jL2)-
L3(jL3))^2*cfpdbar1(jfreq,jb2,jeta)-
2*j*freq(jfreq)*L1^2*L3(jL3)^2*cfpdbar2(jfreq,jb4,jb2,jeta));
          MMfp(jfreq,jb4,jL3,jb2,jL2,jeta)=KKp^2*(Cfp+cfp)-
Gfp(jfreq,jb4,jL3,jb2,jL2,jeta)*(Cfp-cfp)-
```

```
Hfp(jfreq,jb4,jL3,jb2,jL2,jeta)*KKp*(Sfp+sfp);
          NNfp(jfreq,jb4,jL3,jb2,jL2,jeta)=KKp^2*(Sfp+sfp)-
Gfp(jfreq,jb4,jL3,jb2,jL2,jeta)*(Sfp-sfp)-
Hfp(jfreq,jb4,jL3,jb2,jL2,jeta)*KKp*(Cfp-cfp);
          OOfp(jfreq,jb4,jL3,jb2,jL2,jeta)=KKp^(-
1)*(KKp^2*sfp+Gfp(jfreq,jb4,jL3,jb2,jL2,jeta)*sfp+Hfp(jfreq,jb4,jL3,jb2
,jL2,jeta)*KKp*cfp);
          PPfp(jfreq,jb4,jL3,jb2,jL2,jeta)=KKp^3*(Sfp-sfp)-
Ffp(jfreq,jb4,jL3,jb2,jL2,jeta)*(Cfp-cfp)-
Kfp(jfreq,jb4,jL3,jb2,jL2,jeta)*KKp*(Sfp+sfp);
          QQfp(jfreq,jb4,jL3,jb2,jL2,jeta)=KKp^3*(Cfp+cfp)-
Ffp(jfreq,jb4,jL3,jb2,jL2,jeta)*(Sfp-sfp)-
Kfp(jfreq,jb4,jL3,jb2,jL2,jeta)*KKp*(Cfp-cfp);
          RRfp(jfreq,jb4,jL3,jb2,jL2,jeta)=KKp^(-
1)*(KKp^3*cfp+Ffp(jfreq,jb4,jL3,jb2,jL2,jeta)*sfp+Kfp(jfreq,jb4,jL3,jb2
,jL2,jeta)*KKp*cfp);
A1fp(jfreq,jb4,jL3,jb2,jL2,jeta)=(OOfp(jfreq,jb4,jL3,jb2,jL2,jeta)*QQfp
(jfreq,jb4,jL3,jb2,jL2,jeta)-
RRfp(jfreq,jb4,jL3,jb2,jL2,jeta)*NNfp(jfreq,jb4,jL3,jb2,jL2,jeta))/(MMf
p(jfreq,jb4,jL3,jb2,jL2,jeta)*QQfp(jfreq,jb4,jL3,jb2,jL2,jeta)-
PPfp(jfreq,jb4,jL3,jb2,jL2,jeta)*NNfp(jfreq,jb4,jL3,jb2,jL2,jeta));
A2fp(jfreq,jb4,jL3,jb2,jL2,jeta)=(OOfp(jfreq,jb4,jL3,jb2,jL2,jeta)*PPfp
(jfreq,jb4,jL3,jb2,jL2,jeta)-
RRfp(jfreq,jb4,jL3,jb2,jL2,jeta)*MMfp(jfreq,jb4,jL3,jb2,jL2,jeta))/(NNf
p(jfreq,jb4,jL3,jb2,jL2,jeta)*PPfp(jfreq,jb4,jL3,jb2,jL2,jeta)-
MMfp(jfreq,jb4,jL3,jb2,jL2,jeta)*QQfp(jfreq,jb4,jL3,jb2,jL2,jeta));
Dfp(jfreq,jb4,jL3,jb2,jL2,jeta)=abs(A1fp(jfreq,jb4,jL3,jb2,jL2,jeta)*(C
fp-cfp)+A2fp(jfreq,jb4,jL3,jb2,jL2,jeta)*(Sfp-sfp)+KKp^(-1)*sfp);
        end
Dfpmax(jb4,jL3,jb2,jL2,jeta)=max(Dfp(:,jb4,jL3,jb2,jL2,jeta));Dfpmaxsqr
t2(jb4,jL3,jb2,jL2,jeta)=Dfpmax(jb4,jL3,jb2,jL2,jeta)/sqrt(2);
             end
          end
    end
  end
end
%%%% find resonant frequency%%%
for jeta=1:length(eta);
     for jL2=1:length(L2);
         for jb2=1:length(b2);
             for  jL3=1:length(L3);
                 for jb4=1:length(b4);
                     for jfreq=1:length(freq);
            %LLamd(jfreq) = ((mmbar*L1^4*(freq(jfreq))^2)/(E*Im))^0.25;

if(Dfp(jfreq,jb4,jL3,jb2,jL2,jeta)==Dfpmax(jb4,jL3,jb2,jL2,jeta));
               resf(jb4,jL3,jb2,jL2,jeta)=freq(jfreq);
             end
      end
   end
  end
         end
     end
end
for jeta=1:length(eta);
     for jL2=1:length(L2);
         for jb2=1:length(b2);
```

```
            for  jL3=1:length(L3);
                for jb4=1:length(b4);
        b3(jb4,jb2)=0.5*(b2(jb2)-b1-2*b4(jb4));
        dc(jb4,jL3,jb2,jL2)=(0.5*L2(jL2)*b2(jb2)*L2(jL2)-
0.5*L3(jL3)*(b1+2*b4(jb4))*L3(jL3))/(L2(jL2)*b2(jb2)-
L3(jL3)*(b1+2*b4(jb4))); % distance of the mass center to the end of
the HH rectangle using L2,L3,b1,b4
        ds(jb4,jL3,jb2,jL2)=(0.5*L2(jL2)*b2(jb2)*L2(jL2)-
0.5*L3(jL3)*(b1+2*b4(jb4))*L3(jL3))/(L2(jL2)*b2(jb2)-
L3(jL3)*(b1+2*b4(jb4)))-L3(jL3); % distance of the mass center to the
end of the stem using L2,L3,b1,b4
        dc2(jb4,jL3,jb2,jL2)=(0.5*L2(jL2)*b2(jb2)*L2(jL2)-
0.5*L3(jL3)*(b2(jb2)-2*b3(jb4,jb2))*L3(jL3))/(L2(jL2)*b2(jb2)-
L3(jL3)*(b2(jb2)-2*b3(jb4,jb2))); % distance of the mass center to the
end of the HH rectangle using L2,L3,b2,b3
        ds2(jb4,jL3,jb2,jL2)=(0.5*L2(jL2)*b2(jb2)*L2(jL2)-
0.5*L3(jL3)*(b2(jb2)-2*b3(jb4,jb2))*L3(jL3))/(L2(jL2)*b2(jb2)-
L3(jL3)*(b2(jb2)-2*b3(jb4,jb2)))-L3(jL3); % distance of the mass center
to the end of the stem using L2,L3,b2,b3
Jd(jb4,jL3,jb2,jL2)=(1/12)*Pb*L2(jL2)*b2(jb2)*h*(L2(jL2)^2+b2(jb2)^2)+(
dc(jb4,jL3,jb2,jL2)-0.5*L2(jL2))^2*Pb*L2(jL2)*b2(jb2)*h-
((1/12)*Pb*L3(jL3)*(b1+2*b4(jb4))*h*(L3(jL3)^2+(b1+2*b4(jb4))^2)+(ds(jb
4,jL3,jb2,jL2)+0.5*L3(jL3))^2*Pb*L3(jL3)*(b1+2*b4(jb4))*h); % moment of
inertia due to rotation
        md(jb4,jL3,jb2,jL2)=Pb*h*(L2(jL2)*b2(jb2)-
L3(jL3)*(b1+2*b4(jb4))); % mass of the HH
        %%%%%%%%%% Hydrodynamic function including thickness
correction %%%%%%%%%%
Reym(jb4,jL3,jb2,jL2,jeta)=(Pf*resf(jb4,jL3,jb2,jL2,jeta)*b1^2)/(4*eta(
jeta));
Reyd1(jb4,jL3,jb2,jL2,jeta)=(Pf*resf(jb4,jL3,jb2,jL2,jeta)*b2(jb2)^2)/(
4*eta(jeta));
Reyd2(jb4,jL3,jb2,jL2,jeta)=(Pf*resf(jb4,jL3,jb2,jL2,jeta)*b3(jb4,jb2)^
2)/(4*eta(jeta));
           Gammarm(jb4,jL3,jb2,jL2,jeta)=Reym(jb4,jL3,jb2,jL2,jeta)^-
0.5*(0.9003+0.6105*(h/b1)^0.5+2.1722*(h/b1)^1)+(-0.0021*(h/b1)^0.5-
0.1459*(h/b1)^1+0.8255*(h/b1)^1.5+0.8144*(h/b1)^2);
           Gammaim(jb4,jL3,jb2,jL2,jeta)=Reym(jb4,jL3,jb2,jL2,jeta)^-
1*(2.5758-1.3388*(h/b1)^0.5)+Reym(jb4,jL3,jb2,jL2,jeta)^-
0.5*(0.9003+0.7121*(h/b1)^0.5+1.6845*(h/b1)^1+0.8236*(h/b1)^1.5-
0.4178*(h/b1)^2);
           Gammard1(jb4,jL3,jb2,jL2,jeta)=Reyd1(jb4,jL3,jb2,jL2,jeta)^-
0.5*(0.9003+0.6105*(h/b2(jb2))^0.5+2.1722*(h/b2(jb2))^1)+(-
0.0021*(h/b2(jb2))^0.5-
0.1459*(h/b2(jb2))^1+0.8255*(h/b2(jb2))^1.5+0.8144*(h/b2(jb2))^2);
           Gammaid1(jb4,jL3,jb2,jL2,jeta)=Reyd1(jb4,jL3,jb2,jL2,jeta)^-
1*(2.5758-1.3388*(h/b2(jb2))^0.5)+Reyd1(jb4,jL3,jb2,jL2,jeta)^-
0.5*(0.9003+0.7121*(h/b2(jb2))^0.5+1.6845*(h/b2(jb2))^1+0.8236*(h/b2(jb
2))^1.5-0.4178*(h/b2(jb2))^2);
           Gammard2(jb4,jL3,jb2,jL2,jeta)=Reyd2(jb4,jL3,jb2,jL2,jeta)^-
0.5*(0.9003+0.6105*(h/b3(jb4,jb2))^0.5+2.1722*(h/b3(jb4,jb2))^1)+(-
0.0021*(h/b3(jb4,jb2))^0.5-
0.1459*(h/b3(jb4,jb2))^1+0.8255*(h/b3(jb4,jb2))^1.5+0.8144*(h/b3(jb4,jb
2))^2);
           Gammaid2(jb4,jL3,jb2,jL2,jeta)=Reyd2(jb4,jL3,jb2,jL2,jeta)^-
1*(2.5758-1.3388*(h/b3(jb4,jb2))^0.5)+Reyd2(jb4,jL3,jb2,jL2,jeta)^-
0.5*(0.9003+0.7121*(h/b3(jb4,jb2))^0.5+1.6845*(h/b3(jb4,jb2))^1+0.8236*
```

```
(h/b3(jb4,jb2))^1.5-0.4178*(h/b3(jb4,jb2))^2);
mfpmbar(jb4,jL3,jb2,jL2,jeta)=0.25*pi*Pf*b1^2*Gammarm(jb4,jL3,jb2,jL2,j
eta);
cfpmbar(jb4,jL3,jb2,jL2,jeta)=0.25*pi*Pf*b1^2*Gammaim(jb4,jL3,jb2,jL2,j
eta)*resf(jb4,jL3,jb2,jL2,jeta);
mfpdbar1(jb4,jL3,jb2,jL2,jeta)=0.25*pi*Pf*b2(jb2)^2*Gammard1(jb4,jL3,jb
2,jL2,jeta);
cfpdbar1(jb4,jL3,jb2,jL2,jeta)=0.25*pi*Pf*b2(jb2)^2*Gammaid1(jb4,jL3,jb
2,jL2,jeta)*resf(jb4,jL3,jb2,jL2,jeta);
mfpdbar2(jb4,jL3,jb2,jL2,jeta)=0.25*pi*Pf*b3(jb4,jb2)^2*Gammard2(jb4,jL
3,jb2,jL2,jeta);
cfpdbar2(jb4,jL3,jb2,jL2,jeta)=0.25*pi*Pf*b3(jb4,jb2)^2*Gammaid2(jb4,jL
3,jb2,jL2,jeta)*resf(jb4,jL3,jb2,jL2,jeta);
Kp(jb4,jL3,jb2,jL2,jeta)=L1*((resf(jb4,jL3,jb2,jL2,jeta)^2*(mmbar+mfpmb
ar(jb4,jL3,jb2,jL2,jeta))-
1i*resf(jb4,jL3,jb2,jL2,jeta)*cfpmbar(jb4,jL3,jb2,jL2,jeta))/(E*Im))^0.
25;
          KKp=Kp(jb4,jL3,jb2,jL2,jeta);
          Cfp=cosh(KKp);
          Sfp=sinh(KKp);
          sfp=sin(KKp);
          cfp=cos(KKp);
          Gfp(jb4,jL3,jb2,jL2,jeta)=0.5*(E*Im)^(-
1)*(2*resf(jb4,jL3,jb2,jL2,jeta)^2*L1^2*ds(jb4,jL3,jb2,jL2)*md(jb4,jL3,
jb2,jL2)+resf(jb4,jL3,jb2,jL2,jeta)^2*L1^2*(L2(jL2)-
L3(jL3))^2*mfpdbar1(jb4,jL3,jb2,jL2,jeta)-
2*resf(jb4,jL3,jb2,jL2,jeta)^2*L1^2*L3(jL3)^2*mfpdbar2(jb4,jL3,jb2,jL2,
jeta)-j*resf(jb4,jL3,jb2,jL2,jeta)*L1^2*(L2(jL2)-
L3(jL3))^2*cfpdbar1(jb4,jL3,jb2,jL2,jeta)+2*j*resf(jb4,jL3,jb2,jL2,jeta
)*L1^2*L3(jL3)^2*cfpdbar2(jb4,jL3,jb2,jL2,jeta));
          Hfp(jb4,jL3,jb2,jL2,jeta)=(3*E*Im)^(-
1)*(3*resf(jb4,jL3,jb2,jL2,jeta)^2*L1*ds(jb4,jL3,jb2,jL2)^2*md(jb4,jL3,
jb2,jL2)+resf(jb4,jL3,jb2,jL2,jeta)^2*L1*(L2(jL2)-
L3(jL3))^3*mfpdbar1(jb4,jL3,jb2,jL2,jeta)+2*resf(jb4,jL3,jb2,jL2,jeta)^
2*L1*L3(jL3)^3*mfpdbar2(jb4,jL3,jb2,jL2,jeta)+3*resf(jb4,jL3,jb2,jL2,je
ta)^2*L1*Jd(jb4,jL3,jb2,jL2)-j*resf(jb4,jL3,jb2,jL2,jeta)*L1*(L2(jL2)-
L3(jL3))^3*cfpdbar1(jb4,jL3,jb2,jL2,jeta)-
2*j*resf(jb4,jL3,jb2,jL2,jeta)*L1*L3(jL3)^3*cfpdbar2(jb4,jL3,jb2,jL2,je
ta));
          Ffp(jb4,jL3,jb2,jL2,jeta)=(E*Im)^(-1)*(-
resf(jb4,jL3,jb2,jL2,jeta)^2*L1^3*md(jb4,jL3,jb2,jL2)-
resf(jb4,jL3,jb2,jL2,jeta)^2*L1^3*(L2(jL2)-
L3(jL3))*mfpdbar1(jb4,jL3,jb2,jL2,jeta)-
2*resf(jb4,jL3,jb2,jL2,jeta)^2*L1^3*L3(jL3)*mfpdbar2(jb4,jL3,jb2,jL2,je
ta)+j*resf(jb4,jL3,jb2,jL2,jeta)*L1^3*(L2(jL2)-
L3(jL3))*cfpdbar1(jb4,jL3,jb2,jL2,jeta)+2*j*resf(jb4,jL3,jb2,jL2,jeta)*
L1^3*L3(jL3)*cfpdbar2(jb4,jL3,jb2,jL2,jeta));
          Kfp(jb4,jL3,jb2,jL2,jeta)=0.5*(E*Im)^(-1)*(-
2*resf(jb4,jL3,jb2,jL2,jeta)^2*L1^2*ds(jb4,jL3,jb2,jL2)*md(jb4,jL3,jb2,
jL2)-resf(jb4,jL3,jb2,jL2,jeta)^2*L1^2*(L2(jL2)-
L3(jL3))^2*mfpdbar1(jb4,jL3,jb2,jL2,jeta)+2*resf(jb4,jL3,jb2,jL2,jeta)^
2*L1^2*L3(jL3)^2*mfpdbar2(jb4,jL3,jb2,jL2,jeta)+j*resf(jb4,jL3,jb2,jL2,
jeta)*L1^2*(L2(jL2)-L3(jL3))^2*cfpdbar1(jb4,jL3,jb2,jL2,jeta)-
2*j*resf(jb4,jL3,jb2,jL2,jeta)*L1^2*L3(jL3)^2*cfpdbar2(jb4,jL3,jb2,jL2,
jeta));
          MMfp(jb4,jL3,jb2,jL2,jeta)=KKp^2*(Cfp+cfp)-
Gfp(jb4,jL3,jb2,jL2,jeta)*(Cfp-cfp)-
```

```
Hfp(jb4,jL3,jb2,jL2,jeta)*KKp*(Sfp+sfp);
          NNfp(jb4,jL3,jb2,jL2,jeta)=KKp^2*(Sfp+sfp)-
Gfp(jb4,jL3,jb2,jL2,jeta)*(Sfp-sfp)-Hfp(jb4,jL3,jb2,jL2,jeta)*KKp*(Cfp-
cfp);
OOfp(jb4,jL3,jb2,jL2,jeta)=KKp^(-
1)*(KKp^2*sfp+Gfp(jb4,jL3,jb2,jL2,jeta)*sfp+Hfp(jb4,jL3,jb2,jL2,jeta)*K
Kp*cfp);
  PPfp(jb4,jL3,jb2,jL2,jeta)=KKp^3*(Sfp-sfp)-
Ffp(jb4,jL3,jb2,jL2,jeta)*(Cfp-cfp)-
Kfp(jb4,jL3,jb2,jL2,jeta)*KKp*(Sfp+sfp);
          QQfp(jb4,jL3,jb2,jL2,jeta)=KKp^3*(Cfp+cfp)-
Ffp(jb4,jL3,jb2,jL2,jeta)*(Sfp-sfp)-Kfp(jb4,jL3,jb2,jL2,jeta)*KKp*(Cfp-
cfp);
          RRfp(jb4,jL3,jb2,jL2,jeta)=KKp^(-
1)*(KKp^3*cfp+Ffp(jb4,jL3,jb2,jL2,jeta)*sfp+Kfp(jb4,jL3,jb2,jL2,jeta)*K
Kp*cfp);
A1fp(jb4,jL3,jb2,jL2,jeta)=(OOfp(jb4,jL3,jb2,jL2,jeta)*QQfp(jb4,jL3,jb2
,jL2,jeta)-
RRfp(jb4,jL3,jb2,jL2,jeta)*NNfp(jb4,jL3,jb2,jL2,jeta))/(MMfp(jb4,jL3,jb
2,jL2,jeta)*QQfp(jb4,jL3,jb2,jL2,jeta)-
PPfp(jb4,jL3,jb2,jL2,jeta)*NNfp(jb4,jL3,jb2,jL2,jeta));
A2fp(jb4,jL3,jb2,jL2,jeta)=(OOfp(jb4,jL3,jb2,jL2,jeta)*PPfp(jb4,jL3,jb2
,jL2,jeta)-
RRfp(jb4,jL3,jb2,jL2,jeta)*MMfp(jb4,jL3,jb2,jL2,jeta))/(NNfp(jb4,jL3,jb
2,jL2,jeta)*PPfp(jb4,jL3,jb2,jL2,jeta)-
MMfp(jb4,jL3,jb2,jL2,jeta)*QQfp(jb4,jL3,jb2,jL2,jeta));
          xi=sym('xi','real'); % denotes x/L1
X(jb4,jL3,jb2,jL2,jeta)=A1fp(jb4,jL3,jb2,jL2,jeta)*(cosh(KKp*xi)-
cos(KKp*xi))+A2fp(jb4,jL3,jb2,jL2,jeta)*(sinh(KKp*xi)-
sin(KKp*xi))+KKp^(-1)*sin(KKp*xi); % normalized shape function
Xp(jb4,jL3,jb2,jL2,jeta)=KKp*(A1fp(jb4,jL3,jb2,jL2,jeta)*(sinh(KKp*xi)+
sin(KKp*xi))+A2fp(jb4,jL3,jb2,jL2,jeta)*(cosh(KKp*xi)-
cos(KKp*xi))+KKp^(-1)*cos(KKp*xi)); % first derivative of normalized
deflection measns X'
Xpp(jb4,jL3,jb2,jL2,jeta)=KKp^2*(A1fp(jb4,jL3,jb2,jL2,jeta)*(cosh(KKp*x
i)+cos(KKp*xi))+A2fp(jb4,jL3,jb2,jL2,jeta)*(sinh(KKp*xi)+sin(KKp*xi))-
KKp^(-1)*sin(KKp*xi)); % second derivative of normalized deflection
measns X''
BB1(jb4,jL3,jb2,jL2,jeta)=int((real(Xpp(jb4,jL3,jb2,jL2,jeta)))^2, xi,
0, 1);
BB2(jb4,jL3,jb2,jL2,jeta)=int((imag(Xpp(jb4,jL3,jb2,jL2,jeta)))^2, xi,
0, 1);
BB3(jb4,jL3,jb2,jL2,jeta)=int((real(Xpp(jb4,jL3,jb2,jL2,jeta)))*(imag(X
pp(jb4,jL3,jb2,jL2,jeta))), xi, 0, 1);
BB4(jb4,jL3,jb2,jL2,jeta)=int((real(X(jb4,jL3,jb2,jL2,jeta)))^2, xi, 0,
1);
BB5(jb4,jL3,jb2,jL2,jeta)=int((imag(X(jb4,jL3,jb2,jL2,jeta)))^2, xi, 0,
1);
BB6(jb4,jL3,jb2,jL2,jeta)=int((real(X(jb4,jL3,jb2,jL2,jeta)))*(imag(X(j
b4,jL3,jb2,jL2,jeta))), xi, 0, 1);
BB7(jb4,jL3,jb2,jL2,jeta)=(real(A1fp(jb4,jL3,jb2,jL2,jeta)*(cosh(KKp)-
cos(KKp))+A2fp(jb4,jL3,jb2,jL2,jeta)*(sinh(KKp)-sin(KKp))+KKp^(-
1)*sin(KKp)))^2;
BB8(jb4,jL3,jb2,jL2,jeta)=(imag(A1fp(jb4,jL3,jb2,jL2,jeta)*(cosh(KKp)-
cos(KKp))+A2fp(jb4,jL3,jb2,jL2,jeta)*(sinh(KKp)-sin(KKp))+KKp^(-
1)*sin(KKp)))^2;
BB9(jb4,jL3,jb2,jL2,jeta)=(real(A1fp(jb4,jL3,jb2,jL2,jeta)*(cosh(KKp)-
```

```
cos(KKp))+A2fp(jb4,jL3,jb2,jL2,jeta)*(sinh(KKp)-sin(KKp))+KKp^(-
1)*sin(KKp)))*(imag(A1fp(jb4,jL3,jb2,jL2,jeta)*(cosh(KKp)-
cos(KKp))+A2fp(jb4,jL3,jb2,jL2,jeta)*(sinh(KKp)-sin(KKp))+KKp^(-
1)*sin(KKp)));
BB13(jb4,jL3,jb2,jL2,jeta)=(real(KKp*(A1fp(jb4,jL3,jb2,jL2,jeta)*(sinh(
KKp)+sin(KKp))+A2fp(jb4,jL3,jb2,jL2,jeta)*(cosh(KKp)-cos(KKp))+KKp^(-
1)*cos(KKp))))^2;
BB14(jb4,jL3,jb2,jL2,jeta)=(imag(KKp*(A1fp(jb4,jL3,jb2,jL2,jeta)*(sinh(
KKp)+sin(KKp))+A2fp(jb4,jL3,jb2,jL2,jeta)*(cosh(KKp)-cos(KKp))+KKp^(-
1)*cos(KKp))))^2;
BB15(jb4,jL3,jb2,jL2,jeta)=(real(KKp*(A1fp(jb4,jL3,jb2,jL2,jeta)*(sinh(
KKp)+sin(KKp))+A2fp(jb4,jL3,jb2,jL2,jeta)*(cosh(KKp)-cos(KKp))+KKp^(-
1)*cos(KKp))))*(imag(KKp*(A1fp(jb4,jL3,jb2,jL2,jeta)*(sinh(KKp)+sin(KKp
))+A2fp(jb4,jL3,jb2,jL2,jeta)*(cosh(KKp)-cos(KKp))+KKp^(-
1)*cos(KKp))));BB10(jb4,jL3,jb2,jL2,jeta)=sqrt(BB7(jb4,jL3,jb2,jL2,jeta
))*sqrt(BB13(jb4,jL3,jb2,jL2,jeta));
BB11(jb4,jL3,jb2,jL2,jeta)=sqrt(BB8(jb4,jL3,jb2,jL2,jeta))*sqrt(BB14(jb
4,jL3,jb2,jL2,jeta));
BB12(jb4,jL3,jb2,jL2,jeta)=sqrt(BB7(jb4,jL3,jb2,jL2,jeta))*sqrt(BB14(jb
4,jL3,jb2,jL2,jeta))+sqrt(BB13(jb4,jL3,jb2,jL2,jeta))*sqrt(BB8(jb4,jL3,
jb2,jL2,jeta));
            BB16(jb4,jL3,jb2,jL2,jeta)=BB13(jb4,jL3,jb2,jL2,jeta);
            BB17(jb4,jL3,jb2,jL2,jeta)=BB14(jb4,jL3,jb2,jL2,jeta);
            BB18(jb4,jL3,jb2,jL2,jeta)=BB15(jb4,jL3,jb2,jL2,jeta);
            BB19(jb4,jL3,jb2,jL2,jeta)=-
imag(2*A1fp(jb4,jL3,jb2,jL2,jeta)*KKp^2);
                                  for jtau=1:length(tau)
F(jtau,jb4,jL3,jb2,jL2,jeta)=BB1(jb4,jL3,jb2,jL2,jeta)*(cos(jtau))^2+BB
2(jb4,jL3,jb2,jL2,jeta)*(sin(jtau))^2-
2*BB3(jb4,jL3,jb2,jL2,jeta)*(cos(jtau))*(sin(jtau))+(L1^4*mmbar*resf(jb
4,jL3,jb2,jL2,jeta)^2*(E*Im)^(-
1))*(BB4(jb4,jL3,jb2,jL2,jeta)*(sin(jtau))^2+BB5(jb4,jL3,jb2,jL2,jeta)*
(cos(jtau))^2+2*BB6(jb4,jL3,jb2,jL2,jeta)*(cos(jtau))*(sin(jtau)))+(md(
jb4,jL3,jb2,jL2)*L1^3*resf(jb4,jL3,jb2,jL2,jeta)^2*(E*Im)^(-
1))*(BB7(jb4,jL3,jb2,jL2,jeta)*(sin(jtau))^2+BB8(jb4,jL3,jb2,jL2,jeta)*
(cos(jtau))^2+2*BB9(jb4,jL3,jb2,jL2,jeta)*(cos(jtau))*(sin(jtau)))+(2*m
d(jb4,jL3,jb2,jL2)*L1^2*ds(jb4,jL3,jb2,jL2)*resf(jb4,jL3,jb2,jL2,jeta)^
2*(E*Im)^(-
1))*(BB10(jb4,jL3,jb2,jL2,jeta)*(sin(jtau))^2+BB11(jb4,jL3,jb2,jL2,jeta
)*(cos(jtau))^2+BB12(jb4,jL3,jb2,jL2,jeta)*(cos(jtau))*(sin(jtau)))+(md
(jb4,jL3,jb2,jL2)*L1*ds(jb4,jL3,jb2,jL2)^2*resf(jb4,jL3,jb2,jL2,jeta)^2
*(E*Im)^(-
1))*(BB13(jb4,jL3,jb2,jL2,jeta)*(sin(jtau))^2+BB14(jb4,jL3,jb2,jL2,jeta
)*(cos(jtau))^2+2*BB15(jb4,jL3,jb2,jL2,jeta)*(cos(jtau))*(sin(jtau)))+(
Jd(jb4,jL3,jb2,jL2)*L1*resf(jb4,jL3,jb2,jL2,jeta)^2*(E*Im)^(-
1))*(BB16(jb4,jL3,jb2,jL2,jeta)*(sin(jtau))^2+BB17(jb4,jL3,jb2,jL2,jeta
)*(cos(jtau))^2+2*BB18(jb4,jL3,jb2,jL2,jeta)*(cos(jtau))*(sin(jtau)));
Qua(jtau,jb4,jL3,jb2,jL2,jeta)=F(jtau,jb4,jL3,jb2,jL2,jeta)/BB19(jb4,jL
3,jb2,jL2,jeta);
   end
end
  end
end
  end
end
for jeta=1:length(eta);
     for jL2=1:length(L2);
```

```
         for jb2=1:length(b2);
             for  jL3=1:length(L3);
                 for jb4=1:length(b4);
Quaactual(jb4,jL3,jb2,jL2,jeta)=max(double(Qua(:,jb4,jL3,jb2,jL2,jeta))
)end
             end
         end
     end
end
```